UNIVERSITÉ DE LORRAINE | BIBLIOTHÈQUES UNIVERSITAIRES

AVERTISSEMENT

Ce document est le fruit d'un long travail approuvé par le jury de soutenance et mis à disposition de l'ensemble de la communauté universitaire élargie.

Il est soumis à la propriété intellectuelle de l'auteur. Ceci implique une obligation de citation et de référencement lors de l'utilisation de ce document.

D'autre part, toute contrefaçon, plagiat, reproduction illicite encourt une poursuite pénale.

Contact bibliothèque : ddoc-theses-contact@univ-lorraine.fr
(Cette adresse ne permet pas de contacter les auteurs)

LIENS

Code de la Propriété Intellectuelle. articles L 122. 4
Code de la Propriété Intellectuelle. articles L 335.2- L 335.10
http://www.cfcopies.com/V2/leg/leg_droi.php
http://www.culture.gouv.fr/culture/infos-pratiques/droits/protection.htm

SIReNa

LIBio et LCPM

Thèse

Présentée et soutenue publiquement pour l'obtention du titre de

DOCTEUR DE l'UNIVERSITE DE LORRAINE

Mention : GÉNIE BIOTECHNOLOGIQUE ET ALIMENTAIRE

par **Jiaqi WENG**

Sous la direction de Stéphane DESOBRY et Alain DURAND

Encapsulation et Cinétique de Libération de Molécules de Polyphénols à Partir de Particules à Base de Chitosan

Encapsulation and Release Kinetics of Polyphenol Molecules from Chitosan Based Particles

Le 6 novembre 2023

Membres du jury :

Directeur(s) de thèse :	**Monsieur Stéphane DESOBRY**	**Professeur, Université de Lorraine, Nancy**
Codirecteur(s) de thèse :	**Monsieur Alain DURAND**	**Professeur, Université de Lorraine, Nancy**
Président de jury :	**Monsieur Frédéric DEBEAUFORT**	**Professeur, Université de Bourgogne, Dijon**
Rapporteurs :	**Madame Claire BORDES**	**Professeur, Université Claude Bernard-Lyon 1, Lyon**
	Monsieur Pingtian DING	**Professeur, Shenzhen Technology University, Shenzhen**
Examinateurs :	**Monsieur Frédéric DEBEAUFORT**	**Professeur, Université de Bourgogne, Dijon**
	Madame Christine GERARDIN	**Professeur, Université de Lorraine, Nancy**

Table of Contents

Table of Contents **2**

List of abbreviations **4**

Acknowledgments **6**

Remerciement **8**

Résumé **10**

Introduction *10*

Méthode *12*

Résultats *13*

Effet des paramètres du procédé de préparation sur les caractéristiques des particules *13*

Encapsulation *14*

Test de libération *14*

Conclusions et perspectives *16*

General introduction **18**

1 State of the art **20**

1.1 Biopolymer with unique positive charge: chitosan *20*

1.2 CS-TPP particulate systems *29*

1.3 Preparation methods of chitosan-based network and particulate structure *32*

1.4 General introduction of ionotropic gelation *38*

1.5 Nanoparticles *40*

1.6 Polyphenols *48*

1.7 Application of CS-TPP system in delivery of polyphenols *58*

2 Scientific approach **60**

2.1 Context *60*

2.2 Position of this work *60*

2.3 Objectives *61*

2.4 Research questions *61*

2.5 Experimental design *61*

3 Material and methods 62

3.1 Characterization of materials 62

3.2 Preparation of CS-TPP particles 66

3.3 Characterization and morphology of the prepared chitosan particles 73

3.4 Encapsulation of polyphenols into CS-TPP particles 74

3.5 Release properties of polyphenols loaded CS-TPP particles 81

4 Results and discussion 83

4.1 Characterization of materials 83

4.2 Effect of process parameters on particle quality (size control) 108

4.3 Encapsulation 114

4.4 Release of NRG from CS particles 128

5 Conclusion and perspectives 141

List of figures 144

List of Tables 147

Reference 148

Annex I. Preparation conditions of CS-TPP particles 165

Annex II. SEC MALS 168

Annex III. Encapsulation washing step 177

List of abbreviations

Definition	Abbreviation
Alginate	ALG
Atomic force microscopy	AFM
Brunauer Emmett Teller	BET
Catechin	CAT
Chitosan	CS
Cyclooxygenase-2	COX-2
Derjaguin, Verwey, Landau and Overbeek	DVLO
Deuterium chloride	DCL
Design of Experiments	DoE
Degree of deacetylation	DDA
Dimethyl formamide	DMF
Dimethyl sulfoxide	DMSO
Dimethylnitrosamine	DMN
Dynamic light scattering	DLS
Encapsulation efficiency	EE
Ethanol	EtOH
European pharmacopoeia	Ph. Eur
Food and Agriculture Organization	FAO
Food and Drug Administration	FDA
Fourier transform infrared spectroscopy	FTIR
Gastrointestinal	GI
High-performance liquid chromatography	HPLC
International Union of Pure and Applied Chemistry	IUPAC
Ionotropic gelation	IG
Laser doppler velocimetry	LDV
Low-density lipoprotein	LDL
Multiple-angle laser light-scattering	MALS
Nanoparticle	NP
Naringenin	NRG
Naringin	NR
Nitric oxide	NO
Nuclear factor-kappa B	NF-κB
Nuclear Magnetic Resonance spectroscopy	NMR
Number-average molecular weight	Mn
Palladium	Pd
Polydispersity index	PDI
Polyelectrolyte complexation	PEC
Quantity of catechin	Q_{CAT}
Quantity of naringenin	Q_{NRG}
Quantity of naringin	Q_{NR}
Quantum dots	Qdots

Reactive oxygen species	ROS
Scanning electron microscopy	SEM
Size-exclusion chromatography	SEC
Transmission electron microscopy	TEM
Tripolyphosphate	TPP
Ultraviolet–visible	UV-Vis
Weight-average Molecular weight	Mw

Acknowledgments

Here, I would like to express my gratitude to my supervisors, Alain Durand and Stéphane Desobry. Throughout the entire research process, they provided me with guidance and direction. As my mentor, their guidance has been invaluable. I want to thank the members of the CSI committee, Christine Gérardin and Catherine Virot Humeau for their understanding and tolerance regarding deadline extensions caused by the circumstances of the pandemic. I appreciate your trust and encouragement.

I want to especially thank Alain for his academic enthusiasm and friendship, which has always inspired me. Whether it was the joy of success or the setbacks encountered during experimental research and writing, his guidance and encouragement have always been by my side. He provided thorough and generous guidance for the initial draft of my thesis.

I would like to express my gratitude to my colleagues for their contributions inspiration during this research work. They are: Oliver Fabre, Raphael Dos Santos Morais, Carole Jeandel, Carole Perroud, Lise Salsi, Alexandre Collard, Khalid Ferji, Jean-Luc Six, Florentin Michaux, Anne-Marie Revol-Junelles, Frédéric Borges, Erika Paola Fonseca Parra, Aurélie Adam, Aldjia Ait Chekdid, Loubiana Cvetkovska, Faustine Gomand, Kamil Elkhoury, Mohamed Ibrahim, Ali Khalil, Marie Vuillemin, Jordane Jasniewski, Tristan Fournaise, Urielle M'Be, Blandine Simard, Aurélie Seiler, Alexis Dijamentiuk, Mahmoud Hasan, Cécile Mangavel, and Magda Corgneau. Thank you all for your support and collaboration.

Throughout my Ph.D. journey, I have been fortunate to receive invaluable insights and inspiration from numerous friends within and outside the academic community. Their unwavering support, encouragement, and emotional assistance have been instrumental in helping me navigate through challenging times. Despite their diverse backgrounds and lifestyles, they have remained by my side, offering constant companionship and motivating me to keep progressing. They are Pan Wang, Teng Guo, Hao Li, Jiayao Li, Yawen Luo, Ziqing Wu, Chenhui YE, Tianyuan Zhang, Yuzhe Hao, Kou Du, Dang Ning, Wang Tao, Mengxi Zhou, Ruotao Yang, Jia Shang, Fangyu Yang, Chunxiao Li, Hao Wang, Fuhua Yang, Kun Wang, Hasnae, Rod, FTCY, Mengjia ZHU and Erbao. Without your support, my research and writing would not have been possible.

I am extremely grateful to Jasminka for providing me with accommodation and for her exceptional care and support. Whenever I felt lost or overwhelmed, she patiently listened and helped me regain my confidence. Her valuable advice on various matters and life choices has been invaluable to me. Her positive outlook on life and her determination to find solutions in the face of challenges have been a great source of inspiration and strength for me. I deeply admire her genuine and generous nature, her appreciation for beauty, her kindness and generosity, her curious spirit, and her inclusive attitude towards different cultures. The time I spent with her during my PhD, whether it was on weekends, holidays, travels, or Christmas, is truly cherished.

I would also like to thank Jean-Louis for helping me move, providing accommodation, creating a good writing environment, and caring about my health. He accompanied me during the final writing process of this dissertation, and at the same time, constantly encouraged me to persevere to the end. The time spent in Nemours will become a precious treasure and good memory in my life.

Thanks to my mother for her constant support, trust, and love.

We thank the support of the research grant from the LUE-Biomolecule project of the Université de Lorraine.

Remerciement

Ici, je tiens à exprimer ma gratitude envers mes directeurs de recherche en doctorat. Tout au long du processus de recherche, ils m'ont fourni des orientations et des conseils. En tant que superviseurs, leur accompagnement a été inestimable. Je tiens à remercier mes directeurs de recherche et les enseignants du comité CSI pour leur compréhension et leur tolérance à l'égard des délais prolongés dus à des circonstances telles que la pandémie. J'apprécie votre confiance et votre encouragement. Je tiens à remercier également aux autres membre de jury, Mme. Bordes, M. Ding, et M. Debeaufort pour leur participation à la revue de ma thèse et à mon soutenance et leurs questions inspirants pendant la discussion.

Je tiens particulièrement à remercier Alain pour son enthousiasme académique et son amitié, qui m'ont toujours inspiré. Que ce soit la joie du succès ou les revers rencontrés lors de la recherche expérimentale et de l'écriture, ses conseils m'ont toujours accompagné. Il a apporté un soutien attentif et généreux pour la rédaction du premier brouillon de ma thèse après sa finalisation.

Je tiens à exprimer ma gratitude envers mes collègues pour leurs contributions et leurs inspirations au cours de ce travail de recherche. Il s'agit de : Oliver Fabre, Raphael Dos Santos Morais, Carole Jeandel, Carole Perroud, Lise Salsi, Alexandre Collard, Khalid Ferji, Jean-Luc Six, Florentin Michaux, Anne-Marie Revol-Junelles, Frédéric Borges, Erika Paola Fonseca Parra, Aurélie Adam, Aldjia Ait Chekdid, Loubiana Cvetkovska, Faustine Gomand, Kamil Elkhoury, Mohamed Ibrahim, Ali Khalil, Marie Vuillemin, Jordane Jasniewski, Tristan Fournaise, Urielle M'Be, Blandine Simard, Aurélie Seiler, Alexis Dijamentiuk, Mahmoud Hasan, Cécile Mangavel, and Magda Corgneau. Je vous remercie tous pour votre soutien et votre collaboration.

Tout au long de mon doctorat parcours, j'ai eu la chance de recevoir des idées et des inspirations inestimables de la part de nombreux amis au sein et en dehors de la communauté universitaire. Leur soutien indéfectible, leurs encouragements et leur aide émotionnelle ont été déterminants pour m'aider à traverser des moments difficiles. Malgré leurs parcours et modes de vie divers, ils sont restés à mes côtés, m'offrant une compagnie constante et me motivant à continuer de progresser. Il s'agit de Pan Wang, Teng Guo, Hao Li, Jiayao Li, Yawen Luo, Ziqing Wu, Chenhui Ye, Tianyuan Zhang, Yuzhe Hao, Kou Du, Dang Ning, Wang Tao, Mengxi Zhou, Ruotao Yang, Jia Shang, Fangyu Yang, Chunxiao Li, Hao Wang, Fuhua Yang, Kun Wang, Hasnae Joua, Rod, FTCY, Mengjia Zhu et Erbao. Sans votre soutien, mes recherches et mes écrits n'auraient pas été possibles.

Je tiens à exprimer mes sincères remerciements à Jasminka pour m'avoir offert un hébergement et m'avoir accompagné avec une grande attention. Chaque fois que je me sentais perdue ou submergée, elle m'écoutait patiemment et m'aidait à retrouver confiance. Ses précieux conseils sur divers sujets et choix de vie ont été d'une importance inestimable pour moi. Son regard positif sur la vie et sa détermination à trouver des solutions face aux défis ont été une grande source d'inspiration et de force pour moi. J'admire profondément sa nature sincère et généreuse, son appréciation de la beauté, sa gentillesse et sa générosité, son esprit curieux et son attitude inclusive envers les différentes cultures. Le temps que j'ai passé avec elle pendant ma thèse, que ce soit les week-ends, les vacances, les voyages ou Noël, est véritablement précieux.

Je tiens également à remercier Jean-Louis pour m'avoir aidé à déménager, pour m'avoir fourni un logement et créé un bon environnement d'écriture, ainsi que pour s'être soucié de ma santé. Il m'a accompagné tout au long du processus final d'écriture de cette thèse et m'a constamment encouragé à persévérer jusqu'au bout. Le temps passé à Nemours deviendra un trésor précieux et de bons souvenirs dans ma vie.

Merci à ma mère pour son soutien constant, sa confiance et son amour.

Nous remercions le soutien de la subvention de recherche du projet LUE-Biomolécule de l'Université de Lorraine.

Résumé

Introduction

Le chitosan (CS) est un matériau dérivé de la chitine naturellement abondante et présente dans les carapaces de crustacés et les parois cellulaires des champignons. Malgré son intérêt croissant tant du milieu universitaire que des industries, l'utilisation du chitosan reste relativement faible en raison d'un manque de sensibilisation et de connaissances sur ses propriétés et avantages dans les différents secteurs industriels. Les institutions de recherche, universitaires ou industrielles et les initiatives gouvernementales se concentrent sur le développement de méthodes d'extraction durables, l'optimisation des techniques de traitement et la sensibilisation aux avantages et aux applications du chitosan. Avec l'avancement des connaissances et de la technologie, on s'attend à ce que l'utilisation du chitosan augmente à l'avenir.

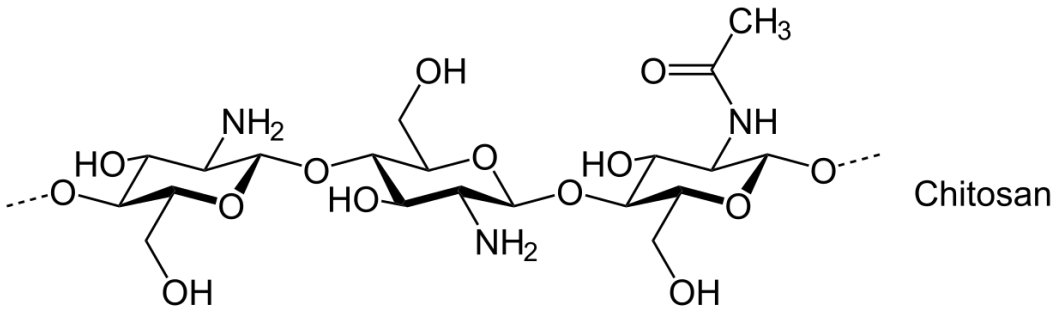


Figure R- 1 Structure chimique du chitosan

Les polyphénols sont un groupe de composés naturellement présents dans divers aliments d'origine végétale, notamment les fruits, les légumes, les céréales complètes, le thé, le café et certaines épices. Les polyphénols offrent de nombreux bienfaits pour la santé tels que l'activité antioxydant, les effets anti-inflammatoires, la protection cardiovasculaire et les propriétés anticancéreuses. La naringénine (NRG), la naringine (NR) et la catéchine (CAT) sont des polyphénols qui présentent un potentiel prometteur pour la santé humaine. Cependant, leurs applications pratiques sont souvent entravées par des questions liées à leur stabilité, à leur biodisponibilité et à leur formulation. Il est donc nécessaire de surmonter ces limitations afin de pleinement exploiter les propriétés bénéfiques de ces polyphénols. Des recherches en cours visent à surmonter ces obstacles en explorant des techniques telles que la nanoencapsulation à l'aide de particules de chitosan, qui peuvent améliorer la stabilité, la libération contrôlée et la délivrance ciblée de polyphénols et d'autres substances.

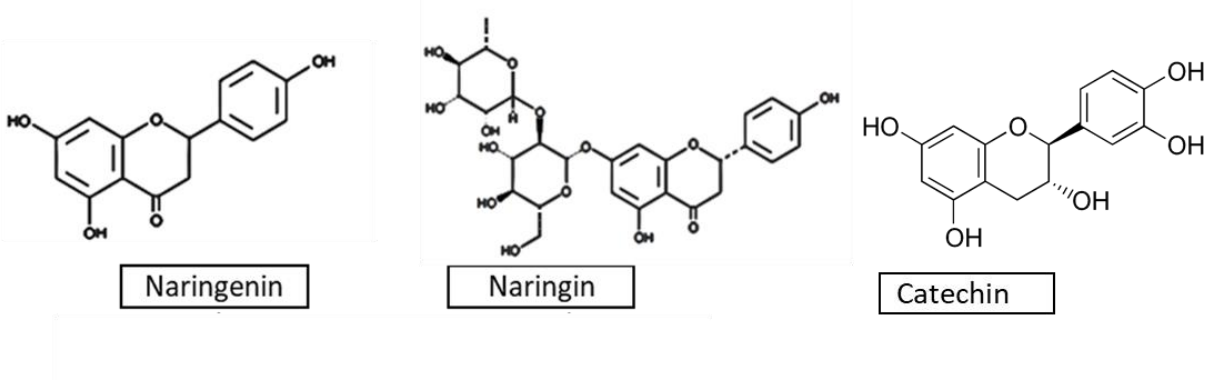


Figure R- 2 Structure chimique de la naringénine, de la naringine et de la catéchine.

Dans la littérature, l'utilisation de particules de chitosan dans l'encapsulation des polyphénols offre une approche polyvalente pour améliorer la stabilité, la libération contrôlée et la délivrance ciblée de diverses substances.

Les particules submicroniques sont couramment utilisées pour l'encapsulation et la libération contrôlée de molécules actives peu solubles dans l'eau. Les caractéristiques de surface de ces particules jouent un rôle crucial dans la détermination de certaines de leurs propriétés, telles que la stabilité colloïdale, la capacité de redispersion après séchage ou lyophilisation, les interactions avec les composants des milieux biologiques et la cinétique de libération des molécules actives. Pour contrôler les propriétés de surface des particules, l'adsorption physique de biopolymères tels que les protéines ou les polysaccharides est souvent utilisée. Ces biopolymères peuvent être utilisés directement ou après fonctionnalisation pour améliorer leurs propriétés d'adsorption. Plus récemment, l'utilisation de complexes de biopolymères, tels que des complexes polysaccharides-protéines, pour le revêtement de surface des particules a été envisagée. L'un des avantages de cette approche est qu'elle élimine la nécessité d'étapes préalables de modification ou de fonctionnalisation, permettant ainsi l'utilisation de biopolymères dans leur état natif. Le choix du biomatériau de revêtement permet également d'introduire des propriétés de surface spécifiques aux particules (par exemple la furtivité pour prévenir ainsi toute réaction immunitaire).

L'objectif de cette étude est d'améliorer la production de particules submicroniques composées de chitosan et revêtues de complexes biopolymères physiquement adsorbés. Les conditions de fabrication seront soigneusement ajustées pour contrôler la distribution de la taille des particules et les propriétés de surface, notamment la charge, l'épaisseur de la couche de surface, la nature et la conformation des macromolécules de surface. De plus, ces particules seront utilisées pour l'encapsulation d'une molécule phénolique hydrophobe.

L'objectif principal de cette étude est également d'examiner les mécanismes de libération et de contrôler le taux de libération de la molécule active en fonction des propriétés du revêtement de surface auto-assemblé et des paramètres physico-chimiques du milieu environnant, tels que le pH et la polarité. De plus, l'objectif est d'explorer et d'établir la corrélation entre la structure du matériau composite et le profil de libération des molécules encapsulées.

La technique de gélification ionique est largement utilisée pour créer des nanoparticules de chitosan (NPs de CS) grâce à l'interaction électrostatique entre le CS et les polyanions tels que le -tripolyphosphate (TPP). Cette méthode est largement appliquée pour la délivrance de médicaments. Notre attention se porte sur les nanoparticules à base de CS (NPs CS-TPP) formées à l'aide du TPP en tant qu'agent de réticulation. Ce choix est dû à son rentabilité et à l'encapsulation rapide qu'il offre, particulièrement adapté aux composés labiles car il n'implique pas de hautes températures, de solvants organiques ou de sonication. L'alginate (ALG), dérivé des algues brunes, est un polysaccharide naturel ayant des propriétés anioniques, ce qui le rend utile pour des applications pharmaceutiques telles que la délivrance de médicaments et l'encapsulation de cellules en raison de sa nature mucoadhésive. Lorsqu'il est combiné avec le chitosan (CS), qui possède des charges électriques opposées dans des environnements acides, une couche peut se former autour des nanoparticules CS-TPP grâce à des interactions électrostatiques. Cette enveloppe a été signalée pour introduire de nouvelles propriétés telles que la mucoadhésion, la protection des molécules et une modification du comportement de diffusion des particules. Dans cette étude, des particules de CS-TPP ainsi que des particules de CS-TPP revêtues d'ALG ont été préparées et caractérisées afin d'explorer leur potentiel en tant que transporteurs de polyphénols.

Méthode

L'approche expérimentale de cette étude a été divisée en trois parties principales :

Partie 1 : Mise au point du processus de préparation des particules de CS-TPP

Le processus de préparation des particules de CS-TPP a été optimisé en prenant en compte diverses variables, telles que la concentration desconstituants, la température de gélification, le rapport de masse des constituants et leur rapport volumique. Des recherches bibliographiques et des expériences préliminaires ont été menées pour déterminer les conditions optimales à l'égard de la distribution de tailles de particules. De plus, un revêtement de sel d'alginate a été appliqué au cœur de CS pour fonctionnaliser la surface des particules. Les particules de CS résultantes, à la fois revêtues et non revêtues, ont été caractérisées à l'aide de techniques telles que la diffusion de la lumière dynamique (DLS), la mesure de potentiel zêta, la microscopie électronique à balayage (MEB) et la granulométrie par diffraction laser pour analyser leurs propriétés telles que la distribution de taille, la charge de surface et la morphologie.

Partie 2 : Encapsulation des molécules cibles

La structure en gel réticulé formée lors du processus de gélification ionique constitue une excellente matrice pour encapsuler divers agents thérapeutiques ou composés actifs. Les particules peuvent contrôler la libération des substances encapsulées, permettant une libération soutenue et contrôlée dans le temps. Ce mécanisme de formation du cœur des particules a également l'avantage de ne pas faire intervenir de solvants autres que des milieux aqueux.

La naringénine, la naringine et la catéchine ont été choisies comme molécules cibles à encapsuler dans les particules de CS-TPP. Ces molécules ont été incorporées dans les particules de CS en les mélangeant avec une solution de CS lors du processus de préparation des particules. Ensuite, une méthode de séparation appropriée a été utilisée pour séparer les particules de CS des molécules

libres en excès dans le milieu continu (non encapsulées). La quantité de molécules libres a ensuite été quantifiée par spectrophotométrie UV, ce qui a permis de déterminer l'efficacité d'encapsulation (EE%) de l'opération.

Partie 3 : Étude des cinétiques de libération

Les cinétiques de libération des molécules polyphénoliques à partir des particules de CS ont été suivies dans différents milieux avec des variations de pH, de composition de solvant et de volume de dissolution. Cela a permis de comprendre de manière exhaustive le comportement de dissolution et la cinétique de libération des molécules chargées à partir des particules de CS.

Résultats

Effet des paramètres du procédé de préparation sur les caractéristiques des particules

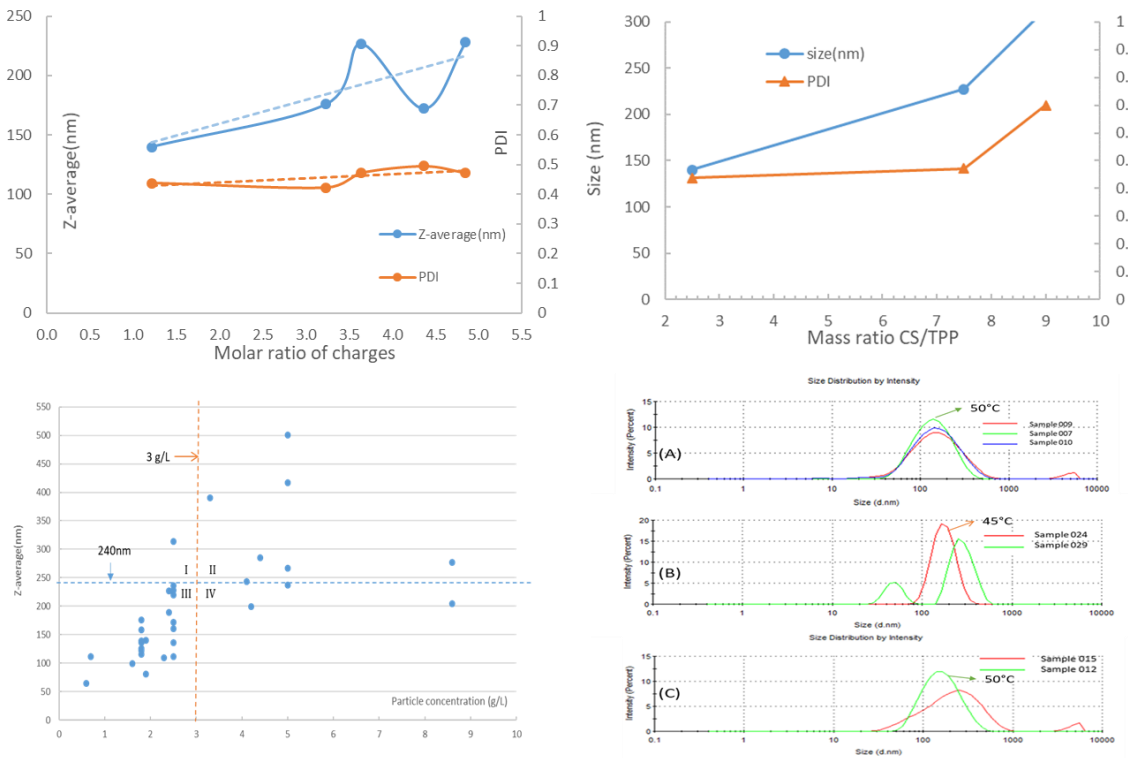


Figure R- 3 Résultats de l'effet des paramètres du processus sur la taille des particules

Selon les conditions de préparation, des particules de CS-TPP ont été préparées avec des tailles allant de 60 nm à 200 µm. Les particules ont été trouvées avoir une forme sphérique, comme confirmé par l'analyse microscopique. De plus, leur charge de surface a été déterminée comme positive à l'aide de mesures de potentiel zêta. Comme attendu, les particules de CS-TPP revêtues d'ALG avaient une charge de surface négative.

Les résultats de la DLS indiquent que lorsque le rapport de charges (${NH_3}^+/{P_3O_{10}}^{5-}$) et le rapport de masse CS/TPP augmentent, la taille moyenne des particules et l'indice de polydispersité (PDI) augmentent dans les conditions définies. À des températures de gélification plus élevées (45/50 °C),

les particules de CS présentent une meilleure homogénéité et une distribution de taille plus étroite, comme l'indique une diminution de l'IPD. La concentration des particules est définie comme la concentration du produit final dans l'environnement aqueux à la fin du processus de préparation des particules. Une observation intéressante est que lorsque la concentration des particules était inférieure à 3 g/L, la taille des particules avait tendance à être inférieure à 240 nm. Cependant, des analyses statistiques supplémentaires sont recommandées pour confirmer cette tendance.

Encapsulation

Les possibilités d'encapsulation de la NRG, la NR et la CAT ont été étudiées dans les particules de CS-TPP en mélangeant leurs solutions avec une solution de CS avant l'ajout de TPP pendant le processus de préparation des particules de CS-TPP. Un protocole permettant de déterminer l'EE% de ces molécules a été établi. La quantité de molécules non encapsulées et en excès dans le surnageant a été déterminée par spectrophotométrie UV-Vis, ce qui a permis de calculer indirectement l'EE% de la molécule à l'intérieur des particules de CS-TPP. Les résultats de notre étude indiquent que le système CS-TPP présente une forte affinité pour la naringénine (NRG), une affinité modérée pour la catéchine (CAT) et une faible affinité pour la naringine (NR). L'EE% de la NRG variait de 70 % à 90 %, en fonction des formulations de CS-TPP utilisées. L'EE% la plus élevée de la CAT était inférieure à 30 %. L'EE% de la NRG a été trouvé pour augmenter avec une plus grande quantité initiale de NRG dans la plage de 1,5 mg à 4,5 mg. D'autre part, la composition du solvant utilisé pour la CAT semblait avoir un impact sur l'EE% de la CAT. Ces résultats suggèrent que le système CS-TPP peut être particulièrement adapté à l'encapsulation et à la délivrance de la naringénine, tandis que d'autres stratégies doivent être explorées pour l'encapsulation efficace de la naringine et de la catéchine. L'encapsulation de la NRG à l'aide de particules de CS-TPP revêtues d'ALG a également été réalisée, mais l'EE% s'est avérée inférieure à celle des particules de CS-TPP. Ceci a été attribué à des pertes occasionnées par les étapes supplémentaires du procédé de préparation.

Test de libération

La faible solubilité de la NRG dans l'eau représente une difficulté pour la réalisation d'un test de libération tout en garantissant des conditions suffisamment loin de la saturation du milieu extérieur tout au long de la durée du test. La solubilité de la NRG dans l'eau a été estimée de manière fiable en dispersant les particules de CS-TPP chargées de NRG (4,4 mg) dans différents volumes d'eau (10,50, 100, 400, 800 mL) (Figure R-4). La solubilité de la NRG dans l'eau à 20°C a été déterminée à 21,6 ± 0,9 mg/L. Un volume de 800 mL a été choisi pour le test de dissolution afin de garantir que la diffusion de la NRG dans l'eau ne soit pas entravée par la saturation.

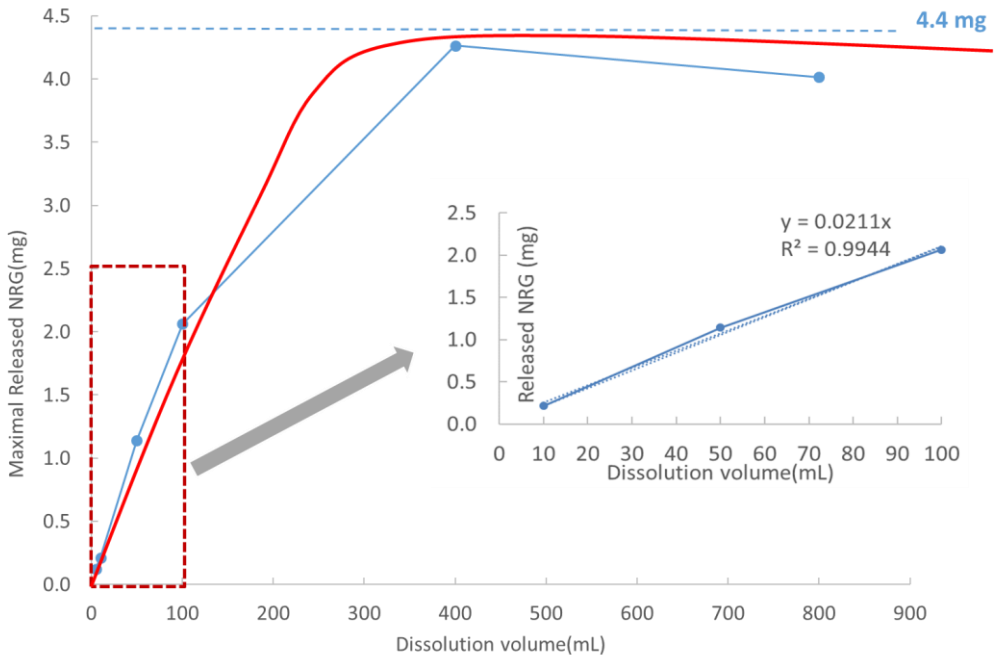


Figure R- 4 Libération de la NRG dans 10, 50, 100, 400, 800 ml d'eau à 20°C.

Les profils de libération de la NRG à partir des particules de CS-TPP, avec ou sans revêtement d'ALG, ont présenté des motifs similaires. La cinétique de libération a montré une phase initiale de libération rapide au cours des 10 premières minutes, avec plus de 70 % de la NRG libérée. Cela a été suivi d'une phase de libération soutenue, caractérisée par un taux de libération plus lent, ce qui a permis la libération progressive de la portion restante de NRG. Au fil du temps, la libération cumulative de la NRG à partir des particules de CS-TPP a atteint 100 % à la fin de la période de test de dissolution (Figure R-5).

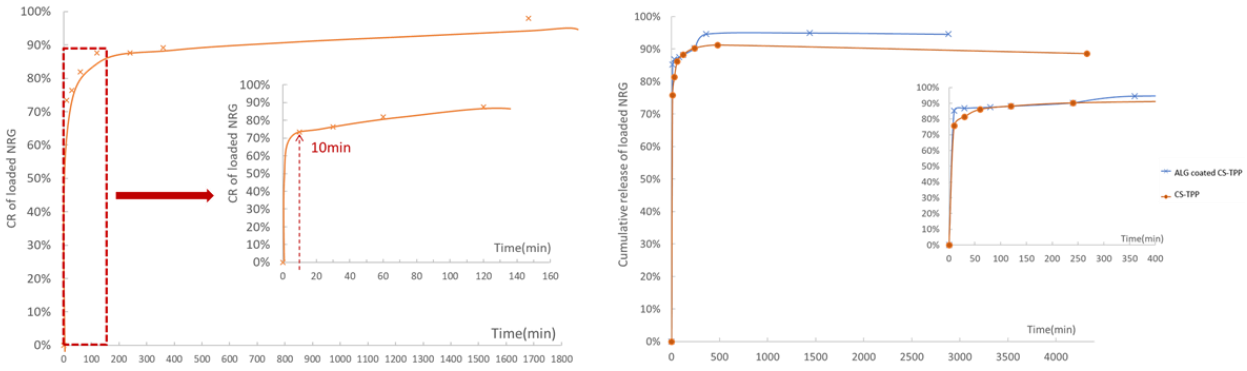


Figure R- 5 Libération cumulative de la NRG à partir des particules de CS-TPP et des particules de CS-TPP revêtues d'ALG dans 800 mL d'eau.

D'autre part, lorsque les particules de CS-TPP chargées de NRG ont été dispersées dans un milieu mixte éthanol (EtOH)-eau, il a été observé que l'ajout d'EtOH jusqu'à une concentration de 33 % n'altérait pas significativement le profil de libération de la NRG à partir des particules. Cependant, la présence d'EtOH dans le milieu pouvait augmenter le niveau global de libération de la NRG. Cela

pourrait être attribué à la solubilité améliorée de la NRG dans le milieu mixte EtOH-eau, en particulier lorsque la libération de la NRG était limitée par sa saturation dans le milieu de dissolution.

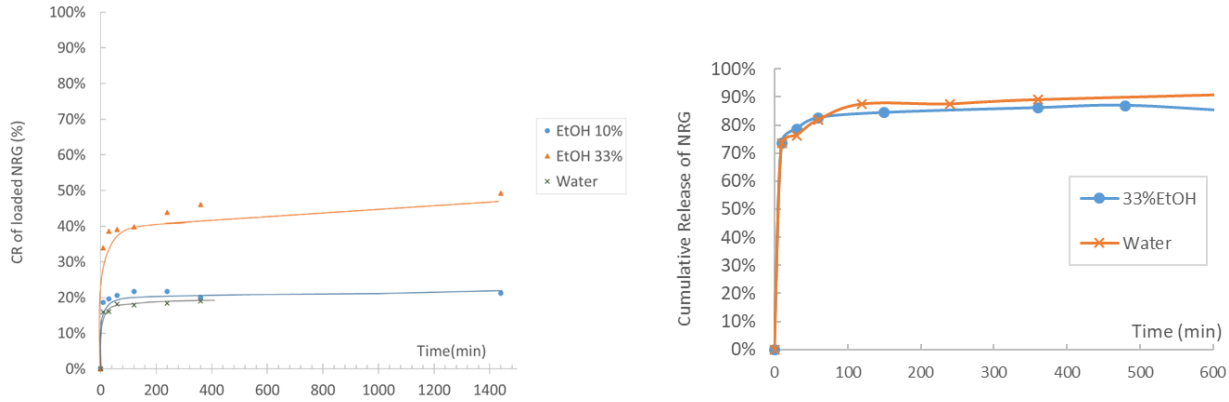


Figure R- 6 Libération de la NRG dans l'eau et les milieux EtOH-eau dans 10 ml (gauche) et dans 800 ml (droite).

Conclusions et perspectives

Le développement, l'optimisation, la caractérisation et l'évaluation des particules de chitosan-tripolyphosphate (CS-TPP) ont été réalisés avec succès dans cette étude. Le processus d'optimisation a impliqué l'étude de différentes variables de processus, notamment la concentration de chitosan (CS), le volume des solutions de CS et de TPP, le rapport de masse CS/TPP et la température. En étudiant systématiquement l'impact de ces variables, il a été possible d'identifier les paramètres clés pour la formulation et la préparation de particules de CS-TPP destinées aux systèmes de délivrance de médicaments. Les résultats de cette optimisation fournissent des informations précieuses et des orientations pour les futures stratégies de formulation et de préparation dans le domaine de la délivrance de médicaments.

Deuxièmement, l'encapsulation de trois molécules polyphénoliques, à savoir la naringénine (NRG), la naringine (NR) et la catéchine (CAT), dans des particules de CS a été réalisée. L'efficacité d'encapsulation (EE%) des molécules actives a été caractérisée à l'aide de la spectrométrie UV-Vis pour évaluer l'affinité entre les particules de CS et les polyphénols. Les résultats ont indiqué que les particules de CS étaient capables d'encapsuler efficacement la NRG et la CAT, comme en témoignent les valeurs élevées d'EE%. Cependant, l'encapsulation de la NR semblait beaucoup moins favorable, probablement en raison des propriétés spécifiques de cette molécule ou de son interaction avec les particules de CS. Les variables susceptibles d'influencer l'EE% ont été étudiées.

L'étude révèle que les particules de CS-TPP présentent des avantages en tant que système d'encapsulation pour la libération contrôlée de la naringénine. L'encapsulation et la libération réussies de la naringénine démontrent le potentiel des particules de CS-TPP dans les applications de délivrance de médicaments. Des recherches supplémentaires sont nécessaires pour explorer pleinement les capacités des particules de CS-TPP pour encapsuler différentes molécules bioactives. De plus, des recherches sur l'affinité entre la naringénine et les membranes à base de cellulose pourraient fournir des informations sur leur compatibilité en tant que stratégie d'encapsulation. Les

matériaux à base de cellulose offrent une biocompatibilité, une biodégradabilité et une libération contrôlée des médicaments, ce qui en fait une voie précieuse pour des systèmes de délivrance de médicaments efficaces(Sun et al., 2019). Explorer le potentiel des dérivés de cellulose ou de la cellulose modifiée pour encapsuler et délivrer de la naringénine pourrait ouvrir de nouvelles opportunités dans ce domaine.

Références

1. Weng, J.; Durand, A.; Desobry, S. Chitosan-Based Particulate Carriers: Structure, Production and Corresponding Controlled Release. *Pharmaceutics* **2023**, *15*, 1455, doi:10.3390/pharmaceutics15051455.

2. Sun, B.; Zhang, M.; Shen, J.; He, Z.; Fatehi, P.; Ni, Y. Applications of Cellulose-Based Materials in Sustained Drug Delivery Systems. *Current Medicinal Chemistry* **2019**, *26*, 2485–2501.

General introduction

Lorraine Université d'Excellence (LUE) is an initiative of Université de Lorraine which was selected for funding in 2016 as an I-SITE initiative in the framework of PIA2 French national program. Since its launch in 2016, LUE initiated various calls for proposals among which IMPACT projects which were aimed at promoting interdisciplinary research as well as transfer to industry.

This PhD thesis took place in the framework of one of these IMPACT projects called "Biomolecules".

The LUE IMPACT Biomolecules project aimed to cover all stages of biomolecule development, from production to testing and application. It involved 17 laboratories (Calbinotox, CITHEFOR, CRAN, DCAC, DynAMic, IAM, IMoPA, L2CM, LAE, LCOMS, LCPM, LERMaB, LIBio, LORIA, LRGP, SIMPA, URAFPA) and 17 industry partners in the Lorraine region, totaling 120 researchers. Its main outcomes focused on identifying novel compounds with anti-proliferative, antioxidant, and anti-inflammatory activities. The project's goal is to create a "Biomolecules – Bioengineering – Bioeconomy Network" (3B Network) that produces new, functionalized, and targeted biomolecules for various industries, including agro-chemistry, biocontrol, agro-food, cosmetics, pharmaceuticals, and medicine.

The project primarily focuses on biomolecules with anti-inflammatory, anti-proliferative, and antioxidant properties, chosen due to the private partners' interests in these markets and the expertise of the consortium's laboratories in these areas. The project's scientific challenges involve studying interactions between living organisms, designing biomolecules inspired by nature, controlling their activity through functionalization or vectorization, and validating their biological efficacy for integration into industrial and pharmaceutical products.

A key strength of the project lies in the complementary expertise of the participating laboratories and companies, allowing them to cover all stages of biomolecule development, from initial discovery to validating their mechanisms of action, ultimately leading to commercialization.

Within the framework of the "Functionalization and Vectorization of Biomolecules" work package in the LUE IMPACT Biomolecules project, which aims to enhance the bioavailability and stability of biomolecules through their encapsulation in an external matrix, this doctoral fellowship was funded by the LUE IMPACT Biomolecules project. It was conducted in collaboration between LIBio and LCPM, under the guidance of Professor Stéphane Desobry (LIBio) and Professor Alain Durand (LCPM).

The LIBio laboratory, located within the Ecole Nationale Supérieure d'Agronomie et des Industries Alimentaires (ENSAIA) at the Université de Lorraine, is dedicated to the creation of carriers and frameworks derived from agricultural resources. Their goal is to modulate the reactivity of these materials, allowing precise control over the transport and release of active compounds, tailored to match the physicochemical conditions of their surroundings. The Laboratory of Physical Chemistry of Macromolecules (LCPM) is a joint research unit affiliated with both CNRS (The French National Centre for Scientific Research) and the Université de Lorraine as UMR 7375. The LCPM conducts research with a transdisciplinary scientific approach, focusing on the design, synthesis, and characterization of molecules and macromolecules with original structures and architectures. This

approach leads to functional and self-organizing properties that have practical applications in three main domains: healthcare, specialized materials, and processes.

Chitosan (CS) is a naturally derived material from chitin found in crustacean shells and fungal cell walls. Despite its abundance, its usage remains limited due to a lack of awareness. Research efforts aim to improve this situation. Polyphenols, found in various plant-based foods, offer numerous health benefits. However, their use is hindered by challenges related to stability and bioavailability. Current research explores techniques like chitosan-based nanoencapsulation to address these issues. Submicron particles are commonly used for encapsulating poorly soluble substances. The choice of coating biomaterial allows for introducing stealth properties to the particles, thus preventing immune reactions.

The study aims to enhance the production of submicron particles composed of chitosan and coated with physically adsorbed biopolymer complexes. It also seeks to understand the release mechanisms of encapsulated molecules based on coating properties and environmental conditions. The experimental approach comprises three main parts: optimization of the CS based particle preparation process, encapsulation of target molecules, and release testing.

In Chapter 1, an extensive literature review was conducted to assess the current status of chitosan, a versatile biopolymer. The review covered its sources, distinctive properties (such as electropositivity, biocompatibility, and antibacterial activity), and various applications. Additionally, a concise overview of chitosan-based network and particulate structures was provided. The production of chitosan particles was explored through numerous methods, with ionic gelation standing out due to its operational simplicity, gentle processing conditions, environmental friendliness, and versatility in generating diverse particles.

Ionotropic gelation (IG), a well-explored method, was highlighted for its ability to create nano- to micro-scaled particles via electrostatic interactions between two ionic species. The non-toxic crosslinking of chitosan with tripolyphosphate (TPP) was identified as a method for obtaining chitosan particles. The chapter also briefly introduced characterization methods for the acquired particles. Naringenin, naringin, and catechin, three polyphenols with significant health potential, including antioxidant, anti-inflammatory, anti-diabetic, and anti-tumor activities, were discussed. Examples from the literature showcasing the delivery of polyphenols through CS-TPP systems were summarized.

Chapter 2 provides a comprehensive overview of the scientific approach undertaken in this research. It outlines the research context, objectives, scientific inquiries to be addressed, and the experimental design. In Chapter 3, the focus is primarily on detailing the methods employed, covering five key aspects: the characterization of materials, the preparation and characterization of CS based particles, the encapsulation of polyphenols, and the analysis of the release kinetics of loaded molecules.

Moving on to Chapter 4, it encompasses the analysis of results, observations, and discussions. Notably, CS-TPP particles of varying sizes were successfully prepared and characterized. The impact of process parameters, particularly size, was explored, with investigations into the effects of

crosslinking temperature, the mass ratio of CS/TPP, the ratio of charges ($NH_3{}^+/P_3O_{10}{}^{5-}$), and particle concentration on CS-TPP particle size. The addition of an alginate coating was found to enlarge particle size and shift the particle surface charge from positive to negative. Results indicated the successful encapsulation of naringenin within the chitosan-based system, unveiling a two-phase release pattern under specific release conditions.

Lastly, Chapter 5 provides a summarization of conclusions drawn from preceding chapters and suggests potential avenues for future research.

1 State of the art[1]

1.1 Biopolymer with unique positive charge: chitosan

Chitosan (CS), derived from chitin through deacetylation, is a natural polymer with enormous potential applications in biotechnology and food engineering. Chitin is a long-chain polymer of N-acetyl glucosamine and the second most abundant natural biopolymer after cellulose on the planet (Martínez et al., 2014; Shit and Shah, 2014; Tharanathan and Kittur, 2003; Zeng et al., 2012). The estimated annual biosynthesis of chitin is roughly 10^{10} tons in the biosphere biosphere(Gooday, 1990; Latańska et al., 2021). It is a sustainable natural resource that is omnipresent but still underexploited commercially. Chitin and cellulose belong to the same class of biopolymers, i.e., polysaccharides. The two other main classes of biopolymers include proteins and nucleic acids.

Chitosan is a linear polysaccharide composed of amino groups, with its structure containing D-glucosamine (deacetylated units) and N-acetyl-D-glucosamine (acetylated units) linked randomly through β-(1→4) bonds(Latańska et al., 2021)(Figure 1-1). Due to its repeatedly reported beneficial characteristics, such as absence of toxicity, biocompatibility, biodegradability, chitosan has found considerable applications in various fields, including environmental engineering, agriculture, aquaculture, agrochemistry, food industry, medical/pharmaceutical and cosmetic industries(Aranaz et al., 2017; Kim, 2010; Martínez et al., 2014; Zhou et al., 2021).

[1] Content modified from our published review, (Weng, Durand, and Desobry 2023)

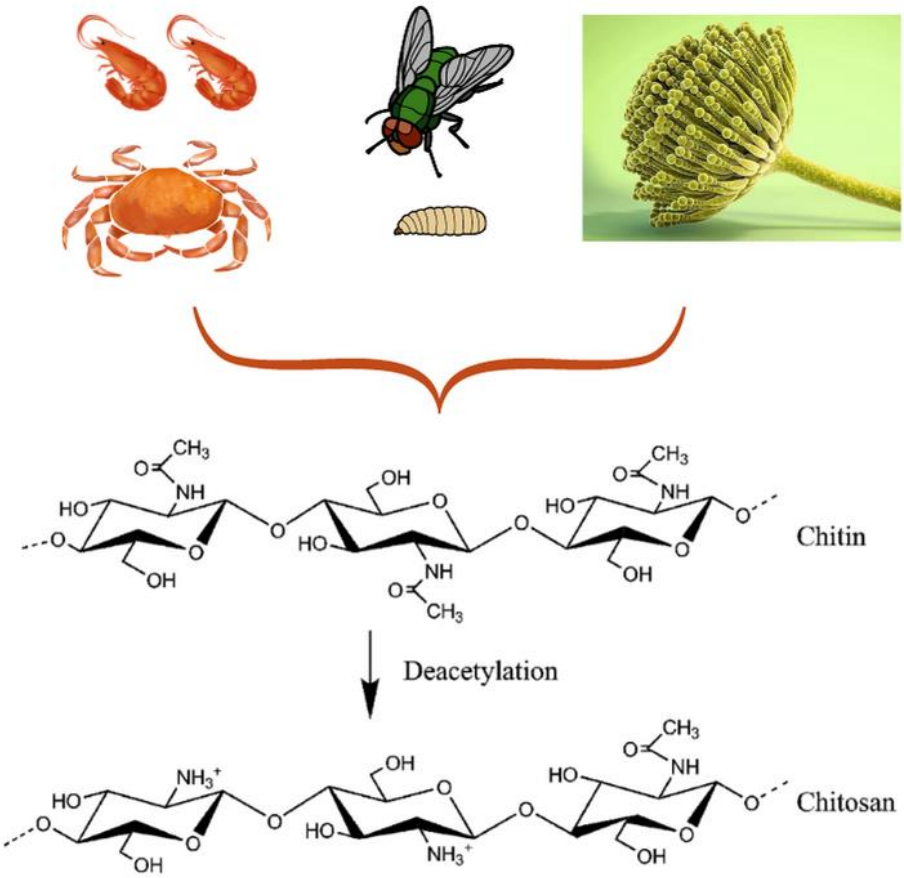


Figure 1-1 Chemical structure of chitin and chitosan and their sources including crustaceans, insects and fungi

Chitin can be found in alga, fungi, arthropods (crab, shrimp, crayfish and insect), plankton and mollusks (squids). Chitosan can be produced from various sources, including shell of crustaceans, insects and cell walls of fungi (Figure 1-1)(El Knidri et al., 2018; Huq et al., 2022; Khayrova et al., 2021; Lee et al., 2022). Nowadays, the main commercial source of chitin and its derives is shells and the exoskeleton of crustaceans, which have been considered as low-value marine wastes for a longtime. Global annual production of shrimp and lobster shells and crab waste was reported between 6 to 8 million tons (Food and agriculture organization of united nations, 2014). According to Food and Agriculture Organization of the United Nations (FAO), on a worldwide basis, production of crustaceans reached to 10 481 319 tons with a value of 76 307 935 000 USD by 2019(FAO, 2019). The chitin content of crustacean shell waste was reported ranged from 15% to 40% (Abdel-Rahman et al., 2015; Mohan et al., 2021; Yan and Chen, 2015).Powder of this grounded marine byproduct can serve as animal-feed supplement but the profitability is very limited compared with its refined high-value chemicals such as chitosan, glucosamine and their derivatives.

Table 1-1 Global annual production and price of chitin, chitosan and Dried shrimp shells.

Product	Industrial production (10^6 Tons per Year)	Price (USD per Ton)
Dried shrimp shells	6 - 8	100 - 120
Chitin	0.02 – 0.04[a]	6 000 - 40 000
Chitosan	<0.1[b]	15 000 - 160 000[c]

[a] Annual production of chitin is probably under 10,000 tons whereas, reliable figures are not available (EUCHIS).
[b] Global industrial production of chitosan is estimated to reach 173.9 thousand tons by 2027(SFly, 2019).
[c] Data from Alibaba (March 2023) (Alibaba, 2023)

Transformation of chitin from marine waste is not complex but it is a process who needs considerable amounts of water and chemical components like strong acids and bases. Preparation of chitin and chitosan from crustacean marine waste involves several steps (Figure 1-2). First, the waste material is collected and washed to remove any debris or impurities. Then, it is subjected to a series of chemical treatments to remove proteins, lipids, and other non-chitin materials. This process typically involves treating the waste with strong acids or bases, followed by several rounds

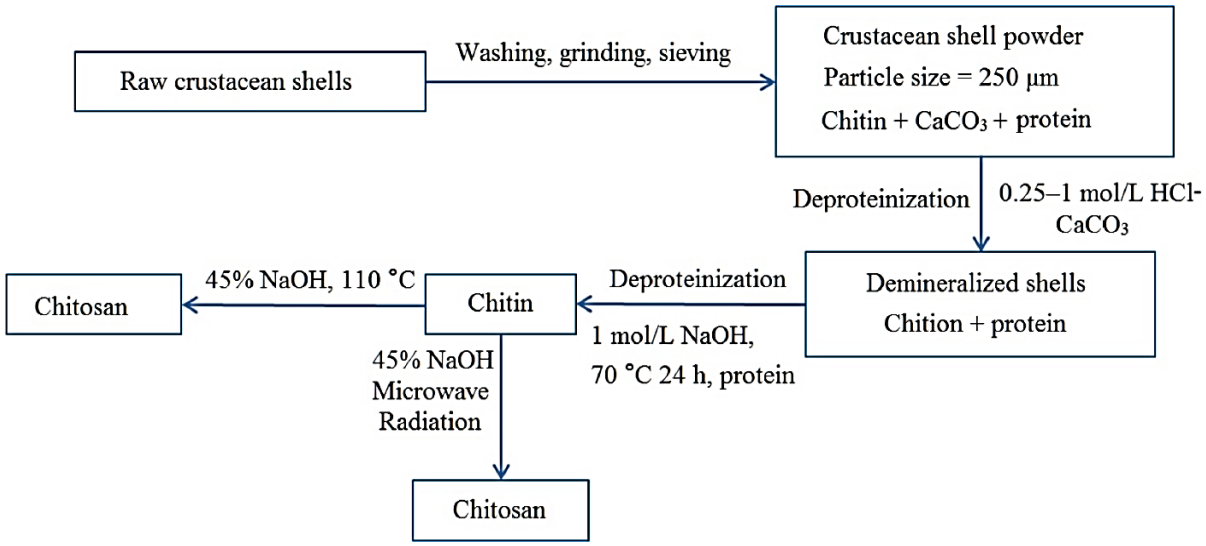


Figure 1-2 Preparation of chitin and chitosan from crustacean marine waste(Sagheer et al., 2009; Huq et al., 2022)

of washing and drying. Once the chitin has been isolated from the waste material, it can be converted to chitosan through a process called deacetylation. This involves treating the chitin with an alkaline solution, which removes the acetyl groups from the polymer chain and converts it to chitosan. The resulting chitosan can then be further processed and purified for use in various applications.

Chitosan from marine waste has several advantages, such as its abundant availability, low cost, and the ability to reduce waste and pollution. However, the production process can be complex, and the purity and quality of the chitosan can vary depending on the source and processing methods (Huq et al., 2022).

The KITOGREEN project is funded by the European Union through the HORIZON 2020 program. Its objective is to investigate alternative methods for the production of chitosan, which is typically extracted from shellfish, by exploring the use of a fungal-derived biopolymer. This innovative technology generates chitosan from vegetal sources, making it a sustainable and eco-friendly option. The use of vegetal sourced chitosan offers multiple benefits, including reduced dependence on fertilizers, improved health implications, lowered CO_2 emissions, elimination of allergens, increased sustainability in agriculture, and expanded applications in other sectors such as healthcare and beverages (CORDIS, 2019).

Chitin can be easily extracted from the cell wall of filamentous fungi, which is a good source of chitin. The amount of waste produced during mushroom cultivation, which can range from 5% to 20% of the production volume. Chitosan derived from fungi can be produced year-round without any seasonal variation. Additionally, it is free from heavy metals and allergenic proteins found in animal sources, making it a favorable option for various applications such as in the food, cosmetic, pharmaceutical, and medical industries. Furthermore, the utilization of chitosan derived from fungi may provide a substitute to conventional chitosan sources for individuals who opt to refrain from animal-derived products due to ethical, religious, or other motives. Nevertheless, commercial-scale production of fungal-based chitosan products is still limited due to the low availability of raw materials and the high cost of production(Ghormade et al., 2017; Huq et al., 2022).

Insects can also serve as a source of chitosan. Chitosan obtained from insects shares similar properties and characteristics with chitosan obtained from other sources(Hahn et al., 2020; Lee et al., 2022). Using chitosan sourced from insects offers the potential benefit of sustainable sourcing, as insects are abundant in nature and can provide a renewable and non-regionally limited source of chitosan. A European startup called SFLY has recently developed a pioneering technology for producing chitin/chitosan from cultured Black Soldier Fly (Hermetia Illucens) insects (SFly, 2019). Their innovative biochemical extraction process aligns with environmentally friendly principles by reducing water consumption, chemical reagents, and energy usage.

Chitosan can also be obtained from other sources, including vegetal or plant-based sources. Vegetal sourced chitosan refers to chitosan that is obtained from plant-based materials, such as fungi, mushrooms, and other non-animal sources. These sources may include cell walls of fungi, mycelium, and other chitin-containing plant tissues.

Vegetal sourced chitosan has similar properties and characteristics to chitosan derived from animal sources, such as high biocompatibility, biodegradability, and antimicrobial properties. It can be used in a variety of applications, including biomedical, pharmaceutical, agricultural, and environmental applications, just like animal-derived chitosan. It's important to note that the properties and characteristics of vegetal sourced chitosan may vary depending on the specific plant source, extraction method, and processing conditions used. Therefore, it is necessary to carefully evaluate the quality and properties of vegetal sourced chitosan through appropriate characterization and testing methods to ensure its suitability for a particular application.

Industrial production of refined chitin/chitosan and its derivatives) remained low by 2016. It reported that less than half of global demand was satisfied ((EUCHIS, 2016.), (SFly, 2019)). Both demand and production for chitosan keep growing in various industries worldwide for these years. The global market volume of chitin and its derivatives was valued nearly 7.1 billion US dollars by 2021 (Facts & Factors, 2022). The global market for Chitin and Chitosan Derivatives was estimated at

7.9 billion US dollars in the year 2022, is projected to reach a revised size of 24.9 billion US dollars by 2030(Reportlinker, 2023).

A multiple-application biopolymer

Chitosan's multiple utilities originate from its relatively rare physical properties; it is the unique cationic polyelectrolyte among known natural biopolymers, we can fabricate composites though electrostatic combination between chitosan and other negatively charged substances; it is a pH sensitive material, because its dissolution and degradation under mild acidic condition; also from its beneficial biological properties, such as non-toxicity, biodegradability, biocompatibility, mucoadhesive property, antimicrobial activities; it is apt to bind with electronegative mucous membranes and it shows low toxicity in vitro and some in vivo models (Munawar et al., 2017). The fact that chitosan chains only dissolve in acidic solution (pH < 6.5) is sometimes considered as a flaw, but substitution or addiction at/onto amine groups of chitosan chains can tackle this solubility problem or even enhance chitosan's antimicrobial property. In a word, its abundant reserves in nature, benign properties and versatile applications rationalize the ongoing research enthusiasm from both academia and industry on chitin/chitosan and its derivatives. Figure 1-3 summarizes chitosan application in variable industries. There would be a predictably continuous increase in chitosan market in following decades.

Emerging Research and Industrial Interest for Chitosan

The first interest in commercializing chitin was held back in the 1930s because of the strong competition with synthesized polymers at that time. Large-scale production of chi-tin regained attention in the mid-1970s, when regulations aiming to reduce the dumping of shellfish waste were introduced. Regarding research interest, 108,025 references concerning "chitin/chitosan" were found using SciFinder (years between 1970 and 2022). A remarkable increase in the number of publications was evidenced at the beginning of the 1990s, indicating a real emerging research interest in the academic world (Figure 1-4). On the other hand, according to statistics from WIPO's database, PATENTSCOPE, the potential commercial applications of CS have grown steadily since the late twentieth century, whereas the number of patent applications concerning CS has exploded in

the last three decades. A total of 51,274 patent application records in English were found from all offices, based on the search on March 1st, 2023 (Figure 1-5).



Figure 1-3 Schematic overview of the versatility of chitosan applications in various

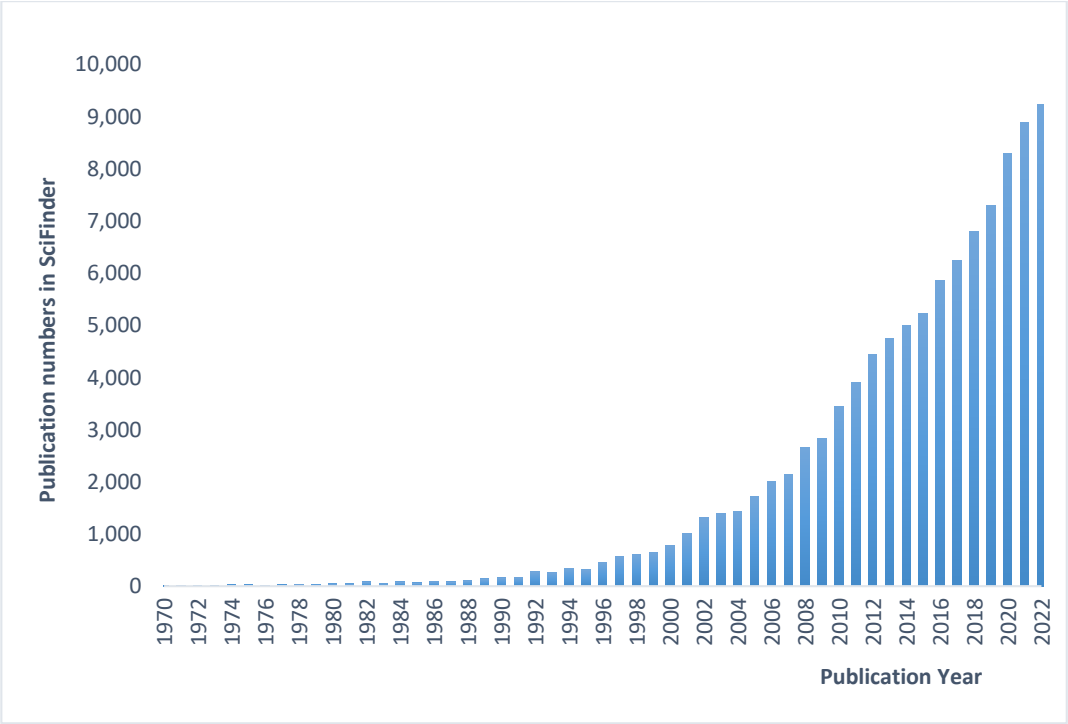


Figure 1-4 Number of publications containing the keywords "chitin" or "chitosan" registered each year in SciFinder. Books, conferences, editorials, journal articles, preprints and reviews included. (Data from SciFinder, March 2023).

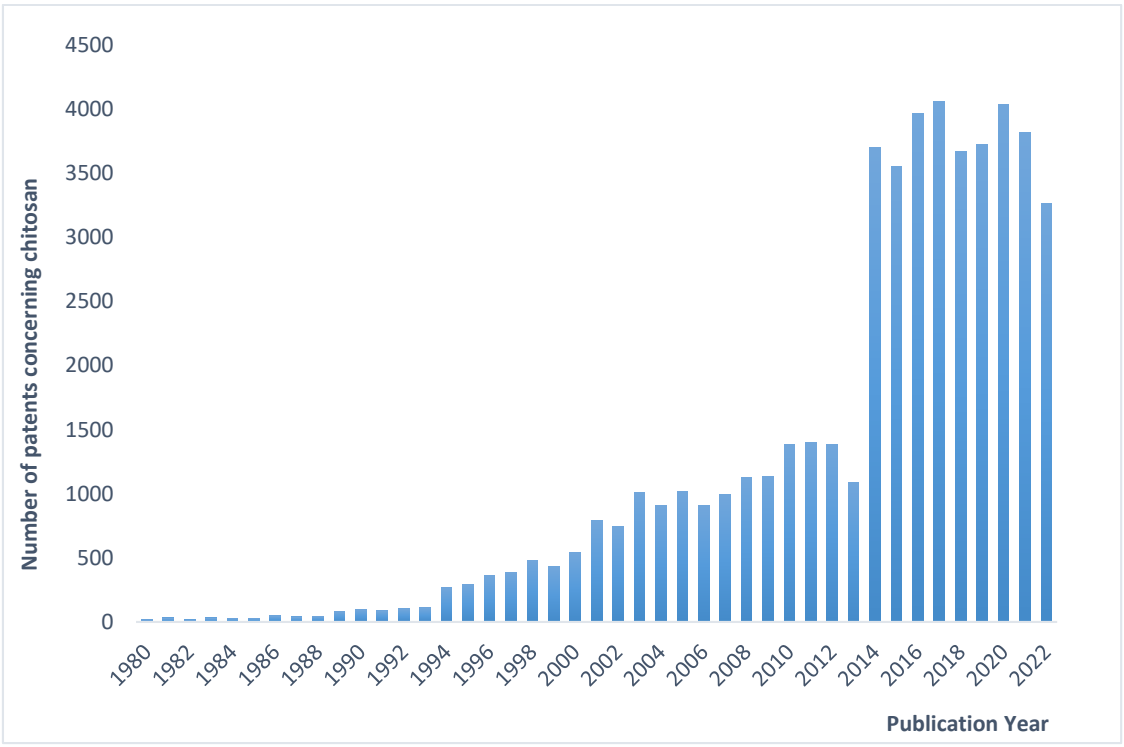


Figure 1-5 Number of patents relevant to the keywords "chitin" or "chitosan" in English published each year. (Data from WIPO, https://patentscope.wipo.int/search/en/result.jsf/(accessed on 1 March 2023)).

1.1.1 Molecular weight (Mw) of chitosan

Mw of chitosan is considered as an important physical property as it was reported having influence on solubility of polymer and on viscosity of polymer solution. CS above 30 kDa usually require acid (except for phosphoric acid) to facilitate its dissolution in water (Herdiana et al., 2022). Chitosan with molecular weight <50 kDa is usually considered as low molecular weight chitosan (Lee et al., 2001; Zielinska et al., 2014). Low-molecular-weight chitosan has been found to exhibit different properties and behaviors compared to high-molecular-weight chitosan, such as improved solubility, higher bioavailability, and increased antimicrobial activity(Herdiana et al., 2022; Lee et al., 2001; Li et al., 2005). Lower molecular weight chitosan has been shown to produce nanoparticles with smaller dimensions, which can lead to altered drug release kinetiCS, pharmacodynamiCS, and more efficient drug delivery (Seidi et al., 2021). Furthermore, chitosan with lower molecular weight was reported associated with lower cellular toxicity (Caprifico et al., 2020).

Determination Mw of chitosan by SEC-MALS

As most biopolymers, chitosan's properties, such as physiochemical and biological functionalities, are highly dependent on its molecular weight, degree of deacetylation and crystallinity(Hwang et al., 2002). Molecular weight of chitosan and its purified product were characterized by size-exclusion chromatography (SEC) coupled to a multiple-angle laser light-scattering (MALS) photometer.

SEC-MALS (Size Exclusion Chromatography with Multi-Angle Light Scattering) is a powerful analytical technique used to characterize the size and molecular weight of macromolecules, such as proteins, polymers, and nanoparticles, in solution(Beri et al., 1993).

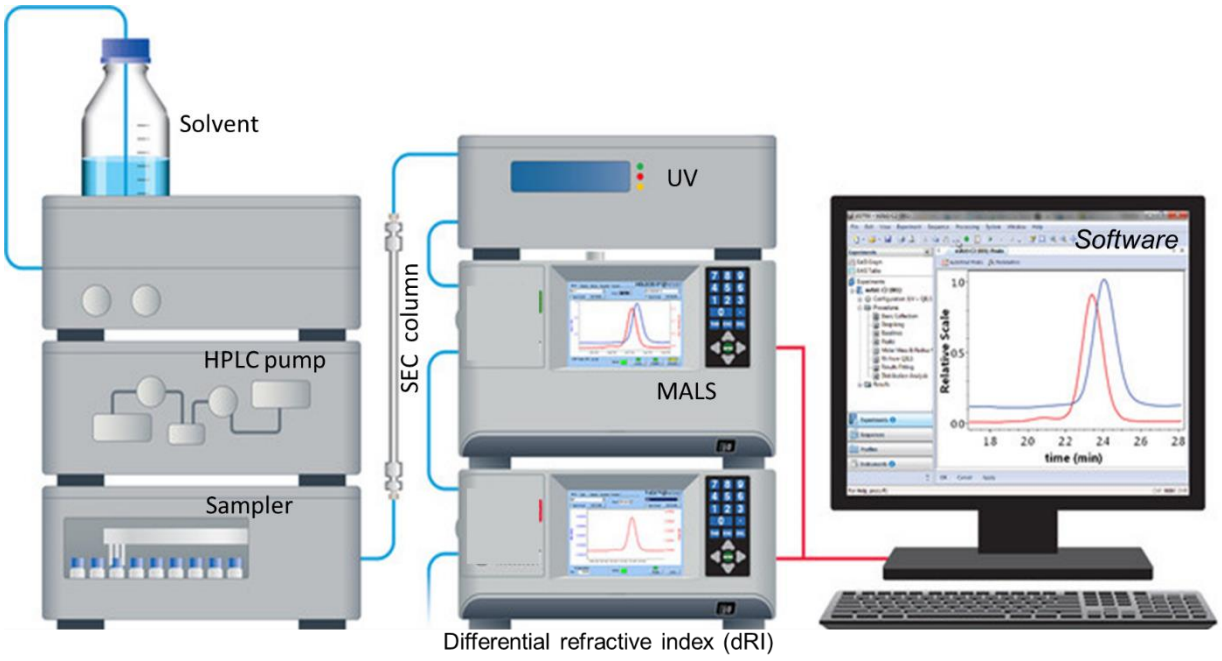


Figure 1-6 Schematic representation of the SEC-MALS system, (Adapted from Some, 2018).

SEC-MALS combines size exclusion chromatography (SEC), which separates molecules based on their size, with multi-angle light scattering (MALS), which measures the scattering of light at different angles. This allows for accurate determination of the absolute molecular weight and size of macromolecules without relying on calibration standards, as in other techniques like conventional SEC. In a typical SEC-MALS experiment, the sample is injected into a SEC column, where the molecules are separated based on their size. As the molecules elute from the column, they pass through a MALS detector that measures the intensity of scattered light at different angles. The

scattered light is then used to calculate the molecular weight, size, and other parameters of the macromolecules in solution. Firstly, molecules dissolved in flow phase pass through the SEC part and are separated by size with the largest eluting first and the smallest last. The signals corresponding to sample were collected by detectors and then analyzed by a software on computer (Figure 1-6).

To describe the distribution of molecular weights of a population of molecules, several definitions could be used. Two common ways to describe the distribution of molecular weight numerically are present below via equations (*eq.*1.1 - *eq.*1.3). In SEC-MALS, Mw/Mn is a ratio of weight-average molecular weight (M_w) to number-average molecular weight (M_n) of a polymer sample. M_w/M_n is a measure of polydispersity, which refers to the distribution of molecular weights in a polymer sample. The narrower the distribution, the smaller the molecular weight range, and the lower the polydispersity.

Weight-average molecular weight (M_w):

$$\overline{Mw} = \frac{\sum M_i C_i}{\sum C_i} \qquad (eq.1.1)$$

where M_i is the molecular weight at the i^{th} data point, and C_i is the concentration (or weight-fraction) at the i^{th} data point.

Number-average molecular weight (M_n)

$$\overline{Mn} = \frac{\sum C_i}{\frac{\sum C_i}{M_i}} \qquad (eq.1.2)$$

Polydispersity(PDI)

$$PDI = \frac{M_w}{M_n} \qquad (eq.1.3)$$

M_i and C_i, can be calculated with the help of light scattering detection provided by the MALS system. Additionally, the light scattering part can also measure intrinsic viscosity and molecular size of the sample.

1.1.2 Determination of deacetylation (DAA, %) of chitosan by ^{1}H NMR

The degree of deacetylation is termed as the molar fraction of N-deacetylated content counting in entire polymer chain of chitosan. The DDA% value decides the quality and essential properties of chitosan such as solubility, viscosity, electrostatic properties and diverse biological activities(Chatelet, 2001; Kasaai, 2009). The effectiveness and behaviors of chitosan were reported repeatedly to be related to DDA% of chitosan in many applications(Sreekumar et al., 2018; Zhang et al., 2011). The degree of deacetylation of chitosan and its derivatives is an important characterization parameter since the charge density of the chitosan molecule is responsible for potential biological and functional effects. Knowledge of the degree of deacetylation is important for an understanding of the functionality of chitosan salts in various applications. (ASTM, 2018). For instance, a reversible cross-linking of chitosan with negatively charged reagent like tripolyphosphate (TPP) at proper condition. The ability of reaction of chitosan in this process is basically from its

positively charged amino groups. Therefore, DDA% of chitosan was found to be one of the most important parameters that influenced on the ability of chitosan to form particles(Sreekumar et al., 2018). Obviously, DDA% as information will assist researchers or/and engineers in choosing the correct chitosan for their particular application.

Up to now, various methods for determination of the degree of N-acetylation of chitin and chitosan have been developed and reported including IR, ^{1}H NMR, ^{13}C NMR, ^{15}N NMR, and UV spectroscopy, titration and enzymatic hydrolysis coupled with calorimetry or chromatography. Applicable range, sensitivity, rapidness, cost, availability of instruments and other factors distinguish those methods (Kasaai, 2009).

1.2 CS-TPP particulate systems

The development of functional polymer nanocarriers is a significant achievement in modern technologies, including medicine, biotechnology, chemistry and photoelectronics. They serve as versatile systems adaptable to various applications, such as drug, nutrients, pesticides and fragrance delivery, navigable (photo)reaction chambers, smart coatings and solar energy storage devices. Although many systems have already been intensely investigated, there is still a considerable area remaining for the development of better, tailor-made materials.

Nanoparticulate systems offer many advantages in drug delivery, by, e.g., improving bioavailability, extending the therapeutic effect of the drug at the target site, and by improving the stability of the drug against chemical and enzymatic degradation like e.g. under gastrointestinal tract conditions. Essential physicochemical properties of nanoparticles include size (distribution), shape, compactness, and surface charge. These properties have been linked to many important drug delivery aspects, such as drug release profiles, bioavailability, biodistribution, and mucoadhesion.

Chitosan is also approved by GRAS (Generally Recognized as Safe by the United States Food and Drug Administration [US FDA]). Crustacean-derived chitosan has a long history of safe use in the food supply. It is currently approved/permitted for use as a natural food additive for general food use in Japan and Korea (JFCRF, 2014; MFDS, 2017) and has broad use as a drug excipient, functional food ingredient, and dietary supplement product in many countries like e.g. the USA., the European Union. Supplement products containing chitosan typically promote weight control and/or maintenance of cardiovascular health (NIH, 2020). On the other hand, fungal-derived chitosan for use as a secondary direct food ingredient in alcoholic beverage production (Chinova, 2021). Chitosan is a biopolymer that combines electrostatic stabilization due to its positive charge and steric stabilization Due to the protonation of amino groups in acidic conditions, its hydrophilic character permits high solubility. The existence of a positive surface charge and the potential of modifying the molecule using electrostatically charged chemicals vitalize the usage of chitosan (Herdiana et al., 2022; Szafraniec-Szczęsny et al., 2020).

Nanoparticulate systems can potentially be used for enhanced drug dissolution and bioavailability, enhanced cellular uptake, improved tumor targeting, and diagnostic purposes. (usage, application) While some nanoparticle-based products are already approved by the U.S. FDA, several others are currently under development and clinical assessment, with anticipated FDA approval in the not so distant future. The public, although moderately knowledgeable about nanotechnology, perceive health benefits as the primary advantage of nanotechnology-based products. While there are ethical issues with respect to the accessibility of products of nanotechnology to the common man, the emergence of new ethical issues is unlikely with this technology. Toxicity of airborne nanoparticles, although a concern, given the prior development of nanoparticle-based products for pharmaceutical purposes, is unlikely to be a major issue. Also, the public is of the opinion that the benefits of the technology will outweigh the risks. The FDA takes a risk-based management approach for products

of new technologies. The manufacturers are ultimately responsible for developing safe and efficacious pharmaceutical products based on nanoparticles.

The chitosan nanoparticles are soluble in aqueous acidic solution thereby avoiding the use of hazardous organic solvents. Chitosan nanoparticles obtained by ionic crosslinking with TPP show attractive features such as formation under extremely mild conditions without use of any environmentally hazardous solvent nor cross-linker(namely aldehydes); a homogeneous size distribution and modifiable size (from nano to micro scale) and a positive surface charge which can be conveniently modulated; a great capacity for the combination with therapeutic agents, like peptides, proteins, vaccines, oligonucleotides, and plasmids; release of the associated molecules at different rates depending upon the composition of the particles; and retention of their integrity and the activity of the associated compounds following freeze-drying and reconstitution(Garg et al., 2019).

1.2.1 Alginate (ALG) coated chitosan particles

Alginate (ALG), the salt of alginic acid, is an edible natural polysaccharide existing in brown algae. ALG is an anionic polymer, which processing excellent mucoadhesive property thus numerous pharmaceutical applications drug delivery and cell encapsulation. As alginate and chitosan are polymers containing groups with opposite electric charges in acidic aqueous environment, polymer chains of ALG and CS or segments of these polymer chains can entangle easily with each other driven by electrostatic force and thus form a coating or a shell outside of CS-TPP nanoparticles. This method is also very eco-friendly and conforms well the vales of green chemistry because of the mild conditions and absence of harsh chemicals.

This outer shell formed via polyelectrolyte complexation of ALG and CS may introduce new properties to CS-TPP particles in terms of:

- Mucoadhesive property
- Protective effect of loaded molecules
- Alter diffusion properties

Alginate has good mucoadhesive properties due to the presence of free carboxyl and hydroxyl groups in the structure. The presence of free carboxyl and hydroxyl groups in its structure endows alginate good mucoadhesive properties. Alginate can become sticky to mucous membranes on hydration, like for example digestive tract. the inner part of the eyelids. nasal and oral cavities and genitals. Mucoadhesive property is an advantage in drug delivery as contact time between drug and mucous membranes as the site of action can be extended (Frent et al., 2022).

CS-TPP nanoparticles were reported tending to swell and collapse in acidic environment but stable in alkaline and neutral pH. ALG loaded microbeads, which entrapped CS-TPP nanoparticles inside. were found more stable in acidic pH and able to achieve much more sustained release of protein at pH 1.2, while faster release at pH 7.2 (Li et al., 2021).

Alginate was reported responsible for the prolonged release of HBsAg from ALG coated CS nanoparticles because the swellness of ALG polymer chain slowed down diffusion of HBsAg. What's more. the same team also announced that the coating of alginate assisted in resistant of the release and protecting the antigen from degradation at acidic pH (Saraf et al., 2020).

1.3 Preparation methods of chitosan-based network and particulate structure

Chitosan particles can be obtained by numerous methods, like ionic gelation, polyelectrolyte complexation, emulsion solvent diffusion, emulsion crosslinking, spray drying, superfluid drying, electrospraying, emulsion-droplet coalescence, reverse micellar/emulsion methods, sieving method. Cross-linking gelation method is one of the most investigated methods due to its simplicity and mild reaction conditions. Gelation method usually generate polymer matrices structure, the coating/shell

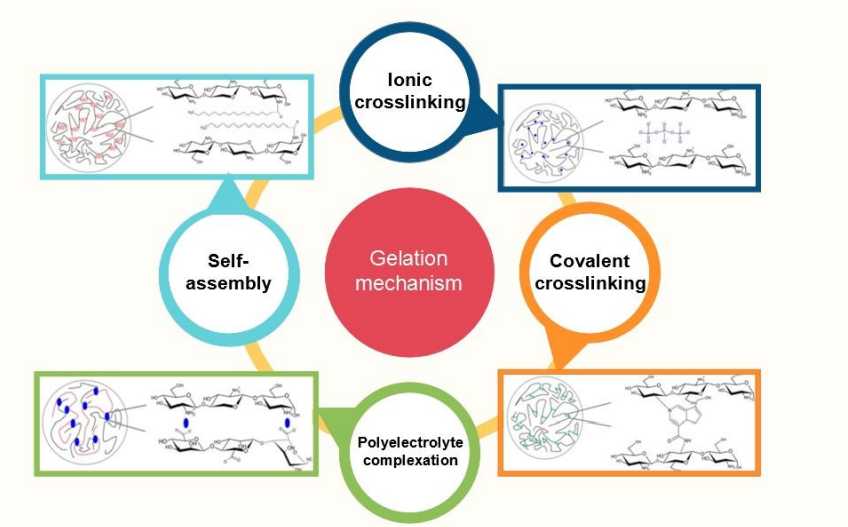


Figure 1-7 Chitosan crosslinking gelation mechanisms. Graph adapted from Bellich et al. 2016

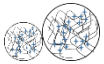
or the core region of core-shell capsules. In a review, Bellich et al. outlined the main characters of chitosan crosslinking gelation mechanisms (Figure 1-7). In principal, spray drying and supercritical process can give birth to monolithic matrix (sphere) structured particles, while capsulate structure could be produced via emulsification (emulsion alkali coacervation/precipitation, emulsion-emulsion coacervation method), electrospraying and microfluidic process. Table 1-2 summarizes frequently-used methods for preparation of chitosan-involved particulate carriers, their advantages and shortages, geometric dimension scale of obtained particles and initial concentration of particle. Specifically, the term" particle initial concentration" was indicated of some methods concerning particle-dispersed discontinuous aqueous phase. It is the concentration of newly-fabricated particles in their dispersing medium after formation yet before any extra operations like separation or dilution for example. This concentration is calculated on available experimental data from literatures (reference listed) and gives a new tool to compare and evaluate different preparation methods.

The structure of particulate carrier is strongly related to preparation method. Process parameters including pH, temperature, concentration of reagents, mass ratio of chitosan and cross-linker/surfactant, agitation speed etc. have strong effect on carrier's structural properties like particle size, particle size distribution, porosity, swelling capacity, degradation rate, diffusivity of drug via the carrier etc. Amounts of researches explored concretely this effect using the Design of Experiments (DoE) method, which is a systematic statistical method to examine quantitively the effect of factors and their interactions on specific carrier parameter(s)(Abdel-Hafez et al., 2014; Sreekumar et al., 2018; Thakur and Taranjit, 2011).

Table 1-2 Preparation methods of chitosan relevant particles. The advantages and shortages of each methods and geometric dimension of obtained particles. The cartoon symbols present structural characteristics of these particles.

Method	Description	Comments		Particulate geometric dimension	Geometry of particle	Particle initial concentration (w/v)	Reference
		Merit(s)	Demerit(s)				
Droplet extrusion method	Form droplets of drug-loaded polymeric solution by extrusion through a nozzle into aqueous solution bath of polyvalent cations	The process is convenient and cost effective and devoid of high temperature and usage of solvent. Available for living-cell encapsulation.	Limited size control/size reduction; Difficulties in large scale production; Teardrop-shaped particles	90µm-7mm		-	Microcapsule (Martins et al., 2017); Microsphere (Lee et al., 2019)
Crosslinking gelation	Electrostatic interaction between (poly-)counterions can be the driven force to form micro/nanoparticles. As the only positive charged natural polymer, chitosan has been broadly investigated to form composite with negative electrolytes by ionic crosslinking (ionotropic gelation) or covalent crosslinking	Mild processing conditions; Simple equipment Ionotropic gelation: Low toxicity, little chance of altering the chemistry of encapsulated drug	Poor stability in non-acid conditions and difficulty in entrapping high molecular weight drugs; toxicity of certain cross-linker (aldehydes)	10nm-3 mm		0.02-1.2%	Microsphere: (Calvo et al., 1997a; Fan et al., 2012; Hasheminejad et al., 2019; Nair et al., 2019; Phan et al., 2019; Soe et al., 2019; Sreekumar et al., 2018) ; Microcapsule(Arozal et al., 2021; Bin-Jumah et al., 2020; Das et al., 2019; Gooneh-Farahani et al., 2020; Hu et al., 2002; Li et al., 2008; Liu et al., 2007, p. 20; Rathore, 2020;

							Saraf et al., 2020; Zhang et al., 2019)
Polyelectrolyte complexation (PEC)	Complex chitosan with synthetic polymers or natural biopolymers via electrostatic interaction	Able to encapsulate macromolecules, like polypeptides and polynucleotides, and also hydrophobic drugs	Toxicity of certain cross-linker (aldehydes)	50-400 nm		0.1-2%	Microsphere: (Hu et al., 2002; Soe et al., 2019) ; Microcapsule: (Mukhopadhyay et al., 2015)
Complex coacervation/precipitation	Chitosan acetic solution was mixed up with a DNA/protein dissolved salty (sodium sulfate) solution to form micro/nanosphere	Narrow particle size distribution; High encapsulation efficiency; Relatively lower cost of processing	Safety issue of toxic cross-linkers; Poor product formation due to poor solubility of active agent (e.g. plant protein)	50-1600 nm		0.25-0.7%	Microsphere: (Hu et al., 2002; Özbaş-Turan et al., 2002)
Emulsion-coacervation (Emulsion-alkali precipitation) method	Disperse drug/oil mixture in chitosan acidic solution under stirring. Then use ultra-sonication/ homogenization to obtain homogeneous emulsion. Microcapsules were produced by dropping alkaline solution into aforesaid emulsion.	Devoid of cross-linker	Suitable for lipophilic drug encapsulation	10-12 µm		0.05-0.19%	Microcapsule: (Huang et al., 2017; Lam et al., 2014; Lim et al., 1997); Double-walled Microspheres: (Liu et al., 2007)
Emulsion cross-linking	Disperse chitosan aqueous solution into oily phase, in the presence of suitable surfactants served as emulsion stabilizers. Thermal cross-linking produce microspheres.	Mild processing conditions;	Complete removal of the un-reacted crosslinking agent may be difficult; Possible toxicity due to residue of certain cross linker(aldehyde);	30-700 µm		0.05-1.66%	Microspheres: (Biró et al., 2009; Patil and Sawant, 2011) Microsphere loaded Core-shell carrier: (Zeng et al., 2017)

Emulsion solvent diffusion method	An o/w emulsion is prepared by mixing organic solvent into a solution of chitosan with stabilizer under mechanical stirring followed by high pressure homogenization/ultra-sonication. AD a large amount of water to the emulsion to form particles.	High encapsulation efficiency of hydrophobic drugs	High shear force involved in the process; Usage of organic solvent	0.1-45 µm		2%	(Niwa et al., 1993) (El-Shabouri, 2002)
Spray drying method	Chitosan was firstly dissolved in an aqueous medium, then the drug is dissolved or dispersed in the previous solution. Cross-linker is aDed to the polymeric solution to overcome the fast drug release of microspheres made of non-cross-linked chitosan. Formation of particles is conducted by atomization and successive solvent evaporation	Less depend on solubility of drug and polymer; Simple, reproducible and easy to scale-up	Degradation due to high temperature or/and high shear rates during atomization	0.2-60 µm		-	Micro-/nanosphere: (Acosta et al., 2015; Aranaz et al., 2017; Budincic et al., 2021; Lu et al., 2011; Ngan et al., 2014)
Supercritical technique	Microsphere fine powders are fabricated by spraying a drug-loaded HCL/DMSO solution into Supercritical CO_2	Small-size particles(<3µm), fast, cost-effective	Multidispersed particle size distribution	6-10 µm		-	Microsphere: (Amidi et al., 2008)
Electrospraying	Chitosan is dispersed/dissolved into a mixture of solvent and blend with drug solution/suspension. The conductive liquids are	Low production cost; uniform particle size; easy-to-control surface properties, and rapid preparation;	Further investigation needed for upscaling; potential toxicity	0.1-1.3 µm		-	Microsphere: (Moreno et al., 2018; Nguyen et al., 2019; Sreekumar et al., 2017)

	atomized under high voltage to form drug-encapsulated particles. The flow rate, the voltage and distance between needle tip and collector are crucial process parameters.	high drug-loading efficiency; gentle condition, without use of harsh solvents;	due to certain solvents				
Reverse microemulsion/micellar method	Organic solvent (containing surfactant), mix with chitosan acidic solution to form reversed micelles. Then drug conjugate and chitosan attach to the micelles via glutaraldehyde (cross-linker) to form nanoparticles. Residual of solvent and surfactant and excess cross-linking agent need to be removed.	Ultrafine particle size (<100 nm); narrow particle size distribution	Application of organic solvent, time consuming preparation process and complex washing step	60–130 nm		0.01%-0.1%	Microsphere: (Cui et al., 2019; Mitra et al., 2001; Sheikholeslami et al., 2017)
Sieving method	A drug loaded chitosan jelly mass is crosslinked then manually passed trough a sieve to get non-sticky particles.	Simple and commercially viable; Easy scale-up; Devoid of tedious processes; High drug loading	Irregular particle shape	500-600 µm		-	Rod or irregular- shape micro particles: (Agnihotri and Aminabhavi, 2004)
Solvent displacement/ interfacial deposition method	Sub-micro capsule nanoemulsion coated with chitosan shell	Suitable to encapsulate lipophilic drug; Rapid and easy operation; Narrow size distribution;	Use of organic solvents	130-500 nm		0.1-0.33%	Nanocapsule: (Calvo et al., 1997b; Hoffmann et al., 2018; Prego et al., 2006)

		Absent of shearing stress					
Microfluidic technique	Dispersed phase and continuous phase are syringe-pumped onto microchannel of the microfluidic chip to get droplets, which are subsequently harden by precipitation or cross-linking	Ultra-uniform size; Able to entrap hydrophilic and/or lipophilic molecules; High cost	Low production rate; Difficulties in mass production (scale-up)	0.2-600 µm		-	Microcapsule: (Huang et al., 2019; Xun et al., 2023; Yang et al., 2016) Multilayer particle :(Ling et al., 2019; Mou et al., 2019; Zhang et al., 2019) Microfiber: (He et al., 2015)

1.4 General introduction of ionotropic gelation

1.4.1 Ionotropic gelation process

Ionotropic gelation (IG) is a process enabling the formation of nanoparticles and microparticles through electrostatic interactions between two ionic species under certain, usually mild conditions. This method was first introduced by P.Calvo et al. in late 90s of last century in order to fabricate hydrophilic nanoparticles (200-1000 nm) possessing remarkable potential in drug delivery(Calvo et al., 1997a). In most cases, the bases of the procedure used by Calvo et al. were followed and have been applied to various pairs of counterions, such as chitosan, alginate, carboxymethyl cellulose and gum arabic and ionic species such as sodium, calcium and magnesium salts have been applied. On the basis of articles in PubMed database by 2019, chitosan and alginate were statistically the most frequently used polymers in IG technique(Pedroso-Santana and Fleitas-Salazar, 2020).

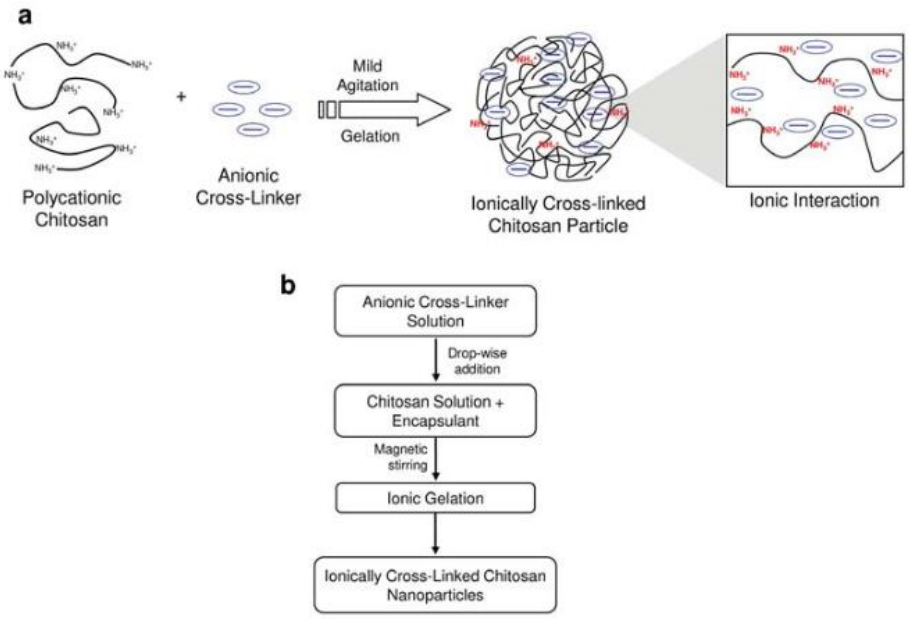


Figure 1-8 (a) Schematic representation of particulate formation through ionotropic gelation ionic gelation between positively charged chitosan and negatively charged counter-ions (e.g.TPP). (b) Schematic diagram of the preparation of ironically cross-linked chitosan nanoparticles via the traditional ionotropic gelation technique (Desai, 2016).

Chitosan is a weak base containing D-glucosamine groups with a pKa value of 6.2-7.0, which makes this polymer insoluble in neutral and alkaline pH solutions. In an acidic medium, the protonation of amino groups of chitosan results in a soluble, positively charged polysaccharide that has a high charge density (with one positive charge on each D-glucosamine unit). The ionic gelation occurs due to the inter- and intra-molecular cross-linking of polycationic chitosan by an anionic cross-linker such as tripolyphosphate (TPP). The ionotropic gelation technique involves mild manufacturing conditions, requiring only the simple mixing of solutions of chitosan, encapsulant, and TPP under mild agitation (Figure 1-8). This technique has drawn a significant amount of research attention and has become more competitive than other encapsulation methods for the preparation of chitosan nanoparticles.

The nano/micro-particle can be formed spontaneously by addition of TPP solution into a solution of chitosan in dilute acetic acid, under mechanical stirring at room temperature. When anionic tripolyphosphate (TPP) is added into dilute chitosan solutions, the TPP ions cross-link the cationic

chitosan chains into micro- and nanogels particles with diameters ranging from tens of nanometers to micrometers. Due to these properties, and their ability to form in mild aqueous environments (which prevents payload degradation), they attracted widespread interest as vectors for the delivery of drugs, cells, and food additives.

Gentle mixing, followed by incubation, of chitosan and TPP solutions generated 'broad' distributions of chitosan–TPP particulate complexes with mean sizes ranging from several nanometers to micrometers. Since particle formation was elicited solely by the tropism of the two oppositely charged macromolecules for one another, these particles were termed 'complexes'.

Due to their sub-cellular and sub-micron size, chitosan–TPP nanoparticles can penetrate deeply into tissues through fine capillaries(Vinogradov et al., 2002). This allows efficient delivery of therapeutic agents to target sites in the body. Also, by modulating nanoparticles characteristics, such as size and surface charge density, one can control the release of a therapeutic agent from nanoparticles to achieve desired therapeutic level in target tissue for required duration for optimal therapeutic efficacy(Panyam and Labhasetwar, 2003).

1.4.2 Merit and demerit of ionotropic gelation method

Thanks to its simplicity in procedure, avoidance of complex and expensive equipment or reagent, this technique is relatively cheap and quick. Furthermore, optimizing formulation may lead to high encapsulation efficiency (> 80%) of loaded molecules (Dudhani and Kosaraju, 2010; Liang et al., 2011), hence improved bioavailability of active molecules. Additionally, by modulating principal process parameters like ratio or concentration of electrolytes, particles with variable dimensions (from nanometers to micrometers) and morphology can be produced. Since this technique is free of any toxic solvent it appears as a bio-safe and green chemical process, which is another advantage.

On the other hand, compared to certain encapsulation techniques like electrospraying and spray drying, particle size distribution of particles obtained by ionotropic gelation is often broader. Polydispersity indices (PDI) obtained from dynamic light scattering, a measure of the heterogeneity of sizes of particles population, are usually higher than 0.1 in the case of ionotropic gelation. However, uniform particles are often desirable to ensure high drug loading and more predictable drug delivery behaviors.

Another limitation of this method may be the low concentration of final product. Dilute solutions are usually used to prepare particles via ionotropic gelation to avoid aggregation of formed complex particles, which are thus dispersed with dilute concentration in aqueous liquid at the end of preparation process. To concentrate those prepared particles, separation methods are introduced to firstly separate particles from its aqueous environment and then redispersed in another liquid with a smaller volume. For that purpose, proper separation method should be applied without changing the initial structure and properties of particles, which introduces extra processing and is not always achievable in practice.

1.4.3 Mechanism and kinetics of ionotropic gelation method

A recent study investigated along the way of the ionic gelation process of chitosan-TPP nanoparticles following an original method via performing aforementioned process in microdroplet reaction. The formation process could be paused by fast dilution of reagent with vast quantity (500 times) of water in an instantaneous way at any desired time point. Then dynamic light scattering (DLS) and scanning electron microscope (SEM) were used to monitor the evolution of particles along time in terms of size distributions and morphology. That was the very first time that ionic gelation process of chitosan particle formation was revealed with experimental evidences.

Results obtained showed the synthesis in a two-step process including quick nucleation (1-5s) of particles followed by growth of developing chitosan nanoparticles.

The cessation of reaction was caused by sharp increase of pH hence considerable deprotonation (90%) of chitosan and also expanded steric distance of molecules due to water dilution. (Kamat et al., 2016).

The kinetics of chitosan/TPP micro- and nanogels formation were reported very sensitive to monovalent salt (NaCl) and ionic crosslinker (TPP) concentrations. The conversion of chitosan polymer to nanoparticles is reported instantaneous(Kamat et al., 2016). The rate of CS-TPP gelation was found decreased through addition of monovalent salt. In another study, the CS-TPP particles formation process was dramatically (by several orders of magnitude) delayed by modulation of the concentration of TPP and NaCl. Using a DM 45K stopped-flow spectrophotometer, the particle formation kinetics were investigated almost instantaneously (millisecond scale). Results of this study display two-stage formation process of CS-TPP particles including first primary small particles (20−50 nm) and secondary the aggregation (100−1000 nm) of previous primary particles(Huang and Lapitsky, 2011).

In conclusion, ionotropic gelation of chitosan with TPP is a spontaneous process that is happening over a very short time scale of the order of millisecond. Researchers have successfully delayed even ceased this process by addition of monovalent salt or by rapid dilution method in order to observe and thus explore the gelation mechanism precisely with conventionally used techniques characterizing nanoparticles like DLS and electron microscopy (SEM, TEM). Usually, this transitory process is thought to be two-staged: first, the initial nucleation stage; and secondly the growth phase where bigger particles formed by infusion of former smaller particles. It is important to notice that presence of salt has great influence during the formation of particles and therefore attention should be payed to control this parameter in preparation of particles via ionic cross-linking of chitosan and TPP.

1.5 Nanoparticles

A nanoparticle or so-called ultrafine particle, gains its name by its nanoscale size. “Nano- “as a common prefix in this work, means one billionth (10^{-9}). The definition of nanoparticles varies on the materials, fields, and applications involved. According to the terminology of International Union of Pure and Applied Chemistry (IUPAC), nanoparticle is defined as a particle of any shape with dimensions between 10^{-9} and 10^{-7} m. On the other hand, in many cases nanoparticles referred to particles with size range from 1 to 100 nanometers, sometimes expanded near to the wavelength of visible light, which is 400 to 500 nm(*Nanoparticle technology handbook*, 2018). In colloidal sciences, special interests devoted on nanoparticles having one dimension below to 500 nm for their unique and versatile properties(Elaissari, 2008). In the scope of drug delivery field, nanoparticles smaller than 300 nm are dominating for efficient transport thanks to their delicate dimension allowing free mobility in available avenues and better penetrability to barriers(Gibaldi and Perrier, 2006).

1.5.1 Activation of surface/ increase in reactivity

All particles are made of atoms or molecules. Atoms or molecules located on the surface of particles are more active due to their free fringe giving more probabilities to bond and further trigger reaction with external active sites. As the size of particle decreases, the fraction of surficial atoms or molecules increases leading to a rise on activity of particle. On the assumption of atomic distance of 0.2 nm, the fraction of surface atoms of a 20 mm cubic particle is only 0.006%, whereas it increases to 0.6% for a 200 nm particle and then it is estimated 49% of the atoms are situated at the surface of a 2 nm particle(*Nanoparticle technology handbook*, 2018).

1.5.2 Higher surface area

The specific surface area increases normally in reversal proportion to the particle size. As the micronization of particles, nanoparticles processing usually relatively immense specific surface area. When a cubic particle of 1 cm is micronized into 10 nm, the specific surface area expands to a million times. As the increase in the specific surface area has direct influence on properties such as the dissolution, adsorption and reaction rates on the surface of the particles, it is one of major reasons for the unique properties of the nanoparticles different from the bulk material in many aspects.

1.5.3 Particle size and relevant properties

1.5.3.1 Size effect of nanoparticles

Effect of particle (grain) size, or so-called size effects, is defined as a series of phenomena associated with a remarkable change in physicochemical properties of substances due to acutely reduction in size of particles. Size effects are observed at the average size of grains of less than 100 nm, and is more broadly observed at the grain size below 10 nm. Quantum dots (Qdots) are small (<10 nm) inorganic nanocrystals that possess particular luminescent properties; their optical properties is stable and can be tuned by varying the particle size or composition. Quantum size effects result in the electronic properties of a substance or material and are linked with a decrease of the dimensions of the electron gas, which leads to a change in the energy spectrum. In biomedical domain, greater uptake by cells of for nanoparticles compared to microparticles has been repeatedly announced(Decuzzi et al., 2008; Prabha et al., 2002).

Qdots have attracted great attention for their applications enable real-time tissue imaging (bioimaging), diagnostics, single molecule probes, and targeting drug delivery, among many other fields.

The surface charge density of a nanoparticle in electrolyte solutions is reported to be highly size-dependent. As the particle diameter decreases to below 10 nm there is remarkable increase in the surface charge density(Abbas et al., 2008). Small nanoparticles also exhibit unique magnetic and optical properties. Ferromagnetic materials were reported to become superparamagnetic when size drooped below around 20 nm(Esenaliev, 2000). Gold and silver nanoparticles show size-dependent optical properties. For example, gold nanoparticles ranging from 9 nm to 100 nm on size can display different colors(Kelly et al., 2003).

The solubility is greatly promoted with decreasing grain size when the size of the matrix nanoparticles is less than 20 nm. In the Fe–Si system, significant enhanced solid solubility has been observed. It can be clearly seen that the solubility of Si in Fe is almost negligible up to a crystallite size of Fe of about 20 nm, below which there is a dissolution of Si. A similar effect was observed for Bi diffusion in Cu. The solubility of Bi in nanocrystalline Cu is quite little around 10^{-6}. Contrastively, the solubility of Bi in nanocrystalline Cu is about 5%, corresponding to a solubility enhancement by about 10,000 times relative to crystalline Cu(Höfler et al., 1993). The absorption of hydrogen atoms in nanocrystalline palladium (Pd) (at concentrations <10–3) is enhanced by a factor about 100 relative to Pd grains(Stuhr et al., 1997).

1.5.3.2 Evaluation of Size of Nanoparticles

As mentioned earlier, the properties and characteristics of nanoparticles are closely related to their size, making it crucial to measure this parameter accurately and reliably using repeatable methods.

1.5.3.2.1 Microscopy: Transmission electron microscope (TEM) and Atomic force microscopy (AFM)

As for the tiny size of nanoparticles, sophisticated high-resolution microscopes are often employed to produce images of nanoparticles to explore their dimensions as well as morphology including shape, surface structure, even internal structure with help of cross-section technique.

TEM (Figure 1-9) is high spatial resolution electron microscopy technique whereby a beam of electrons is transmitted through an ultra-thin specimen, interacting with the specimen as it passes through. An image is formed from the interaction of the electrons transmitted through the specimen.

The technique is well applied in metrology at resolutions of less than 0.2nm, which permits the instrument to capture ultra fine detail even as small as a single column of atoms, which is 1000 times smaller than a resolvable object seen in a conventional optical microscope.

Nevertheless, it is important to notice that TEM can produce directly information of particles size and also the particle size distribution with images under conditions that particles on the sample mount are properly prepared and well dispersed to make sure good representativeness of the sample to the particle population.

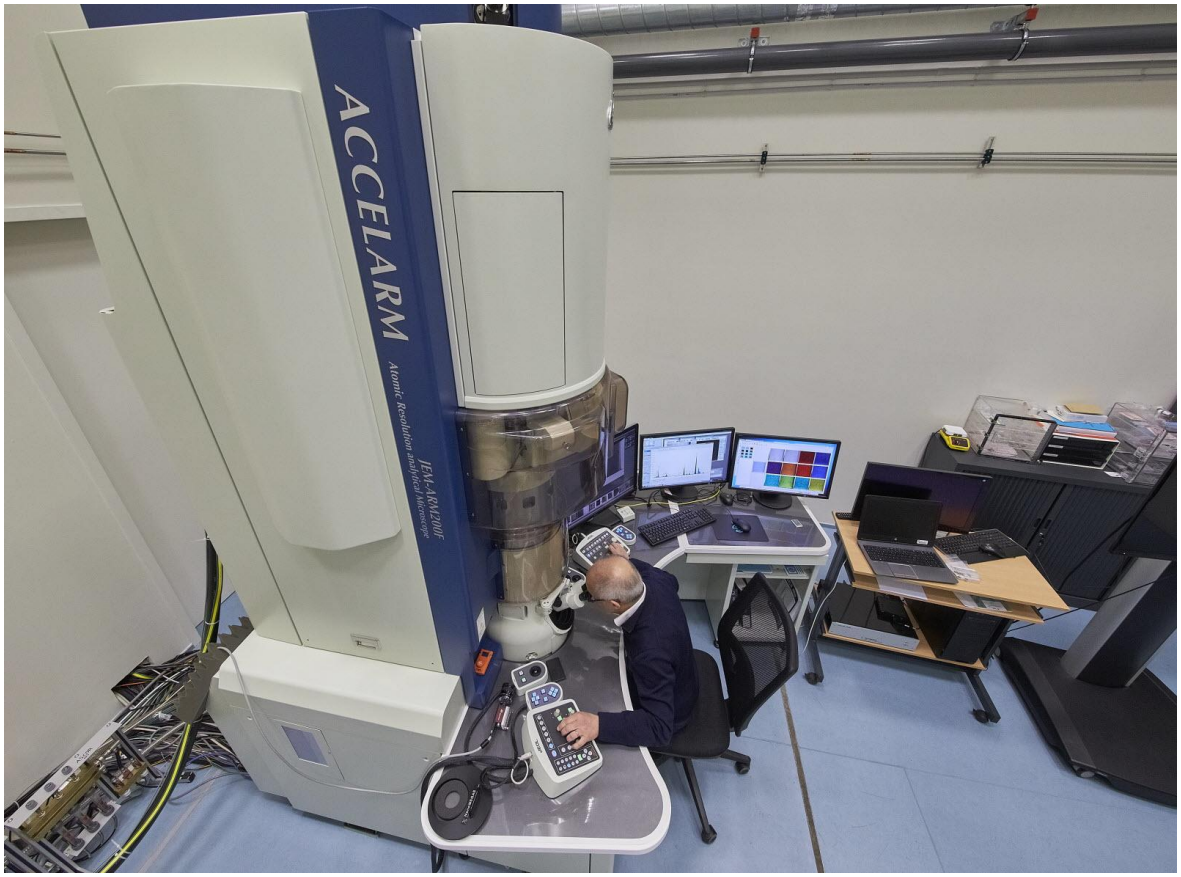


Figure 1-9 Transmission electron microscope, Institute Jean Lamour, campus ARTEM, Nancy

AFM

Atomic force microscopy is a high-resolution scanning probe microscopy, with demonstrated resolution in the range of few nanometers. The information is gathered by contacts between surface and a mechanical probe.

The Configuration of AFM (Figure 1-10) consists of a cantilever with a very fine tip (probe) at its end, typically silicon with a few nanometers, which is utilized to scan the sample surface. During scanning, the forces between the cantilever tip and the sample cause deflection of the cantilever, which can be detected by using a laser spot reflected from the top area of the cantilever.



Figure 1-10 Atomic force microscopy (SMENA NT-MDT Microscope), Laboratoire Charles Coulomb (L2C), Montpellier

AFM is wildly applied for characterization of nanoparticles not only because it can provide dimensional information of object but also its ability to furnish both qualitative and quantitative information about the sample topology, including morphology, surface texture and roughness with 3D scanning images(Montasser et al., 2002).

The major difference between atomic force microscopy and competing technologies such as optical microscopy and electron microscopy is that AFM does not use lenses or beam irradiation. Hence, it is not limited in spatial resolution due to diffraction and aberration, and preparing a space for guiding the beam (by creating a vacuum) and staining the sample are unnecessary(“Atomic force microscopy,” 2022).

1.5.3.2.2 Dynamic light scattering (DLS)

Dynamic light scattering is another wildly utilized technique for measuring the size and size distribution, specifically in the submicron range, of molecules and particles dispersed or dissolved in a liquid. The Brownian motion of these particles or molecules causes rapid fluctuation of the intensity of the scattered light. DLS measures the temporal fluctuations of the light scattered, when a solution containing the particles passing in the path of a monochromatic beam of light. Analysis of these short-term intensity fluctuations yields the speed of the Brownian motion and hence the particle size,

employing the Stokes-Einstein law. This technique affords hydrodynamic diameter of particle along with the polydispersity index, which explains heterogeneity of the sample.

1.5.3.2.3 Laser diffraction

Furthermore, the laser diffraction analysis, also called as laser diffraction spectroscopy, working on the Fraunhofer diffraction theory and Mie scattering theory has also been broadly employed for measuring geometrical dimensions of (sub)micron-sized particle. The angle of the laser beam is in inverse proportion to particle size, where the laser beam angle decreases as particle size increases and vice versa (McCave et al., 1986) Unlike DLS, the laser diffraction technique can also measure the volume distribution directly, whereas the DLS measures an intensity- based mean particle diameter. Another unique advantage of laser diffraction analysis is not only the wide size range (10 nm to 3.5 mm) but also its capability to measure dry powders and aerosols.

Laser diffraction instruments typically consist of a laser light source, a sample dispersion unit, a detection system, and a software package for data analysis. The laser light source produces a beam of light that is focused through a lens to form a narrow beam. The sample dispersion unit disperses the sample into the beam, and the detection system measures the scattered light at different angles. The software analyzes the scattering pattern to determine particle size distribution. Different laser diffraction instruments may have variations in the specific components and configurations, as well as differences in measurement capabilities such as size range, sensitivity, and resolution.

1.5.3.2.4 Brunauer Emmett Teller (BET)

Then Brunauer Emmett Teller (BET) method based on BET theory is the designated method in international standard ISO 9277 for the determination of the specific surface area of solids by gas adsorption, which is often applied as a simple method to evaluate the size of nanosized particles. By this method, it is possible to estimate the particle size from the specific surface area under the assumption of spherical particle shape. This equivalent particle size based on the specific surface area is a calculated value useful for the evaluation of nanoparticle size, though it may differ from the particle size detected by other techniques depending on the surface state and the inner structure of the particles.

Coupling of several different methods, may lead to discrepancy in the nanoparticle size determination. This is mainly caused by the preparation of samples. Since during DLS measurement, particles are dispersed in an aqueous environment where they are hydrated and slightly larger in size due to swelling. Contrastively, samples for TEM usually suffered a drying treatment to satisfy the requirement of vacuum degree of the method. In this case, particles may lightly or largely shrink after drying, depending on the constituting material, hence a reduction in size.

1.5.4 Surface charge

In the 1940s, the scientists Derjaguin, Verwey, Landau and Overbeek developed a theory which dealt with the stability of colloidal systems. DVLO theory suggests that the stability of a particle in solution is the balance of several competing contributions including repulsion and attraction. The attraction is mainly due to van der Waals forces among particles which is strongly depending on temperature. While the repulsive potential comes from two fundamental mechanisms: the steric and electrostatic stabilization. Electrostatic stabilization involves the effect on particle interaction due to the distribution of charged species in the system and can be conducted via altering the concentration of ions in the system, which is a reversible process and less expensive compared to varying steric stabilization. For a colloidal system to remain stable, the repulsive forces must be dominant.

A particle suspended in a solution containing ions is surrounded by an electrical double layer of ions and counterions. The potential that exists at the hydrodynamic boundary of the particle is known as the zeta potential (ζ).

1.5.4.1 Zeta potential and the Electrical double layer

The surface charge or the surface charge density is an important property of nanoparticles dispersed in suspensions, which depends upon the nature of the particle and its surrounding medium. Zeta potential is a physical property used to help estimate surface charge of nanoparticles, and its magnitude is used to predict the long-term stability of colloidal systems like e.g. suspension, emulsion and to anticipate possible surficial interactions. Figure 1-11 Schematic illustrates of zeta potential and the Electrical double layer.

The zeta potential can be calculated by determining the Electrophoretic Mobility and then applying the Henry equation. The electrophoretic mobility is determined by performing an electrophoresis experiment on the sample and measuring the velocity of the particles using Laser Doppler Velocimetry (LDV).

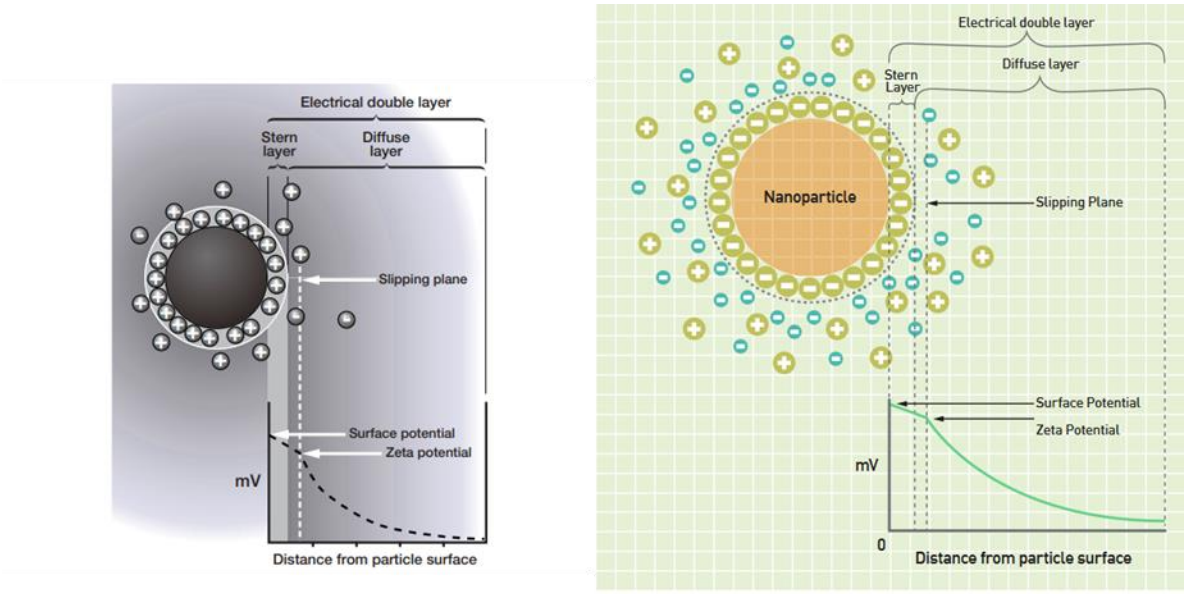


Figure 1-11 Schematic illustration of zeta potential and the Electrical double layer (from: Zetasizer Nano User Manual p229)

1.5.4.1.1 Factors Affecting Zeta Potential

Understanding the factors that affect zeta potential is critical for the design and optimization of colloidal systems for a wide range of applications.

- pH

In aqueous media, as net charge on a particle is significantly influenced by the concentration of protons (H^+) in its surrounding environment, the pH of the sample is one of the most important factors that affects its zeta potential. As the pH changes, the surface charge on the particle changes, and this can alter the zeta potential. The isoelectric point, is the pH at which an object carries no net electrical charge or is electrically neutral (zeta potential equals to zero). From a practical consideration, this is a physical quantity of importance to know, because it is normally the point where aggregation is most likely and hence the colloidal system is least stable (Malvern Instruments, 2005).

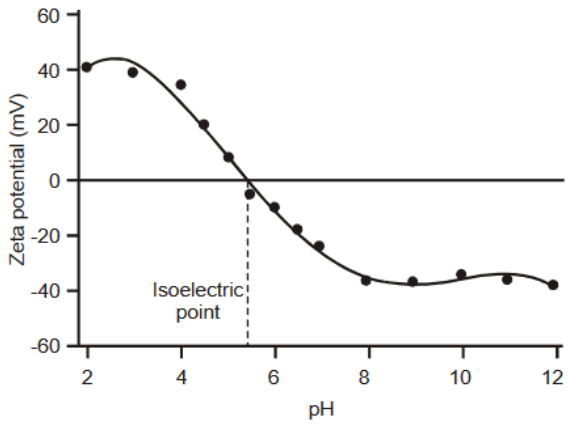


Figure 1-12 Zeta potential versus pH, Isoelectric point(Malvern Instruments, 2005)

- Ions strength

The thickness of the double layer depends upon the concentration of ions in solution and can be calculated from the ionic strength of the medium. The valency of the ions will also influence double layer thickness. A trivalent ion such as Fe^{3+} will compress the double layer to a greater extent in comparison with a monovalent ion such as Cl^{-}. Adsorption of ions onto a particle surface can introduce an impressive effect on the zeta potential of the particle dispersion in certain cases. The ionic strength of the solution can also influence the zeta potential. As the concentration of ions in the solution increases, the electrostatic repulsion between particles decreases, and this can lead to a decrease in the zeta potential(Hunter, 2013; Lyklema, 2005).

- Temperature

Changes in temperature can alter the zeta potential by affecting the solubility of ions in the solution, and altering the mobility of charged species in the solution.

- Particle size

Particle size is another factor that can affect zeta potential. When particles are large, they tend to settle more quickly and can form aggregates, which can decrease the surface charge and lead to inaccurate zeta potential measurements. Smaller particles are less likely to aggregate and will remain suspended in solution for longer periods, allowing for more accurate zeta potential measurements.

In addition, the size of the particles can affect the zeta potential value itself. For example, smaller particles may have a larger surface area relative to their volume, leading to a higher surface charge density and a higher zeta potential. Conversely, larger particles may have a lower surface charge density and thus a lower zeta potential.

Therefore, it is important to consider particle size when measuring zeta potential to ensure accurate and reliable results. Techniques such as dynamic light scattering (DLS) or laser diffraction can be used to measure particle size and inform zeta potential measurements.

In general, the dividing line between stable and unstable suspensions is considered at either +30mV or -30mV. Particles with zeta potentials more positive than +30mV or more negative than -30mV are normally considered stable (Gibaldi and Perrier, 2006).

1.5.5 Chitosan nanoparticles

Nanoparticulate systems can potentially be used for enhanced drug dissolution and bioavailability, enhanced cellular uptake, improved tumor targeting, and diagnostic purposes. While some nanoparticle-based products are already approved by the U.S. FDA, several others are currently under development and clinical assessment, with anticipated FDA approval in the not so distant future. The public, although moderately knowledgeable about nanotechnology, perceive health benefits as the primary advantage of nanotechnology-based products. While there are ethical issues with respect to the accessibility of products of nanotechnology to the common people, the emergence of new ethical issues is unlikely with this technology. Toxicity of airborne nanoparticles, although a concern, given the prior development of nanoparticle-based products for pharmaceutical purposes, is unlikely to be a major issue. Also, the public is of the opinion that the benefits of the technology will outweigh the risks. The FDA takes a risk-based management approach for products of new technologies. The manufacturers are ultimately responsible for developing safe and efficacious pharmaceutical products based on nanoparticles.

A nanoparticle is a microscopic particle with the average size ranging from 1 to 100 nm (Acosta, 2009). Particularly, in pharmaceutical science, particles with size below 1000 nm can still be classified as nanoparticles because of their unique physicochemical properties compared to bulk materials (Li et al., 2011). Nanoparticles are being increasingly used in drug delivery systems. Their advantages include the size and surface characteristics of nanoparticles can be easily manipulated, and this versatility could be used for both passive and active drug targeting. Nanoparticles can also be made to control and sustain release of drug/bioactive molecules under GI tract conditions. Moreover, since distribution and subsequent clearance of drug from the body can be altered, an increase in drug therapeutic efficacy and reduction of side effects can be achieved.

Chitosan particles exhibit characteristic mucoadhesive properties and have been reported having high retention to gastric mucosa and a longer time than alginate and alginate-starch particles (Phuong Ta et al., 2021). Chitosan possesses positive charge following the removal of acetyl units from D-glucosamine residues, unlike most polysaccharides. Apart from being non-toxic, biocompatible, and biodegradable, chitosan also exhibits antibacterial properties. This antibacterial activity is attributed to the electrostatic interactions between the amine groups of chitosan and the anionic sites on the bacterial cell wall, which are present due to the presence of carboxylic acid residues and phospholipids (Hejazi and Amiji, 2003). Chitosan may be fundamental to overcome the intrinsic poor mucosal bioavailability of biopharmaceutical drugs.

Chitosan nanoparticles have several advantages over other types of nanoparticles, including their biocompatibility, biodegradability, low toxicity, and ability to be easily synthesized and modified. They have been shown to improve drug bioavailability, reduce toxicity, and enhance drug stability, making them promising candidates for drug delivery applications. Additionally, they have been explored for gene therapy and tissue engineering applications due to their ability to efficiently deliver genetic material and promote cell growth (Huh et al., 2017; Sargazi et al., 2022). In summary, the ability of chitosan nanoparticles to increase retention time, ultrafine size, and sustained drug/bioactive molecule release (Khan et al., 2014; Liang et al., 2017) make them promising delivery vehicles.

1.6 Polyphenols

Polyphenols constitute a heterogeneous group of molecules that vary according to their chemical structure, and due to the considerable diversity of their structures, polyphenols are considered even more efficient than other antioxidants (Galanakis, 2018). Over the past three decades, there has been a significant accumulation of scientific knowledge on polyphenols, fueled by their recognized beneficial biological activities. Since 1990, more than 68,000 research articles on this topic have been published by researchers worldwide, and this number continues to grow steadily, as evidenced by the Web of Science (Index-SCI Expanded). The interest of scientists and consumers for polyphenols mainly comes from the wildly recognition of their antioxidant properties, their vast abundance in human daily diet, and their likely role in the prevention of numerous diseases associated with oxidative stress and in improvement of human health(Scalbert et al., 2005a).

1.6.1 Definition, classification

Polyphenols can be classified by different ways, such as the source of origin, natural distribution, biological function and the mostly used classification method, by chemical structure. Based on the structural elements in a polyphenol, the most frequent classification of polyphenols according to literature review would cover five classes: phenolic acids, flavonoids, stilbenes, lignans, and others (Figure 1-13, Galanakis, 2018).

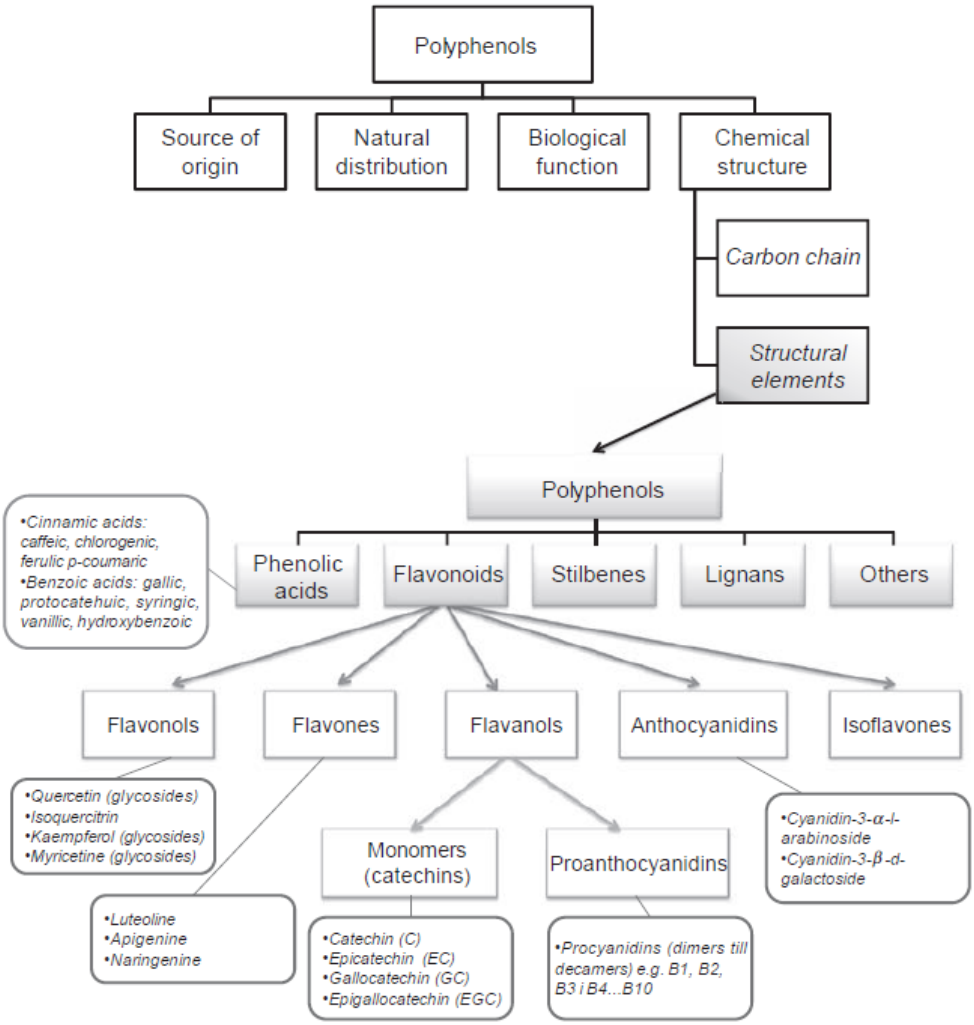


Figure 1-13 Classification of polyphenols (Galanakis, 2018)

Flavonoids are a widely distributed group of phytochemicals having benzo-pyrone nucleus, for that reason flavonoids are often responsible for the different colors in many plants as fruits, vegetables and herbs. More than 8,000 flavonoids have been described and categorized into flavonols, flavones, flavanones, isoflavones and anthocyanidins (Patel et al., 2018; Raja Kumar et al., 2019).

Phenolic acids are compounds characterized by having a benzenic ring, a carboxylic group, and one or more hydroxyl and/or methoxyl groups. These compounds can be divided into two groups: benzoic acids and cinnamic acids and derivatives thereof (Figure 1-14). The benzoic acids have seven carbon atoms (C6-C1) and are the simplest phenolic acids found in nature, while cinnamic acids have nine carbon atoms (C6-C3) and are rarely found in their free form in plants.

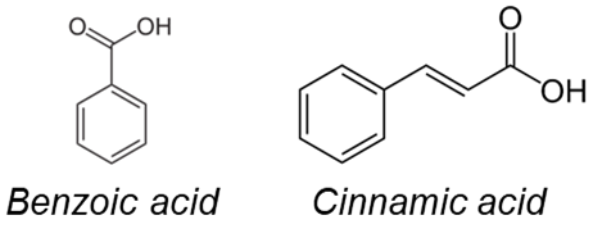


Figure 1-14 Structure of benzoic acid and cinnamon acid

Lignans are formed of two phenylpropane units. Lignans are precursors to phytoestrogens. The richest dietary source is linseed. They might play a role as antifeedants in the defense of seeds and plants against herbivores.

Stilbene, of which there are two forms [trans-1,2-diphenylethylene ((E)-stilbene) and cis-1,2-diphenylethylene ((Z)-stilbene)], is an aromatic hydrocarbon with the formula $C_{14}H_{12}$. Stilbenes are found in only low quantities in the human diet. One of these, resveratrol, for which anticarcinogenic effects have been shown during screening of medicinal plants, has been extensively studied, and is found in low quantities in wine.

1.6.2 Applications of polyphenols in health promotions

Polyphenols are compounds with biochemical activities and as they are the most abundant antioxidants in the diet, increasingly significant research interests are aroused on the propose to cast on light the benefits of polyphenol-containing foods and beverages. The application of dietary polyphenols is reported helpful on promotion of health in a far-sighted way, or say well-leveraged, by avoiding diseases or poor health conditions or/and reducing the progress and the limitations of disability of a disease(Watson et al., 2014).

Health benefits of polyphenols in preventing diseases

Consumption of tea, especially green tea, was reported repeatedly relevant to reduction risks of several diseases including coronary artery disease, non-fatal myocardial infarction, hyperglycemia, dyslipidemia, and elevated blood pressure and even cancers (Khan and Mukhtar, 2007; Scalbert et al., 2005b; Thielecke and Boschmann, 2009). Through altering lipid and energy metabolism, polyphenols have shown in various studies their potentials to facilitate weight loss and hamper weight gain, all of which introduces benefits to the condition of obesity(Giacalone et al., 2011; Peng et al., 2011). Reduction of blood pressure and lipid levels due to grape seed and chokeberry extracts has been seen in small human trials(Cherniack, 2011) . Flavanol-rich foods, especially cocoa and its derivatives, have been demonstrated to possess antihypertensive effects in humans. These effects could be related to the maintenance of optimal NO (Nitric oxide) levels, and could be associated with depressing superoxide anion production in the vasculature(Fraga et al., 2011).

1.6.3 Limited bioavailability of polyphenols

Despite the potential health benefits of phenolic phytochemicals, their low bioavailability remains a challenge. Several factors contribute to this issue, such as low solubility in aqueous solutions, instability in the gastrointestinal tract, and active efflux mechanisms. Naturally low aqueous solubility, poor gastrointestinal stability, passive diffusion, and active efflux of phenolic phytochemicals in the gastrointestinal tract result in such low absorption. These factors can limit the absorption of phenolic phytochemicals and reduce their bioavailability, which ultimately affects their potential health benefits.

- Stability and degradation: Polyphenols can be sensitive to factors such as light, heat, pH, and oxygen, leading to their degradation and loss of bioactivity. For example, the different pH conditions in the gastrointestinal segments can also lead to the degradation of phenolic phytochemicals. Maintaining the stability of polyphenols during processing, storage, and formulation is a challenge.

- Bioavailability: The bioavailability of polyphenols refers to their ability to be absorbed and utilized by the body. Many polyphenols have low bioavailability due to factors like poor solubility, limited absorption in the gastrointestinal tract, rapid metabolism, and rapid elimination from the body. Enhancing the bioavailability of polyphenols remains a significant challenge for developing their application.

- Poor solubility: The aqueous solubility of phenolic phytochemicals is influenced by their affinity to water molecules, with molecular weight playing a primary role (Gao and Hu, 2010). Higher molecular weight compounds, such as proanthocyanidin polymers, have lower aqueous solubility and absorption rates compared to monomers and oligomers.

Incorporating polyphenols into formulations such as food products, beverages, supplements, and pharmaceuticals can be challenging. Polyphenols often have specific solubility requirements, which may necessitate the use of solvents, emulsifiers, or encapsulation techniques. Finding suitable formulation approaches that preserve the stability and bioactivity of polyphenols can be complex.

- Interactions and compatibility: Polyphenols can interact with other compounds, such as proteins, minerals, or other additives, affecting their stability and bioavailability. Compatibility issues need to be addressed to prevent undesirable interactions and optimize the performance of polyphenol-containing products.

1.6.4 Naringenin(NRG), Naringin(NR), Catechin(CAT)

It is well known that natural plants, herbs, and food materials contain compounds that have the potential to be utilized for various value-added applications, such as the treatment of diseases. As an alternative to synthetic preservatives and flavoring agents, active molecules extracted from plants have been used for a long time in traditional medicine or in food processing industries. However, these bioactive compounds are susceptible to degradation and disintegration from environmental conditions such as temperature, moisture, pH, and enzymatic catalyzed degradation. Therefore, it is essential to preserve these valuable compounds to ensure their high bioavailability. Encapsulation is closely linked to the use of bioactive compounds of biological origin, as it can protect these compounds from environmental conditions. Additionally, bioactive compounds can be entrapped in carriers for targeted delivery in home care products, drugs, and diagnostic reagents, in addition to preserving their bioavailability.

Because of their proved low biotoxicity, chitosan-based systems are broadly studied and used in encapsulation of various materials including bioactive compounds like e.g. antioxidants, anti-cancer drugs, anti-inflammation agents etc. and proteins, as well as vaccines (Lam et al., 2014; Li et al., 2008; Maity et al., 2017, 2017; Md et al., 2019; Mukhopadhyay et al., 2015; Tsirigotis-Maniecka et al., 2021).

Natural products with diverse bioactivities are becoming an important source of novel agents and have different pharmaceutical potential. Flavonoids are the most abundant antioxidants in plants and the human diet. They have attracted a great deal of attention in recent years due to their antioxidative, mild estrogenic, antibacterial, antitumor, anti-inflammatory, antimutagenic, myocardial protecting, vasodilator, and hepatoprotective activities (Bhathena and Velasquez, 2002; Oršolić et al., 2011). NAR, NR and CAT are all promising polyphenols with dissociated physicochemical properties (Table- 1-3).

Table 1-3 Solubility and partition coefficient of naringenin, naringin and catechin.

Polyphenol	Naringenin	Naringin	Catechin
Solubility in water at 25°C*	$0.95\ 10^{-6}$	$3.54\ 10^{-6}$	$386\ 10^{-6}$
Solubility in ethanol at 25°C*	0.0104	$4.07\ 10^{-5}$	0.0307
LogP(o/w)**	2.7	-0.13	0.30

* In mole fraction

**Partition coefficient (Luo et al., 2011)

1.6.4.1 Naringenin

Naringenin is chemically named as 2, 3-dihydro-5, 7- dihydroxy-2-(4-hydroxyphenyl) - 4H-1-benzopyran-4-one (Figure 1-15) with a molecular weight of 272.3 g/mol. It is almost insoluble in water while soluble in organic solvent like ethanol, methanol, dimethyl formamide (DMSO) and dimethyl formamide (DMF). Its poor aqueous solubility induces difficulties of application in health engineering due to subsequent limited bioavailability.

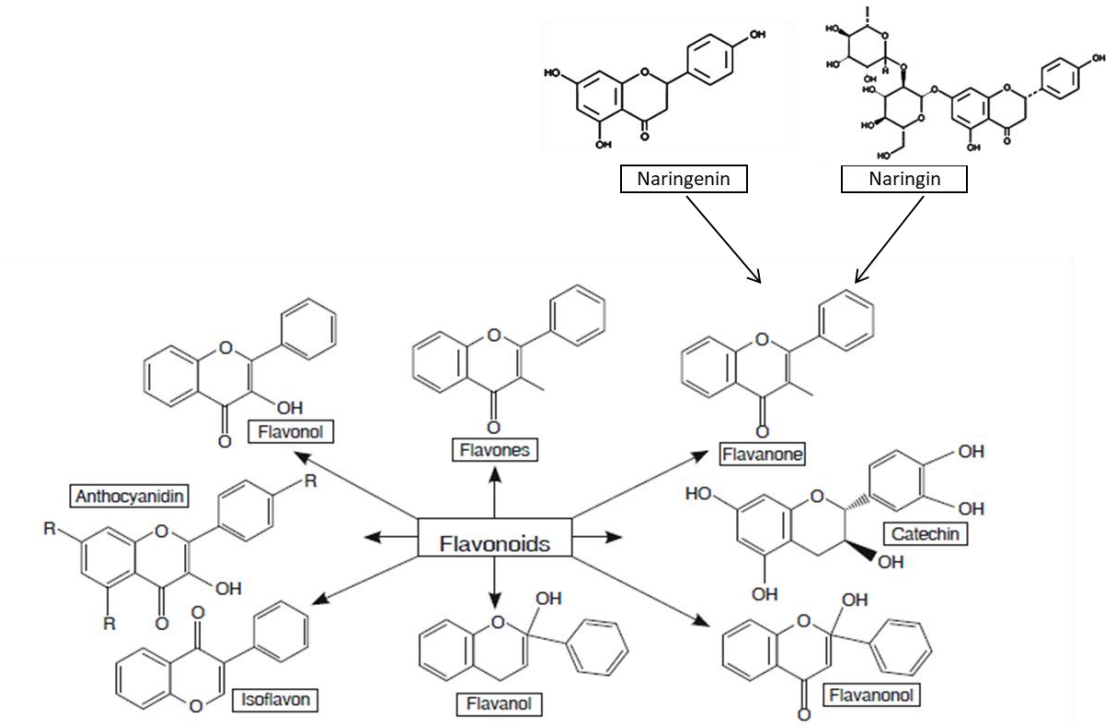


Figure 1-15 Chemical Structures of Different Flavonoids. Chemical structure of naringenin, naringin and catechin(reprinted from Galanakis, 2018).

Naringenin (4',5,7-trihydroxy flavonone, NRG) is one of the most abundant flavonoids in grapes, tomatoes, and citrus fruits (Renugadevi and Prabu, 2010). Moreover, NRG is known as a safe natural product with various bioactive effects, including antioxidative, anti-inflammatory, anticancer, hepatoprotective, and nephroprotective activities (Cavia-Saiz et al., 2010; Fuior et al., 2019; Renugadevi and Prabu, 2010).

Naringenin has been shown to exhibit strong antioxidant activity, which helps to scavenge free radicals and protect against oxidative stress. Naringenin exhibited high antioxidant capacity though chelation with transition metallic ions and its superoxide radical scavenger efficiency(Cavia-Saiz et al., 2010).

Additionally, naringenin was also one of the flavonoids that shown to stabilize membranes through a decrease in lipid fluidity and thus slow down free radical reactions (Arora et al., 2000). The flavanone was effective in reducing DNA damage. It has been shown to reduce oxidative damage to DNA in vitro as well as in animal studies. Findings support that naringenin might have a biological effect in protecting alloxan-induced diabetic mice against oxidative stress (Oršolić et al., 2011).

Naringenin has been shown to exhibit anti-inflammatory effects by inhibiting the production of inflammatory cytokines and enzymes, such as interleukin-6 (IL-6), tumor necrosis factor-alpha (TNF-α), and cyclooxygenase-2 (COX-2). Additionally, naringenin may play a protective role by reducing mucous production during airway inflammation through downregulation of reactive oxygen species (ROS) production and inhibition of nuclear factor-kappa B (NF-κB) activity in human airway epithelial cells (Garbacki et al., 2005). In a study conducted on chlamydia trachomatis-infected macrophages, naringenin was also found to exert anti-inflammatory effects by downregulating cytokines and chemokines(Yilma et al., 2013).

Recently, the inhibition effect of naringenin on the assembly and long-term production of hepatitis C virus has been demonstrated by several research teams(Goldwasser et al., 2011) (Shulman et al., 2011). Oral administration of naringenin is reported effective against dimethylnitrosamine (DMN) induced liver injury and helpful in improvement of several liver function indexes such as aspartate transaminase, alanine transaminase, bilirubin, and alkaline phosphatase levels. Naringenin treatment lowered the DMN-induced accumulation of collagen in the liver thereby protected against hepatic fibrosis(Hernández-Aquino and Muriel, 2018; Lee et al., 2004) .

Estrogen (or oestrogen) is a category of sex hormone in charge of the development and maintenance of the reproductive system and secondary sex characteristics in female(Huether and McCance, 2019; Satoskar et al., 2017). Naringenin is a weak estrogen that also exhibits partial antiestrogenic activity in the female rat uterus and MCF-7 human breast cancer cells(Ruh et al., 1995). As one of main active ingredients of Rhizoma drynariae (Gusuibu) total flavonoids, naringenin is proven effective in treating osteoporosis and bone non-union due to its estrogenic and anti-estrogenic activity(Guo et al., 2011).

Numerous studies showed that naringenin inhibited glucose uptake thus detention of growth and proliferation in cancer cells (Harmon and Patel, 2004; Kanno et al., 2005). On the other hand, naringenin was observed cytotoxic to leukemic cells and various cancerous cell lines of human, which leads to apoptosis and thereby helpful in curing diseases caused by above pathogens, such as leukemia, breast cancer, stomach cancer, liver cancer, gervix cancer, colon cancer and so on.

Neuroprotective activity: Naringenin has been shown to exhibit neuroprotective effects by protecting against oxidative stress, reducing neuroinflammation, and promoting neuronal survival(Shadab et al., 2019).

In summary, naringenin shows promising potential as a bioactive compound with health benefits, and ongoing research is actively investigating its therapeutic potential in various diseases.

1.6.4.1.1 Physical and chemical properties

Solubility evaluation is very important for the pharmaceutical product design, because the drug solubility affects the drug efficacy directly, as well as its future developments and formulation optimizations, influencing the pharmacokinetic properties, such as release, transport, and absorption.

Naringenin (2,3-Dihydro-5,7-dihydroxy-2-(4-hydroxyphenyl)4H-1-benzopyran-4-one, MW = 272.3) is a weak acid (pKa_1 = 6.8; pKa_2 = 9.6; pKa_3 = 11.6 (Zhu et al., 2019)) compound with a low water solubility. Naringenin's low solubility in water makes it a challenging compound to work with in aqueous environments. The solubility of naringenin can also be affected by the pH of the solution. Complexation with β-cyclodextrin can enhance the solubility of naringenin in a positive linear way(Ficarra et al., 2002; Jovanovic et al., 1994). In absence of cyclodextrins, the solubility of naringenin in water at pH 8.0 is higher than at pH 4.0, as it is 0.35 mg/ml while the latter is very low, about 0.08 mg/ml; this is due to the ionization of naringenin in basic media as it tends to easily solubilize, giving pale yellow colored solutions (Tommasini et al., 2004).

Naringenin is insoluble in water, soluble in ethanol (50 mg/mL), DMSO, methanol (LKT Labs). The solubility of naringenin gradually increases as the temperature increases (from 280 to 330 K). The solubility of naringenin also increases when the mole fraction of ethanol in solvent increases. (Figure 1-16, P. Zhang et al., 2013).

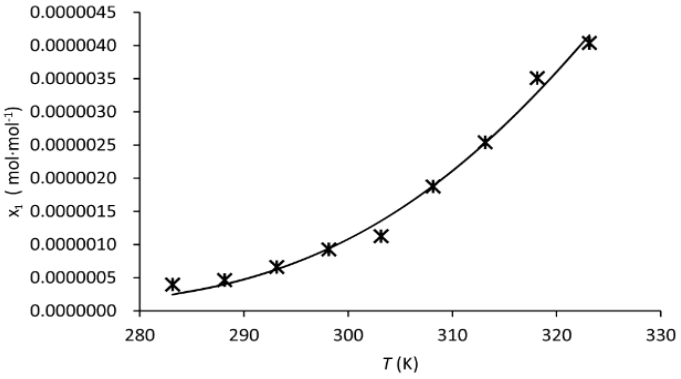


Figure 1-16 The solubility of naringenin in water gradually increases as the temperature increases. pH=4, temperature. (Reprinted form P. Zhang et al., 2013)

Solubility data of naringenin found in the literature range very broadly from 14 to 475 mg/L (Table 1-4).

Table 1-4 Solubility data of naringenin from chemical suppliers and in the literature

Solubility (mg/L)	Reference	Method
14.2	(Zhang et al., 2013)	Water, T=298.15K
34	(Md et al., 2020)	Water
43.8	(Semalty et al., 2010)	pH7.2
214	(Fuior et al., 2019, p. 1); DrugBank.[(accessed on 26 July 2019)]	Water

UV-Vis absorption of NRG

Naringenin exhibits UV-Vis absorption in the range of 200-400 nm, with maximum absorption(λ_{max}) occurring at around 288 nm (Table 1-5). The absorption spectrum of naringenin typically shows two major peaks, one at around 288 nm and another at around 323 nm. The absorption peak at 288 nm is attributed to the n→π* transition of the carbonyl group in the flavanone ring, while the peak at 323 nm is attributed to the π→π* transition of the aromatic ring.

The UV-Vis absorption spectrum of naringenin can be used for quantitative analysis of this compound in various samples. This technique is commonly used in the food and pharmaceutical industries for quality control purposes. The absorbance of naringenin at its maximum absorption wavelength can be measured and used to determine the concentration of the compound in a sample using Beer–Lambert law.

Overall, the UV-Vis absorption spectrum of naringenin provides important information about the electronic transitions and chemical structure of this bioactive compound, and can be used for analytical and quality control purposes.

Table 1-5 λ_{max} of Naringenin in literature

λ_{max} (nm)	Reference	Note
288	(P. Zhang et al., 2013)	283-323 K; in binary solvent system of ethanol and water; UV−vis spectroscopy
285	(Tommasini et al., 2004)	HPLC, with or without cyclodextrins
288	(Maity et al., 2017)	UV–Vis spectrophotometer (Jasco V-630)
288	(Cordenonsi et al., 2017)	Ultraviolet spectroscopy
290	(Khokhar et al., 2022)	HPLC, pH=7.2
210, 323	(Zhu et al., 2019)	UV–Vis spectrophotometry, pH=7, 37°C
289	(Zhu et al., 2019)	UV–Vis spectrophotometry, pH=5, 37°C
245, 323	(Zhu et al., 2019)	UV–Vis spectrophotometry, pH=11, 37°C

1.6.4.2 Naringin

Naringin (4',5,7-trihydroxy flavonone-7-rhamnoglucoside) is a predominant flavonoid found in many plants mainly citrus fruits and their bitter taste is usually ascribed to existence of naringin.

In fact, naringenin is metabolization product of naringin, and is theorized to be responsible for the well-known interaction between grapefruit juice and several pharmaceutical drugs. Naringenin exhibited higher antioxidant capacity and hydroxyl and superoxide radical scavenger efficiency than naringin(Cavia-Saiz et al., 2010). Similar to naringenin, solution process of naringin in the binary system solvent mixtures show positive relation with ethanol proportion in the solvent mixture and with temperature. The solubility of naringenin was significantly higher than naringin in in methanol, isopropanol, ethyl acetate, petroleum ether, n-butanol, and hexane because of the higher polarity of naringenin.

Naringin was reported to be effective on several metabolic disorders like obesity, hyperlipidemia, hyperglycemia, hypertension, diabetics(Raja Kumar et al., 2019). In vitro studies employing naringin have shown that this flavonoid compound processes higher inhibition effect on dipeptidyl peptidase-4 (DPP-4) than sitagliptin, the first commercial DPP-4 inhibiting oral drug for diabetes treatment in pharmaceutical market(Parmar et al., 2012). Neuroprotective effect of naringin was reported and it was

effective in conditions related to cognitive decline and neuronal injury. Naringin mitigated mitochondrial dysfunction and memory deficits in rats, which both may lead to Alzheimer's disease(Sachdeva et al., 2014). Recently, studies exploring the hepatoprotective effect of naringin are emerging. It is interesting to find the strong candidature of naringin in hepatic function improvements thanks to its potential against hepatotoxicity and improvement on lipid metabolism(Akamo et al., 2021; Hassan et al., 2021; Zhang et al., 2021). Recently, naringin has been studied for its renoprotective effects under certain conditions and been found an agent with great potential in improvement of renal functions(Sehrawat et al., 2021). Naringin was reported having high antioxidant capacity, as 20 mM of naringin produced a free radical scavenger efficiency as high as 95%(CariÑo-Cortés et al., 2010).

UV-Vis absorbance of naringin

Naringin has a characteristic UV-Vis absorption spectrum with a maximum absorbance at 285 nm, and the absorption intensity is affected by factors such as pH, solvent, and temperature(Cordenonsi et al., 2017). λ_{max} of naringin found in literature can be seen in Table 1-5.

Table 1-6 λ_{max} of Naringin

λ_{max} (nm)	Reference	Note
283	(Zhang et al., 2015)	UV spectrophotometer
285	(Cordenonsi et al., 2017)	UV spectrophotometer
283	(Ebrahimi et al., 2020)	UV spectrophotometer

1.6.4.3 Catechin

Catechin((2R,3S)-2-(3,4-dihydroxyphenyl)-3,4-dihydro-2H-chromene-3,5,7-triol) is a flavan-3-ol, a type of secondary metabolite providing antioxidant roles in plants. It belongs to the subgroup of polyphenols called flavonoids. Natural sources of catechin include tea leaves, grape seeds, and the wood and bark of trees such as acacia and mahogany. Catechin has attracted great scientific attention not all for its abundances in human diet but also for its versatile benefits repeatedly reported as anti-inflammatory, antimicrobial, cardio protective, hepato-protective, neural protection, antimalarial and other biomedical applications(Abdulah et al., 2017; Mandel et al., 2005). Figure 1-17 depict chemical structure of catechin.

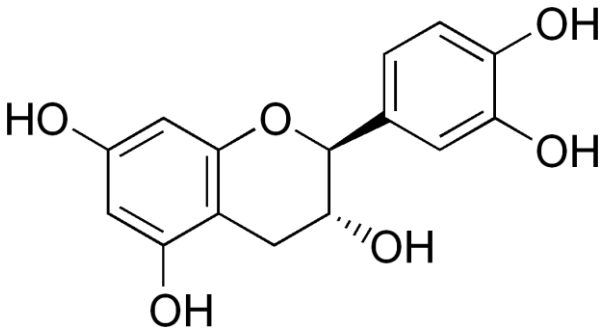


Figure 1-17 Chemical structure of catechin

Catechins are very common in daily diet and beverages e.g. in many types of fruits (apricots, which contain 250 mg/kg fresh weight, are the richest source) and in red wine (up to 300 mg/L), and by far the richest sources are green tea and chocolate. An infusion of green tea contains up to 200 mg catechin (Lakenbrink et al., 2000). Tea is now recognized as the most important polyphenol-rich beverage,

because a growing body of evidence reveals that plant polyphenols in foods and medicinal plants contribute to human health and have done so for many years.

Catechin is a polyphenolic compound who possesses two benzene rings and a dihydropyran heterocycle with a hydroxyl group. Upon contact of enzymes in internal environment after the breakage of integrity of cells, enzymatic oxidation of catechin begins, which is the most important biochemical process. Additionally, as one of the most reducing polyphenols, catechin also involves in the autoxidation (nonenzymatic oxidation) by O_2 mediated by transition metal traces. Catechins are potent antioxidants that can scavenge free radicals and protect against oxidative stress. They can help neutralize reactive oxygen species (ROS) and prevent damage to cells and tissues(Musial et al., 2020). Oxidation of catechin is reported pH-dependent and lower oxidative activity was observed at acidic pH (Bark et al., 2011; Guyot et al., 1995). In deaerated basic buffer solution, the oxidation of catechin molecules seemed to carry through slowly(Bark et al., 2011). Some of the major biological activities of catechins are as follows:

First, they exhibit potent antioxidant activity by neutralizing reactive oxygen species and protecting against oxidative stress (Prasanth et al., 2019). Second, they possess anti-inflammatory effects by inhibiting the production of inflammatory cytokines and enzymes, thus reducing inflammation and alleviating related conditions (Musial et al., 2020). Third, catechins have cardio-protective effects by improving lipid metabolism, inhibiting platelet aggregation, and reducing the risk of cardiovascular diseases (Liang et al., 2017; Mori et al., 2019; H. Zhang et al., 2013). Fourth, they exhibit anti-cancer activity by inhibiting tumor growth, suppressing angiogenesis, and promoting apoptosis (Khan and Mukhtar, 2013). Fifth, catechins have anti-diabetic effects by improving insulin sensitivity, reducing blood glucose levels, and regulating glucose metabolism (Brimson et al., 2023). Sixth, they have potential in weight management by increasing fat oxidation, reducing fat absorption, and improving thermogenesis(Brimson et al., 2023). Finally, catechins exhibit neuroprotective effects by protecting against oxidative stress, reducing neuroinflammation, and promoting neuronal survival, making them potentially useful in the prevention and management of neurodegenerative diseases (Prasanth et al., 2019).

However, the catechins bioavailability is shown to be very low (0.1–1.1%) in humans and also they rapidly oxidize 80% is in just 1 h, thus limited therapeutic potential. As a result, delivery systems were developed to enhance absorption of chitosan in GI tract and improve its stability and hence bioavailability. Nanoparticles based on chitosan has been thoroughly studied as an efficient vehicle to transport catechins with high encapsulation efficiency (Dube et al., 2010; Mandal et al., 2019).

The solubility data of polyphenols, including (+)-catechin, is limited(Cuevas-Valenzuela et al., 2014, p. 6). According to the product information sheet from a supplier (Cayman Chemical), the approximate solubility of (+)-catechin (hydrate) in ethanol and DMF is 100 mg/mL and 50 mg/mL in DMSO, respectively. In PBS (Phosphate-buffered saline) at pH 7.2, the solubility of (+)-catechin (hydrate) is approximately 1.6 mg/mL.

UV-Vis absorption of catechin

Catechins, which are a type of flavonoid compound, exhibit UV-Vis absorption in the range of 200-400 nm, with maximum absorption occurring at around 270-280 nm. The absorption spectrum of catechins typically shows one or more major peaks in this wavelength range, depending on the specific catechin compound and its chemical environment. The literature contains the λmax data of catechin, which can be found in Table 1-6

The specific absorption peaks and intensities in the UV-Vis spectrum of catechin can vary depending on factors such as the presence of other functional groups, pH, temperature, and solvent conditions. UV-

Vis spectroscopy is a commonly used technique to study the electronic transitions and chemical properties of catechin and other flavonoid compounds, and it provides important information about their structural characteristics and potential bioactivity.

It is important to note that the UV-Vis absorption spectrum of catechin can vary depending on the specific catechin compound, as catechin belong to a larger group of flavonoid compounds with diverse chemical structures. Therefore, it's always recommended to refer to specific literature or experimental data for the UV-Vis absorption spectrum of the particular catechin compound of interest.

Table 1-7 λ_{max} data of catechin found in literature

λ_{max} (nm)	Reference	Details
279	(Zu et al., 2006)	HPLC, mobile phase was methanol–acetonitrile–water (40:15:45, v/v/v) containing 1.0% acetic acid
276	Wikipedia	In water
280	(Guyot et al., 1995)	HPLC, pH=3
275	(Bark et al., 2011)	In deaerated water
280	(Li et al., 2012)	HPLC; Mobile phase: 0.1% TFA Trifluoroacetic acid in Milli-Q water (pH=2) mixed with methanol at the volume ratio of 75:25

1.7 Application of CS-TPP system in delivery of polyphenols

Free radicals generated in the body cause oxidative stress, leading to the development of various diseases. Naturally occurring polyphenols have therapeutic potential, but their use is limited due to their short half-life and rapid metabolism. Chitosan, with its biodegradability, biocompatibility, antimicrobial, and antioxidant properties, has been widely used. However, its low solubility and inability to donate H-atoms limit its use as an antioxidant. To overcome this limitation, chitosan has been conjugated with polyphenols to enhance their therapeutic potential and synergistic effects. The use of chitosan-polyphenol conjugates has been reported to be beneficial in the treatment of various diseases for human health(Pattnaik et al., 2022). Figure 1-18 summarizes the advantages of chitosan-polyphenol and the limitations of chitosan and polyphenol.

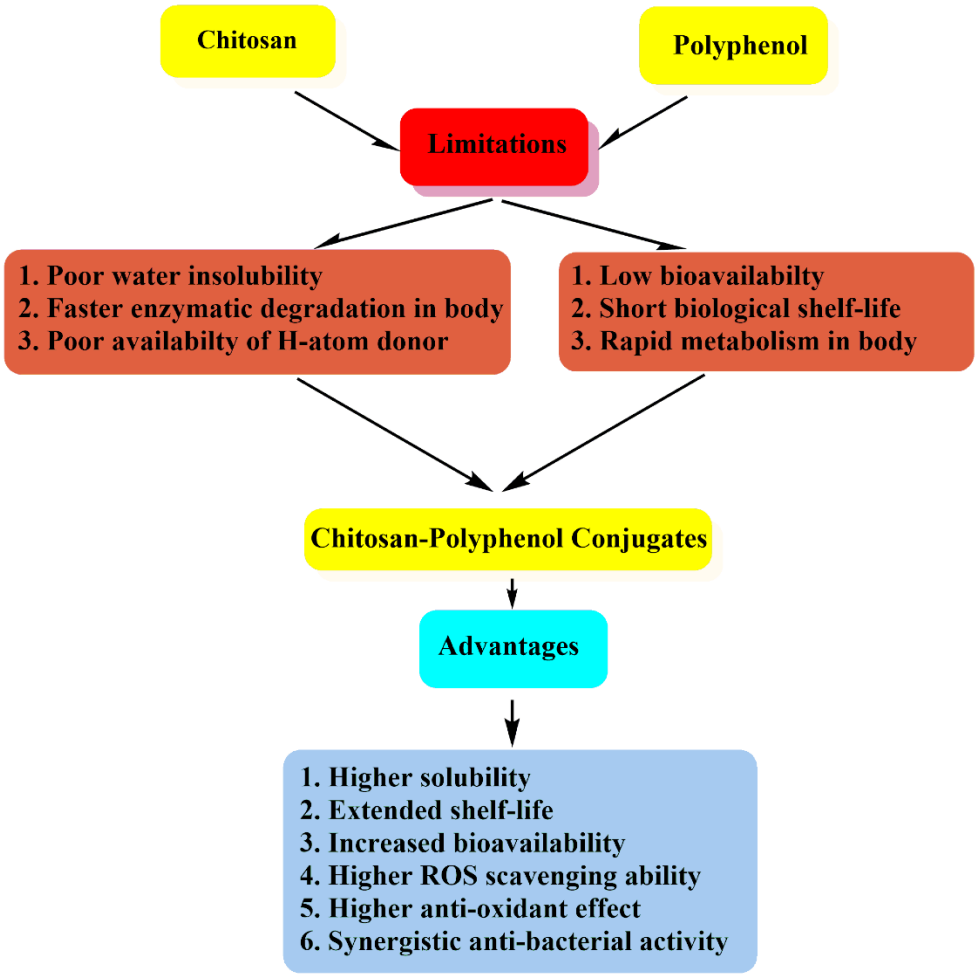


Figure 1-18 Limitations of chitosan and polyphenol, and advantages of chitosan-polyphenol (Reprinted from (Pattnaik et al., 2022), Copyright 2022, Pattnaik et al).

The CS-TPP system has been extensively investigated for its potential in polyphenol delivery due to its numerous advantages. In general, the CS-TPP system has shown great potential for the delivery of polyphenols in various applications, providing opportunities for improved stability, bioavailability, and efficacy of polyphenols in tremendous fields. Overall, the CS-TPP system has demonstrated significant promise for polyphenol delivery in various fields, offering opportunities for enhanced solubility, stability, bioavailability, and effectiveness of polyphenols(Di Santo et al., 2021; Pattnaik et al., 2022; Tang et al., 2013). Between 2010 and 2020, there were more than 60 publications on the subject of "Polyphenol-loaded CS-TPP" (Di Santo et al., 2021). Table 1-7 provides a summary of several examples of Polyphenol-loaded CS-TPP systems that have demonstrated high efficiency in various applications, including drug delivery, food preservation, and tissue engineering.

Table 1-8 Examples of polyphenols loaded CS-TPP

Polyphenols	Particle size (nm)	EE%	Reference
Naringenin	408	70	(Kumar et al., 2015)
Naringenin	88	91	(Shadab et al., 2019)
Naringenin	150-305	57-98	(Maity et al., 2017)
Catechin	129	24-53	(Hu et al., 2008)
Catechin	130	90	(Dudhani and Kosaraju, 2010)
Catechin	138	17	(Kailaku, 2014)
Tea polyphenol	383	97	(Zhang and Zhao, 2015)
Curcumin	261-412	77-85	(Chuah et al., 2013)
Gallic Acid	140-700	64-84	(Lamarra et al., 2016)
Naringin	93	---*	(Malathy and Priya, 2018)

*not informed; EE%= encapsulation efficiency (%)

Additional investigations are required to fine-tune the CS-TPP system to cater to distinct polyphenols and applications, as well as to gain deeper insights into the mechanisms involved in polyphenol release from CS-TPP nanoparticles or microspheres.

2 Scientific approach

2.1 Context

Chitosan (CS) is a naturally abundant material derived from chitin found in crustacean shells and fungal cell walls. Despite its abundance in nature and growing interests in both academia and industries, the utilization of chitosan remains relatively low due to a lack of awareness and knowledge about its properties and benefits across industries. Efforts are being made to address these challenges Research institutions, industry collaborations, and government initiatives are focusing on developing sustainable extraction methods, optimizing processing techniques, and raising awareness about the benefits and applications of chitosan. As knowledge and technology continue to advance, it is expected that the utilization of chitosan will increase in the future.

Similarly, polyphenols found in fruits and vegetables have numerous health benefits but face challenges such as stability, bioavailability, and formulation. Ongoing research aims to overcome these obstacles by exploring techniques like nanoencapsulation using chitosan particles, which can enhance stability, controlled release, and targeted delivery of polyphenols and other substances.

Strategies such as nanoencapsulation, complexation with other CS based delivery systems, coupling with formulation optimization can be used to improve stability, bioavailability, and applicability of polyphenols in various industries. In the literature, the use of chitosan particles in encapsulation of polyphenols offers a versatile approach to enhance the stability, controlled release, and targeted delivery of various substances.

2.2 Position of this work

Sub-micron particles are commonly employed for the encapsulation and controlled release of poorly water-soluble active molecules. The surface characteristics of these particles play a crucial role in determining their properties, such as colloidal stability, redispersion capability after drying or lyophilization, interactions with components of biological media, and release kinetics of the active

molecules. To control the surface properties of the particles, physical adsorption of biopolymers such as proteins or polysaccharides is often employed. These biopolymers can be used directly or after functionalization to enhance their adsorption properties. More recently, the use of biopolymer complexes, such as polysaccharides or polysaccharide-protein complexes, for surface coating of particles has been considered. One of the advantages of this approach is that it eliminates the need for modification or functionalization steps, allowing the use of biopolymers in their native state. The choice of the coating biomaterial also enables the introduction of stealth properties to the particles, thereby preventing any immune reactions.

The objective of this study is to advance the production of sub-micron particles composed of chitosan and coated with physisorbed biopolymer complexes. The fabrication conditions will be carefully adjusted to control the particle size distribution and surface properties, including charge, surface layer thickness, and the nature and conformation of surface macromolecules. Furthermore, these particles will be utilized for the encapsulation of hydrophobic phenolic molecules.

The main purpose of this study is also to investigate the release mechanisms and control the release rate of the active molecule based on the properties of the self-assembled surface coating and physicochemical parameters of the surrounding medium, such as pH and polarity. Furthermore, the aim is to explore and establish the correlation between the structure of the composite material and the release profile of the encapsulated molecules. This knowledge will be valuable for designing novel delivery systems that can accurately target specific sites and achieve controlled release, thus addressing the specific requirements of various industries.

2.3 Objectives

- Prepare and characterize controllable CS-TPP particles
- Entrap polyphenol molecules into CS-TPP particles
- Obtain the release profile of encapsulated molecules in various dissolution media and explore the its relationship with particulate structure

2.4 Research questions

This research work revolves around the following three group of questions:

1. Which are the factors that influence particle properties (size distribution and surface charge) and what are their impacts?
2. Which are proper operation under which conditions to achieve successful encapsulation of polyphenol molecules in CS-TPP particles? What are their encapsulation efficiency (EE, %)of each case? Is there any obvious relationship between EE% and particle properties?
3. Release properties of loaded molecule from CS-TPP particles? What factors could influence release profiles?

2.5 Experimental design

The experimental approach was built in three successive parts:

Part 1: Optimization of preparation process of blank CS-TPP particles

The preparation process of CS-TPP particles was explored by considering various variables such as the concentration of materials, gelation temperature, mass ratio of materials, and volume ratio of materials, as reported in the literature and preliminary experiments. To further functionalize the particle structure, a coating of alginate salt was applied to the CS core through the polyelectrolyte complexation of ALG and CS. The resulting CS particles and uncoated CS particles were thoroughly characterized using multiple techniques, including DLS, SEM, and laser diffraction size analyzer, to analyze their properties in terms of size distribution, size evolution, surface charge, and morphology.

Part 2: Encapsulation

The crosslinked CS based network formed during the ionic gelation process provides an excellent matrix for encapsulating various therapeutic agents or active compounds. The particles can control the release of encapsulated substances, allowing for sustained and controlled release over time.

Naringenin, naringin and catechin were selected as candidate molecules to be entrapped in CS-TPP particles. These molecules were incorporated into CS particles by mixing them with a CS solution during the particle preparation process. After separating the CS particles using an appropriate method, the amount of free molecules (unloaded portion) was measured using UV spectrophotometry. This indirect measurement method allowed for the calculation of the encapsulation efficiency (EE, %) of the molecules.

Part 3: Release of molecule

To ensure appropriate conditions for the dissolution testing, the solubility of the loaded molecules was investigated. The release properties of the molecules from the CS particles were monitored in different media with varying pH, solvent composition, and dissolution volume. This allowed for a comprehensive understanding of the dissolution behavior and release kinetics of the loaded molecules from the CS particles.

3 Material and methods

Chitosan (C2395, 5-20mPa.s, 0.5% in 0.5% Acetic Acid at 20°C) was purchased from TCI (Tokyo). Naringenin (CAS No.: 67604-48-2, W530098, Mw: 272.25 g/mol), naringin (CAS No.: 10236-47-2, 71162, Mw: 580.53 g/mol), catechin (CAS No.: 154-23-4, 43412-10MG, Mw: 290.27 g/mol), sodium alginate (CAS No.: 9005-38-3, W201502) and sodium tripolyphosphate (TPP) (CAS No.: 7758-29-4, 238503, Mw: 367.86 g/mol) were purchased from Sigma-Aldrich.

3.1 Characterization of materials

3.1.1 Chitosan

3.1.1.1 UV-Vis

A series of chitosan solutions were prepared by dissolving chitosan powder into 1% acetic acid (v/v). Concentration of chitosan solutions were 0.25, 0.5, 0.75, 1.0 and 1.5 g/L, respectively. Then the samples were subjected to full-wavelength scanning from 200 to 500 nm using Jasco V-770 UV-Visible spectrophotometer with a resolution of 0.5 nm. Sample temperature was fixed at 20°C with the help of a Heidolph RotaChill Small Chiller.

3.1.1.2 Transform infrared spectroscopy Fourier (FTIR)

The FTIR spectrum of chitosan was analyzed using FTIR spectrometer (Brucker, Germany) equipped with a DTGS pyroelectric detector. 30–50 mg of chitosan was mixed with a pinch of potassium bromide and

compressed to a tablet by a punch on the crystal. 64 scans were carried out at a resolution of 6 cm^{-1} and at an acquisition frequency of 10 kHz at room temperature in a spectral range from 400 to 4000 cm^{-1}. A Fourier transform was applied to the interferogram in order to obtain spectra in using the OPUS software (Brucker).

3.1.1.3 ^{1}H NMR

Deuterium chloride (DCl) and Deuterium oxide (D_2O) were purchased from Sigma-Aldrich. All NMR spectra were recorded using a Bruker Avance II NMR spectrophotometer. Magnet NMR-frequency used was 300 MHz, unless otherwise specified. Table 3-1 present experimental conditions of ^{1}H NMR spectroscopy in details.

Table 3-1 Experimental details of ^{1}H NMR spectroscopy

Instrumentation	
NMR Spectrometer	BRUKER Avance II
Magnet NMR-Frequency	300 MHz
Probe Head	5mm PABBO BB
Nuclei	^{1}H
Experimental Conditions	
Solvent	D_2O-DCl =98:2
Temperature	343 K
Sample Concentration	5 g/L

Sample preparation and the DDA% determination of chitosan

10 mg of sample (commercial chitosan and purified chitosan) was dissolved in a solution composed of 1.96 mL of D_2O and 0.04 mL of DCl (2%, v/v) at room temperature with stirring during at least 30 minutes to ensure complete dissolution. Then previous solution was filtrated by cotton to remove any possible impurities. 0.5-0.6 mL of dissolved sample solution was transferred into a clean 5 mm diameter NMR tube via a glass dropper and a cap was added on the top of the tube. The sample tube was inserted in the magnet and allowed to reach thermal equilibrium by waiting 15 min before performing the experiment.

^{1}H NMR spectra were recorded on a BRUKER Avance II NMR spectrometer using a 5mm PABBO BB probe. The experiments were run at 343 K and 300 K, temperature to avoid interference of solvent (HOD) peak with any of chitosan's peaks (Lavertu et al., 2003).

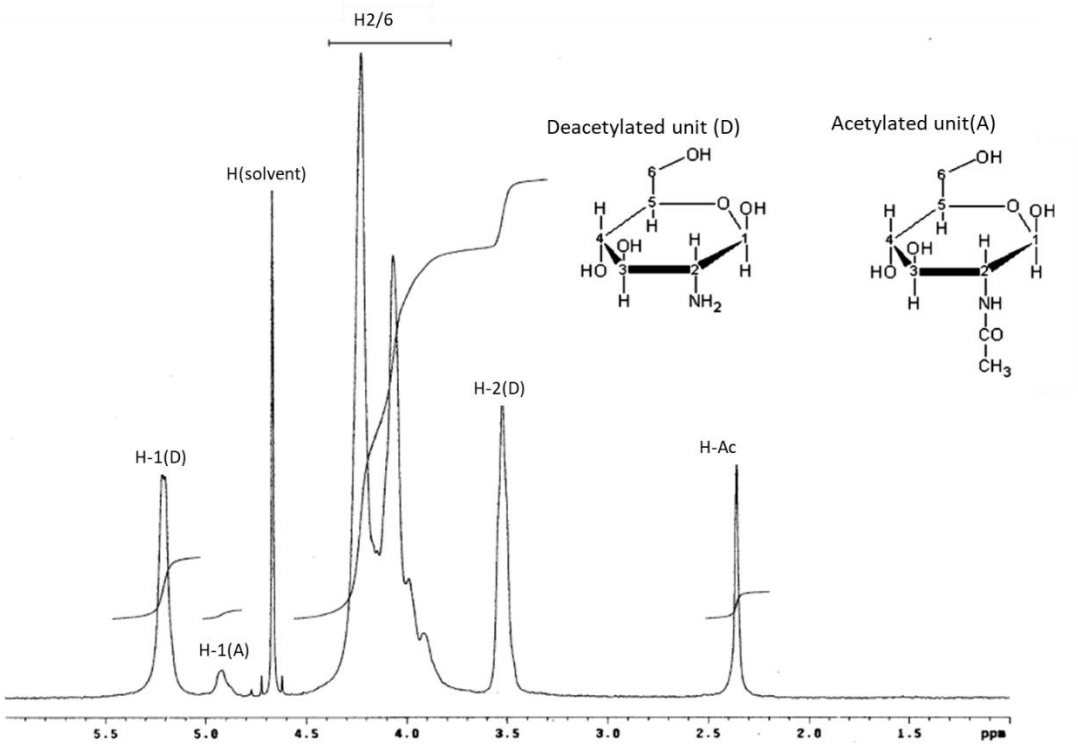


Figure 3-1 chitosan structure and Chitosan ^{1}H NMR spectrum at 343 K.

Figure 3-1 presents chitosan structure and ^{1}H NMR spectrum of chitosan at 343 K. Chitosan is a biopolymer that consists of the acetylated unit and the deacetylated unit and both units display characteristic ^{1}H NMR signals the intensity of which can be estimated and utilized to calculate DDA%. For example, ^{1}H NMR signal of Acyl-H (HAc) can characterize acetylated unit for its absence in deacetylated unit. Similarly, the sum of both units can be represented by the signal from protons H2, H3, H4, H5, H6 (H2/6), as they are in common in both monomers. Following *Eq.*3.1 summarize one way to calculate DDA% in chitosan (Hirai et al., 1991):

$$\mathrm{DDA\%} = \left(1 - \left(\frac{\frac{\mathrm{HAc}}{3}}{\frac{\mathrm{H2/6}}{6}}\right)\right) \times 100\% \qquad (Eq.\,3.1)$$

Likewise, as the integrals of the peak of proton H_1 in deacetylated unit(H_1-D), DDA% can also be calculated by *Eq.*3.2:

$$\mathrm{DDA\%} = \left(\frac{\mathrm{H1D}}{\mathrm{H1D} + \frac{\mathrm{HAc}}{3}}\right) \times 100\% \qquad (Eq.\,3.2)$$

DDA% of samples were calculated by those two methods to compare and confirm the accuracy of results.

3.1.1.4 Mw determination of chitosan by SEC-MALS

Size exclusion chromatography (SEC-MALS, Size exclusion chromatography with multi-angle laser light scattering detectors) allows the determination of the average molar masses and the investigation of the molar mass distribution of commercial and purified chitosan.

For each sample, a solution was made by dissolving the polysaccharide to be tested in an acetate buffer (acetic acid 170 mM, ammonium acetate 200 mM, pH=4.5). This buffer was filtered on a membrane with a porosity of 0.45 µm (Durapore® 47 mm diameters, Millipore) at 20°C. Buffer acetate also served as the mobile phase for chromatography. The analyzes were carried out at 30°C at a flow rate of 0.35 mL/min utilizing a polymethyl-methacrylate column (Malvern, A4000). A SEC-MALLS VISCOTEK 305 TDA (Malvern instruments) and a Shimadzu HPLC pump (Shimadzu) were used for the molar mass determination.

To explore proper concentration of each sample, solutions of 2.5g/L, 5g/L and 10g/L of commercial chitosan and purified chitosan were prepared in pH 4.5 buffer. Then 100 µL of each sample was injected and pumped into a Malvern A4000 Polymethyl-methacrylate column at a flow rate of 0.35 mL/min. RALLS detector was used to detect and collect light scattering signals processed by software OmniSEC (version 11.01, Malvern Panalytical).

3.1.2 Polyphenols

Naringenin, naringin and catechin were characterized by both ^{1}H NMR spectroscopy and UV-VIS spectrophotometry.

3.1.2.1 ^{1}H NMR

10 mg of naringenin, 20 mg of naringin and 80 mg of catechin were dissolved in 2 mL of DMSO-d_6, respectively. Then, these solutions were shaken on a horizontal shaking bed for one night. After filtration by cotton to remove insoluble substances, 0.5 mL of each solution was added into a 5 mm NMR tube for NMR analysis. ^{1}H NMR spectra were acquired on a BRUKER Avance II NMR spectrometer using a 5mm PABBO BB probe at 400 MHz. The experiments were run at 298 K. The sample tube was inserted in the magnet and allowed to reach thermal equilibrium by waiting 10 min before performing the experiment.

3.1.2.2 UV-Vis

Solutions of naringenin were obtained by serial dilution of an ethanol stock solution of naringenin with water to desired concentration (3.3, 4.4, 10 ,13.3, 20 and 40 mg/L, respectively). Those solutions were analyzed by UV-Vis spectrophotometry at 20°C. UV-VIS absorbance of samples was read and plotted against corresponding concentrations of solutions to establish calibration curve. With the help of this calibration curve, the absorbance results collected through experimentation could be directly transformed into concentration by extrapolating through the linearity range.

Similarly, solutions of naringin and catechin were prepared and the corresponding calibration curves were obtained the same way. Linearity range of UV absorbance of naringin and catechin were 6-37 mg/L (0.011-0.065 mmol/L) and 5 -100 mg/L (0.02-0.34 µmol/L), at 282nm and 280nm, respectively.

3.2 Preparation of CS-TPP particles

Ionic gelation of chitosan and TPP (tripolyphosphate) is a widely used method for the preparation of chitosan-based nanoparticles or microparticles. It relies on the electrostatic interactions between the positively charged amino groups of chitosan and the negatively charged TPP ions.

The resulting CS-TPP particles exhibit characteristics such as controlled release properties, biocompatibility, and potential for encapsulation of various therapeutic agents or active compounds. They have applications in drug delivery systems, wound healing, tissue engineering, and other biomedical fields.

It's worth noting that the specific parameters and conditions for the ionic gelation of chitosan and TPP can be adjusted based on the desired particle properties and the intended application.

3.2.1 Purification of chitosan

Among available commercial chitosan materials, shell of crustaceans is the most common source. Remaining protein after chemical deacetylation process i.e. vigorous treatment by acids and bases at high temperature, is the main impurity in commercial chitosan. As chitosan is considered as an interesting biopolymer in medical applications, protein contamination should be strictly limited to avoid slightest potential safety issues. On the other hand, high purity of starting chitosan material is also a good guaranty for the high integrity and quality of product in nanoparticle fabrication process. For this purpose, in this work, further purification of purchased chitosan was carried out by the following steps (Figure 3-2).

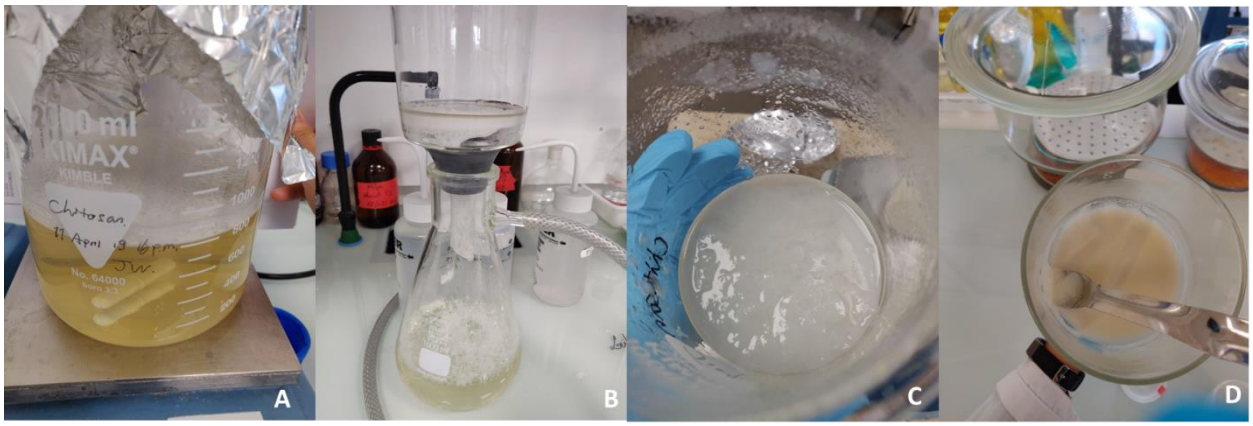


Figure 3-2 Process of purification of commercial chitosan.

Dissolve bulk chitosan into proper volume of 1M NaOH solution. Heat and maintain temperature at 70°C of above mixture under constant magnetic stirring for 2 hours. (A) Dissolution of raw chitosan material into strong base; (B) Vacuum filtration of chitosan basic solution to remove insoluble impurities; (C) Adjust pH value of filtrate solution to 8. Yellowish solution turned into more viscous white slurry; (D) Vacuum filtrate above slurry to remove excess water, then let the filter cake dry in a 40 °C oven for one night.

Filtrate roughly above mixture via glass filter funnel (Por.1, VitraPOR® ROBU), discard filtrated liquid then wash filtrated mass by proper volume of distilled water (around 8 times of original volume) until pH of filtrate liquid close to 8. Then vacuum filtrate above chitosan slurry to remove further residue water and then dry filtrated mass in a 40°C oven overnight.

Dissolve dried chitosan mass into 0.2M acetic acid solution, keep at 40°C under magnetic stirring for 3-4 hours. Remove insoluble impurities via vacuum filtration then adjust pH of filtrated liquid to 7-8. Filtrate obtained chitosan slurry (white) to remove extra water then freeze dry to obtain final product. Filtrated chitosan and raw commercial chitosan were characterized afterwards by FTIR and ^{1}H NMR spectrometry and SEC-MALS.

3.2.2 Preparation of particles

Ionic gelation method was utilized for preparation of CS-TPP particles for its ease in operation and mild conditions. Generally, chitosan was dissolved in 1% (v/v) acetic acid and diluted properly to prepare CS solutions with various concentrations: 0.06%, 0.1%, 0.2%, 0.3%, 0.4%, 0.5%, 1%, 3% (w/v). Likewise, TPP was dissolved in MilliQ ultrapure water and diluted properly to obtain TPP solutions with different concentrations: 0.05%, 0.1%, 0.267%, 0.5% (w/v). Certain volume of CS solution is poured into a container put on a magnetic stirrer (equipped with hotplate and temperature probe). Then desired amount of TPP solution is added drop by drop into CS solution under magnetic stirring. After addition of TPP, the container is then sealed by an Eppendorf Parafilm (a stretchable, moldable, waterproof, and self-adhering thermoplastic film). Keep stir for at least 30 minutes to make sure fully crosslinking. The crosslinking of chitosan and TPP has been often reported as a modulable process by varying operational parameters such as concentrations of crosslinking agents, temperature, mass ratio of crosslinking agents, ratio of opposite charges, pH and so on.

Series of experiments were designed and conducted to explore effect of these factors on particle properties in terms of size distribution, morphology, surface charge, encapsulation capacity, etc. For experimental condition details of the preparation of those samples see Annex I.

3.2.2.1 Preliminary factors

3.2.2.1.1 Purification of chitosan

To explore if difference exists among particles prepared by raw purified chitosan, sample-010 and 015 as well as sample-007 and 012 were compared in pair. Except for the chitosan source, within each group, samples were prepared under same concentrations (concentration and volume of crosslinking agents and at the same temperature).

3.2.2.1.2 Stirring speed

All of these experiments were carried-out at the same magnetic stirring rate at 600 rpm, unless otherwise specified herein. Higher stirring rate (800 rpm) was reported inducing smaller particle size but moderate rate (400 rpm) might lead to optimum interaction between the chitosan solution and the TPP droplets thus lower PDI of generated particles (Abdel-Hafez et al., 2014).

3.2.2.1.3 Scale of batch

To explore the influence of batch volume, i.e. is the total volume of crosslinking agent solutions, on CS-TPP particle quality specially in terms of particle size and its distribution, three samples were designed and prepared by syringe dropping 0.1% (w/v) TPP solution into 0.2% (w/v) chitosan solution following conditions listed in details in Table 3-2. Volume of crosslinking agents varied but volume ratio of CS/TPP and other conditions were kept unchanged, and as a result, batch volume was the single variable to be examined. Here, batch volume of sample-013 is 5 times of the one of sample-014 and batch volume of sample-011 is twice of the one of sample-013 and 10 times of sample-014.

Table 3-2 Samples prepared with different scale of batch to explore influence of batch volume on CS-TPP particle size and size distribution.

Sample	C_{CS} (mg/mL)	C_{TPP} (mg/mL)	V_{CS}(mL)	V_{TPP}(mL)	Batch Volume(mL)	Temperature(°C)
011	2	1	100	30	130	RT
013	2	1	50	15	65	RT
014	2	1	10	3	13	RT
026	3	1	10	3	13	45
028	3	1	50	15	65	45

3.2.2.2 Factors influence particle size

3.2.2.2.1 Cross-linking temperature

To explore crosslinking temperature influence on particle size, two groups of samples with various chitosan concentration were prepared. The crosslinking temperature was set up at room temperature (20±2°C) or 45/50°C. The heat plate and the thermal probe equipped on the magnetic stirrer were used for temperature control (Figure 3-3): (A) Gelation of CS and TPP at room temperature (20±2°C). Real-time temperature was monitored by a thermal probe. (B) Crosslinking of CS and TPP at 45 °C. (C) Syringe addition of TPP solution into CS solution drop by drop under continuous stirring. Visible opacity occurred instantly when TPP drops were dripped into CS solution in the container. (D) After addition of TPP solution, continue to stir for at least 30 minutes to make sure fully crosslinking of CS and TPP. The suspension remained opaque but no visible precipitate was observed. Experimental conditions details are shown in Annex I_preparation conditions of CS-TPP particles.

To explore effect of preparation temperature on properties of CS-TPP particles, samples were prepared following conditions listed in Table 3-3. Sample-009 and Sample-010 were prepared by following steps. 33 ml of 0.1% (w/v) TPP solution was added into 100 ml of 0.2% (w/v) chitosan solution drop by drop under magnetic stirring at 600 rpm for 30 min at room temperature (20±2°C). Sample-007 was prepared with the same conditions except that chitosan solution was heated to and maintain at 50°C all along the formation of particles.

Sample-012 and Sample-015 were prepared using raw chitosan without purification. Sample-012 was prepared by dropping 30 ml of 0.1% (w/v) TPP solution into 100 ml of 0.2% (w/v) chitosan (CS(b)) solution under magnetic stirring. Sample-015 was prepared with the same conditions except that crosslinking temperature was set up at 50°C all along the formation of particles.

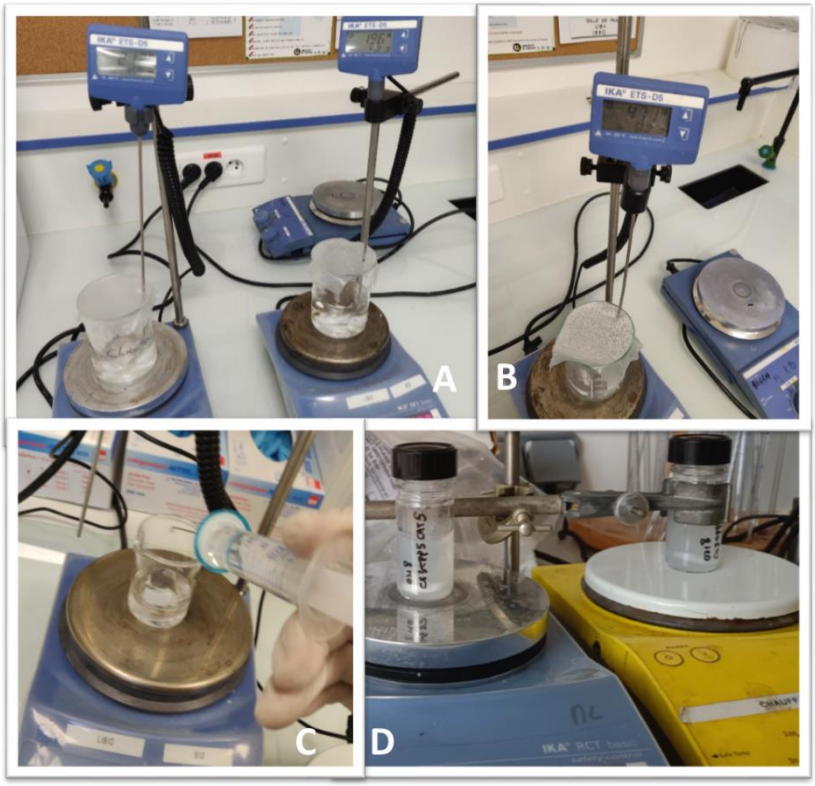


Figure 3-3 Experimental photos of preparation CS-TPP particles via crosslinking under magnetic stirring at various temperatures.

Sample-029 was prepared by adding 3.3 ml of 0.1% (w/v) TPP solution into 10 ml of 0.3% (w/v) chitosan solution drop by drop under magnetic stirring at 600 rpm for 30 min at room temperature (20±2°C). On the other side, sample-024 was prepared with the same conditions except that chitosan solution was heated and maintain at 45°C all along the formation of particles.

Table 3-3 Experimental conditions of samples prepared at room temperature and higher temperatures. Volume ratio of CS/TPP of those samples was fixed to 3.

Sample	C_{CS} (mg/ml)	C_{TPP} (mg/ml)	V_{CS}(ml)	V_{TPP}(ml)	Temperature(°C)
007	2	1	100	33	50
009	2	1	100	33	RT
010	2	1	100	33	RT
012	2	1	100	30	50
015	2	1	50	15	RT
024	3	1	10	3.3	45
029	3	1	10	3.3	RT

3.2.2.2.2 Concentration of chitosan

Concentration of chitosan has been repeatedly reported related to particle size in a large amounts of research articles (Gan et al., 2005 ; Hu et al., 2008; Li et al., 2021; Sreekumar et al., 2018). To explore the influence of concentration of chitosan on particle size, a series of samples (sample-014, 029, 037, 040 and 041, detailed conditions can be seen in *Annex_I*) were prepared with various concentration of chitosan from 0.1% to 0.5% (v/v) at room temperature. Similarly, another series of samples (sample-008, 024, 038; detailed preparation conditions can be seen in *Annex_I*) were prepared with various concentration of chitosan from 0.2% to 0.4% (v/v) at 45°C. With pre-established conditions that, CS/TPP volume ratio of those samples is fixed at 3; all experiments were conducted under magnetic stirring at 600 rpm for 30 min.

3.2.2.2.3 CS/ TPP mass ratio

Mass ratio of CS/TPP has been reported as a factor which can affect CS-TPP NPs size in lots of researches(Abdel-Hafez et al., 2014; Gan et al., 2005; Hu et al., 2008; Sreekumar et al., 2018). But contradictory discoveries were found on effect of CS/ TPP mass ratio on particle size. Q. Gan et al. have reported that CS/ TPP mass ratio had positive effect on particle size at the range from 3:1 to 7:1 (Gan et al., 2005). Whereas, Hu et al. found that the particle size decreased linearly with the increasing CS/TPP mass ratio (Hu et al., 2008). On the other hand, S.M. Abdel-Hafez et al. announced the increase in CS/TPP mass ratio had a fluctuating effect on the particle size (Abdel-Hafez et al., 2014).

3.2.2.2.4 Molar ratio of charges ($NH_3{}^+/P_3O_{10}{}^{5-}$)

Essentially, the ionic gelation of chitosan and TPP is driven by the interaction between positive charges of NH_3^+ groups in chitosan polymer chains and the negative charges of $P_3O_{10}{}^{5-}$ from TPP molecules. So the molar ratio of charges might significantly influence CS-TPP particle formation process.

Molar ratio of charges ($NH_3{}^+/P_3O_{10}{}^{5-}$) can be calculated by following equations:

$$n_{positive} = n_{NH_3{}^+} = m_{cs} \div \left(M_n + \frac{1 - DDA}{DDA} * M_m\right)$$

$$n_{negative} = n_{P_3O_{10}{}^{5-}} = 5 \times n_{\mathrm{TPP}}$$

Where,

$n_{NH_3{}^+}$ is the molar quantity of $NH_3{}^+$;

$n_{P_3O_{10}{}^{5-}}$ is the molar quantity of $P_3O_{10}{}^{5-}$;

n_{TPP} is the molar quantity of TPP;

m_{cs} is weight of chitosan used;

M_n is molecular weight of deacetylated molecule in chitosan polymer;

M_m is molecular weight acetylated molecule in chitosan polymer;

DDA is the degree of deacetylation of chitosan.

3.2.2.2.5 Concentration of particles

Concentration of particles depends on total mass used in the formation of particles and the final volume of liquid where final product was dispersed. It may also affect size of formed CS-TPP particles as individual particle may be intend to aggregate and form larger particles when the suspension is too concentrated. In addition, from the point of view of industries, it is an interesting parameter to know as it expresses ratio of gain (particles) to waste (liquid in this case).

$$\text{Concentration of particles} = \frac{C_{CS} \times V_{CS} + C_{TPP} \times V_{TPP}}{V_{Total}}$$

To explore effect of CS/TPP mass ratio, ratio of charges and particle concentration on CS-TPP particle formation, sample-003, 023, and 029 were prepared. A solution of 0.3% (w/v) purified chitosan (CS(p)) was prepared in 1.0% (v/v) glacial acetic acid. Solution of 0.1% (w/v) TPP was prepared. By varying volume mixed of TPP solution with chitosan solution, mass ratio of CS/TPP, molar ratio of charges ($NH_3{}^+/P_3O_{10}{}^{5-}$) , and concentration of particles were altered. All experiments above were conducted at room temperature under magnetic stirring at 600 rpm for 30 min. Values of above three parameters of those samples were listed in Table 3-4. Preparation condition details are present in *Annex I*.

Table 3-4 Three samples with various mass ratio CS/TPP and their size information.

Sample	Ratio Mass CS/TPP	Molar ratio of charges ($NH_3{}^+/P_3O_{10}{}^{5-}$)	Particle concentration (g/L)	Z-average(nm)	PDI
023	2.5	1.2	1.9	140	0.44
027	7.5	3.6	2.4	227	0.47
079	9.0	4.4	2.5	172	0.50

3.2.2.3 Preparation of CS-TPP Microparticles

While the individual factors of CS and TPP did not exhibit a direct proportional relationship with particle size, there was a trend observed where an increase in both factors resulted in an increase in particle size, which could even exceed the nanoscale to become micro-sized. Additionally, it was observed that instead of dropping TPP solution into CS solutions, the reverse approach of adding CS solution dropwise into TPP solution under magnetic stirring could also result in the formation of larger particles. Based on these two ideas, a series of experiments were designed in this work to prepare CS-TPP microparticles

Solutions of 0.3%, 0.5%, 1% (w/v) of chitosan in 1% (v/v) glacial acetic acid were prepared. Aqueous solution of 0.5% (w/v) of TPP was prepared. The fabrication steps of CS-TPP microparticles are similar to CS-TPP nanoparticles and used the same apparatus. The sonication effect on particle size was also studied by treating newly prepared CS-TPP microparticle suspension with an ultrasonic processor (Vibra-Cell™, VCX 750). During the treatment of ultrasonic probe. CS-TPP suspension was immerged into an ice bath to compensate the heat release effect of probe and to keep temperature at the selected value.

Mastersizer was employed to analyze particle size beyond the range of the ZETASIZER (DLS), which can only measure particles in the nanometer to micrometer range. The surface area moment mean D[3,2] was used as the size measurement since it is relevant for cases where specific surface area is important, such as bioavailability, reactivity, and dissolution. This measurement is particularly sensitive to the presence of fine particulates in the size distribution. On the other hand, the volume-based distribution gives more weight to larger particles in the population.

In this study, both D[3,2] and volume size distribution were used to represent the overall size distribution of CS-TPP particles since the final product consists of individual CS-TPP particles and their agglomerates. This approach considers both the size of individual particles and the presence of larger agglomerates in the particle population, providing a comprehensive representation of the particle size distribution.

Ultrasonication treatment

To achieve more uniform particle size, ultrasonication was utilized.

A CS5TPP5R2.5 sample was prepared by mixing 32 ml of 0.5% (w/v) TPP solution with 80 ml of 0.5% (w/v) CS solution under 600 rpm magnetic agitation at room temperature for at least 1 hour. Subsequently, approximately 20 ml of the resulting CS-TPP suspension was subjected to ultrasonic treatment using a Vibra-Cell™ ultrasonic processor (amplitude: 30%, duration: 2 min 30 s, pulse mode: 1 s ON/1 s OFF). The size of the CS5TPP5R2.5 sample before and after sonication was measured using a Laser Diffraction size analyzer to obtain size information.

3.2.2.4 TPP-CS microparticles (Reverse addition of CS into TPP)

The addition way of TPP into chitosan is usually vaguely stated in the literature and some has reported the drop speed of TPP could be a factor that influence particle propertied like for instance particle size and its distribution. To the best of our knowledge, very few research has reported what would have happened if conversely add CS solution into TPP solution in details. Keep this question on mind, a series of experiments were designed to explore the answer by curiosity. Would larger particles be formed in this way or otherwise?

Reverse the way of addition in CS-TPP preparation process. in other words, drop chitosan solution into TPP solution under magnetic agitation. To distinguish with normal preparation method, i.e. drop-wisely add TPP solution into CS solution to produce CS-TPP particles, samples prepared by this reverse method was noted “reverse” to underline its abnormality.

3.2.2.5 Preparation of ALG coated CS-TPP particles

The synthesis of the ALG coated CS core-shell nanoparticle was performed according to previously described method of Maity et al., (2017) with modification. Sodium alginate solids was dissolved in DPBS (Dulbecco’s Phosphate-buffered saline. pH 7.1-7.5) buffer. Briefly, blank CS-TPP nanoparticles (CS-NPs) were firstly prepared as above mentioned. To obtain ALG coating CS-NPs. suspension of CS-NPs was added drop by drop into ALG solution under sonication (Vibra Cell, Model 75043, 750 Watt, Figure 3-4) in an ice bath to counteract the heat effect caused by sonication. After addition of CS-TPP NPs, the mixed suspension was magnetically stirred (750 rpm) for 30 min followed by centrifugation to remove extra ALG. Then $CaCl_2$ solution was added into the mixture to gel with and form ALG coating. Centrifugation was then utilized to remove extra Ca^{2+}. Afterward pellets were redispersed into Milli-Q water to wash established particles.



Figure 3-4 Addition of CS-TPP into ALG solution under sonication within an ice bath. and the pulse on mode was used to help temperature control of samples during sonication treatment

Size evolution of ALG coated CS-TPP particles

To investigate the size evolution during the ALG coating process, samples-026, 030, 035, and 072 were chosen as examples. The CS-TPP particles were prepared as described previously at a temperature of 45°C, and the ALG shell was added through polyelectrolyte complexation. The experimental conditions can be found in the supplementary materials (Annex I). Sample 026 was prepared by adding TPP solution to a chitosan solution under stirring, as specified in the sample list. Sample-035 was obtained by crosslinking CS-TPP nanoparticles from sample-026 with alginate sodium. Sample-072 was prepared by adding a $CaCl_2$ solution to the suspension of sample-035, followed by two washes with water. The size evolution during this process was monitored using dynamic light scattering (DLS) to measure the particle sizes.

3.3 Characterization and morphology of the prepared chitosan particles

The morphology of particles refers to their physical structure, shape, and size distribution Depending on the synthesis method employed, particles may exhibit a range of shapes, from simple spherical to more complex structures such as rods, cubes, and others. The morphology of particles plays a crucial role in determining their properties, including stability, surface area, drug loading capacity, and release kinetics. Consequently, achieving optimal particle morphology is critical for successful application in various fields. Techniques used to analyze particle morphology are outlined below.

Dynamic Light Scattering (DLS)

The Dynamic Light Scattering (DLS) technique was utilized to determine the mean particle size and zeta potential. The analysis of the nanoparticle dispersions was conducted at a viscosity of 0.908 cp and a refractive index of 1.33, and the measurements were based on intensity. The intensity of autocorrelation was measured at a scattering angle of 173° at 25 °C., and the particle size was calculated using the Stokes-Einstein equation with the Zetasizer Nano ZS instrument from Malvern Panalytical (UK). The mean and standard deviations were calculated based on triplicate measurements.

Laser Diffraction

Particle size of chitosan microparticles was determined by laser particle size analyzers (Mastersizer 2000/3000, Malvern Panalytical, UK) utilizing laser diffraction methodology. It achieves this by detecting the intensity of light scattered when a laser beam interacts with a dispersed particulate sample. Subsequently, this information is evaluated to determine the size of the particles responsible for generating the scattering pattern. The D_{50}, which is the particle size at which 50% of the cumulative volume of particles is reached in the particle size distribution profile, along with the particle size distribution span (span = (D_{90} - D_{10}) / D_{50}) were determined. The D_{90} and D_{10} correspond to the particle sizes at which 90% and 10% of the cumulative volume of particles are reached, respectively, in the particle size distribution profile.

The CS microspheres were suspended in a liquid medium and injected into wet dispersion units with a stirrer to prevent aggregation between the microspheres. The stirrer was operated at a speed of 2000 rpm. The average volume mean particle size was then measured by conducting the experiment in triplicate.

Scanning Electron Microscopy (SEM)

Chitosan particles were visualized using Scanning electron microscopy (SEM) (Hitachi S4800, Japan). The CS particle suspension was applied onto an aluminum pad and allowed to air dry at room temperature for 48 hours. After drying, the sample was coated with a thin layer of carbon using a metallization process. The pictures were taken at an excitation voltage of 3 kV and a magnification of 0.6, 2.2, 6, 18, 20, 45, 60, 80 or 110 k.

3.4 Encapsulation of polyphenols into CS-TPP particles

Figure 3-5 and Figure 3-6 schematically present encapsulation experiments of polyphenol molecules into CS-TPP particles and ALG coated CS-TPP particles.

3.4.1 Encapsulation Efficiency (EE, %)

Encapsulation efficiency is an indicator used to evaluate a formulation's ability to trap desired molecules within particles. Mathematically, it is calculated as the percentage of loaded molecule in comparison to the total amount of substance. Determination of EE (%) can be accomplished by direct method and indirect method. By direct method, EE (%) can be calculated using the following formula ($Eq.3.3$):

$$EE\ (\%) = \frac{Amount\ of\ substance\ encapsulated}{Total\ amount\ of\ substance\ added} \times 100 \qquad (Eq.3.3)$$

Because of the difficulty to determine directly the amount of substance encapsulated within the particles, indirect method is commonly used. By indirect method, the Encapsulation Efficiency can be determined by subtracting the amount of unencapsulated drug by UV spectrometry.

In this work, active molecules were encapsulated into CS-TPP particles and ALG coated CS-TPP particles respectively.

The amount of non-encapsulated drug equals to the sum of the amount in the supernatant after centrifugation or filtration of molecule-loaded CS-TPP solutions(*S*), and the amount in the two supernatants after twice washing (*W1* and *W2*). UV-Vis spectrophotometer results shown that after twice washing, signals of molecules residual in washing liquid decreased strongly, which indicates that free molecules have been eluted after two washings (More details presented in Annex III. Encapsulation-washing step).

In the case of ALG coated CS-TPP particles, mixture of active molecule and CS-TPP particles was dropped into ALG aqueous solution then centrifuged. The amount of active molecule in the supernatant after this first centrifugation was determined by UV spectrometry (*S*). The pellet was redispersed into $CaCl_2$ aqueous solution and was centrifuged after incubation. The amount of active molecule in this supernatant after centrifugation was determined by UV spectrometry (*W1*). The pellet was then washed by water and centrifuged. Amount of active molecule in the supernatant after this third centrifugation was measured UV spectrophotometrically (*W2*).

So, EE (%) can, therefore, be calculated by dividing that unencapsulated amount by the total amount of drug added (*T*, which is known) ($Eq.3.4$).

$$EE(\%) = \left(1 - \frac{S + W1 + W2}{T}\right) \times 100\% \qquad (Eq.3.4)$$

Where,

T: Total mass of molecule (g)

S: Mass of molecule in supernatant after first centrifugation or in the filter liquor after filtration (g)

$W1$: Mass of molecule in first washing liquid (g)

$W2$: Mass of molecule in second washing liquid (g)

3.4.2 Loading capacity (LC%)

Loading capacity is another evaluation of performance of encapsulation, i.e. the amount of active substances loaded per unit weight of the delivery system, indicating the amount of drug that can be loaded onto the drug delivery system relative to the total weight of the system. Achieving a high loading capacity is often desirable, as it allows for a higher concentration of drug to be delivered to the target site, potentially increasing therapeutic efficacy while reducing side effects.

Loading capacity can be calculated by the amount of total entrapped drug divided by the total nanoparticle weight $(Eq.3.5)$. In drug delivery, yield, given as a percent, is a reflection of the amount of drug delivered per amount encapsulated.

$$LC\% = \frac{M_x}{M_{cs} + M_{TPP} + M_x} \times 100\% \qquad (Eq.3.5)$$

Where,

M_x : weight of loaded molecules (g)

M_{cs} : weight of chitosan (g)

M_{TPP} : weight of TPP (g)

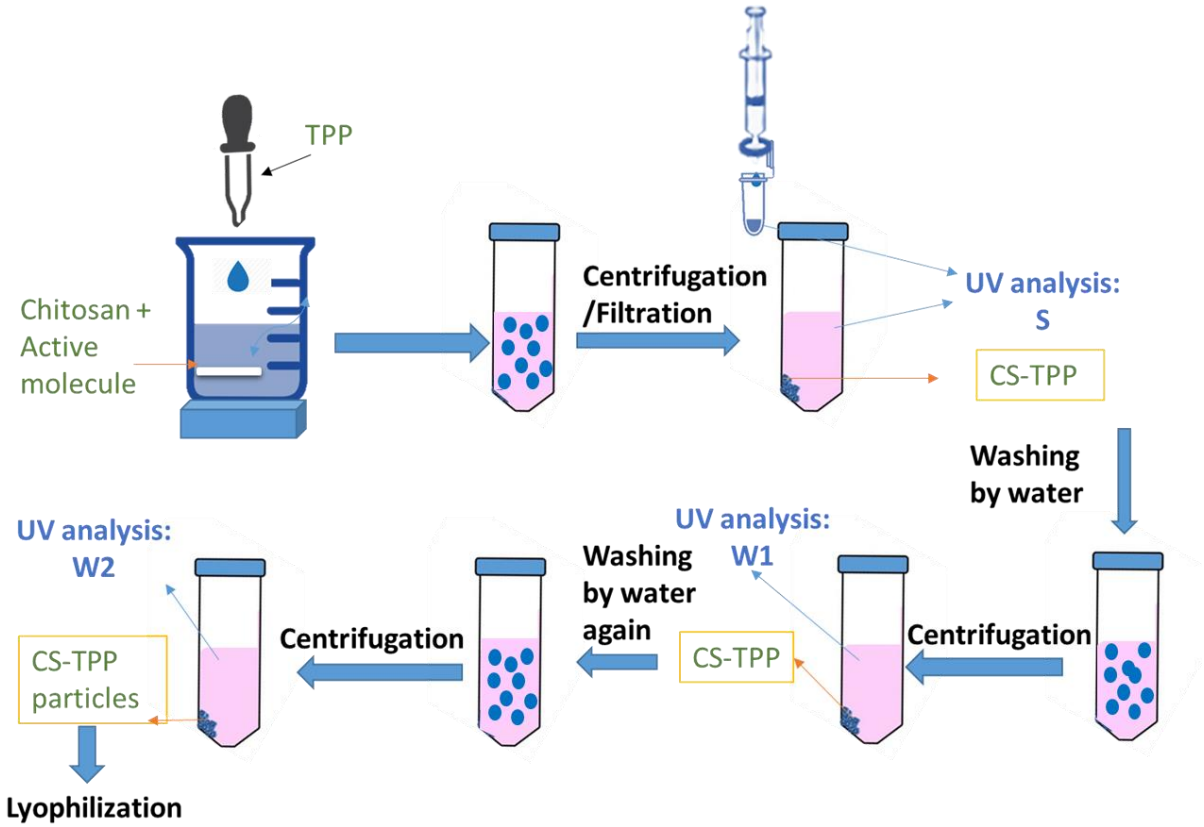


Figure 3-5 Schematic introduction of encapsulation of active molecule by CS-TPP particles.

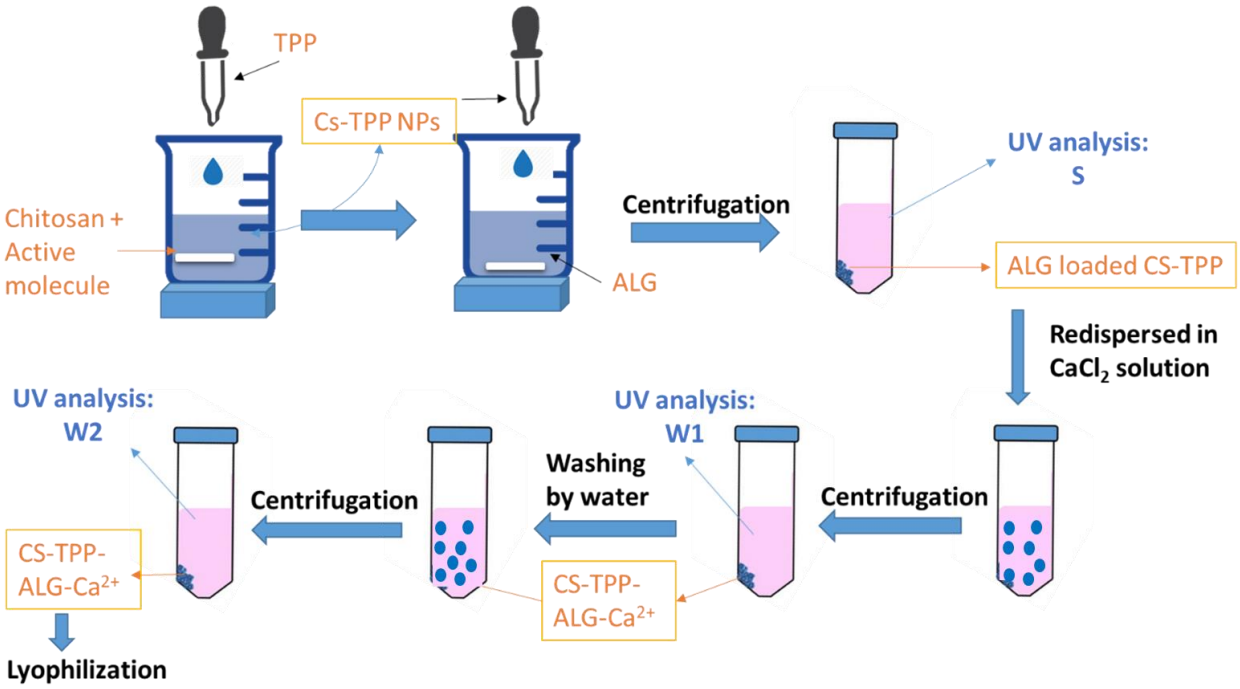


Figure 3-6 Schematic introduction of encapsulation of active molecule by ALG coated CS-TPP particles.

Different CS-TPP formulations were prepared to explore the feasibility to encapsulate those polyphenol molecules. Certain volume of solution of the active molecule was mixed with chitosan acetic acid solution in advance. Then appropriate amount of TPP aqueous solution was added dropwise to the above mixture under magnetic stirring. Thanks to crosslinking of chitosan polymer chain with the crosslinker, TPP, active molecules can be enclosed into spherical network formed by CS and TPP at mild conditions.

UV-Vis spectrometer was used to determine the content of these molecules as all of them possessing UV absorption functional group in the structure hence strong UV absorption at UV-Vis wavelength. To exclude all absorption of other substances apart from expected material, a blank control group was prepared at the same time with the sample. For the blank sample, “active molecule” solution was replaced by equal volume of solvent (usually ethanol). Apart from that, this blank sample was prepared via the same preparation steps as its corresponding sample. UV-Vis spectra of supernatants and filtrated liquid of blank samples were used as baselines to “correct” spectra of corresponding samples by canceling out UV-Vis absorption from all compounds except the target molecule, which can also absorb UV-Vis light within the determined region.

The indirect method was used to calculate EE% of particulate formulation of certain molecule loaded. Because of the difficulty to determine directly content trapped in capsules, this value was calculated by taking out entrapped part from total quantity added of the molecule.

As indicated in $Eq.3.4$, UV-Vis absorption in S, W1 and W2 were measured by UV-Vis spectrometer. With help of calibration equation at specific wavelength, molecule concentration and thus content of this molecule in liquids can be calculated (since volumes of liquids are known).

3.4.3 Limitation of method

As the fabrication is a complex process with multistep procedures, special attention should be paid since there are several potential sources of error that may affect the results of the study:

- Inaccuracy of liquid volume

Liquid volume cannot be accurately measured by precise instrument each time in actual operation. What's more, slight difference among each experiment does exist but it would be arduous to take this into consideration. The solution was to repeatedly measure the volume of liquids in each step and then use the average value for calculations. If liquid volume is underestimated, EE% would be overestimated. Likewise, if liquid volume is overestimated, EE% would be underestimated and even generating negative result.

- Incomplete separation of unloaded molecules

In some situation, complete separation is not achieved by centrifugation so that part of loaded particles may stay in supernatant and disturb UV-Vis absorption of free molecules thus introducing inaccuracy in EE% determination.

Particle size analysis of all prepared formulations indicated the presence of nanoparticles with dimensions smaller than the pore size of the membrane filter used. This suggests that some of the nanoparticles may have passed through the filter and dispersed in the filtrate. In the case where the active molecule loaded nanoparticles also exhibit UV-Vis absorption, this may result in an overestimation of the unloaded CAT and therefore an underestimation of EE%.

- Errors from UV measurement

Another possible source of error could be related to the UV spectrophotometer measurement. Since UV-Vis spectrometry is a very precise quantitative method with high sensitivity, disturbance may come from any substances with UV-Vis absorption at the same determination region.

Overall, it is important to acknowledge these potential sources of error and take them into account when interpreting the results of the study.

Strategies can be used to minimize these uncertainties:

- A blank sample without adding target molecule can be prepared and determined with exactly the same methods as a sample. The UV-Vis spectra of this blank sample can be used as background to eliminate "noise" absorption from irrelevant substances and thus correct UV-Vis spectra of its corresponding sample.
- Repeated measurements will reduce random errors and increase reliability of the measurements

3.4.4 Choice of molecules

In this work, we selected several polyphenols as typical examples: naringenin, naringin and catechin. All three of them are reported high-value polyphenol molecules with numerous beneficial bioactive effects like: antioxidant activity, anti-inflammatory activity, anti-cancer activity and anti-obesity activity (more details, examples and references can be seen in previous chapter 1. State of art -1.7 Polyphenols). Although these molecules offer numerous health benefits, their low water solubility and susceptibility to the internal environment significantly limit their applications.

The incorporation of these delicate molecules into CS particulate systems aims to protect them from rapid oxidation and degradation, while enhancing their bioavailability and stability. Additionally, reducing the particle size can lead to a larger surface area, potentially enhancing the bioavailability of the encapsulated compounds.

3.4.5 Separation method used in encapsulation

Ascertaining the exact quantity of encapsulated molecules directly can be impractical. Instead, the amount of unencapsulated molecules was determined and subsequently subtracted from the total amount of molecules added during encapsulation to indirectly determine the quantity of encapsulated molecules. Hence, it is necessary to utilize an effective separation method to isolate the unencapsulated drug from the loaded particles. Two commonly employed methods, namely filtration and centrifugation, were explored in this regard.

3.4.5.1 *Filtration*

To investigate whether the cellulose membrane introduced any additional effects, such as absorption, which could potentially disrupt the UV-Vis absorbance results. If this were the case, filtration would not be a suitable method for separation. NRG, NR and CAT solutions were diluted and passed through a cellulose membrane via filtration. Subsequently, the filtrates were analyzed using a UV-Vis spectrometer and the results were compared with those of the unfiltered samples.

3.4.5.2 *Centrifugation*

Centrifugation is a commonly used separation method. The main parameter of centrifugation is the gravitational force or centrifugal force, which is determined by the speed of rotation, the radius of the rotor, and the mass of the particles being separated. Sedimentation speed of particles, i.e. the rate at which particles in a fluid settle under the influence of gravity, is useful to design centrifuges and optimize their operation. Generally, settling velocity depends on the size and shape of the particle, the density of the particle and the fluid, and the viscosity of the fluid (Eason and Campbell, 1978). Observations were made on the sedimentation behavior of CS-TPP particles, including settling velocity and the compactness of the sedimentation cake. The centrifugation conditions for these samples were established and optimized by considering the sedimentation rate and empirical findings.

3.4.6 Encapsulation of polyphenols

3.4.6.1 Encapsulation of NRG

Solutions of 0.3%, 0.5% (w/v) chitosan were prepared in 1.0% (v/v) glacial acetic acid. Solutions of 0.25%, 0.5% (w/v) TPP was prepared. Solutions of 0.5%, 0.8%, 1%(w/v) naringenin were prepared by dispersing naringenin solids in ethanol absolute and magnetically stirred for one hour.

A sample was prepared by adding 3.3 ml of 0.25% (w/v) TPP solution into 10 ml of 0.3% (w/v) chitosan solution. And another two samples were prepared by adding 3.3 ml of 0.5% (w/v) TPP solution into 10 ml of 0.3% (w/v) chitosan and 10 ml of 0.5% (w/v) chitosan, respectively. In all above experiments, TPP solutions were dropped dropwise under magnetic stirring at 600 rpm for 30 min at 45°C. Specific volume of NRG EtOH solution was added in CS solution and stirring for at least 30 min before addition of TPP solution.

3.4.6.2 Encapsulation of NR

Naringin is a natural flavanone glycoside formed from naringenin and neohesperidose. Like naringenin, naringin has also very poor aqueous solubility. Efforts were taken to encapsulate naringin molecules into CS-TPP-ALG particles with similar preparation method like naringenin with slight modifications.

Solutions of 2%(w/v) naringin was prepared by dispersing naringin solids in ethanol absolute and magnetically stirred for one hour. Various quantity of NR (Q_{NR}=1 mg, 3mg, 5mg, 7.5mg, 10mg) of NR were tested to explore Q_{NR} effect on EE% of NR. NR loaded CS-TPP samples were prepared and separated by above mentioned methods like NRG. Encapsulation efficacy (EE%) of NR was also determined by indirect method by UV-Vis spectrometry.

Additionally, after loading NR into CS-TPP particles, the particles were redispersed in water and the amount of released NR was measured using spectrophotometry.

3.4.6.3 Encapsulation of CAT

Verification of solubility of CAT in water at room temperature

Catechin is reported sparklingly soluble in water and is more soluble in organic solvents like for example ethanol (27.1g/100g, Matsubara et al., 2014), DMF, DMSO, etc. The water solubility of (+)-catechin at room temperature was reported between 3.6 to 7.7 g/L (Cuevas-Valenzuela et al., 2014; Matsubara et al., 2014).

To verify water solubility of our CAT product, 50 mg of CAT was dissolved in 10 ml (5 g/L) of distilled water at room temperature while being stirred magnetically.

Various solvents were evaluated for the dissolution of CAT. Solutions containing 2 mg of CAT were prepared by dissolving it in water, 50% EtOH (water: EtOH =1:1, v/v), and pure EtOH, and then added to CS solutions. TPP solutions were then added dropwise to the CS-CAT mixture to generate CAT-loaded CS-TPP particles. In addition, a solution containing 5 mg of CAT dissolved in EtOH was also utilized to produce CAT-loaded CS-TPP particles using the same procedure. EE% of CAT within different CS-TPP formulations were calculated indirectly by determining content of unloaded CAT via UV spectrophotometer.

Extra CAT was separated from CAT-loaded particles via membrane filtration other than centrifugation. Suspensions of CAT-loaded particles were filtrated by cellulose membrane syringe filter. Then clear filtrates were diluted properly and measured by UV-Vis spectrometry to calculate EE% of CAT.

3.4.7 Polyphenol loaded ALG coated CS core-shell nanoparticle

The synthesis of polyphenol loaded particles is similar to blank particles except mixing of polyphenol solution with chitosan solution before addition of TPP. Solutions of 0.12%, 0.5%, 0.64%, 0.8%, 1.0%, 2.3% (w/v) of naringenin in ethanol were prepared. Solutions of 0.25%, 1.0%, 2.0% (w/v) of naringin in ethanol were prepared. Solutions of 0.5%, 1.0% (w/v) of catechin in ethanol were prepared.

The polyphenol solution was added dropwise into the chitosan solution under moderate agitation (750 rpm) for a minimum of 30 minutes. The subsequent steps of preparing the blank ALG-coated CS-TPP particles were followed to obtain the loaded particles.

3.5 Release properties of polyphenols loaded CS-TPP particles

3.5.1 Determination of solubility of naringenin

Naringenin exhibits poor solubility in water at room temperature. Water solubility values reported in the literature vary significantly, ranging from 14.2 to 214 mg/L (Table 1-3). To determine naringenin water solubility at 20°C, same amount of lyophilized NRG loaded CS-TPP particles (containing 4 mg of NRG) were dispersed in various volume (5, 10, 50, 100, 400, 800 mL) of water. NRG concentration in suspensions were monitored by determining NRG content UV-spectrophotometrically in the supernatants of samples taken at prescheduled time intervals.

3.5.2 Establishment of drug release conditions

3.5.2.1 Separation method

Naringenin diffusing from dialysis tube

10 ml of NRG solution that contains 0.32 mg of NRG was added into a dialysis tube. This tube was immersed into a baker containing 20 ml of water. At prescheduled time interval from 10 to 7200 min, the amount of NRG was calculated.

Filtration of naringenin

To evaluate the potential impact of filtration processes on the UV absorption of the NRG solution, a solution containing NRG at a concentration of 9 mg/L was measured using a UV spectrometer (V-770 UV-visible/NIR Spectrophotometer, JASCO) both before and after being filtered through a syringe filter.

3.5.2.2 Media volume

Dissolution volume of media was explored to make sure free diffusion during dissolution testing. NRG loaded CS-TPP particles were dispersed in 10 mL, 50mL, 100mL, 400mL and 800mL of water in 20°C, respectively.

3.5.3 Release testing

As described before, CS3TPP5 formulation was chosen as best candidate to encapsulate naringenin molecule. And the encapsulation efficiency (EE%) of NRG was found around 90%. Now, we are interested in the release properties of entrapped NRG in these particles. Alginate coated CS3TPP5 particles were also investigated to see if ALG coating can alter drug delivery. In addition, release properties of NRG loaded particles with ultrasonication treatment were also monitored. Last but not least, composition and pH of dissolution media were also investigated as factors that may affect release properties of NRG.

3.5.3.1 CS-TPP particles

Freeze-dried NAR loaded of CS-TPP particles were dispersed in 800 mL of water at 20°C with continuous magnetic stirring. Content of NRG in media was measured UV spectrophotometrically at prescheduled time intervals.

3.5.3.2 Ultrasonic treated CS-TPP particles

High physical forces may change particles structure and alter drug release properties from particles. To explore the effect of ultrasonic treatment on release behavior of loaded molecule from CS-TPP particles,

before centrifugation step, CS-TPP suspensions were treated by an ultrasonic probe during 0.5min, 1min and 5min, respectively.

3.5.3.3 ALG coated CS-TPP particles

Freeze-dried ALG coated CS-TPP particles (containing 4.4 mg of NRG) were dispersed in 800 mL of water at 20°C with continuous magnetic stirring. Content of NRG in media was measured UV spectrophotometrically at prescheduled time intervals.

3.5.4 Effect of composition of media

For poor soluble substance in aqueous media like naringenin, addition of a solvent in which it is more soluble may facilitate the dissolution. We investigated if addition of EtOH into dissolution media could alter release behavior of NRG loaded CS-TPP particles.

NAR loaded CS-TPP particles were dispersed in water, 10% EtOH and 33% EtOH, respectively. NRG content in dissolution media was monitored by UV-VIS spectrophotometry at prescheduled time intervals.

4 Results and discussion

Chitosan (C2395, 5-20 mPa·s, 0.5% in 0.5% Acetic Acid at 20°C) was purchased from TCI (Tokyo). Naringenin (CAS No.: 67604-48-2, W530098, Mw: 272.25 g/mol), naringin (CAS No.: 10236-47-2, 71162, Mw: 580.53 g/mol), catechin (CAS No.: 154-23-4, 43412-10MG, Mw: 290.27 g/mol), sodium alginate (CAS No.: 9005-38-3, W201502) and sodium tripolyphosphate (TPP) (CAS No.: 7758-29-4, 238503, Mw: 367.86 g/mol) were purchased from Sigma-Aldrich.

4.1 Characterization of materials

4.1.1 Characterization of chitosan

Table 4-1 summarized the chitosan samples utilized in this work. The molar mass and degree of deacetylation were determined and were found consistent with the specification provided by the suppliers.

Table 4-1 Product information of the three chitosan commercial samples used in this work

Chitosan abbreviation	Supplier	Product Number	M_w (kDa) from suppliers	M_w [i] (kDa)	Degree of deacetylation(%) from suppliers	Degree of deacetylation [ii] (%)
Cs(b)	TCI Tokyo	C2395	around 50-100	44	75-85 % (calculated on dried substance)	81
Cs(p)	Prepared in-house	C2395	-	36	-	77

[i] M_w determined by SEC-MALS
[ii] DDA% determined by ^{1}H NMR

Commercial chitosan sample as well as purified chitosan samples were characterized using UV-Vis spectrometry, FTIR, ^{1}H NMR, and SEC-MALS.

4.1.1.1 UV–Vis absorption spectra of chitosan

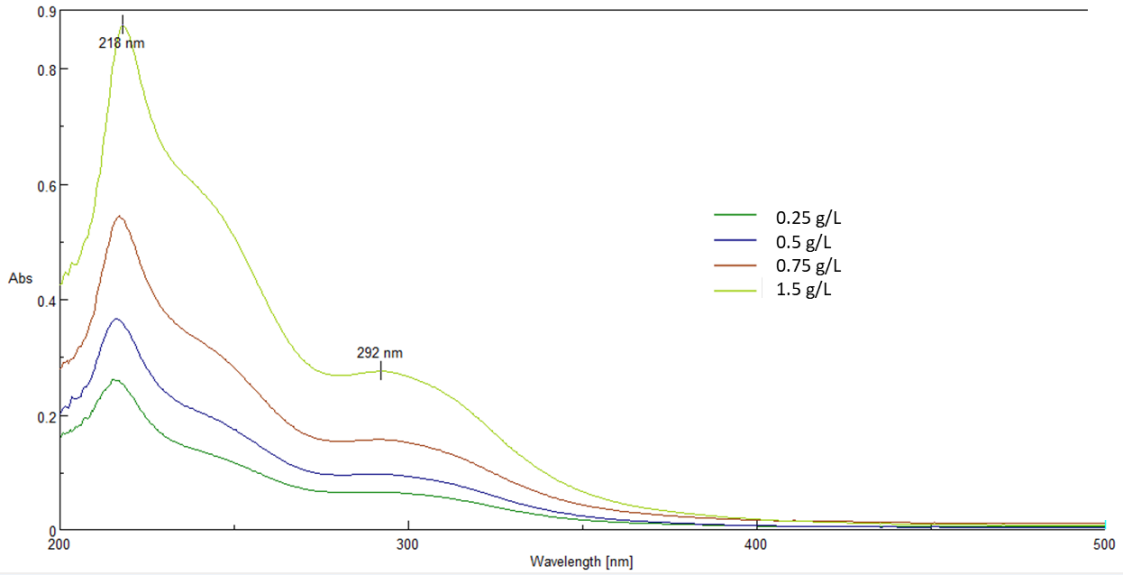


Figure 4-1 UV–Vis spectra of chitosan solutions (0.25, 0.5, 0.75, 1.5 mg/L, 1% acetic acid) at the range 200-500 nm.

The UV-Vis spectra of chitosan solutions at various concentrations (Figure 4-1) exhibited two peaks with maxima at λ_{max} equal to 218 nm and 292 nm in accordance with literature (Amidi et al., 2008). This result confirmed the purity of commercial sample.

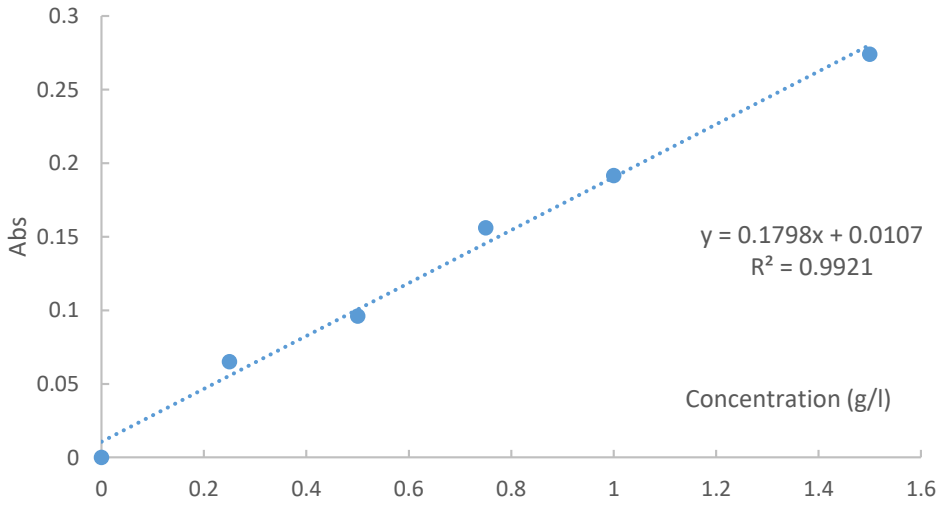


Figure 4-2 UV absorbance at 292 nm vs concentration of chitosan solutions (1% acetic acid, v/v) and calibration curve with regression equation.

As chitosan solutions with high concentration possess significant absorbance at 292 nm which is the same value as for λ_{max} of naringenin, the calibration curve of chitosan was used to estimate the UV absorbance contribution from chitosan (Figure 4-2).

4.1.1.2 Fourier transform infrared spectroscopy (FTIR) of chitosan

FTIR spectra were recorded in the mid-infrared (4000 cm^{-1} to 500 cm^{-1}) with a resolution of 4 cm^{-1} at room temperature (20±2°C). The samples for FTIR analysis were prepared by grinding the dry blended powders of chitosan with KBr, and then compressed to form tablets.

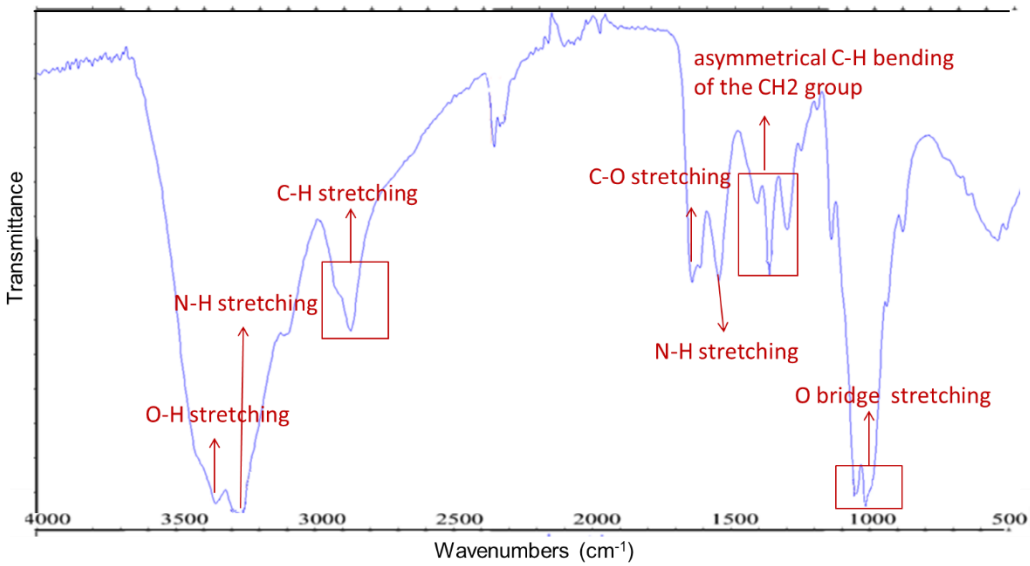


Figure 4-3 Infrared spectrum of commercial chitosan in the field 4000–500 cm^{-1} with assigned characteristic bonds (KBr tablet).

Different characteristic bands were assigned from the FTIR spectra of chitosan (Figure 4-3): 3386 cm^{-1}, 3270 cm^{-1} (O-H stretching, N-H stretching), 2918-2867 cm^{-1} (C-H stretching), 1650 cm^{-1} (amide II band, C-O stretching of the acetyl group), 1592 cm^{-1} (amide II band, N-H stretching) 1485–1380 cm^{-1} (asymmetrical C-H bending of the CH_2 group) and 1036 cm^{-1} (O bridge stretching) of the glucosamine residue. These characteristic bands were in good consistence with data found in the literature (Dara et al., 2020; Kumirska et al., 2010; Paulino et al., 2006), which confirmed chemical structure integrity and purity of chitosan.

4.1.1.3 ^{1}H NMR of chitosan

4.1.1.3.1 Solvent: DCl-D_2O vs. CD_3COOD-D_2O

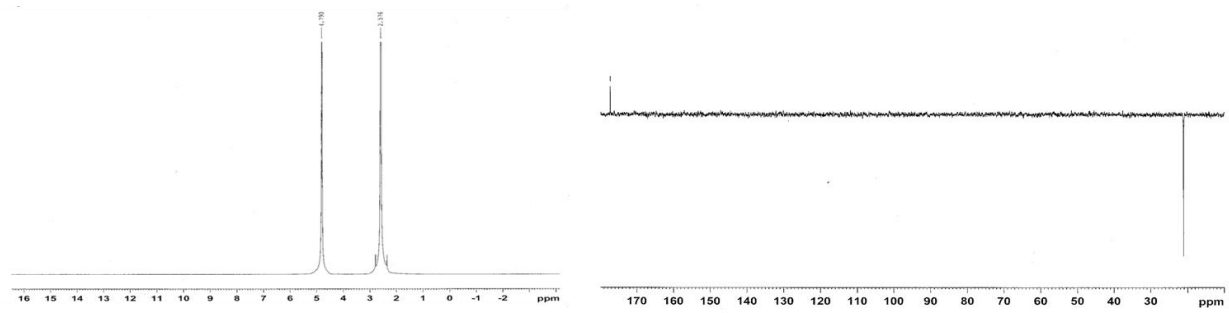


Figure 4-4 ^{1}H NMR spectrum of CD_3COOD-D_2O(2%, v/v) at 343 K (left) and ^{13}C NMR spectrum of CD_3COOD-D_2O(2%, v/v) at 343 K (right).

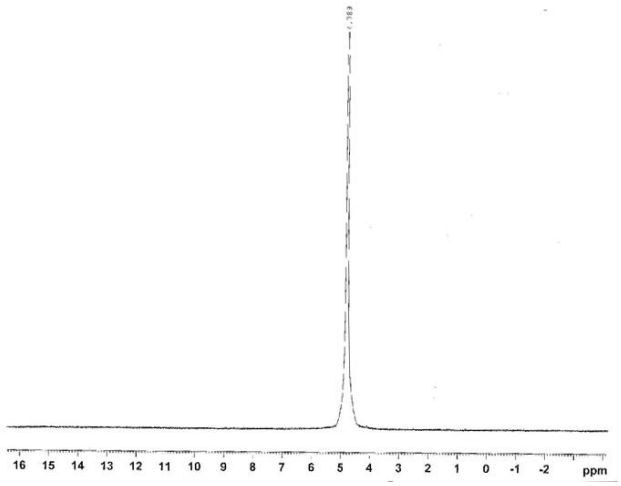


Figure 4-5 ^{1}H NMR spectrum of DCl-D_2O (2%, v/v) at 343 K.

Chitosan is insoluble either in neutral pH aqueous conditions or in common organic solvents. Thus, proper amount of acid is needed to ensure complete dissolution of chitosan. ^{1}H NMR spectrum at 343 K of CD_3COOD-D_2O (2%, v/v) revealed solvent peaks of HOD and CD_3COOH were seen at 4.8 ppm and 2.6 ppm, respectively (Figure 4-4). Only one peak of HOD appeared at 4.8 ppm in ^{1}H NMR spectrum at 343 K of DCl-D_2O (2%, v/v, Figure 4-5). As chemical shift of proton in methyl group of acetylated units (A) is close to 2.5 ppm 'which is close to the peak of CD_3COOH), we finally chose DCl-D_2O as solvent of chitosan, to avoid possible interference of solvent peak with peaks of chitosan.

4.1.1.3.2 Temperature: 300k vs 343k

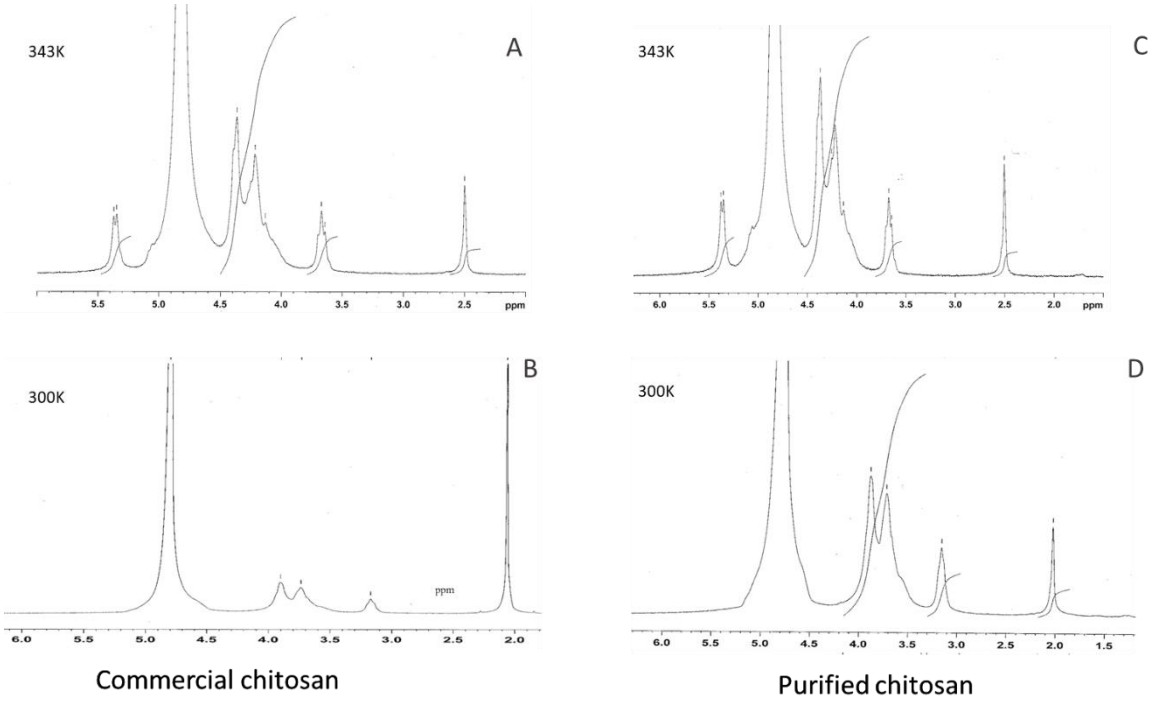


Figure 4-6 ^{1}H NMR spectra of commercial (A,B)and purified chitosan (C,D) at 343K and at 300K. Obviously, 1H NMR spectra at 343K has stronger proton signal and the peaks of H-1(D) at 5.4 ppm were not visible at 300K for both commercial chitosan and purified chitosan.

Commercial chitosan and purified chitosan were characterized by ^{1}H NMR spectroscopy at 300K and 343K (Figure 4-6), respectively. ^{1}H NMR spectra with assigned protons can be seen in Figure 4-7. Chemical shift and integrals of protons were listed in Annex I. Chitosan's ^{1}H NMR spectra were in good consistence with literature (Hirai et al., 1991; Lavertu et al., 2003), and confirmed its chemical structure and purity.

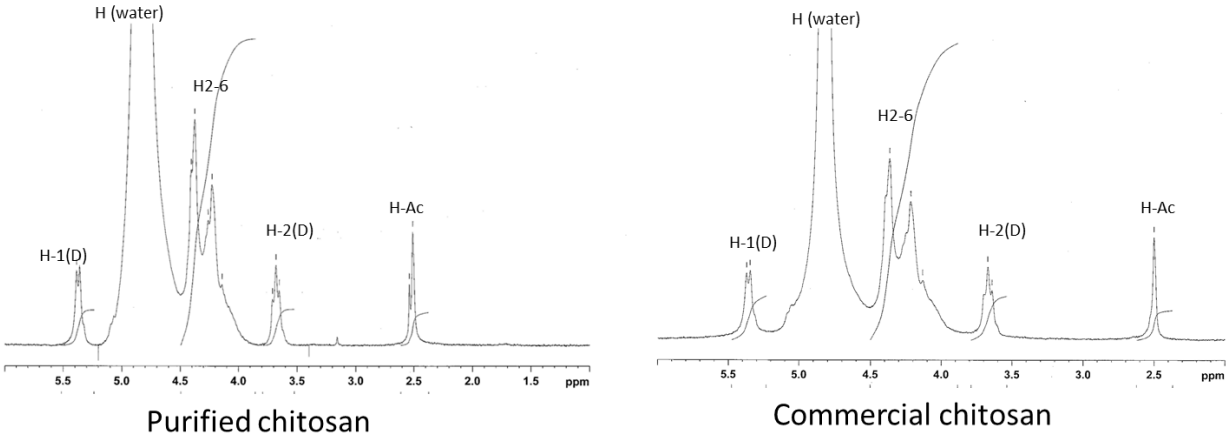


Figure 4-7 ^{1}H NMR spectrum of purified chitosan (left) and our commercial chitosan (right) in DCl-D_2O (2%, v/v) at 343 K. Protons were assigned in following orders: H-Ac, H-2(D), H2-6, H-1(D).

4.1.1.3.3 DDA% determination of chitosan by ^{1}H NMR

DDA% of purified chitosan and commercial chitosan were determined by ^{1}H NMR with above mentioned methods (Hirai et al., 1991) (calculated DDA% presented in Table 4-2).

Table 4-2 Assigned protons of ^{1}H NMR spectrum chitosan in D_2O/DCl at 343K.

		Protons			
		H-1(D)	HAc	H2-6	H-2(D)
Chemical shift (ppm)	Commercial chitosan	5.4	2.5	4.1-4.4	3.7
	Purified chitosan	5.4	2.5	4.1-4.4	3.7
Integrals of signals	Commercial chitosan	1.0000	0.6781	6.7942	1.0012
	Purified chitosan	1.0000	0.9390	8.7127	1.0234

Table 4-3 Deacetylation degree (DDA, %) determined of chitosan samples

Sample	DDA (%) determined using *Eq.3.1*	DDA (%) determined using *Eq.3.2*	Average DDA(%)
Commercial chitosan	80	82	81
Purified chitosan	78	76	77

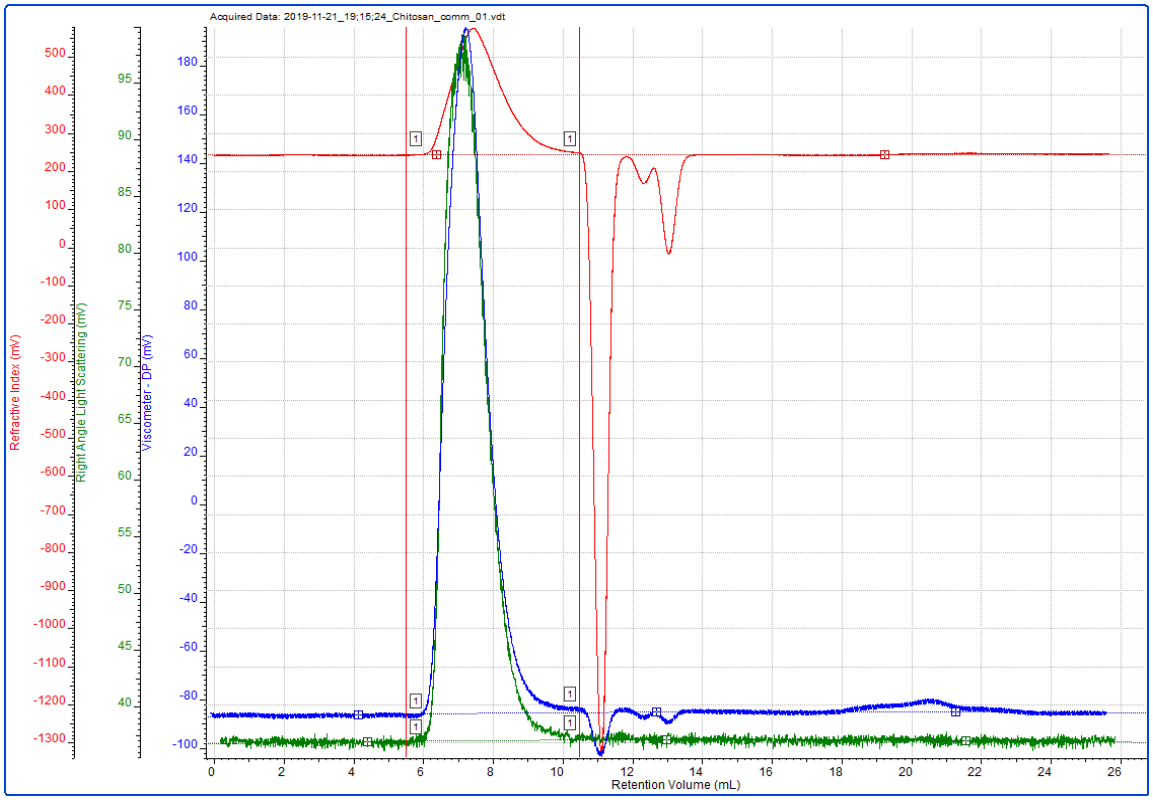
The DDA% results of the commercial chitosan showed good consistency with the DDA% data provided by the supplier (TCI chemicals, TCI, 2018), as seen in Table 4-3. The slight reduction in DDA% of chitosan after purification is likely attributed to the deacetylation of the acetyl group during the purification process.

4.1.1.4 Mw determination of chitosan by SEC-MALS

Calibration of system was performed by PEO 24k before and during measurement of samples (Spectra seen in Annex II SEC-MALS).

Optimization of chitosan concentration

According to SEC-MALS spectra (seen in *Annex II SEC-MALS*), 10 mg/L as concentration was too high for the system, while 2.5 mg/L as concentration was too low. 5 mg/L appeared as the optimal concentration of chitosan solution for SEC-MALS analysis. SEC-MALS spectra of commercial chitosan and purified chitosan are shown in Figure 4-8 and Figure 4-9, respectively.



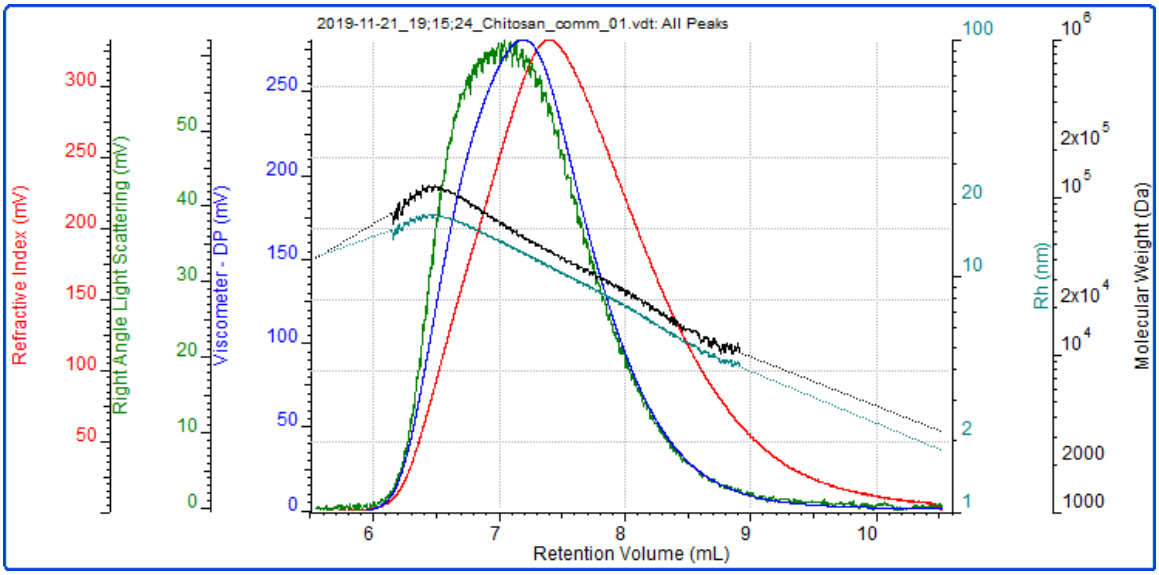


Figure 4-8 SEC-MALS spectrum of commercial chitosan (5 mg/L).

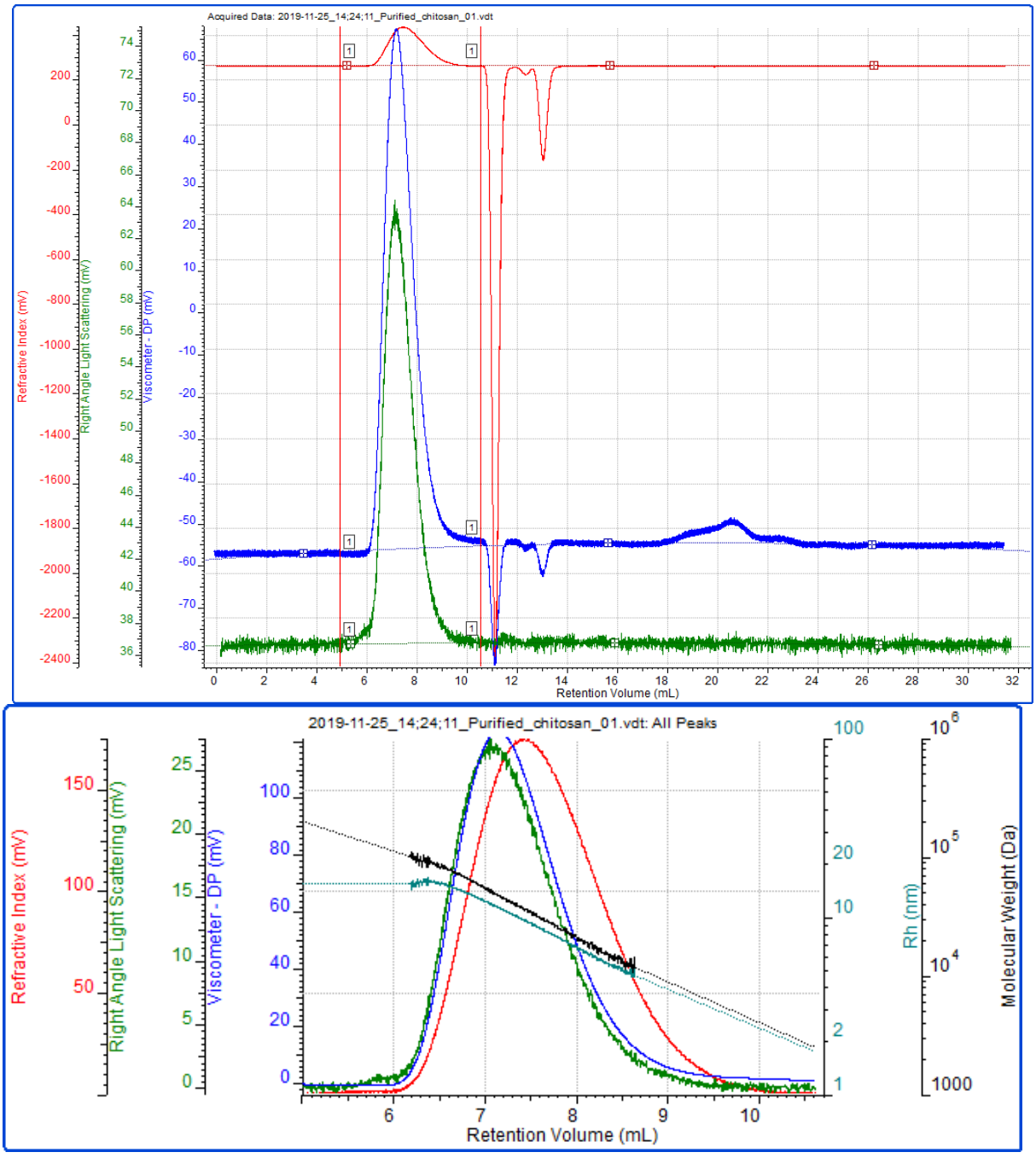


Figure 4-9 SEC-MALS spectrum of purified chitosan (5 mg/L).

According to the supplier (TCI), the Mw of commercial chitosan should be around 50-100 kDa. Mass-average molar mass of commercial chitosan and purified determined by SEC-MALS were 44 kDa and 36 kDa (Table 4.3), respectively. The determined Mw of commercial chitosan is near to lowest value of supplier's information. A slight reduction of Mw of chitosan was observed after purification process, during which chitosan was submitted to treatment by strong base at relative high temperature (70°C). Partial hydrolysis of chitosan chains may exist during purification, which explains lower Mw of purified chitosan. Mw of commercial CS extracted from marine waste was reported ranging from 100 kDa to

1,200 kDa (Hahn et al., 2020; Hossain and Iqbal, 2014). Therefore, samples of CS used in this work can be classified as low molecular weight CS (<150 kDa; Agirre et al., 2014).

Table 4-4 Average molar masses of commercial and purified chitosan samples determined by SEC-MALS.

	Commercial sample	Purified sample
Mw (kDa)	44	36
Mw/Mn	1.7	1.6

Table 4.3 shows that the polydispersity indices (Mw/Mn) of the chitosan samples were 1.7 and 1.6, respectively, before and after purification. These values are considered relatively low for chitosan samples, according to Zielinska et al. (2014), indicating that both the commercial and purified chitosan polymer samples have a relatively narrow range of molecular weights.

Effect of purification of chitosan on particle size

The DLS results (Figure 4-10) shows that CS-TPP nanoparticles made of purified chitosan (CS(p)) are slightly smaller than those made of raw chitosan without purification (CS(b)).

To explore if difference exists among particles prepared by raw chitosan and purified chitosan, sample-010 and 015 as well as sample-007 and 012 were compared in pair. Except for the type of chitosan, within each group, samples were prepared under same conditions (concentration and volume of crosslinking agents and at the same temperature). Size distribution and average size results of these samples showed that chitosan samples recovered after purification would lead to CS-TPP particles with slightly smaller size but with better homogeneity. Slight decrease in molecular weight after purification of chitosan may be responsible for the reduction in size of particles. Indeed, it has been reported that chitosan with lower molecular weight could form smaller particles by mild crosslinking method(Desai, 2016; Wan et al., 2008). Removal of impurities in raw chitosan by purification process may be answerable for better homogeneity of formed particles. Because impurities like proteins may possess charges, which could disturb the ionic crosslinking between chitosan and TPP to produce homogenous particles. For these reasons, purified chitosan is more recommended to be used to prepare CS-TPP nanoparticles with smaller size and narrower size distribution. These conclusions were not modified when switching from room temperature to 50 °C.

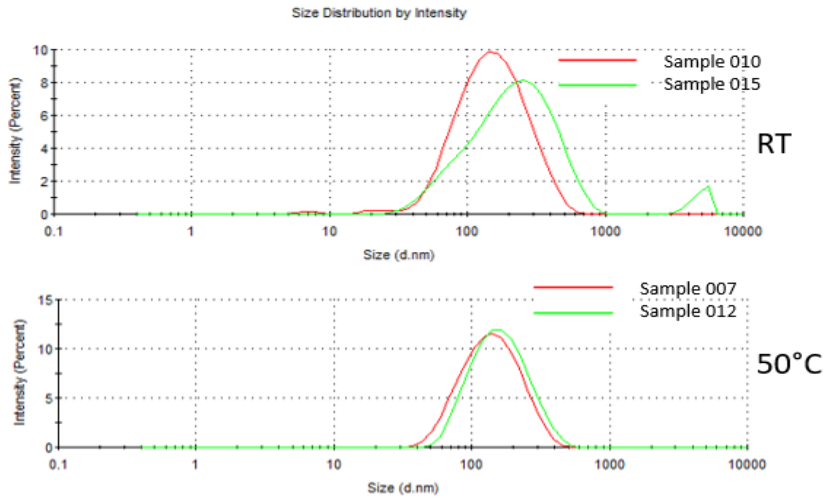


Figure 4-10 Size distribution by intensity of samples prepared using raw chitosan (green) and purified chitosan (red). Upper side are samples prepared at room temperature, whereas below are samples prepared at 50°C.

Particle characteristics including but not limited to particle size, surface charge, particle morphology, stability, release rate, are profoundly influenced by type of the polymer, which is defined by M_w (molecular mass), disparity, and DDA%.

4.1.2 Characterization of polyphenols

4.1.2.1 Characterization of naringenin

4.1.2.1.1 UV–VIS absorption spectra of naringenin

UV-VIS spectra of naringenin dilute solutions and absorbance data at 288 nm were present in Figure 4-11. The wavelength (λ_{max}) of maximum UV absorbance of naringenin was 289 nm. Another characteristic peak of naringenin was detected at 211 nm but it was convoluted with other signals and thus less convenient for our work. The characteristic λ_{max} appearing at 211 nm and 289 nm in the UV-VIS spectra of NRG were in good agreement with literature data.

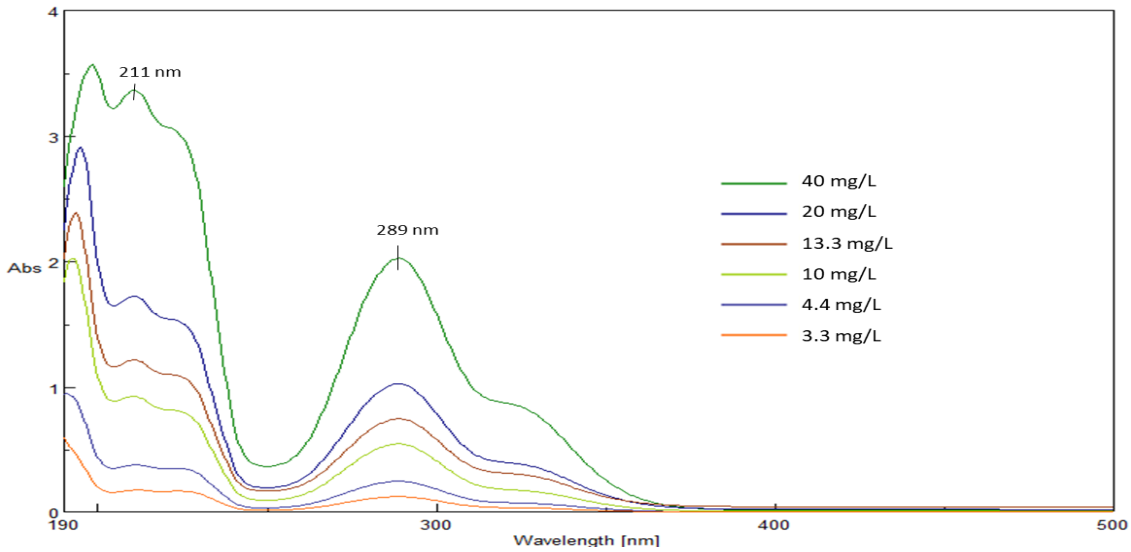


Figure 4-11 UV-VIS spectra of naringenin diluted solutions from 190 nm to 500 nm.

To quantitatively determine the content of naringenin, a calibration curve was established using above five solutions of NRG with known concentrations. The UV absorbance of NRG solution at 289 nm presents a linear relationship versus the NRG concentration and a linear regression equation was calculated by Excel 2016 (Figure 4-12).

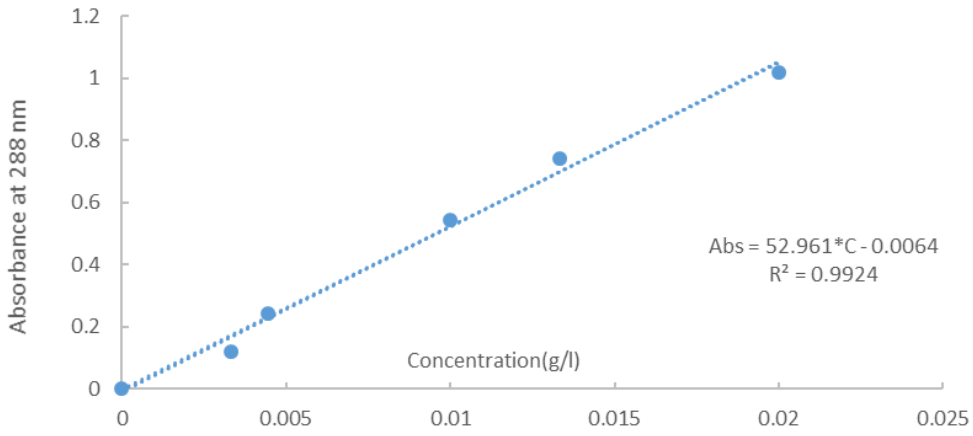


Figure 4-12 UV-Vis absorbance of naringenin aqueous solutions with various concentrations at 289 nm.

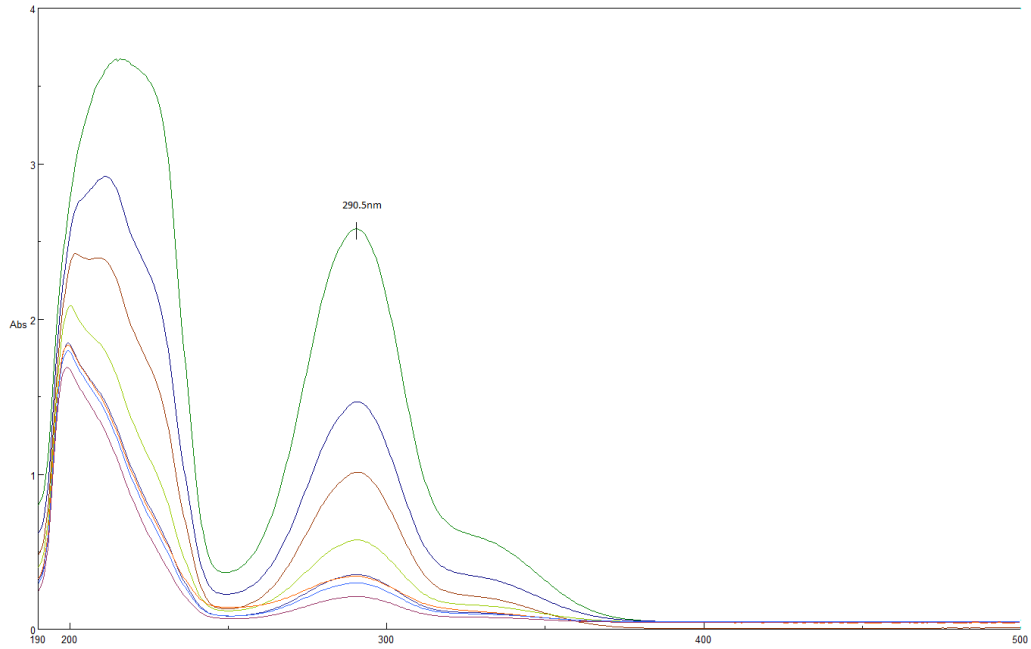


Figure 4-13 UV-Vis absorbance spectra of naringenin dissolved in 33% EtOH

On the other side, when NRG was dissolved in 33% EtOH, the λ_{max} of UV derived to 290.5nm (Figure 4-13), which is close to the one (289 nm) of NRG aqueous solution.

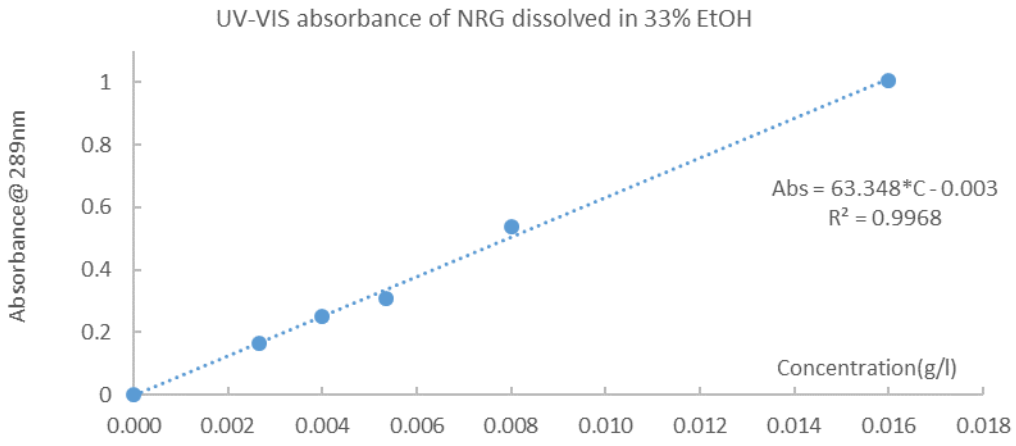


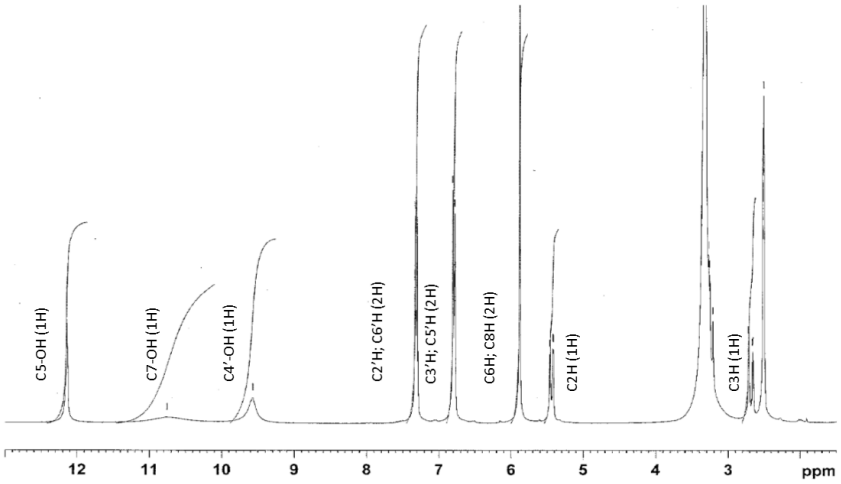
Figure 4-14 UV-Vis absorbance of naringenin dissolved in 33% EtOH at 289 nm.

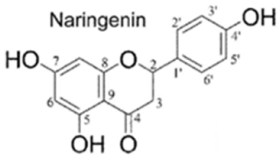
Furthermore, the best linear relationship between the concentration and UV-Vis absorbance of naringenin dissolved in 33% EtOH was observed at 289 nm (Figure 4-14).

4.1.2.1.2 ^{1}H proton NMR spectra of naringenin

The assignment of naringenin peaks have already been reported in the literature (Álvarez-Álvarez et al., 2015; Cordenonsi et al., 2017). Figure 4-15 presents ^{1}H NMR spectrum (on left side), chemical structure (on upper right corner) of naringenin and the assigned chemical shifts of naringenin protons signals and

data in literature; (A): DMSO-d_6, 400 MHz, 300K) ;(B) : in DMSO-d_6, 600 MHz (Maltese et al., 2009) ; (C): in metanol-d4, 600 MHz, 298K (Álvarez-Álvarez et al., 2015)).





Proton	Chemical shift (ppm) (A)	(B)	(C)
C3H cis	2.7	2.7	2.7
C3H trans	3.3	3.4	3.2
C2H	5.4	5.6	5.4
C6H,C8H	5.8	5.9	6.0
C3'H,C5'H	6.8	6.8	6.9
C2'H,C6'H	7.3	7.4	7.4
C4'-OH	9.6	-	-
C7-OH	10.8	-	-
C5-OH	12.1	-	12.2

Figure 4-15 ^{1}H NMR of naringenin in DMSO-d_6 at 300 K with assignments.

^{1}H NMR and chemical shift of protons of naringenin were consistent with data found in literature (Álvarez-Álvarez et al., 2015; Gustavo et al., 2019), which confirmed the structure integrity. In addition, the absence of unidentified peaks indicated the purity of naringenin sample.

4.1.2.2 Characterization of naringin

4.1.2.2.1 UV–VIS absorption spectra of naringin

UV-VIS spectra of naringin dilute solutions (from 6 mg/L to 37 mg/L) and absorbance data at 282 nm were present in Figure 4-16. The wavelength of maximum (λ_{max}) UV absorbance of naringin was 282 nm. Another characterized peak of naringin was seen at 212 nm. These characteristic λ_{max} match well UV-Vis spectrophotometric data in literature (J. Zhang et al., 2015, Cordenonsi et al., 2017, Ebrahimi et al., 2020)

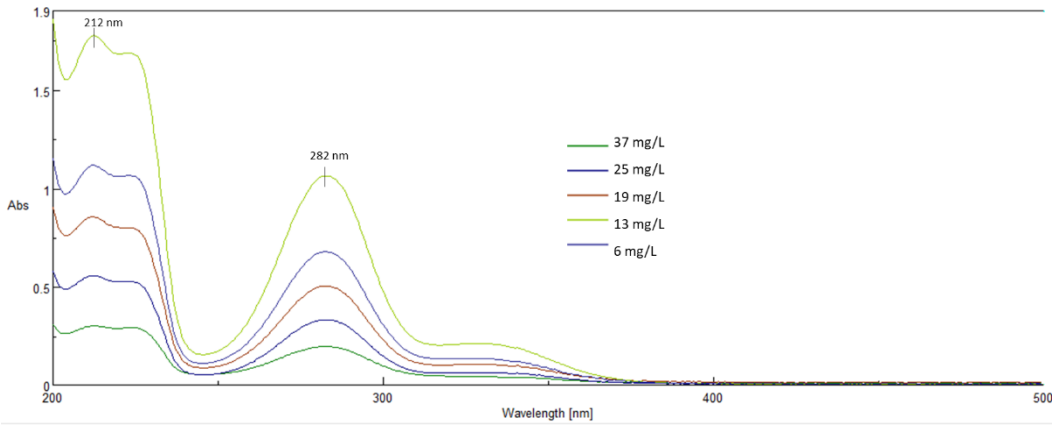


Figure 4-16 UV-VIS spectra of naringin dilute solutions and absorbance data from 200 to 500 nm.

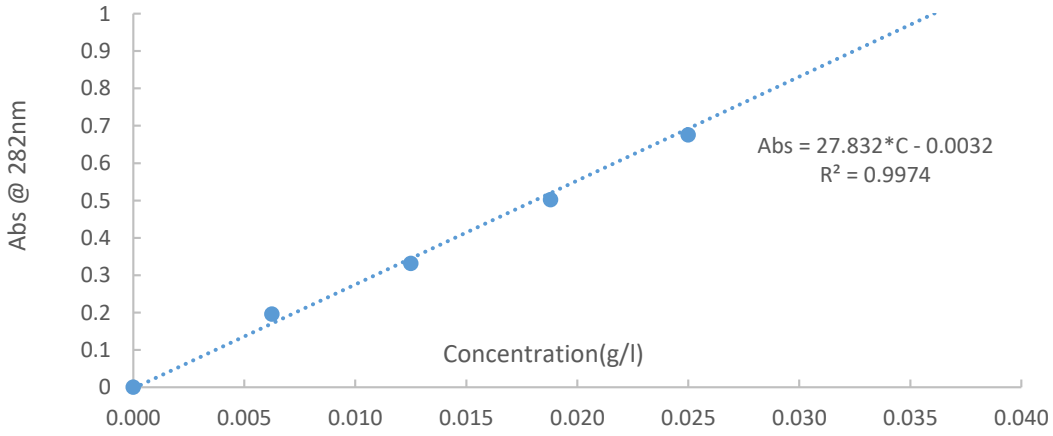


Figure 4-17 Calibration curve for UV-Vis spectrophotometric determination of naringin in aqueous solution (λ_{max} = 282 nm)

Absorbance of naringin solutions at 282 nm was plotted with concentration (Figure 4-17). A linear variation was observed over the whole range of concentrations.

4.1.2.2.2 ^{1}H proton NMR spectra of naringin

^{1}H NMR spectrum of naringin in DMSO-d_6 at 298K with assigned signals are presented in Figure 4-18.

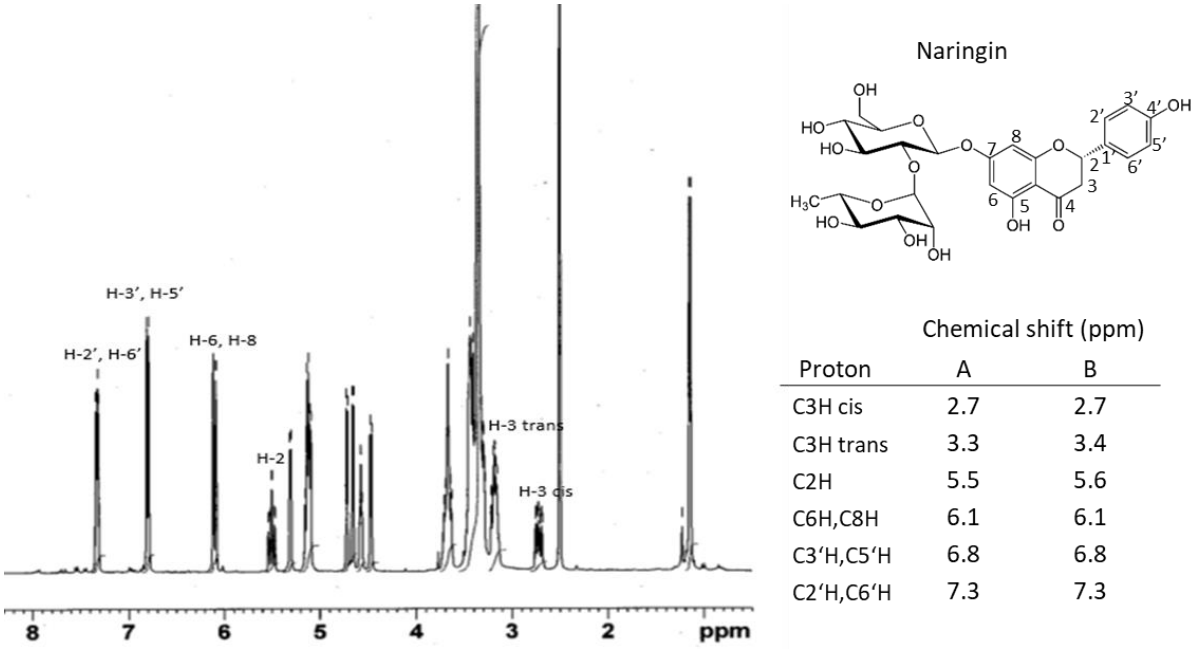


Figure 4-18 ^{1}H NMR spectrum of naringin in the range δ 7.5– δ 2.5 (298K, 400 MHz). Sample was dissolved in DMSO-d_6. The signals are assigned as follows: (1) H-3 cis (2) H-3 trans (3) H-2, (4) H-6 and H-8, (5) H-3' and H-5', (6) H-2' and H-6'.

The signals were assigned as follows: (1) H-3 cis (2) H-3 trans (3) H-2, (4) H-6 and H-8, (5) H-3' and H-5', (6) H-2' and H-6'. Chemical shift of assigned protons of this work (A) and from work of Maltese et al. (B, 600 MHz, DMSO-d_6) were listed in the table on lower right corner. Consistence in results was found with another article describing analytical methods of identification of flavanone glycosides by proton NMR

spectroscopy (Maltese et al., 2009), where NMR spectroscopic data (600 MHz, DMSO-d_6 , 298K) for naringin were given. ^{1}H NMR spectrum of naringin confirmed chemical structure and no appearance of unknown peaks confirmed the purity of naringin sample.

4.1.2.3 Characterization of catechin

4.1.2.3.1 UV–VIS absorption spectra of catechin

UV-VIS spectra of dilute catechin solutions were present in Figure 4-19. A very sharp and strong absorption maximum (λ_{max}) peak at 280 nm in the UV-vis absorption spectrum of catechin, which corresponds to results in literature (Merghem et al., 2004; Zu et al., 2006).

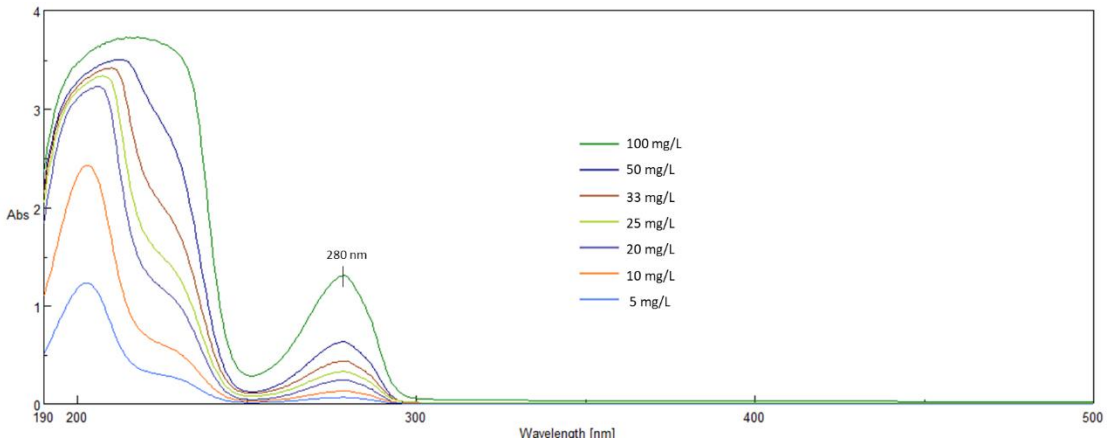


Figure 4-19 UV-VIS spectra of catechin dilute solutions at range from 190 to 500 nm.

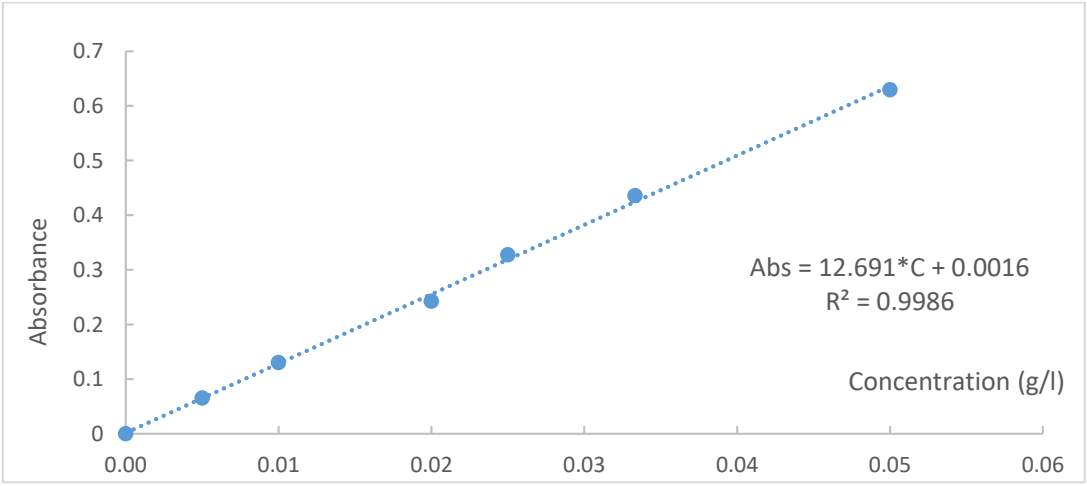


Figure 4-20 Calibration curve of catechin at 280 nm.

Absorbance values of UV of catechin solutions with known concentration (from 5 mg/L to 100 mg/L) were plotted and the regression equation of this calibration curve (the tendency line) was calculated (Figure 4-20). The wavelength of peak maximum (λ_{max}) UV absorbance of catechin was 280 nm. UV spectra of catechin were compatible of UV spectrometry information in literature (Guyot et al., 1995; Li et al., 2012). Chemical structure integrity and purity were confirmed UV-VIS spectrophotometrically.

Absorbance of light of catechin at 280 nm were in good linear relation with concentration of sample (R^2>0.99).

4.1.2.4 UV-VIS absorption of polyphenols

Table 4-5 summarizes regression equations of calibration curves of substances with experiment details.

With the assistance of regression equations that demonstrate the linear correlation between the concentration and absorbance of UV light for molecules, the content of polyphenols can be accurately measured using UV-Vis spectrophotometry.

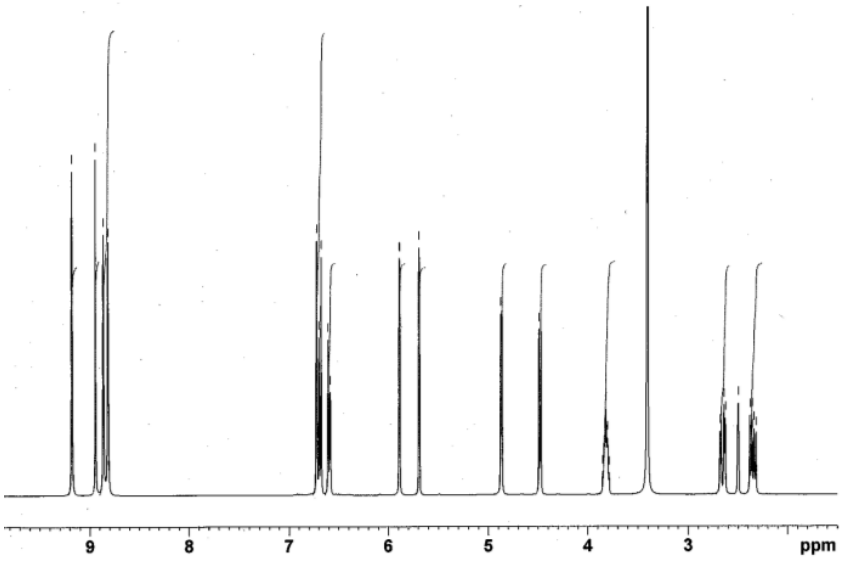
Table 4-5 Linear regression equations of calibration curves of polyphenols

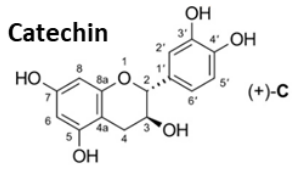
Molecule	Solvent	Concentration range (mmol/L)	Concentration range (mg/L)	Wavelength (nm)	Equation[i]
Naringenin	water	0.061-0.010	2.8-16.7	288	Abs = 63.521*C - 0.0064
Naringenin	33% EtOH	0.059-0.010	2.7-16	289	Abs = 63.348*C - 0.0030
Naringin	water	0.065-0.011	6-37	282	Abs = 27.832*C - 0.0032
Catechin	water	0.020-0.340	5-100	280	Abs = 12.752*C - 0.0035

[i] *Correlation coefficient (r^2) of all equations here were higher than 0.99.*

4.1.2.4.1 ^{1}H NMR spectrum of catechin

As seen in Figure 4-21, ^{1}H NMR spectrum of catechin in DMSO-d_6 at 298K (Figure 4-21A) was compatible with the referred spectrum (Figure 4-21B, Pauli et al., 2006) in terms of peak areas and chemical shifts. ^{1}H NMR spectrum of catechin confirmed chemical structure of catechin and absence of impurity within this chemical substance.





Proton	Chemical shift (ppm) A	B
C3H	3.8	3.8
C2H	4.5	4.5
C4H-α	2.7	2.6
C4H-β	2.3	2.3
C6H	5.9	5.9
C8H	5.7	5.7
C3-OH	4.9	4.9
C5-OH	8.9	8.9
C7-OH	9.2	9.2
C3'-OH C4'-OH	8.8	8.8

Figure 4-21 ^{1}H NMR spectrum of catechin in DMSO-d_6 (10 mg/mL, 400 MHz, 298K) and assigned proton signals(A); (B) chemical shifts of catechin in DMSO-d_6 (5.33 mg/mL, 600 MHz; 298K, reprinted from Pauli et al., 2014).

4.1.3 Characterization of chitosan particles

4.1.3.1 Morphology

The morphology of nanoparticles refers to their shape, and physical structure. Depending on the synthesis method employed, particles may exhibit a range of shapes, from simple spheres to more complex structures such as rods, cubes, and others. The morphology of particles plays a crucial role in determining their properties, including stability, surface area, drug loading capacity, and release kinetics. Consequently, identifying and achieving optimal particle morphology is critical for successful application in various fields. Techniques used to analyze particle morphology are outlined below.

SEM utilizes an electron beam to generate a 3D image of particle surfaces, allowing for the determination of individual particle size and particle size distribution. However, it is important to note that a sufficient amount of sample must be used to ensure a representative analysis.

- SEM Microscopy images of chitosan particles

For surface morphology and shape analysis, CS-TPP nanoparticle suspension was dropped on aluminum studs, dried at room temperature and observed under a Scanning Electron Microscope (SEM, Hitachi S-4800) at an acceleration voltage of 3 kV.

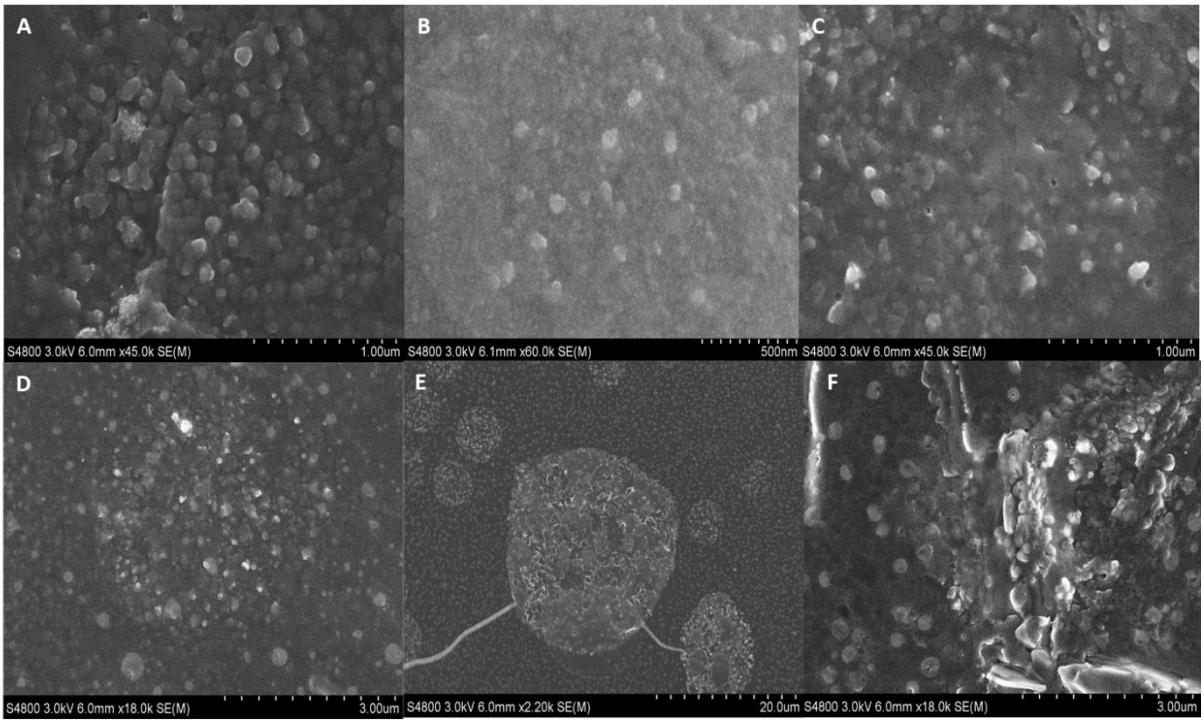


Figure 4-22 SEM micrographs of CS-TPP particles prepared by crosslinking of CS and TPP. experimental details including concentration volume. A: sample-021; B: sample-038; C,D: sample-012; E,F: sample-019

In the SEM images (Figure 4-22), individual sphere-shaped CS-TPP nanoparticles can be clearly seen. In the SEM photo of sample-022(Figure 4-22A), spherical nanoparticles with size about a hundred nanometers can be clearly seen. Based on this picture, particles seem rather monodisperse; In the SEM photo of sample-038 with magnifications of 60k (Figure 4-22B), CS-TPP nanoparticles can be seen with brighter contrast compared to the background. Those particles exhibited sphere forms with diameters

around 100 nm. Figure 4-22C, D are two SEM pictures of sample-012 with magnifications of 45k and 18k, respectively. Nanoparticles with sphere and oval shapes can be seen in both photos and some particles with larger size around 200-300 nm can been seen with lower depth of view in Figure 4-22D. Figure 4-22E, F are two SEM micrographs of sample-019 with magnifications of 2.2k and 18k. respectively. Both sphere microparticles with diameters of several micrometers and numerous nanoparticles could be seen in Figure 4-22E. Figure 4-22F shows that spherical nanoparticles are not only dispersed individually but also adsorbed onto the surface of the polymer with a glazed surface and lamellar structure.

The SEM micrographs confirmed formation of CS-TPP particles by ionic crosslinking method. Large agglomerations of nanoparticles were also observed in several samples. Small nanoparticles were absorbed on the surface and might also be inside those large structure with several to dozens of micrometers in size (cannot seen by SEM). Temperature and the way of crosslinking (TPP into CS or CS in to TPP) are detailed in *Annex I*.

By reversing the preparation process, i.e. dropping CS solution into TPP solution, larger particles can be formed with broader particle size distribution from nanoscale to microscale, as confirmed by SEM micrographs of samples. Particle size distribution of sample-019 seemed broader than the ones of sample-021 and sample-038. In the SEM images of sample-019, individual nanoparticles with diameters about 300-500 nm can be seen in Figure 4-22.). Microparticles with several micrometers in diameter were also observed (Figure 4-22E).

4.1.3.2 Particle size

4.1.3.2.1 Nanoparticles

Combination of DLS and SEM

Combining several methods for characterizing particles is commonly used to obtain more accurate and comprehensive information about particle size and morphology. One commonly used combination of techniques is dynamic light scattering (DLS) and scanning electron microscopy (SEM). DLS provides information on the hydrodynamic size of the particles in solution, while SEM allows for visualization of the particles' morphology and size distribution.

In addition, it is important to note that the results may be affected by factors such as sample preparation and instrument limitations. Thus this has to be taken into account when comparing data obtained with different techniques.

In addition to the qualitative information about the surface morphology of the particles, SEM provides also knowledge on particle dimensions (lengths and widths), especially for irregularly shaped particles that cannot be characterized easily with traditional methods including laser diffraction and dynamic light scattering (DLS).

Micrographs of SEM with particle dimensions and particle size distribution of DLS of CS-TPP samples were presented together in Figure 4-23. For each sample, the DLS result was compatible with SEM micrographs (only one image of each sample was showed here). In its SEM micrograph particle size of sample-021 was ranging from about 50 to 150 nm. Likely, in the case of sample-012 and sample-038 were 50-200 nm and 50-800 nm, respectively. Average size determined by DLS of sample-021, sample-012 and sample-038 were 81, 138 and 396 nm, respectively. Particle size of samples determined by these two methods were in the same order of magnitude and thus were in good consistence.

Slight reduction in particle size observed by SEM may due to the dehydration of Cs-TPP particles. Dehydration of particles during the drying for preparation of sample may be responsible for this observation.

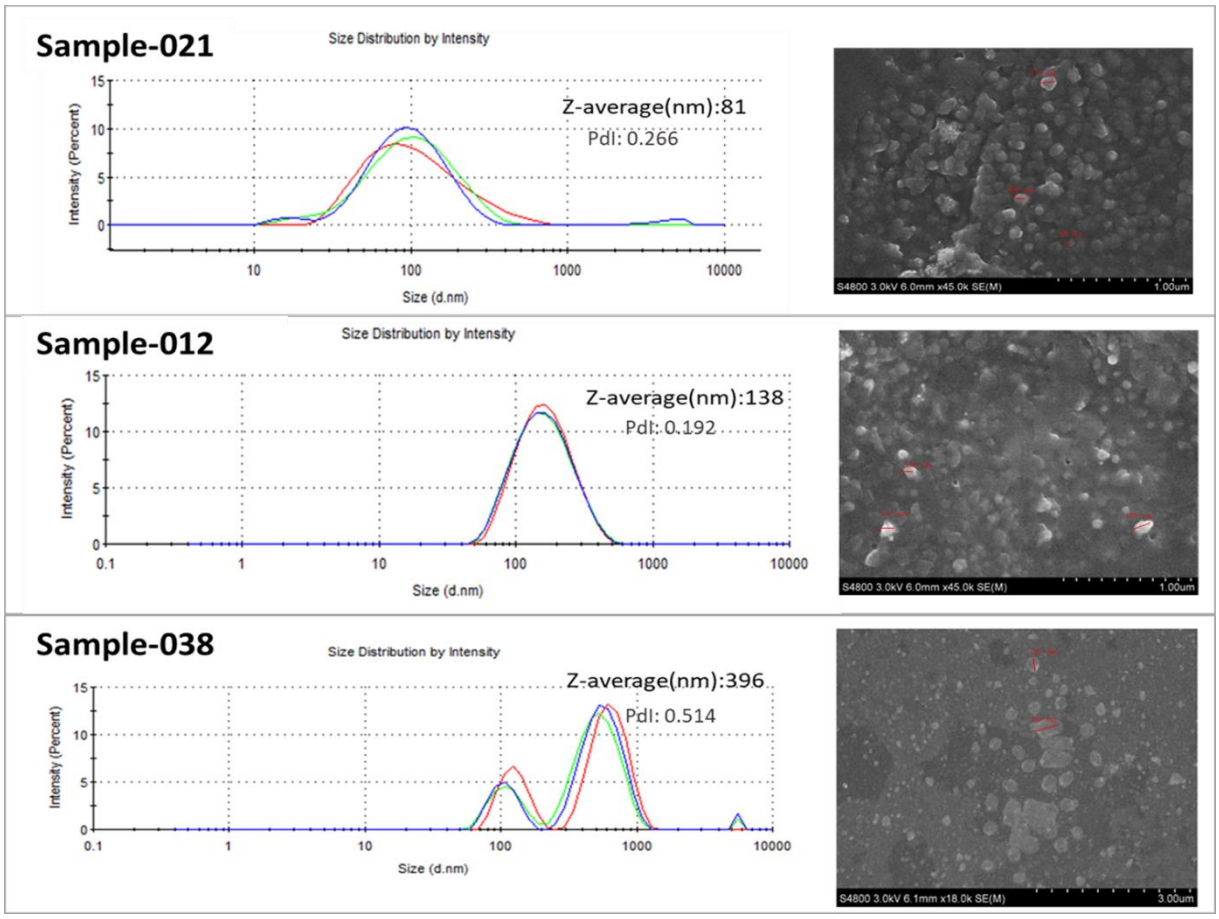


Figure 4-23 Combination of results of DLS (left) and SEM images (right) of sample-021, 012 and 038.

4.1.3.2.2 Microparticles

By increasing concentration of CS or/and TPP, average size of CS-TPP particles increases from nanoscale to microscale.

Observations

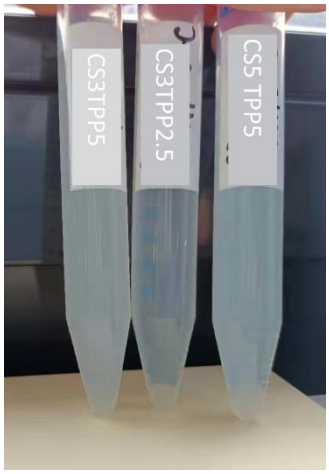


Figure 4-24 Appearance of samples. After addition of TPP and agitation for 1 hour. It was observed that the formed nanoparticle suspension became less turbid in following order: CS3TPP5> CS5TPP5> CS3TPP2.5.

instantaneous opacity appeared as soon as first drop of TPP solution was mixed with CS solution, and this opacity was strengthened along the addition of TPP. Different formulation had visible difference in turbitity. Three samples were prepared with various solutions of CS or TPP thus various mass ratios of CS/TPP and molar ratios of charges (detailed experimental conditions seen in Table 4-6).

Table 4-6 Three CS-TPP samples prepared with various solutions of CS and TPP. Those samples were named based on the concentration of solutions used for preparation of these samples The mass ratio of CS/TPP and molar ratio of charges were also calculated.

Sample	C_{CS}(g/l)	C_{TPP}(g/l)	V_{CS}(ml)	V_{TPP} (ml)	Mass Ratio CS/TPP	Molar Ratio of charges
CS3TPP5	3	5	10	3.3	1.8	1.0
CS5TPP5	5	5	10	3.3	3.0	1.6
CS3TPP2.5	3	2.5	10	3.3	3.6	1.9

When mass ratio of CS/TPP increased from 1.8 to 3.6 and molar ratio of charges from 1.0 to 1.9, the CS-TPP sample became more turbid(Figure 4-24).

Rapid settling was observed of CS-TPP microparticle suspensions. After several hours, clear separation between transparent supernatant and sendiment was seen (Figure 4-24). CS3TPP5 underwent very quick settling. As for CS5TPP5 and CS3TPP2.5 samples, no clear separation could be seen even after 48-hour still putting on bench. This was an indication of better colloidal stability of those two samples.

When mass ratio of CS/TPP increased from 1.8 to 3.6 and molar ratio of charges from 1.0 to 1.9, the CS-TPP sample became more turbid (Figure 4-24). The higher the molar ratio of charges(CS/TPP), the higher the excess of positive charges of chitosan as compared to negative charges of TPP. Electrostatic repulsion among excessives positive chages lead to a relatively stable state of particles. When molar ratio of charges equaled to 1 (no positive charge was in excess), the poorest stability of suspension was indicated by the quickest sedimentation and visually obvious settling of particles.

Settlement speed of CS-TPP formulations were also different. CS3TPP5 formulation seemed settled more quickly than other samples (Figure 4-25). This observation indicates that, finding proper ratio of charges is essential to obtain CS-TPP particle suspensions with convenient colloidal stability.

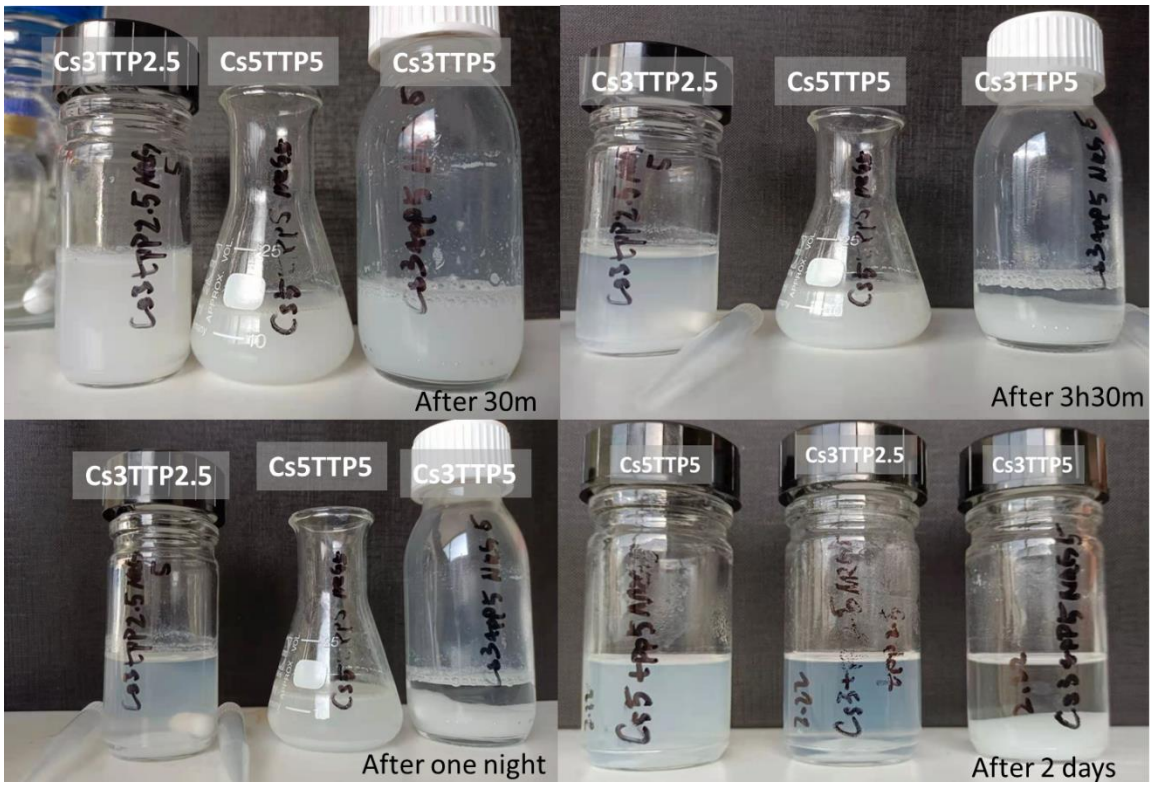


Figure 4-25 CS-TPP particle suspensions, put them still on the bench and observe: newly prepared sample, after 30 min, after 3h30min, after one night and 2 days after preparation.

4.1.3.2.2.1 Size distribution

These particles possess size ranging from several micrometers to around 100 micrometers commonly with unimodal distribution. Exceptionally, sample-048 (Formula: CS5TPP5R4) and sample-076 (Formula: Cs3TPP5) exhibited bimodal distributions. Overall, the value of D[3,2] of CS-TPP microparticles ranged from 2 to 74 µm, while the SPAN values ranged from 0.87 to 3.75.

Table 4-7 D [3, 2], SPAN and distribution mode of some CS-TPP microparticle samples.

Sample	Formulation	D[3,2](µm)	Span	Distribution mode
045	Cs5TPP5	11	2.63	Unimodal
048	Cs5TPP5R4	2[i]	3.75	Bimodal
058	Cs10TPP5R5	16	3.62	Unimodal
075	Cs5TPP5R2.5	20	1.86	Unimodal
076	Cs3TPP5	23[ii]	1.63	Bimodal
080	Cs10TPP5R2.5	6	1.57	Unimodal

[i] D[3,2] (µm)= 0.35; 11.24 for each mode; [ii] D[3,2] (µm)= 17; 318 for each mode

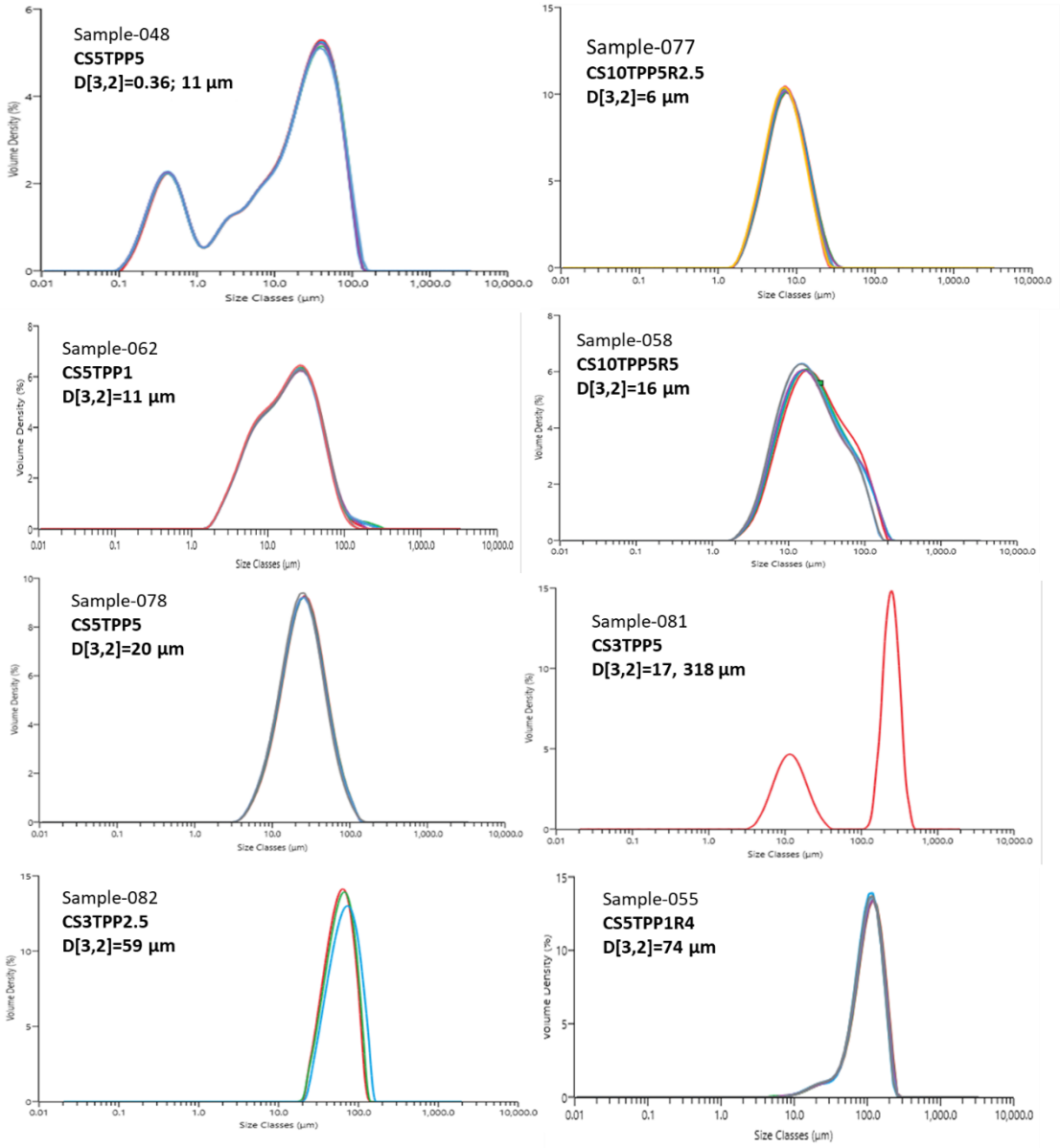


Figure 4-26 Particle size distribution on volume of CS-TPP microparticle (R= CS-TPP Mass Ratio).

The laser diffraction analysis of CS-TPP microparticles is presented in Figure 4-26, which shows various patterns of particle size distribution, including unimodal, bimodal, and even multimodal shapes. These patterns suggest the presence of aggregates of small particles (submicroparticles). To produce samples with narrower size distributions, ultrasonication was applied to break the corresponding aggregates.

Effect of ultrasonication on size distribution

Figure 4-27 Particle size distributions of sample-075 (CS5TPP5R2.5) before (A) and after (B) sonication treatment.

The results indicate that the size distribution changed from a unimodal distribution with a D[3,2] of 19 µm to a bimodal distribution, with a smaller peak ranging from nano to micro scale (D[3,2] = 0.15 µm) and a larger peak at 42 µm. This suggests that the high energy introduced by ultrasonication caused

some agglomerates to break into smaller particles, while simultaneously forming larger clusters of particles.

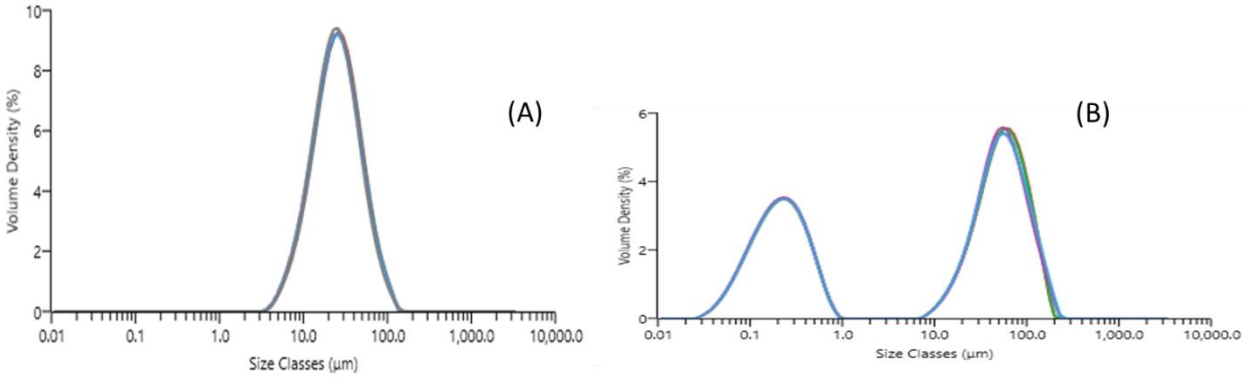


Figure 4-27 Size distribution of sample-075 sample before(A) and after(B) ultrasonication.

4.1.3.2.2.2 TPP-CS microparticles

Sample-009 that was prepared by normal method, i.e. dropping TPP into CS solution. sample-042, 006 and 019 were prepared by reverse method, namely dropping CS into TPP solution. Average size and PDI of above samples are listed in Table 4-8.

DLS results indicates the presence of both small particles and large aggregates in these samples. The particle populations were rather heterogeneous, and the particle size was closer to the micrometer range than the nanometer range. The size distribution of these three samples was multimodal, with large particle peaks appearing in the micrometer region. Both sample-042 and 006 exhibited broad size distributions, with high PDI values (near to 1 in case of sample-006).

Table 4-8 Size information of samples prepared by normal method and reverse method.

Symbol in Figure 4-27	Number in the sample list	Z-average(nm)	PDI	Method
A	009	125	0.39	normal
B	042	550	0.50	
C	006	115	0.96	reverse
D	019	4303	0.28	

4.1.3.2.2.3 ALG coated CS-TPP particles

There are two clear indications of the successful formation of an ALG coating around CS-TPP particles. The first piece of evidence is the increase of particle size after the coating step. The addition of ALG resulted in the particles size distribution shifting towards larger values (micro scale). The second evidence, which strongly supports the successful assembly of an ALG layer around the CS-TPP particle surface, is the reversal of surface charge from positive (prior to coating) to negative (after coating). This overturn in charge can be attributed to chitosan being a positively charged polyelectrolyte at acidic pH, while alginates are negatively charged polymers.

Another interesting experimental observation is that, CS-TPP-ALG (CS-TPP particles with ALG coating) samples can be more easily re-dispersed in liquid after centrifugation step. Without ALG coating, CS-TPP particles alone were found difficult to redisperse in aqueous environment like for instance in $CaCl_2$ solution or water. Consequently, mechanical forces were often needed to adequately redisperse particles. Above mentioned forces may include but not limited to rotation shaking force (Vortex, IKA). ultrasonic force (Vibra cell ™, VCX 750).

4.1.3.2.2.3.1 Size evolution of ALG coated CS-TPP particles

To investigate the size evolution during the ALG coating process, samples-026, 030, 035, and 072 were chosen as examples. The CS-TPP particles were first prepared as described previously at a temperature of 45°C, and afterwards the ALG shell was added through polyelectrolyte complexation. The experimental conditions can be found in the supplementary materials (Annex I). Sample 026 was prepared by adding TPP solution to a chitosan solution under stirring (see sample list). Sample-035 was obtained by coating CS-TPP nanoparticles from sample 026 by adding sodium alginate. Sample-072 was prepared by adding a $CaCl_2$ solution to the suspension of sample 035, followed by two washing steps with water. The evolution of average particle size during this process was monitored.

Table 4-9 summarizes the average size and zeta-potential evolution of CS-TPP particles during the ALG coating process. Upon addition to the ALG solution, the average size of CS-TPP particles increased from 220 nm to 378 nm. Subsequently, when the ALG-coated CS-TPP particles were redispersed in a $CaCl_2$ solution, their size further expanded to 634 nm (sample-026→030→035→072, Figure 4-28). Each step led to roughly doubling the average particle size. This enlargement in size might due to fixation of Ca^{2+} of more ALG polymer chains surrounding ALG coated CS-TPP core. In addition, centrifugal force applied during centrifugation may lead to agglomeration of individual particles. However, during the washing step, the particle size remained relatively unchanged. Figure 4-29 illustrates the size progression of ALG-coated CS-TPP particles during the coating process in a schematic manner.

Table 4-9 Size and zeta-potential evolution of CS-TPP particles during ALG coating process.

Sample code	Sample number	Z-average diameter(nm)	PDI	Zeta potential (mV)
CS-TPP 45°C	026	220	0.37	+34
CS-TPP-ALG	030	378	0.25	-32
CS-TPP-ALG-Ca	035	634	0.14	-29
CS-TPP-ALG-Ca-W	072	637	0.33	-27

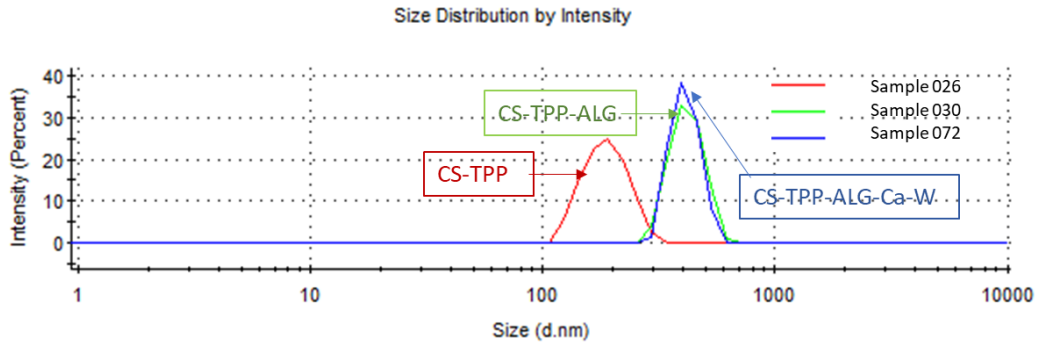


Figure 4-28 Size distribution by intensity of sample-026, sample-030 and sample-072.

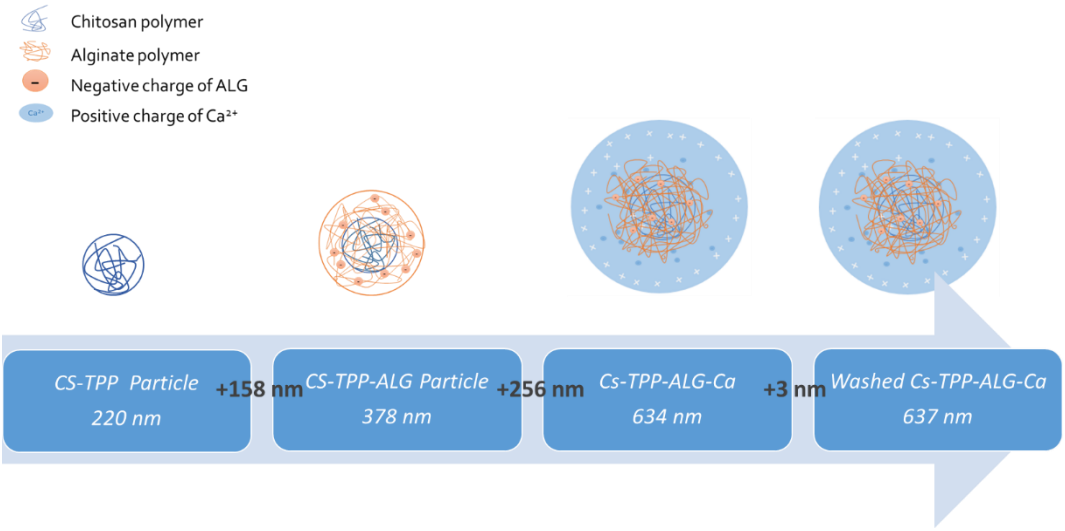


Figure 4-29 Size evolution of ALG coated CS-TPP particles during coating process.

4.1.3.2.2.3.2 Zeta potential evolution of ALG coated CS-TPP particles

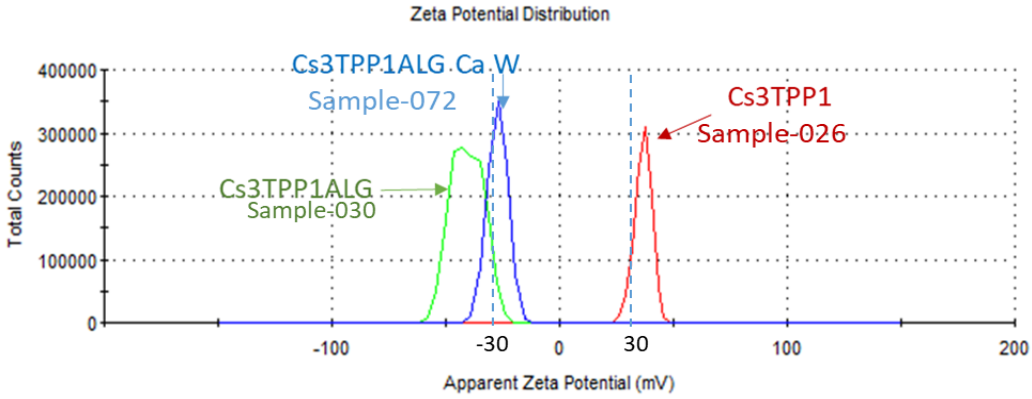


Figure 4-30 Zeta potential distribution of CS-TPP(sample-026, in red). CS-TPP-ALG (sample-030, green) and CS-TPP-ALG-Ca-W (sample-072, blue) samples.

Zeta potential of sample-026 was +34 mV, after addition of ALG (sample-030), the zeta potential turned from positive charge to negative charge -32 mV, then after incubation in $CaCl_2$ solution and washing step (sample-072), zeta potential slightly decreased (absolute value) to -27 mV. The protonation of amino group of chitosan polymer in acidic environment explains the positive charges of CS-TPP particles. The presence of deprotonated carboxylic groups imparts a negative charge on alginate, and thus negative zeta potential of ALG coated CS-TPP particles. Then incubation in $CaCl_2$ solution slightly reduced surface charge of particles (from -32 mV to -29 mV) because of the charge neutralization of Ca^{2+} with negative charges of alginate. In final washing step of process, excess $CaCl_2$ and alginate were washed away. No significant change but slight reduction of surface charge was observed. All above absolute values of zeta

potential of those particles were higher than or close to 30, which indicate good colloidal stability of those samples.

4.2 Effect of process parameters on particle quality (size control)

4.2.1 Concentration of chitosan (C_{CS})

Due to complexity of process. it is hard to explore influence of a single factor without changing other factors at the same time. According to our results, as a single factor, the effect of concentration of chitosan has fluctuant effect on size and PDI of particles and no linear relationship between particle size and concentration of chitosan was observed (Figure 4-31). On the left side of the figure, the samples were prepared at room temperature, while on the right side, the samples were prepared at 45°C. In both figures, the samples are arranged in increasing order of chitosan concentration, from left to right. The influence of chitosan concentration on particle size and polydispersity index (PDI) can be observed to fluctuate, both at room temperature and at 45°C. Consistently, it has been reported that the interaction between the concentration of polymer and the mass ratio of chitosan to TPP has a more significant effect on particle size compared to individual factors such as the concentration of chitosan, concentration of TPP, and duration of cross-linking (Desai, 2016). In conclusion, although no clear correlation between chitosan concentration and particle size was observed, it is still possible that chitosan concentration plays a significant role either as a single factor or in combination with other factors to influence particle size.

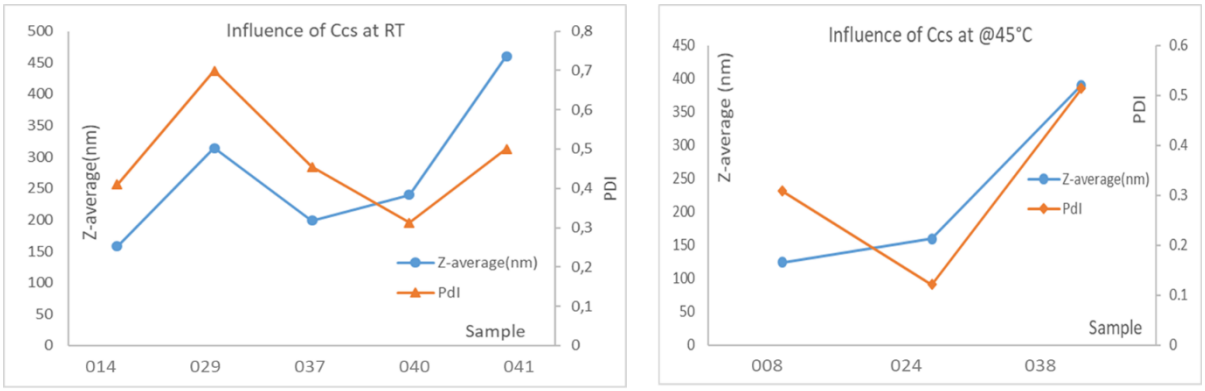


Figure 4-31 Influence of concentration of chitosan on particle size and PDI.

4.2.2 Influence of crosslinking temperature on particle size

Average size and PDI measured by DLS of above samples are listed in Table 4-10 and size distribution by intensity of those samples can be seen in Figure 4-32. Particle size of these sample-007, 009,010 were unimodal distributed between 100-200 nm region, and mainly overlapped with each other. While sample-009 possessed a tiny peak appearing around 5000 nm region (Figure 4-32A). Size distribution of sample-024 was a narrow unimodal distribution and sample-029 was a bimodal distribution (Figure 4-32B). Sample-015 had a broader size distribution spread over tens to thousands nanometers and small tail peak appeared around several micrometers (Figure 4-32C).

Size distribution of sample-007,009 and 010 were all unimodal distribution and their average particle size values given by DLS were very close, which are 122, 125 and 126 nm respectively. PDI of above mentioned samples were not broad (< 0.4). Sample-007 was the most monodispersed and had the lowest PDI as 0.18.

Average size of sample-012 (138 nm) was smaller than sample-015 (176 nm). PDI of sample-012 (0.19) was also narrower than sample-015 (0.42). Similar results were observed in those samples prepared using purified chitosan.

Table 4-10 Particle size and polydispersity index of samples prepared at room temperature and higher temperatures.

Sample	Z-average(nm)	PDI	Temperature(°C)
007	122	0.18	50
009	125	0.39	RT
010	126	0.27	RT
012	138	0.19	50
015	176	0.42	RT
024	160	0.12	45
029	314[i]	0.70	RT

[i] Bimodal distribution

Size distribution of sample-029 were a bimodal distribution having a small peak at 20-90 nm and another peak at 100-500 nm with a very broad PDI (0.70), which indicated that this particle population was very broad. Average size of sample-029 was 314 nm which was almost twice that of sample-024, but given to the high PDI of sample-029, the average size value in fact can no more very well present the overall particle population. Whereas, as a control group of sample-029 prepared at high temperature, sample-024 exhibited a much lower value of PDI (0.12).

The results obtained from DLS indicate that increasing the temperature of the step of particles' formation up to 45/50 °C has a significant impact on the size distribution, resulting in improved homogeneity indicated by lower PDI of the particle population. This effect is observed regardless of the concentration and type of chitosan used. Furthermore, a noticeable decrease in PDI is observed for both CS3TPP1 and CS2TPP1 formulations as the cross-linking temperature increases. It is worth noting that a temperature of 45°C is shown to achieve similar effects as 50°C but with better energy efficiency. In the size distribution analysis by intensity using DLS, it can be observed that at high temperatures (45°C), the particle population exhibits a mono-disperse broad peak instead of multiple peaks.

This phenomenon may be attributed to the increased Brownian motion of molecules at higher temperatures, resulting in an increased mobility of negatively charged species and thus to the formation of more compact and monodisperse particles. Another possible explanation for the smaller particle size is the decrease in viscosity of the chitosan solutions at higher temperatures. This lower viscosity promotes the movement of the cross-linker (TPP) through the chitosan chains, thereby enhancing the interaction between the chitosan and the cross-linker.

A homogeneous size distribution is advantageous in various characterization techniques as it enables more accurate measurements. In cases where mathematical models for analyzing data from inhomogeneous samples are not readily available, a homogeneous size distribution simplifies the analysis process. Additionally, in many industries such as the food industry and drug delivery, mono-disperse particles are desired. This is because they offer better control over product quality and efficiency, leading to improved performance.

In summary, samples prepared at higher temperatures exhibit a more monodisperse particle size distribution, resulting in narrower polydispersity indices (PDI) compared to samples prepared at room

temperature. To ensure the production of homogeneous CS-TPP particles, a crosslinking temperature of 45°C was selected for the preparation of CS-TPP nanoparticles in subsequent studies.

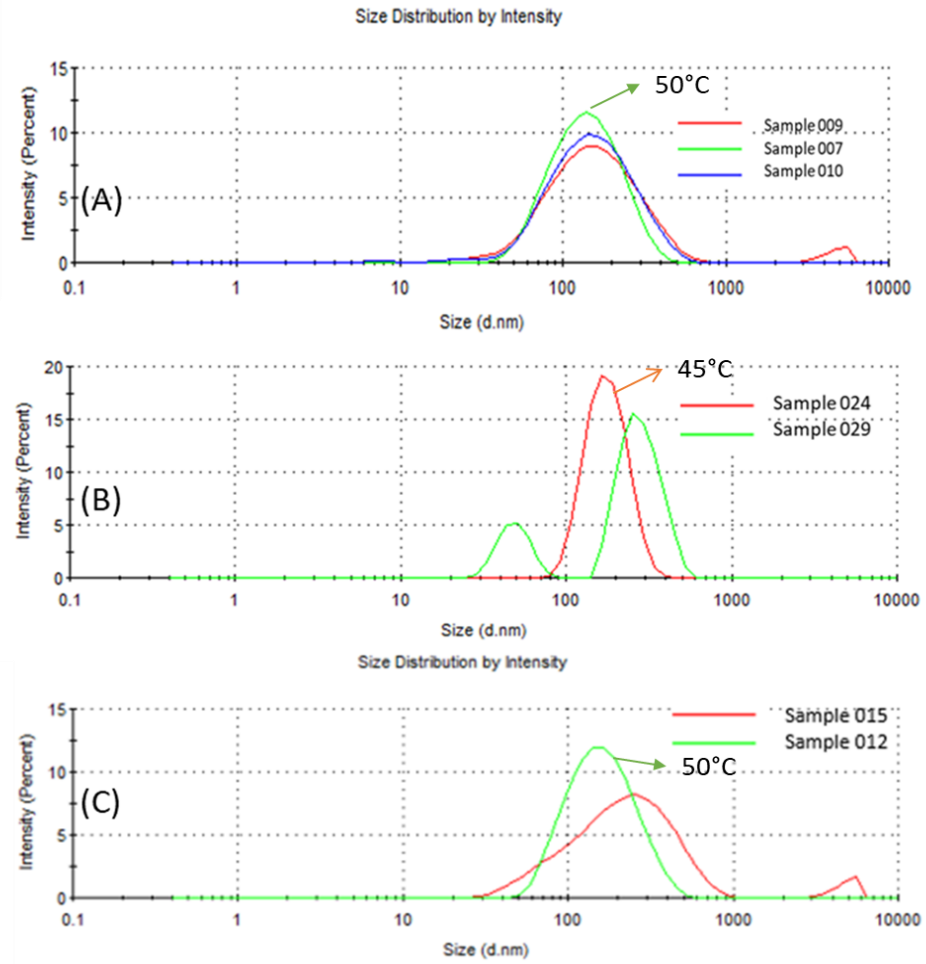


Figure 4-32 (A)Size distribution by intensity of sample-009 (red), 007 (green) and 010 (blue). (B) Size distribution by intensity of sample-024 (red) and sample-029 (green). (C) Size distribution by intensity of sample-015 (red) and sample-012 (green).

4.2.3 Mass ratio of CS/TPP

Sample-023, 027 and 079 are three samples prepared by mixing 0.3%(v/v) CS solution with 0.1%(v/v) TPP solution at room temperature. These samples containing various ratio mass CS/TPP were characterized by DLS (results seen in Table 4-11).

Table 4-11 Preparation conditions of two samples with low mass ratio of CS/TPP.

Sample	C_{CS} (mg/ml)	C_{TPP}(mg/ml)	V_{CS}(ml)	V_{TPP}(ml)	Ratio Mass CS/TPP	Z-average(nm)	PDI
023	3	1	10	12	2.5	140	0.44
027	3	1	50	20	7.5	227	0.47
079	3	1	39	13	9	172	0.50

Results of DLS (Figure 4-33) showed that CS/TPP mass ratio had fluctuant effect on particle size when the concentration of CS was fixed. Whereas, the fact that PDI increased indicating higher heterogeneity of CS-TPP particle population when CS/TPP mass ratio increased.

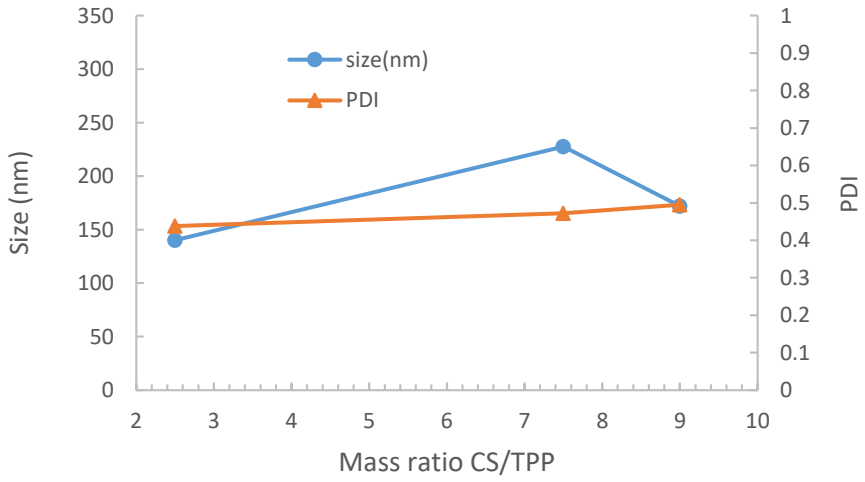
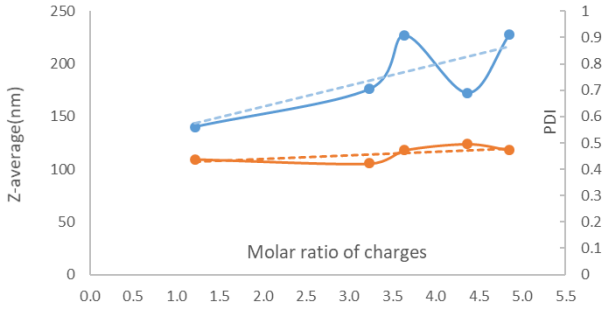


Figure 4-33 Influence of Mass ratio of CS/TPP on particle size and PDI. Mass ratio of CS/TPP ranging from 2.5 to 9 had fluctuant effect on particle size, while PDI increased slightly when mass ratio of CS/TPP increased.

4.2.4 Ratio of charges ($NH_3^+/P_3O_{10}^{5-}$)

A series of samples were prepared with same CS solution (3 mg/L) and various ratio of charges at room temperature to explore effect of molar ratio of charges on particle size and particle distribution. As shown in Figure 4-34, an increase of molar ratio of charges led to an overall increase of particle size when varying over the range from 1.2 to 4.8. The PDI did not seem to be significantly affected by the molar ratio of the charges. As mass ratio of charges increased, particle size had tendency to increase with fluctuation. Those particles were all broadly dispersed (PDI> 0.4). No significant relation between PDI and mass ratio of charges was observed. Experiment details can be found in *Annex I*.

The influence of molar ratio of charges (positive to negative) may be related to the decrease of the number of physical cross-links per chitosan macromolecule.



Sample	Molar ratio of charges	Particle concentration (g/L)	Z-average(nm)	PdI
023	1.2	1.9	140	0.44
015	3.2	1.8	176	0.42
003	3.6	2.4	227	0.47
079	4.4	2.5	172	0.49
027	4.8	2.5	228	0.47

Figure 4-34 Influence of molar ratio of charges on particle formation(Average size(nm) in blue; PDI in orange).

4.2.5 Concentration of particles

As a mentioned before (*3.2.2.2.5 Concentration of particles*), the concentration of particles is an invented term, that has taken both materials used and the total volume into consideration. It indicates concentration of final product in the aqueous environment at the end of particle preparation process.

After observation of 36 CS-TPP samples on focusing on their size and concentration of particles (Data seen in Table Annex I- 4-12). It is interesting to mention that, when particle concentration is below 3 g/L, particle size was often smaller than 240 nm (Expect for sample-037 and 073). Whereas, particles larger than 240 nm usually had particle concentration beyond 3 g/L. Figure 4-35 visualized this trend by tracking down particle size on concentration of particle of those samples, where samples dots were more likely to disperse in II and III zones but less likely in I and IV zones.

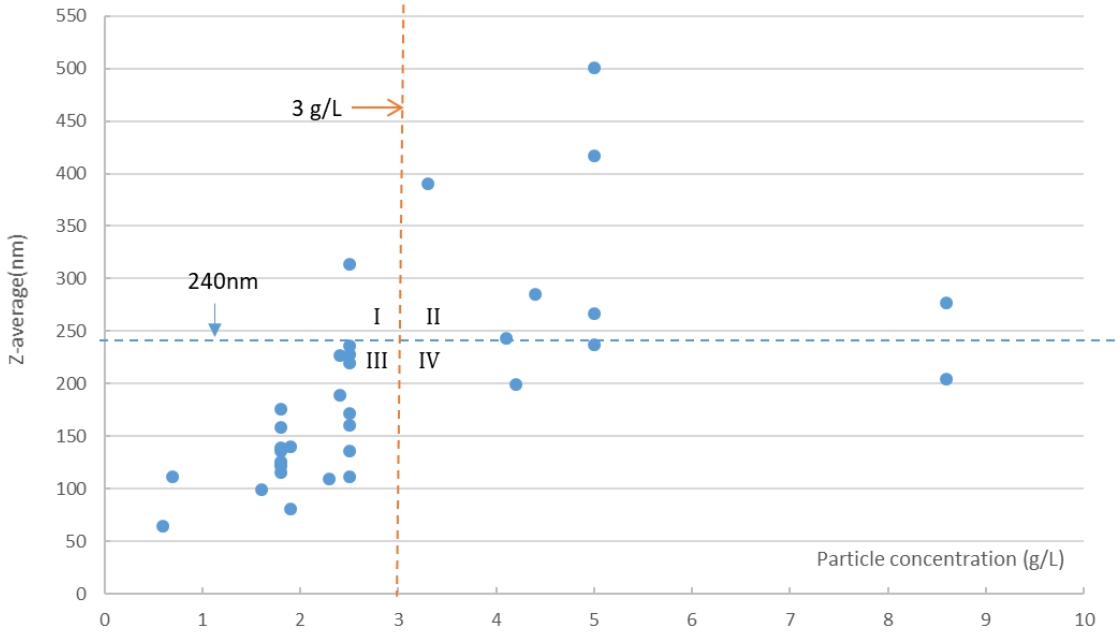


Figure 4-35 Distribution of samples in terms of particle size and particle concentration

However, some exceptions were observed like for example sample-029(appeared in zone I), the particle concentration was 2.5 g/L, the average particle size was 314 nm (>240 nm). This founding can give a rough prediction on particle size based on particles concentration. Like for example, if one wants to produce CS-TPP nanoparticles with a dimension around 100-200 nm, particle concentration less than 3 g/L should be considered preferentially. Statistics analysis of these result data would be recommended to further confirm this observation mathematically.

Although observation of relationship between the particle concentration and size remained sketchy, the particle concentration could still be a useful tool to locate thresholds of experimental conditions somehow, once that the desired size of particles is decided.

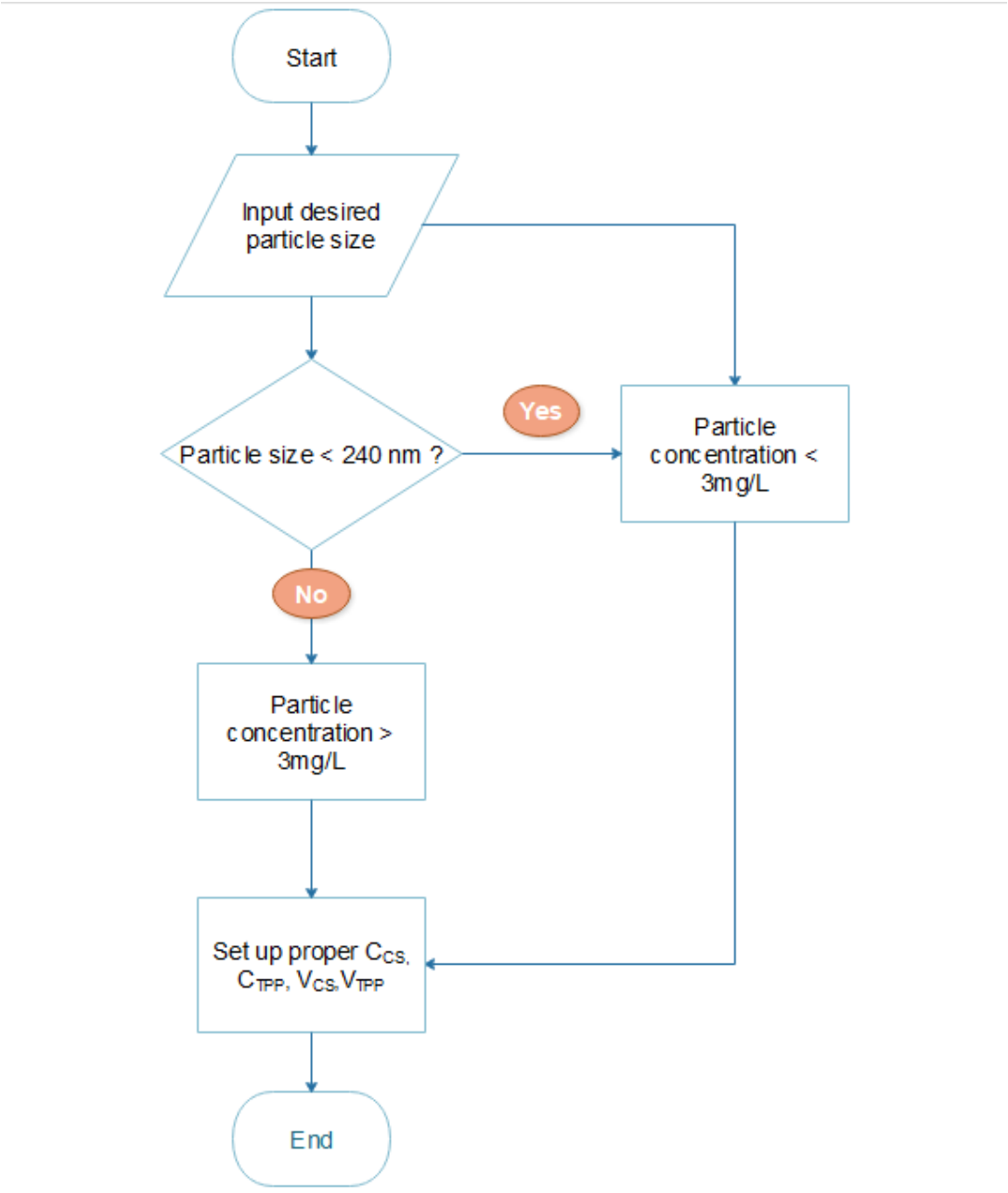


Figure 4-36 Process to start up preparation conditions of particles with expected size.

With the help of particle concentration, one could settle upon experimental conditions to prepared CS-TPP particles with desired size. Based on above mentioned idea, a flowchart was present in Figure 4-36 The flowchart outlines the process for establishing the preparation conditions (C_{CS}, C_{TPP}, V_{CS}, V_{TPP}) necessary to obtain particles of a desired size.

4.3 Encapsulation

Successful preparation of CS-TPP particles was achieved using the ionic gelation method. The particles were characterized in terms of their size distribution, surface potential, and morphology. In contrast to CS-TPP particles, the particles coated with ALG exhibited a negative surface charge. Our attention now turns to evaluating the potential of these prepared particles as carriers for encapsulating and delivering active molecules, specifically polyphenols. Based on a literature search and availability in our laboratory, naringenin, naringin, and catechin were selected as the candidates for encapsulation. The encapsulation efficiency of the CS-based particles in delivering these molecules was determined to assess their efficacy as a drug delivery system. Additionally, the choice of a proper separation method is critical in evaluating the performance and effectiveness of the delivery system. Therefore, the feasibility of using filtration and centrifugation as separation methods was investigated and compared.

4.3.1 Choice of separation method

4.3.1.1 Filtration of NRG, NR and CAT

To evaluate the UV absorbance of the molecules after filtration, separate solutions of catechin, naringin, and naringenin were prepared. The UV spectrophotometric measurements were conducted both before and after passing these solutions through a 0.45 µm cellulose membrane filter.

According to the findings depicted in Figure 4-37, there was no apparent variation observed in the UV-Vis spectrum of the aqueous solution containing catechin (CAT) before and after filtration. The UV spectra of both solutions exhibited almost identical patterns, indicating that there was no substantial alteration in UV absorbance subsequent to filtration. This suggests that the separation of free catechin molecules from catechin-loaded CS-TPP particles using a cellulose membrane filter is a viable approach.

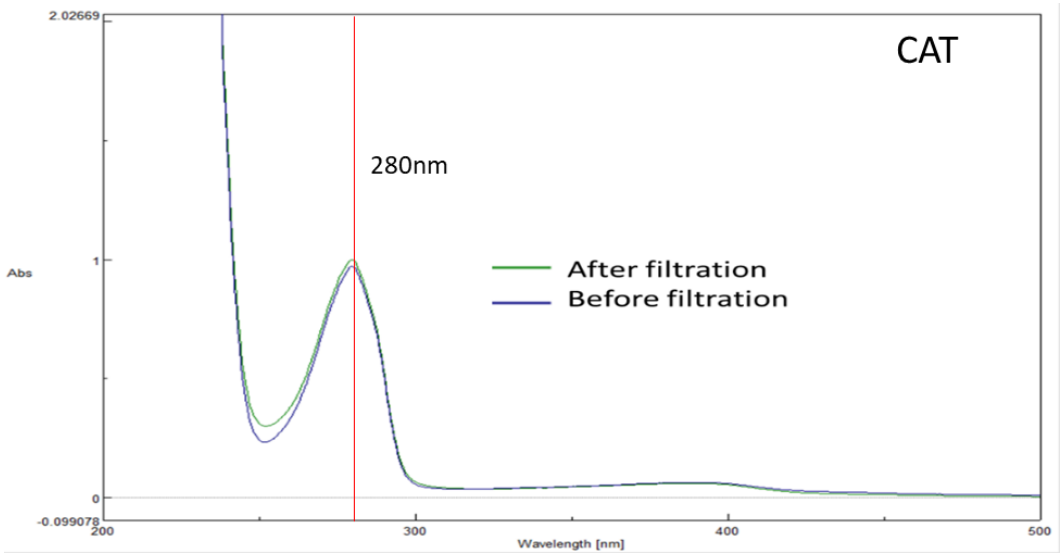


Figure 4-37 UV-Vis spectra of CAT solution before (blue) and after (green) filtrated through 0.45 µm cellulose membrane filter.

Unlike catechin (CAT), noticeable reductions in UV absorbance were observed at the respective λmax wavelengths for naringenin (NRG) and naringin (NR) solutions after undergoing filtration using a cellulose membrane filter, as illustrated in Figure 4-38 and Figure 4-39. This indicates that the filtration process resulted in a significant decrease in the concentration of naringenin and naringin in the solution. Therefore, alternative separation methods, such as centrifugation, were employed for the

encapsulation process of naringenin and naringin to ensure the preservation of their UV absorbance properties.

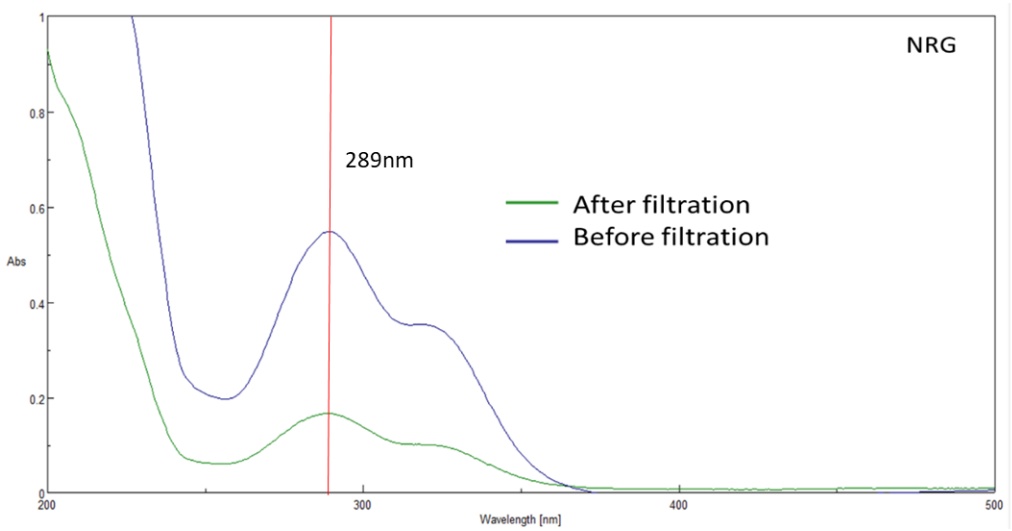


Figure 4-38 UV-Vis spectra of NRG solution before (blue) and after (green) filtrated through 0.45 µm cellulose membrane filter.

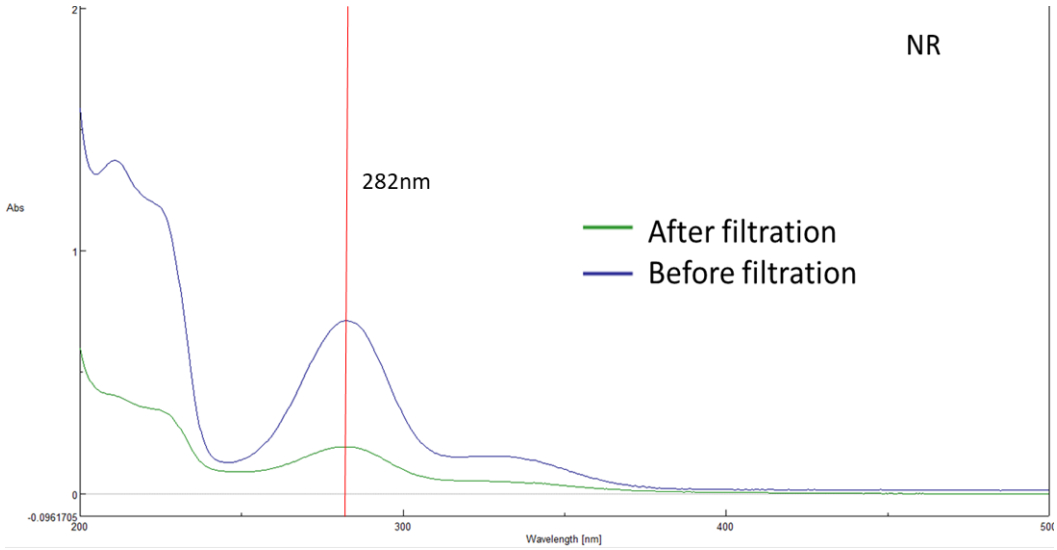


Figure 4-39 UV-Vis spectra of NR solution before (blue) and after (green) filtrated through 0.45 µm cellulose membrane filter.

The observed interactions between naringenin (NRG) and cellulose-based membranes, such as filtration membranes, suggest a potential affinity between NRG and cellulose. Further investigation into the interactions between NRG and cellulose could provide valuable insights into their compatibility and potential as an encapsulation strategy. Cellulose-based materials have been widely used in various drug delivery systems due to their biocompatibility, biodegradability, and ability to control drug release (Sun et al., 2019). Therefore, exploring the potential of cellulose-based materials, such as cellulose derivatives or modified cellulose, for the encapsulation and delivery of NRG could offer new avenues for developing effective drug delivery systems.

4.3.1.1.1 Centrifugation and Filtration of CAT

A suspension of catechin (CAT) loaded CS-TPP particles was divided into two parts for further processing. One half of the sample underwent centrifugation, while the other half was subjected to filtration using a membrane filter. The supernatant and filtrate were subsequently measured UV-Vis spectrophotometrically. UV-Vis spectra showed that no significant difference of UV absorbance was observed of the filtrate and the supernatant of CAT loaded CS-TPP suspension at λ_{max}, 280 nm (Figure 4-40).

This observation indicates that filtration is equally effective as centrifugation in separating unloaded catechin (CAT) molecules from CAT-loaded CS-TPP particles. Considering its user-friendliness and the advantage of requiring a smaller sample volume compared to centrifugation, filtration was chosen as the preferred method for separating free CAT and determining the amount of encapsulated CAT, based on the known initial loaded quantity.

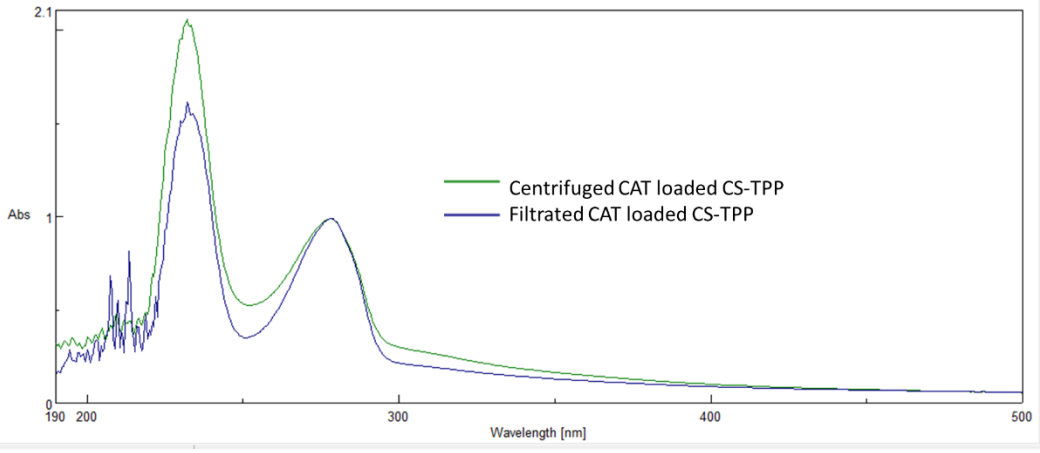


Figure 4-40 UV-Vis spectra of CAT loaded CS-TPP's supernatant obtained via centrifugation (green) and filtrate obtained via filtration (blue).

4.3.1.2 Centrifugation

Sedimentation speed of CS-TPP microparticles

The selection of optimal centrifugation parameters for each sample is crucial to achieve effective separation. The sedimentation speed of the suspension should be considered in order to determine the appropriate centrifugation conditions. Generally, particles that settle more rapidly require milder centrifugation conditions. By taking into account the sedimentation characteristics of the particles, the optimal parameters can be set to ensure a good separation effect of the samples.

Three CS-TPP formulations, namely CS5TPP5, CS3TPP2.5, and CS3TPP5, were chosen as potential candidates for the delivery vehicle.

It was observed that after addition of TPP, the turbidity increased in the following order: CS3TPP5 > CS5TPP5 > CS3TPP2.5. CS3TPP5 was the one that settled most quickly, followed by CS3TPP2.5 and then CS5TPP5. After 2 days of settling, the sedimentation cake of CS3TPP5 was the most densely packed, followed by CS5TPP5 and then CS3TPP2.5.

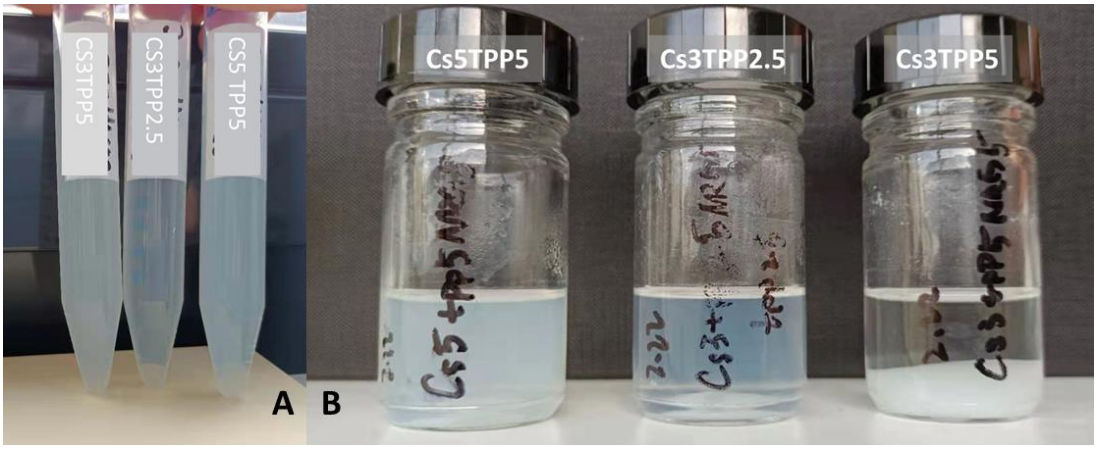


Figure 4-41 Appearance of samples (A) After addition of TPP (B) CS-TPP particle suspensions after 2 days of preparation: CS5TPP5, CS3TPP2.5, CS3TPP5 (from left to right)

CS3TPP5 exhibited the highest sedimentation rate, requiring milder centrifugation conditions, while CS3TPP2.5 encountered challenges during centrifugation with the equipment and conditions available in our laboratory, resulting in incomplete particle separation from the liquid environment and thus inaccurate measurement of encapsulation efficiency.

The centrifugation conditions for these samples were determined and optimized based on the sedimentation rate and empirical results, as presented in Table 4-13. Typically, a higher speed of rotation and longer duration will be required for samples with low settling rate.

Table 4-13 Centrifugation conditions of samples

Sample	Code	Speed (RPM)	Centrifugation time (min)	Temperature(°C)
081	CS3TPP5	3500	5	15
082	CS3TPP2.5	12000	30	15
083	CS5TPP5	5000	20	15

In summary, the separation method employed for catechin (CAT) was filtration, while centrifugation was used for naringenin (NRG) and naringin (NR)

4.3.2 NRG encapsulation

To investigate the impact of naringenin (NRG) encapsulation on the properties of CS-TPP particles, the NRG-loaded particles were subjected to characterization studies focusing on particle size and surface charge.

4.3.2.1 Size evolution of NRG loaded CS-TPP nanoparticles

Sample-073, which represents naringenin (NRG) loaded CS-TPP nanoparticles, was prepared according to the conditions outlined in Annex I. Subsequently, sample-073 was dispersed in an alginate solution while undergoing sonication to generate ALG coated particles, denoted as sample-074. Further, sample-075 denotes the particles obtained after solidification with calcium, and sample-076 represents the particles after being washed with water.

Figure 4-42 illustrates the size distribution by intensity, and Table 4-14 provides information on the Z-average diameter and zeta potential of the particles.

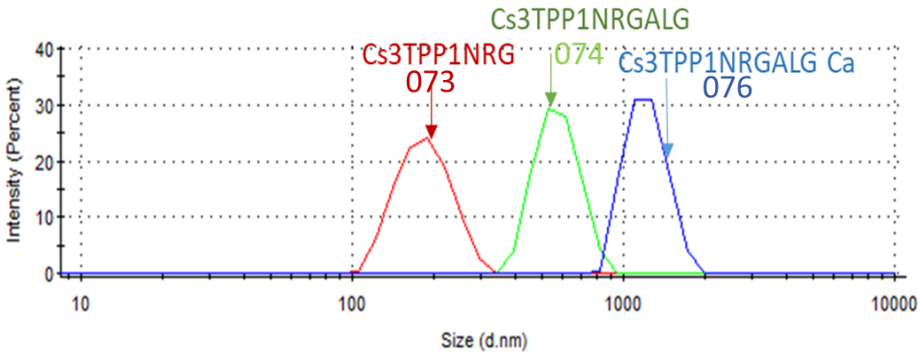


Figure 4-42 Particle size evolution of ALG coated NRG loaded CS-TPP particles during coating process. The particle size greatly increased after addition of ALG and continuously increased after addition of Ca^{2+}.

Table 4-14 Particle size, PDI and zeta potential of ALG coated NRG loaded CS-TPP particle.

Sample	Code	Z-average diameter (nm)	PDI	Zeta potential (mV)
073	CS3TPP1NRG	204	0.35	+40
074	CS3TPP1NAR ALG	501	0.24	-32
075	CS3TPP1NARALGCa	1154	0.29	-29
076	CS3TPP1NARALGCaW	1159	0.37	-53

In comparison to blank CS-TPP particles (sample-026) with a size of 220 nm, the naringenin (NRG) entrapped particles (CS-TPP-NRG) appeared to be more compacted as a slight reduction in average size was observed. Conversely, similar to the NRG-free particles, the addition of ALG resulted in a significant increase in particle size in the NRG-loaded CS-TPP particles (CS-TPP-NRG-ALG), with the size expanding from 204 nm to 501 nm (an increase of 145% in percentage). Additionally, the particle's hydrodynamic diameter continued to increase upon the introduction of Ca^{2+}.

4.3.2.2 Size evolution of Cs-TPP microparticles after encapsulation of active molecules

Three formulations of CS-TPP were chosen for encapsulation of active molecules (sample-081, 082 and 083, for preparation details see in *Annex I*). Particle size and size distribution curve of blank CS-TPP microparticles and active molecule loaded CS-TPP particles were measured by laser diffraction size analyzer (Mastersizer 2000 and Mastersizer 3000, Malvern). Table 4-15 depicts size distribution results.

The surface mean diameter (D[3,2]) and the width of the size distribution (Span) for CS-TPP particles with and without active molecules are presented in Table 4-15. The D[3,2] values for the blank samples (sample-081, 082, and 083) were 51 µm, 57 µm, and 25 µm, respectively. The volume-weighted particle size distribution results shown in Figure 4-43 indicate that blank sample-081 (CAT3TPP5) exhibited a

bimodal distribution, while blank samples 082 (CS3TPP2.5) and 083 (CS5TPP5) displayed a unimodal distribution.

Table 4-15 Particle size of blank CS-TPP particles and active molecule loaded CS-TPP particles

Sample	Formulation	D[3,2](µm)	Span
081	CS3TPP5	51[a]	1.53
	CS3TPP5 (CAT)	47	1.71
	CS3TPP5 (NRG)	34	1.47
082	CS3TPP2.5	57	0.94
	Cs3tpp2.5 (NRG)	82	0.98
083	CS5TPP5	25	2.34
	CS5TPP5 (NRG)	16	5.15

[a] Bimodal: D[3,2] = 23, 309 µm

Encapsulation of active molecules resulted in a decrease in D[3,2] for sample-081 (CS3TPP5) and sample-083 (CS5TPP5). However, for sample-082 (CS3TPP2.5) particles loaded with NRG, the D[3,2] increased from 57 to 82 µm. Furthermore, the particle size distribution of all active molecule-loaded CS-TPP particles exhibited a bimodal pattern, as shown in Figure 4-43. The reduction in the average size of CS3TPP5 and CS5TPP5 particles after encapsulation could be attributed to a higher proportion of smaller particles. The span values, which represent the range of particle size distribution, were relatively broad for these samples. Therefore, it can be concluded that the encapsulation of polyphenol molecules did not lead to significant changes in the particle size of CS-TPP particles.

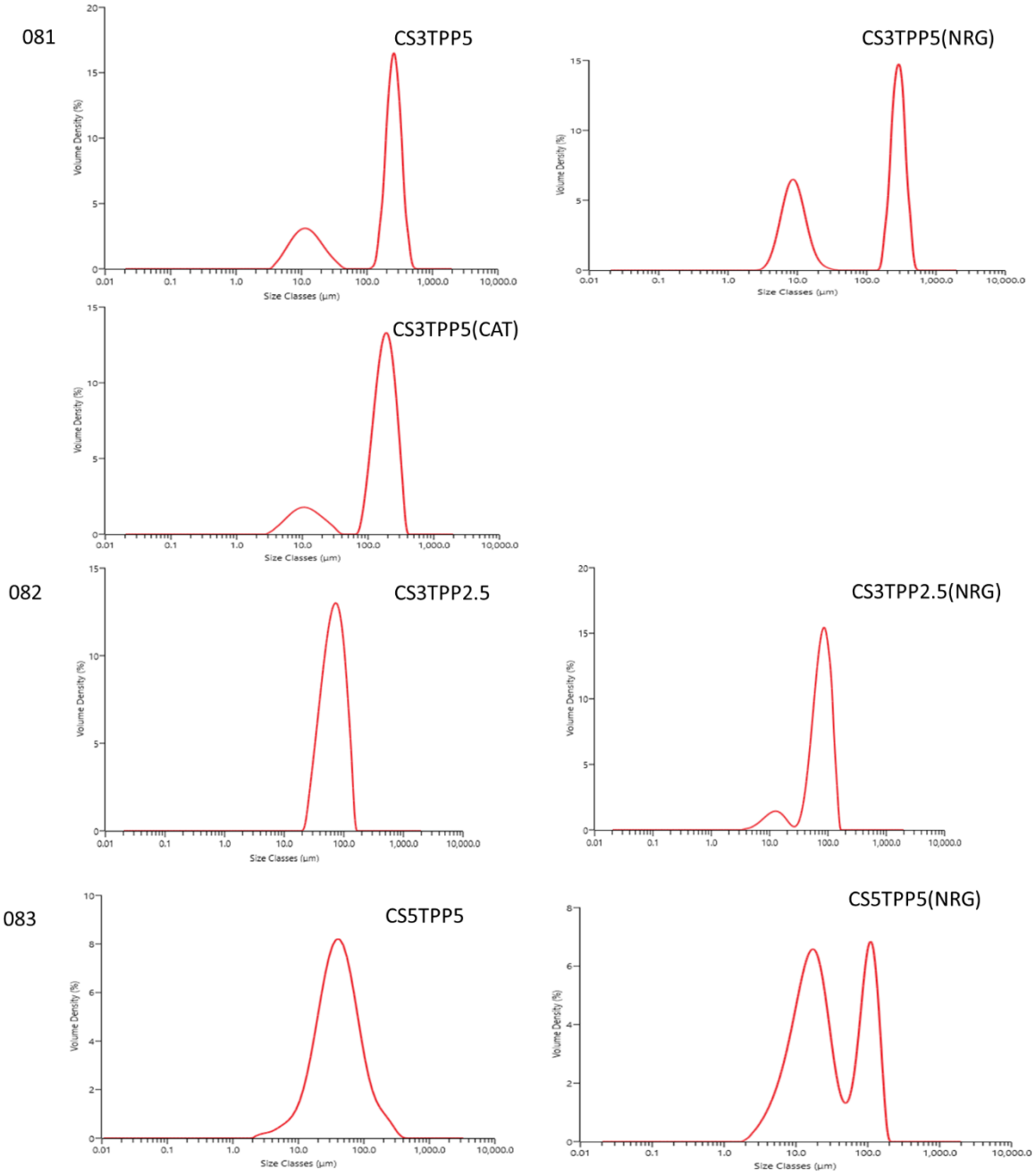


Figure 4-43 Volume weighted particle size distribution of blank CS-TPP particles and NRG/CAT loaded CS-TPP particles

4.3.2.3 Surface charge evolution of NRG loaded CS-TPP nanoparticles

Before the addition of ALG coating, the zeta potential of CS-TPP nanoparticles was positive and relatively high, approximately +40 mV. However, after the addition of the coating, the zeta potential became negative, with a reduction of about 25% in the absolute value of the zeta potential, resulting in a value

of -29 mV. In the final product, sample-076, the absolute value of the zeta potential was extremely high, with a value of 53 mV (Table 4-14).

It is worth noting that after incubation in $CaCl_2$ solutions, the particles were more easily redispersed in aqueous liquid after centrifugation, without the need for extra operation introducing external physical force such as sonication, rotation, or vibration. This was observed for both blank particles and particles loaded with NRG, and may be related to a change in the surface characteristics of the CS-TPP particles coated with ALG.

4.3.2.4 EE% of NRG loaded in CS-TPP particles

High encapsulation efficiencies (> 80%) of naringenin were achieved successfully with various CS-TPP particulate formulations, while slight differences existing in different formulations. CS3TPP5 is the formulation with highest EE% and relatively low deviation. Initial quantity of naringenin (Q_{NRG}) molecules introduced in the system also have influence on EE% values. Higher initial molecule quantity led to higher EE% in all CS-TPP formulations. For formulations loading 2mg of NRG, EE% were about 80%, while for those entrapping 5mg of NRG, EE% achieved to about 90%. What's more, in all CS-TPP formulations, when Q_{NRG} increased from 2mg to 5mg, increase in EE% were observed.

Regardless of Q_{NRG}, EE% decreased in the following order: CS3TPP5 > CS3TPP2.5 > CS5TPP5, and differences among these formulations remain quite small.

Table 4-16 EE% of NRG in CS-TPP particles.

Sample	Q_{NRG}(mg)	EE%[a]	SD (%)
082	2	82	2
081	2	85	1
083	2	82	2
082	5	93	0
081	5	94	1
083	5	89	3

[a] All experiments were repeated twice. Results present here are the arithmetic mean values.

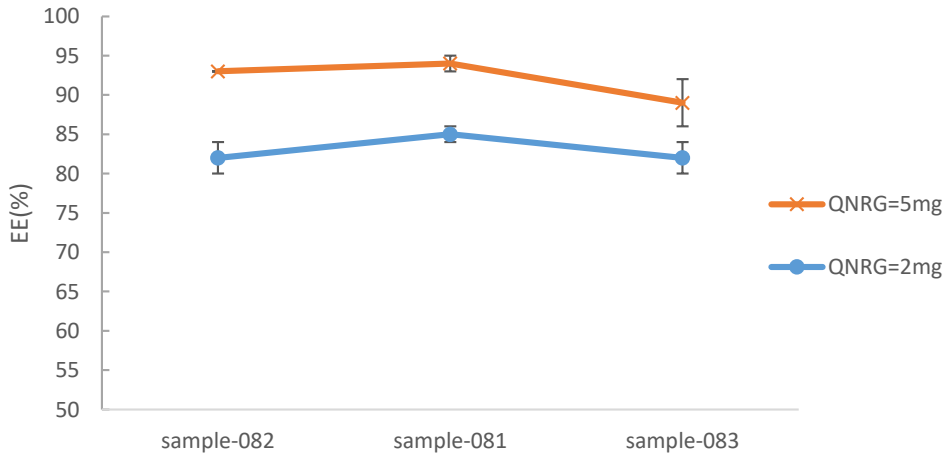


Figure 4-44 EE% of NRG loaded in various CS-TPP systems (x: Q_{NRG}=5 mg; ●: Q_{NRG}=2 mg)

4.3.2.5 EE% of NRG loaded in ALG coated CS-TPP particles

The encapsulation efficiency (EE%) of NRG loaded CS-TPP-ALG particles was compared to that of CS-TPP particles, and a reduction in EE% was observed in the CS-TPP-ALG formulations. This reduction can be attributed to the loss during the additional fabrication steps involved in the preparation of CS-TPP-ALG particles. However, the EE% of NRG in the CS-TPP-ALG formulations remained relatively high, exceeding 50% as shown in Table 4-17. Among the formulations, sample-083 (Formulation: CS3TPP5) was selected for further investigation due to its good colloidal stability and high EE%. Although the preparation process of CS-TPP-ALG particles is more complex, the CS-TPP-ALG particulate system is also an efficient vehicle for the encapsulation of polyphenol molecules such as naringenin. The introduction of extra steps in the preparation of CS-TPP-ALG particles, such as the washing step and the dilution effect due to ALG solution, may contribute to the decrease in EE% of the loaded molecules. However, the overall encapsulation efficiency of the system is still satisfactory, highlighting its potential as a delivery system for polyphenols.

Table 4-17 EE% of NRG loaded in ALG coated CS-TPP particles.

Sample	Q_{NRG}(mg)	EE%	SD (%)
083	1.6	51	3
083	2.4	71	2
083	4.0	82	2

Influence of quantity of naringenin (Q_{NRG}) on EE%

Figure 4-45 demonstrates the relationship between the initial quantity of NRG and the encapsulation efficiency (EE%) of NRG-loaded CS-TPP particles. It is evident that in all CS-TPP formulations, a higher quantity of naringenin leads to a higher EE% within the range of 1.5 mg < Q_{NRG} < 4.5 mg. This observation can be attributed to the relatively stable loss of entrapped molecules during each step of the particle preparation process. As the total amount of molecules increases, the proportion of molecules lost in the process decreases. This results in a higher proportion of loaded molecules and, consequently, an increase in the encapsulation efficiency.

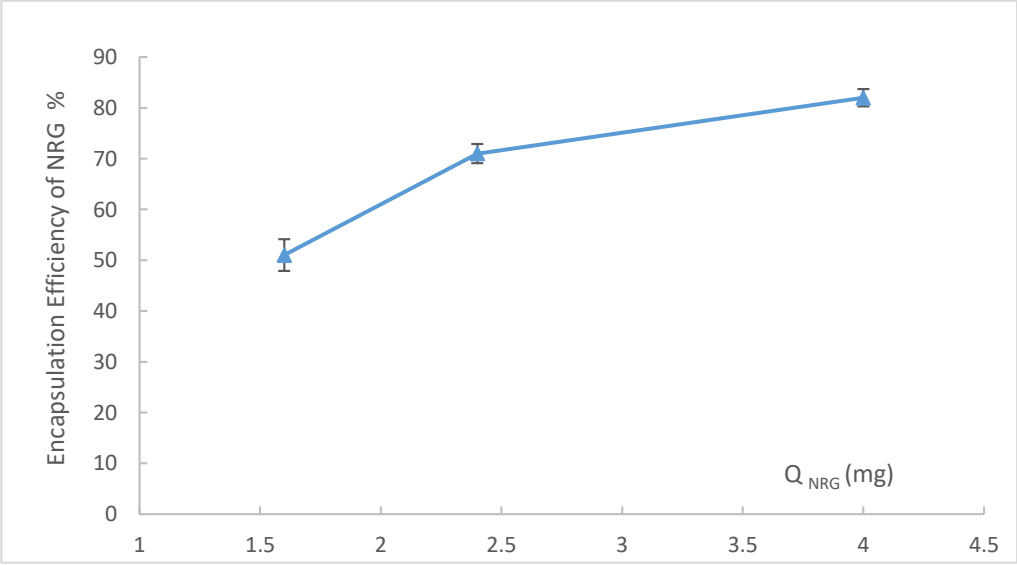


Figure 4-45 Influence of Q_{NRG} on EE% of CS-TPP-ALG particles

In contrast to the findings in the current study, another article reported conflicting results when using similar CS-TPP nanoparticles for the delivery of NRG. In that study, an increase in the concentration of NRG from 0.1 to 0.25 mg/mL resulted in a significant decrease ($p \leq 0.05$) in the encapsulation efficiency (EE%) from 74.6 ± 4.09% to 59.19 ± 5.36%(Shadab et al., 2019). These differing results suggest that the encapsulation efficiency of NRG in CS-TPP nanoparticles can be influenced by various factors, such as the specific formulation, preparation method, and concentration of the active molecule. Further investigation is needed to understand the underlying mechanisms and optimize the encapsulation process for achieving consistent and high encapsulation efficiency.

4.3.3 Naringin entrapped in CS-TPP particles

EE% of NR loaded CS-TPP particles was either not detectable or very low, less than 10% (as shown in Table 4-18). After dispersing the CS-TPP particles loaded with NR in water, drug release was monitored using a UV-Vis spectrometer at specific time intervals. However, no detectable absorption was observed in the UV-Vis spectra when the initial amount of NR (Q_{NR}) was either 3 or 10 mg. On the other hand, a slight absorption was detected when the initial amount of NR (QNR) was 1 and 5 mg. However, in some cases, the baseline of UV-Vis spectra drifted (Figure 4-46), indicating poor quality of certain measurements. This could be attributed to the insufficient amount of NR molecules inside the CS-TPP particles, which made it difficult to accurately detect them using UV-Vis spectrometry.

This results suggest that the use of CS-TPP particulate system may not be a suitable method for encapsulating the naringin molecule.

Table 4-18 EE% of NR in CS-TPP particles

Q_{NR}(mg)	EE%
1	8%
3	---*
5	5%
10	---*

* No detectable encapsulation

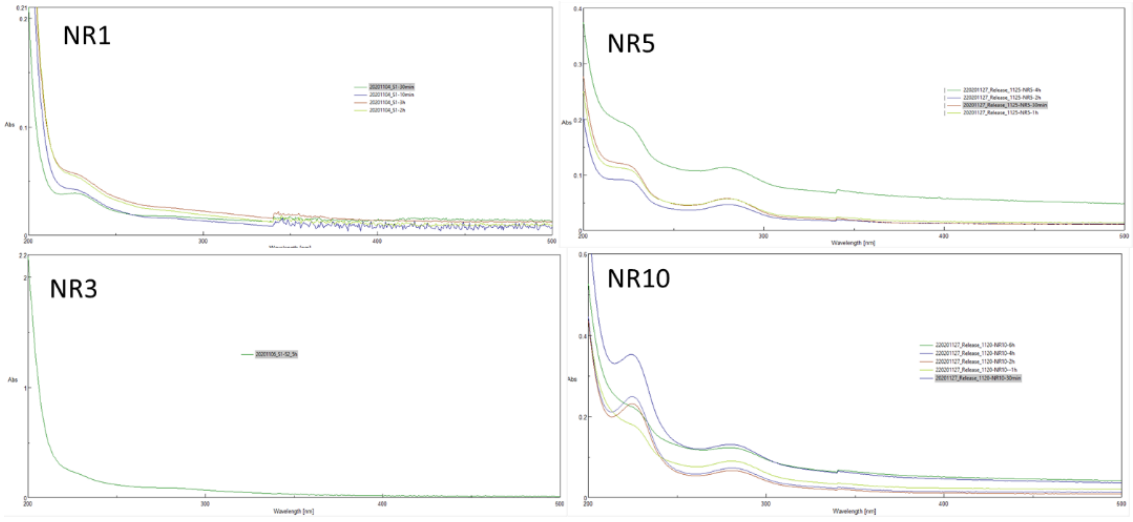


Figure 4-46 UV-Vis spectra of redispersed NR-loaded CS-TPP particles to monitor release of NR from these particles

4.3.3.1 EE% of NR loaded in ALG coated CS-TPP particles

The results obtained when loading 5 mg and 10 mg of NR into ALG coated CS-TPP particles (formulation: CS3TPP5) showed undetectable encapsulation efficiency (EE%) of NR. This suggests that the use of ALG coated CS-TPP particulate system may not be suitable for effectively encapsulating the naringin molecule. It is possible that the characteristics of naringin, such as its solubility or interaction with the particle matrix, hinder its successful encapsulation within the ALG coated CS-TPP particles. Alternative methods or formulations may need to be explored to achieve efficient encapsulation of naringin or other similar molecules.

4.3.4 CAT entrapped in CS-TPP particles

4.3.4.1 Verification of solubility of CAT in water at room temperature

After 4-hour dissolution, no visible impurities were detected in the transparent light orange/yellowish solution, as shown in Figure 4-47. The exact solubility of the CAT substance used is unknown, but it was found to dissolve completely in water at a concentration of 5 g/L at room temperature. This result is consistent with previously reported data in the literature (Cuevas-Valenzuela et al., 2014; Matsubara et al., 2014).

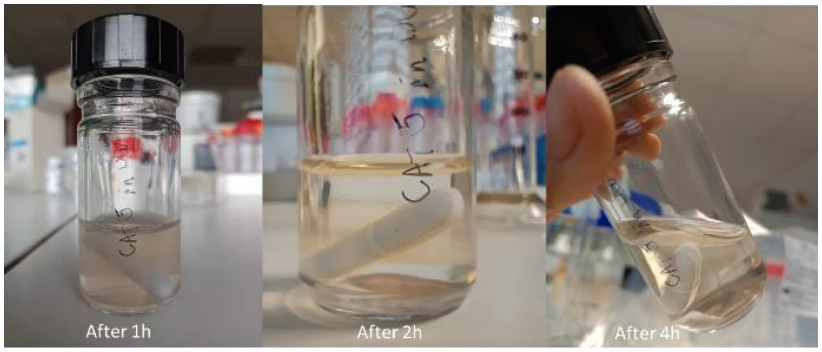


Figure 4-47 CAT water solution with concentration of 5g/L at room temperature

4.3.4.2 EE% of CAT in CS-TPP particles

Figure 4-48 presents the preparation process of CAT loaded CS-TPP particles. Before addition of TPP, the mixture of CS and CAT solution was transparent. While after addition of TPP solution into above mixture, turbidity appeared within seconds.



Figure 4-48 Mixture of chitosan and catechin solution before(A) and after(B) addition of TPP solution

Table 4-19 displays the encapsulation efficiency (EE%) of different CS-TPP formulations for CAT dissolved in solutions with varying proportions of ethanol. The results show that the highest EE% achieved for CAT was 29%. However, in some cases, the amount of free CAT detected by UV spectrophotometry was equal to or greater than the amount of CAT added (Q_{CAT}), which is not practical. Therefore, these cases were recorded as non-detectable in the table. Furthermore, sample-082 showed a very low EE%, regardless of the solvent used to dissolve CAT.

Table 4-19 Encapsulation capacity of CS-TPP formulations of CAT(dissolved in water, in 50% EtOH and in EtOH).

Sample	Q_{CAT}(mg)	EE%	Formulation	Solvent of CAT
081	2	---*	CS3TPP5	Water
082	2	---*	CS3TPP2.5	Water
083	2	---*	CS5TPP5	Water
081	2	6	CS3TPP5	50% EtOH
082	2	---*	CS3TPP2.5	50% EtOH
083	2	13	CS5TPP5	50% EtOH
081	2	10	CS3TPP5	EtOH
082	2	1	CS3TPP2.5	EtOH
083	2	17	CS5TPP5	EtOH
081	5	29	CS3TPP5	EtOH
082	5	---*	CS3TPP2.5	EtOH
083	5	28	CS5TPP5	EtOH

* No detectable encapsulation

4.3.4.3 Influence of solvent composition of CAT on EE%

The results obtained from the encapsulation of CAT into CS-TPP formulations (sample-081, 082, and 083) indicate that the solvent composition of CAT has a significant effect on the encapsulation efficiency

(EE%). When CAT was dissolved in water, the encapsulation into CS-TPP particles was unsuccessful, as reflected by the low EE% values reported in Table 4-19.

When CAT was dissolved in 50% EtOH (EtOH:water=1:1) or pure EtOH, successful loading of CAT into certain CS-TPP formulations was achieved, although the encapsulation efficiency percentages were below 20%. Furthermore, it was observed that the encapsulation efficiency percentages of CAT in pure EtOH were higher than those in 50% EtOH, as shown in Figure 4-49.

These findings suggest that the choice of solvent during the encapsulation process plays an important role in determining the encapsulation efficiency of CAT in CS-TPP particles. The use of EtOH, particularly pure EtOH, appears to be more favorable for achieving higher encapsulation efficiency percentages. The underlying reasons for these solvent-dependent effects on encapsulation efficiency could be attributed to the solubility and interactions between CAT and the CS-TPP particle matrix. Further investigation and optimization of the encapsulation process with different solvent compositions may be necessary to enhance the encapsulation efficiency of CAT in CS-TPP particles.

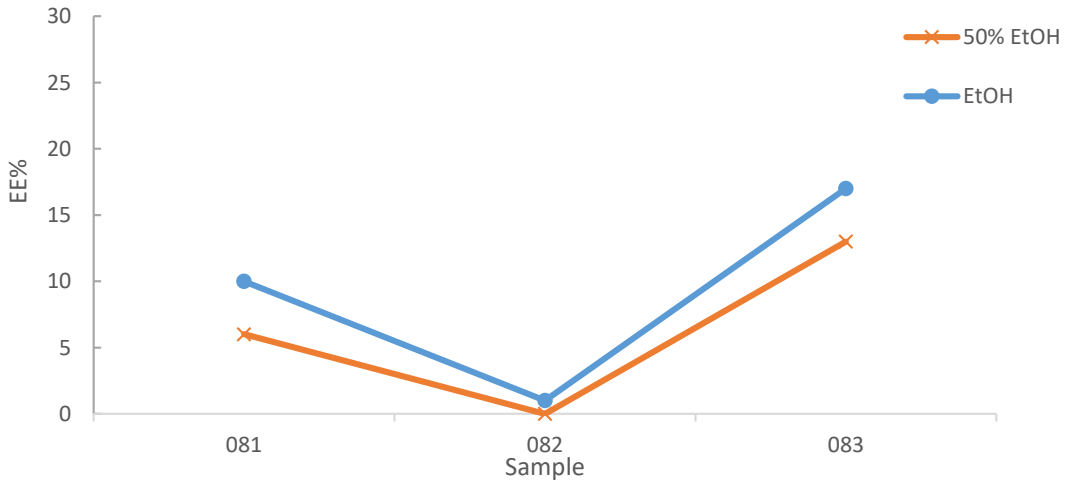


Figure 4-49 EE% of CAT loaded CS-TPP samples, Q_{CAT}=2mg (x: CAT was dissolved in 50%EtOH; ●: CAT was dissolved in EtOH)

Despite the confirmation of full dissolution of CAT in water at room temperature, it was found that increasing the proportion of EtOH in the solvent of CAT was beneficial for the encapsulation of CAT into CS-TPP particles.

4.3.4.4 Influence of Q_{CAT} on EE% of CAT

An ethanol solution containing 5 mg of CAT was utilized to encapsulate CAT into the CS-TPP formulations mentioned above. It was observed that when the amount of CAT increased from 2 mg to 5 mg, the encapsulation efficiency percentages of CAT increased to nearly 30% for samples-081 and 083 (Figure 4-50).

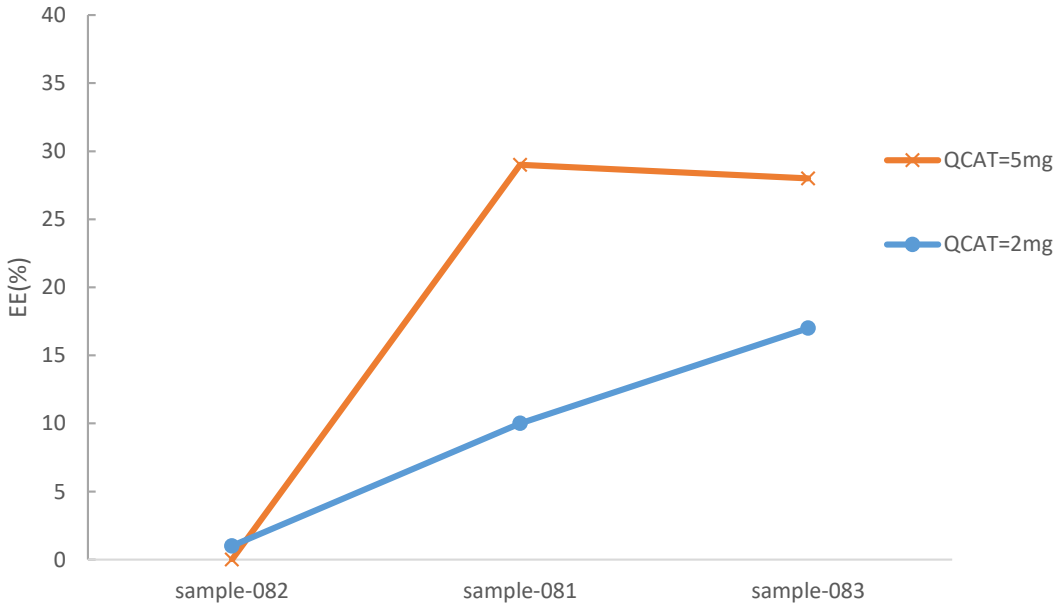


Figure 4-50 EE% of CAT (in EtOH) loaded CS-TPP in different CS-TPP formulations (x: Q_{CAT} =5 mg; ●: Q_{CAT} =2 mg).

Additionally, the EE% of sample-082 remained almost negligible, regardless of quantity of CAT added. Therefore, this particular formulation (CS3TPP2.5) is deemed unsuitable for CAT encapsulation.

In conclusion, the encapsulation efficiency (EE%) of CAT in CS-TPP particles is lower than that of NRG overall. However, a higher proportion of ethanol in the solvent of CAT may promote a greater EE% of CAT. The highest EE% of CAT, reaching approximately 30%, was obtained when a higher quantity (Q_{CAT} =5 mg) of CAT was dissolved in EtOH.

Additionally, errors in measurement and analysis may have arisen from inaccuracy in volume measurements and the presence of nanosize particles that could pass through the filter and cause overestimation of unloaded CAT and underestimation of EE%.

In summary, among these three polyphenol molecule candidates, naringenin is the best choice for further investigation i.e. release properties, due to its high EE% and also for good repeatability of experiment results.

4.3.4.5 EE% of CAT loaded in ALG coated CS-TPP particles

When attempting to load 5 mg of CAT into ALG coated CS-TPP (formulation: CS5TPP5), the encapsulation efficiency (EE%) of CAT was determined to be 4% with a standard deviation of 4%.

4.3.5 Easier redispersion of particles after lyophilization

After centrifugation of suspensions of CS-TPP nanoparticles, massive pellets of NPs were concentrated at the bottom of Eppendorf tube due to centrifugal force. The opalescent pellet seemed very compact

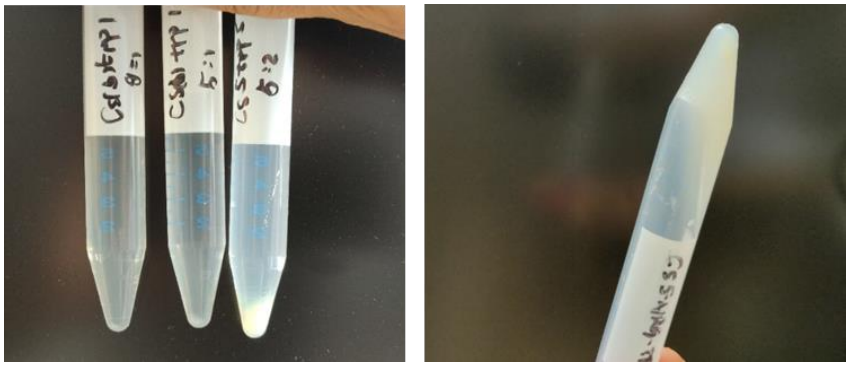


Figure 4-51 Two photos of newly prepared CS-TPP particles after centrifugation. Precipitate (pellet) of CS-TPP nanoparticles at the bottom of Eppendorf tube after centrifugation.

and difficulty was encountered to redisperse these pellets in aqueous liquid even with the help of a Vortex mixer or an ultrasonic water bath. White pellet of CS-TPP particles aggregation was still seen in redispersed suspension (Figure 4-51).

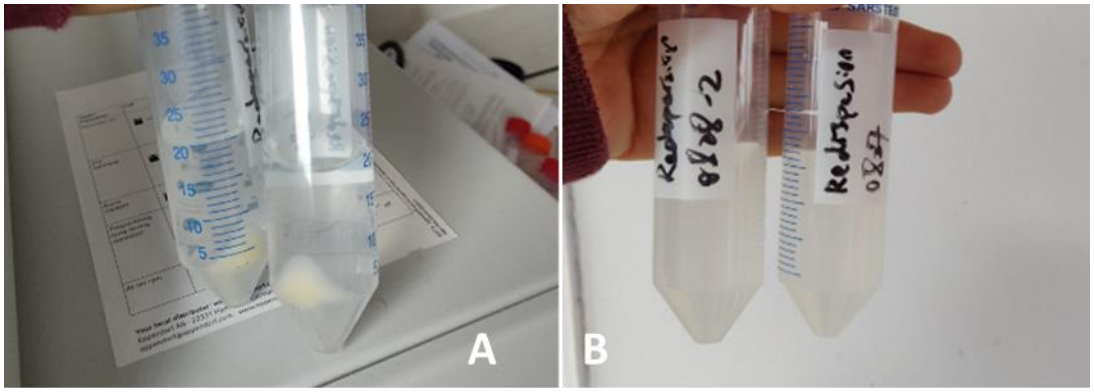


Figure 4-52 The appearance of pellet CS-TPP particles after centrifugation(A), and redispersed suspension of lyophilized CS-TPP particles (B)

On the other hand, lyophilized CS-TPP NPs can be more easily redispersed. The new suspension seemed very homogeneous and no precipitate was visible (Figure 4-52). Unlike newly prepared CS-TPP NPs, lyophilized CS-TPP NPs could be redispersed in water by shaking by hand with ease. No extra external force need to be introduced to obtain homogeneous suspension of lyophilized CS-TPP NPs particles. Possible explanation of this phenomena might be that lyophilization operation induced more loose porous structure of particles during freezing and drying process of water contained in samples.

4.4 Release of NRG from CS particles

As mentioned earlier, three polyphenol molecules, namely naringenin, naringin, and catechin, were attempted to be encapsulated using CS-TPP particles prepared with different formulations. The encapsulation of naringenin and catechin was successful, while encapsulating naringin proved to be challenging. Additionally, naringenin showed a higher affinity towards CS-TPP carriers, resulting in

significantly higher encapsulation efficiency compared to catechin. Therefore, naringenin was selected as the loaded molecule for further investigation of its release kinetics in specific media.

4.4.1 Establishment of release kinetics experimental conditions

In order to ensure the proper measurement of release kinetics and obtain accurate and reliable results, careful investigations were conducted regarding the experimental conditions. Several aspects were considered, including the volume of the release media, the method of separation, and the composition of the media.

4.4.1.1 Media volume

In pharmaceutics, during the dissolution testing, the dissolution volume is usually 5 to 10 times greater than the volume present in the saturation solution of target substance. So, concentration of dissolved substance should be 5 to 10 times lower than the saturated concentration in this medium. That is because the dissolution rate will progressively decrease when the concentration gets close to the saturated point, which can cause faulty test results (Ghosh and Jasti, 2004; Liu, 2008).

In the context of release testing, a "sink condition" refers to a situation where the concentration of the substance in the release medium is significantly lower than its solubility. In a perfect sink condition, the drug is rapidly and completely dissolved, ensuring that the dissolution rate is not limited by the solubility of the substance. The exact threshold for a perfect sink condition may vary depending on the specific molecule and its solubility characteristics. However, commonly accepted value is to keep the concentration in the release medium below 10% of its solubility. Maintaining a sink condition is crucial for accurate and reliable release testing, as it allows for a consistent and reproducible assessment of the drug's dissolution behavior. It ensures that the release process is not solubility-limited and provides meaningful data for determining drug release rates and dissolution profiles.

To establish the appropriate volume of release media that ensures sink conditions throughout the release process, it is essential to have a comprehensive understanding of the solubility of NRG. This is particularly important as solubility data for NRG available in the literature span a wide range. (14-214 mg/L, Table 1-3).

4.4.1.1.1 Determination of solubility of NRG

The release kinetics of NRG (4.4 mg) were evaluated in various volumes of release medium ranging from 10mL to 800mL, and the results were plotted over time (Figure 4-53). The final concentration of naringenin in each release medium was determined when the concentration reached a plateau. In water, regardless of the volume, the release profile of NRG exhibited a rapid initial release within the first 120 minutes, followed by a more sustained and stable release in the subsequent phase.

The cumulative release of NRG differed among different water volumes. In 10mL, 50mL, and 100mL of water, the cumulative release of NRG was distinct at each time interval and eventually reached 5%, 30%, and 55%, respectively. Conversely, in 400mL and 800mL of water, the loaded NRG was completely released by the end of the dissolution period (over 4320 minutes). This was in contrast to the other cases where the dissolution of NRG was limited and reached a certain amount. Furthermore, the release profile of NRG in 400mL of water was similar to that in 800mL from the initial point, and the maximum amounts released in these two samples were relatively close to each other (close to 100%).

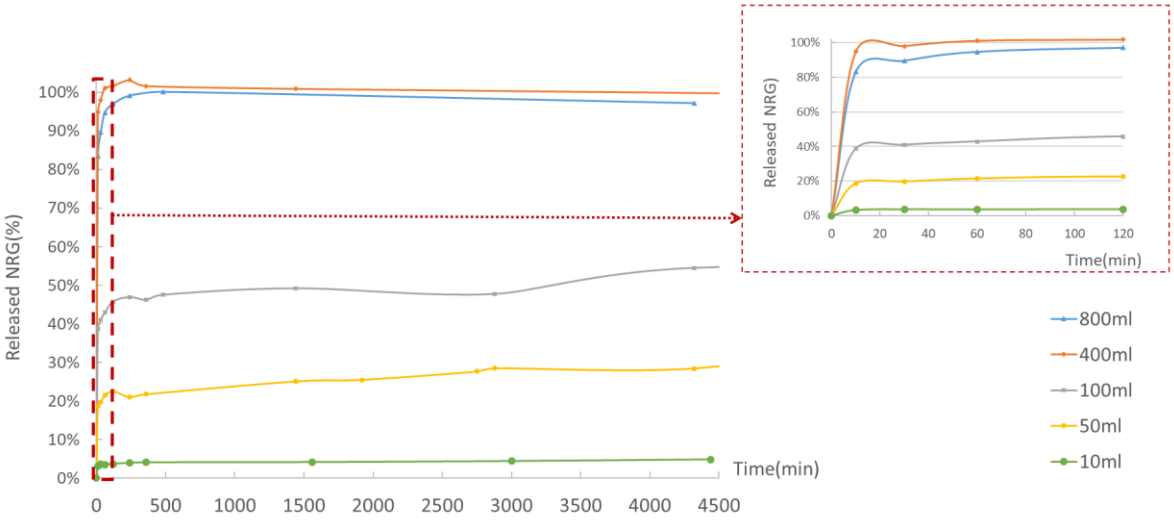


Figure 4-53 Release of NRG from CS-TPP particles in various volume of water at room temperature.

Dissolution volume, amount of released NRG and the final concentration of NRG in the media at the end of dissolution (calculated by dividing released NRG by dissolution volume) were present in Table 4-20.

Table 4-20 : Maximal concertation of naringenin during dissolution testing in media with various volume

Dissolution Volume (mL)	Released NRG (mg)	Maximal concentration (mg/L)
10	0.213	21.3
50	1.141	22.8
100	2.064	20.6
400	4.264	10.7
800	4.016	5.0

The results revealed that the final concentrations of NRG were approximately 21 mg/L when the dissolution volume ranged from 10 mL to 100 mL. These concentrations corresponded to the solubility limit of NRG in our experimental setup. The release of NRG from within the particles was hindered by the saturation of NRG in the surrounding dissolution media. However, when the dissolution volume was increased up to 400 mL and 800 mL, the final concentration of NRG was lower, indicating that the solution was not saturated. Interestingly, in these two cases, the final release amount approached the total amount (4.4 mg) of naringenin loaded in CS-TPP particles, indicating that all the NRG was dissolved in the media.

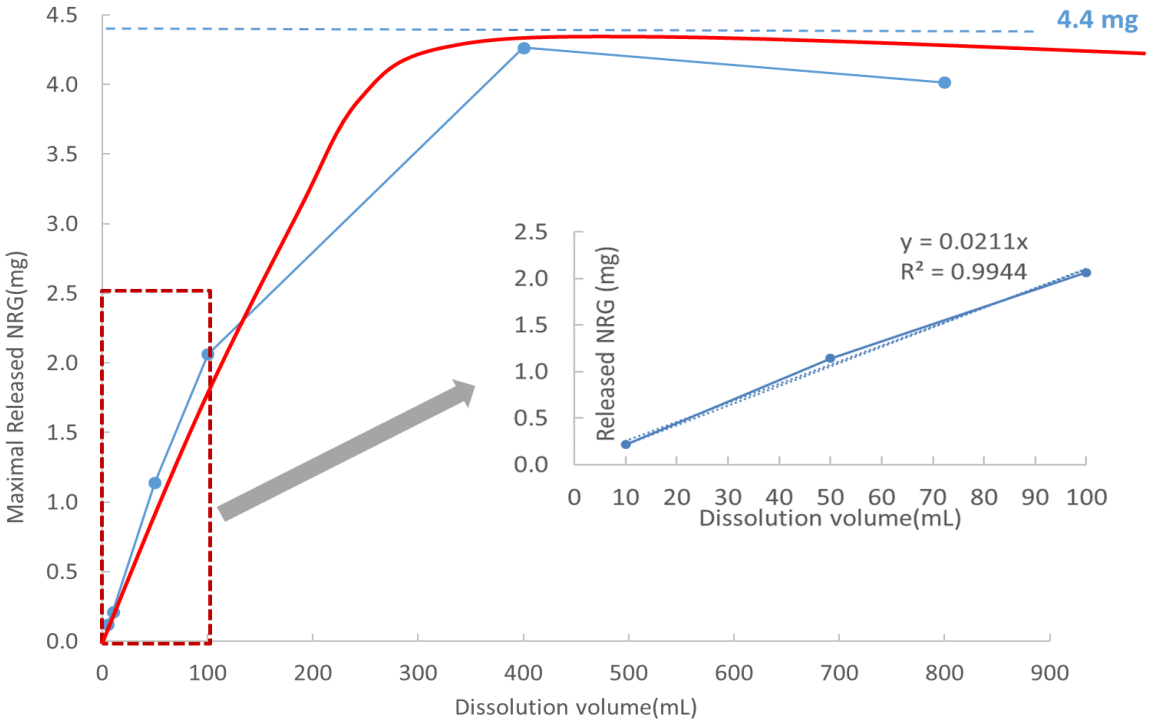


Figure 4-54 Maximal amount of NRG *released from CS-TPP particle within aqueous media with various volumes. When dissolution volume ranging from 10 ml to 100 ml, amount of released NRG was in good linear relation (R^2> 0.99) with dissolution volume (Seen in the figure on upper side corner).*

In Figure 4-54, significant linear relationship (R^2>0.99) between dissolution volume and released NRG amount can be clearly seen when dissolution volume was below 100 mL. Whereas, when dissolution volume was 400 mL and 800 mL, maximal amount of released NRG achieved to totality of loaded amount (4.4 mg, marked out by a dot line in blue). In these two cases, the complete release of NRG confirmed good sink condition were maintained during dissolution testing of NRG. That is to say, release of NRG was not limited to its solubility, when release media volume was 400mL or 800mL for 4.4 mg of NRG.

The slope of the trend line obtained through linear regression analysis represents the approximation towards the saturated concentration of naringenin at 20±2°C. Using this method, the water solubility of naringenin at 20°C, which corresponds to the saturated concentration of the substance in water, was calculated as 21.1 mg/L, under the premise of artificially setting the intercept to zero.

Additionally, good linear relationship indicated that dissolution media were saturated of NRG when dissolution volume was below 100 mL. Therefore, there is another way to determine water solubility of NRG, which is to calculate average value of maximal concentration of NRG in saturated solutions (Dissolution volume = 10, 50 and 100 mL). Through this method, solubility of NRG in water at 20°C was determined as 21.6±0.9 mg/L.

Results of these two methods were compatible. Calculated solubility of NRG is closer to low values but is still in consistence with data listed in Table1-3. According to European Pharmacopoeia (Ph. Eur.)

solubility criteria, naringenin should be classified into practically insoluble chemical (*European Pharmacopoeia*, 2016).

In pharmaceutics, during the dissolution testing, the dissolution volume is usually 5 to 10 times greater than the volume present in the saturation solution of target substance. So, concentration of dissolved substance should be 5 to 10 times lower than the saturated concentration in this medium. That is because the dissolution rate will progressively decrease when the concentration gets close to the saturated point, which can cause faulty test results (Ghosh and Jasti, 2004; Liu, 2008).

Considering the calculated solubility of naringenin at 21.1 mg/L, the maximum concentration should be kept below 4.12 mg/L, which corresponds to one-fifth of the saturated concentration. As shown in Table 4-20, the maximum concentration of NRG dissolved in 800 mL was 5 mg/L, which is close to the 4.12 mg/L threshold. Furthermore, when selecting the dissolution volume, it is important to consider the sensitivity of the analytical method. If the media volume continues to increase, the UV signals of the samples may become too low to be detected by the UV-Vis spectrometer.

Taking the aforementioned reasons into consideration, a dissolution volume of 800 mL was selected to ensure unobstructed dissolution rate during the release of 4 mg of naringenin in water at 20°C.

4.4.1.2 Separation method

4.4.1.2.1 NRG dissolution through dialysis membrane

Dissolution amount of NRG on percentage of total amount of NRG through a dialysis tube made of dialysis membrane was followed (*Figure 4-55*). The dissolution curve of NRG through the dialysis membrane exhibited a two-phase pattern, characterized by rapid dissolution during the first 360 minutes, followed by a prolonged dissolution phase.

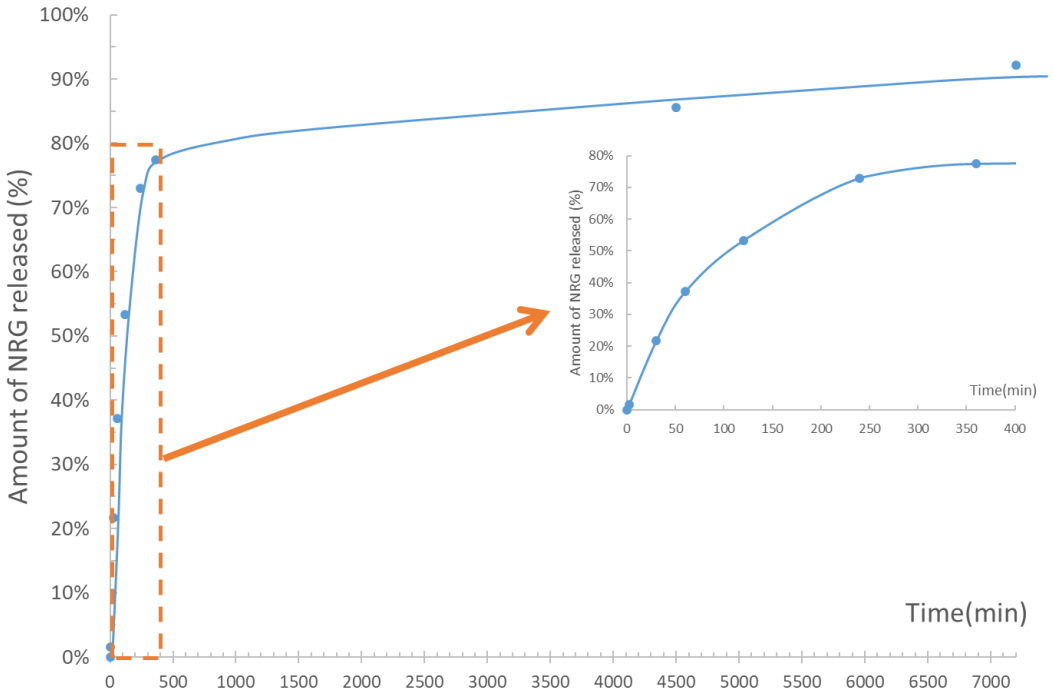


Figure 4-55 Dissolution of NRG from dialysis tube along time. Dissolution curve from 0 to 360 min was logarithmic shaped (Seen in upper right corner).

To examine if dissolution in first phase followed Fickian diffusion rule, amount of NRG dissolution was traced along square root of time ($\sqrt{T}$). As seen in Figure 4-56, significant linear relationship between dissolution of NRG and square root of time was observed as R^2 was 0.9725, higher than 0.8. This indicates dissolution of NRG from dialysis tube was dominant by diffusion in the first 360 min. After 360 min, only 80% of NRG was diffused through dialysis membrane.

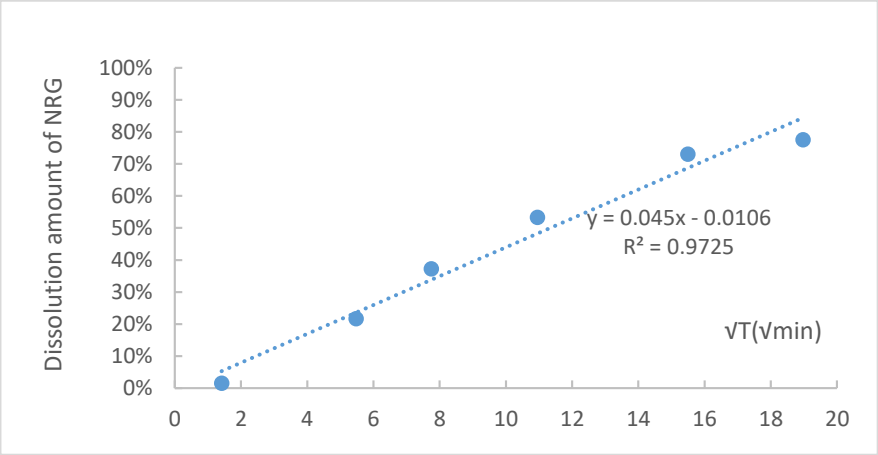


Figure 4-56 Dissolution of NRG from dialysis tube in the first 360 min was plotted against square root of time.

UV absorbance measurements were conducted on the liquids inside and outside the dialysis tube after 7200 minutes of dissolution. Figure 4-57 depicts the UV absorption, showing that the liquid inside the dialysis tube had a slightly higher UV absorption compared to the liquid outside. This finding indicates that, at the 7200-minute mark, although the concentration of naringenin in the release medium approached that inside the dialysis tube, a slight disparity in NRG concentration still persisted. After calculation, approximately 92% of the initial mass of naringenin had passed through the dialysis membrane.

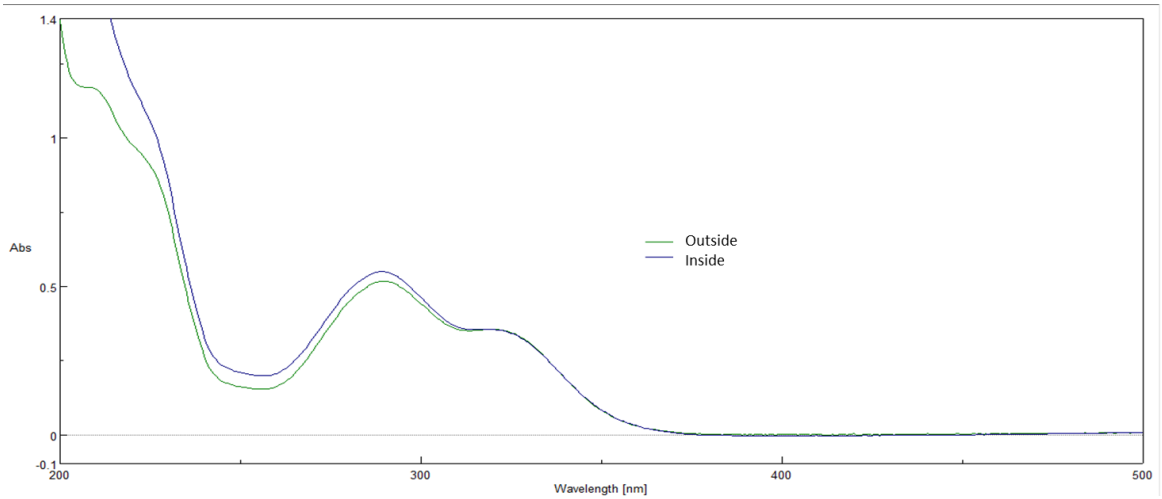


Figure 4-57 UV absorbance of NRG liquids inside and outside the dialysis tube at 7200 minutes.

This gives us a hint that, dialysis method would be improper to use in dissolution test of NRG because the dissolution is not instant due to the low diffusion rate of NRG through the dialysis membrane.

Based on the calculations, it was determined that around 92% of the initial mass of naringenin (NRG) had diffused through the dialysis membrane. This observation suggests that the dialysis method may not be suitable for conducting the dissolution test of NRG, as the dissolution process is not immediate due to the slow diffusion rate of NRG through the dialysis membrane.

4.4.1.2.2 Filtration of naringenin

As previously mentioned, a significant decrease in UV absorbance was noticed after filtration, suggesting a possible adsorption of naringenin (NRG) molecules onto the filter membrane. This adsorption effect during filtration makes it unsuitable as a separation method for the NRG release test. Similarly, dialysis is not suitable for separating NRG molecules, as the diffusion through the dialysis membrane was observed to be very slow. Therefore, centrifugation emerged as the preferred separation method for the dissolution test of NRG-loaded particles.

Furthermore, hindered diffusion was observed during both dialysis and filtration of NRG, suggesting a possible interaction between NRG and the cellulose membranes used in these operations. Unfortunately, the ambiguous product specifications provided by the suppliers, such as regenerated cellulose or cellulose mixed ester, make the exact composition of these membranes unknown. As a result, we lack the necessary information to further investigate the underlying cause of these observed phenomena.

4.4.1.3 Composition of dissolution media

The composition of the dissolution media plays a crucial role in the release of drugs from dosage forms during dissolution testing. In the case of NRG, it has higher solubility in EtOH compared to water. Consequently, using an EtOH-water mixed media allows for a smaller volume of media while still maintaining sink conditions during drug release. Additionally, altering the composition of the release media can influence the partition coefficient (or dissolution coefficient) of NRG, potentially resulting in a different release profile.

On the other hand, we are curious to know impact of the composition of media on CS-TPP particles. As known, when chitosan is added to ethanol, it tends to form aggregates or precipitates due to the reduced polarity and interactions between chitosan and the ethanol solvent. The interaction between chitosan and ethanol can indeed might have an impact on the particle structure of CS-TPP particles and subsequently influence their delivery efficiency.

EtOH-water media

The NRG-loaded CS-TPP particles were redispersed in 10 mL of EtOH-water mixed media with EtOH concentrations of 10% and 33%, respectively. In addition, the release of NRG in 10 mL of water was investigated as a control group.

Figure 4-58 illustrates that all three samples exhibited similar two-phase release profiles, characterized by an initial burst release within the first 10 minutes, followed by a sustained release in the second stage. The release profiles in water and 10% EtOH were comparable, with both reaching around 20% of the loaded mass. However, the release in 10% EtOH was slightly higher than in water. In contrast, the release in 33% EtOH was significantly higher than in the other two media. At the 10-minute mark, more than 30% of NRG was detected in the release medium. Subsequently, there was a gradual release, reaching approximately 50% of the loaded NRG at 1440 minutes.

By checking maximal concentration of NRG in dissolution, rather low release level of these three samples might be explained. Sink condition was no longer remained when amount of NRG increased at certain period during dissolution process. Although NRG release was limited by solubility in these experiments, the results still demonstrated that release profile of NRG was not altered in EtOH-Water media. Moreover, the observed reduction in NRG release could be attributed to a combination of factors, including differences in solubility and potential alterations in the behavior of CS-TPP in the EtOH-water systems. However, the exact contribution of each factor remains unclear due to the lack of precise solubility information for NRG in these specific EtOH-water systems.

To investigate the impact of the 33% EtOH-water mixed solution on NRG release, an experiment was conducted using the same amount of NRG-loaded CS-TPP particles dispersed in 800 mL of the 33% EtOH solution. By choosing a larger volume, sink conditions were ensured throughout the release process.

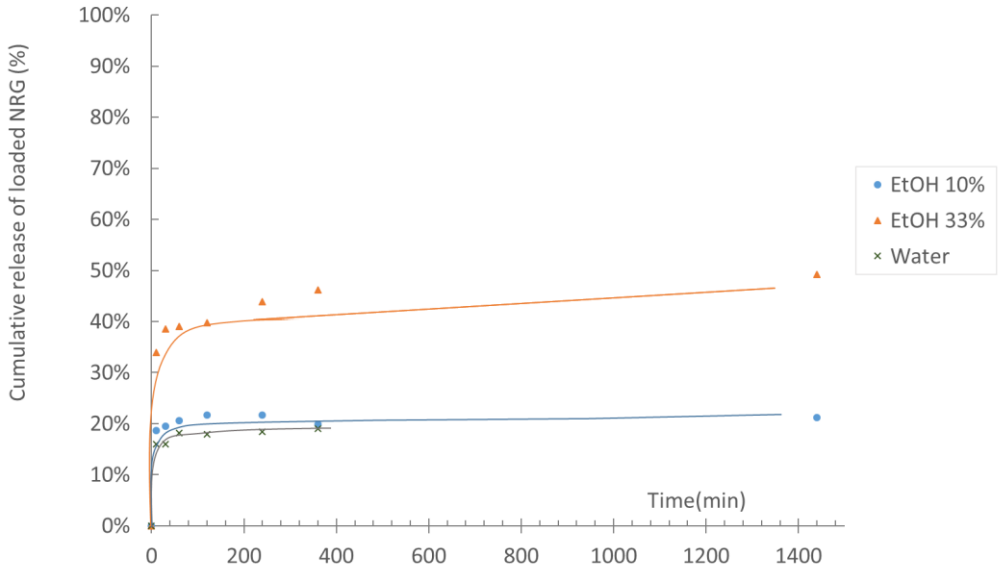


Figure 4-58 Release profile of NRG loaded CS-TPP dispersed in 10 mL of water, 10% EtOH and 33% EtOH.

The release profile of NRG-loaded CS-TPP particles dispersed in 800 mL of 33% EtOH was compared to the release profile in water, as shown in Figure 4-59. The similarity in the release profiles of these two conditions was remarkable. Moreover, complete release indicating that the presence of 33% EtOH did not significantly alter the release properties of NRG from the CS-TPP particles, when sink condition is ensured. That is to say, CS-TPP particles structure was not significantly changed in 33% EtOH. Instead of

aggregation or precipitation in the media, a suspension of chitosan particles might be formed in Ethanol-Water.

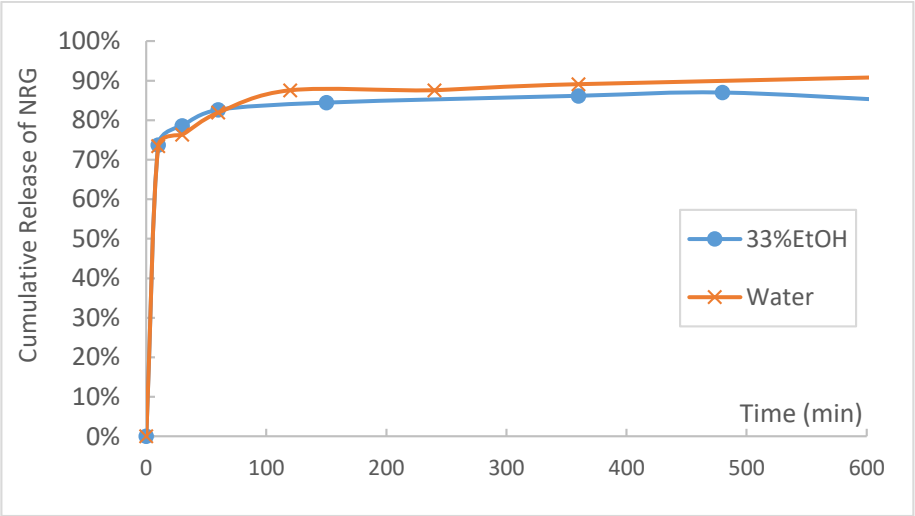


Figure 4-59 Release profile of NRG loaded CS-TPP particles were dispersed in 800 ml of 33% EtOH and in water.

The addition of EtOH into the dissolution media does not appear to alter the pattern of the release profile of NRG from CS-TPP particles. However, it may increase the overall release level of NRG by enhancing its solubility in the release medium. It should be noted that this phenomenon may not be observed if the sink condition is already established before the addition of ethanol.

In conclusion, the dissolution media for CS-TPP particles loaded with 4.4 mg of NRG was determined to be 800 mL of water. Centrifugation was chosen as the method to separate the CS-TPP particles from the release media, allowing for the measurement of NRG content in the media at prescheduled time intervals.

4.4.2 Release of NRG from CS particles

As mentioned earlier, the CS3TPP5 formulation was selected as the most suitable option for encapsulating the naringenin molecule, exhibiting an encapsulation efficiency (EE%) of approximately 90%. Our current focus is on exploring the release characteristics of the entrapped naringenin within these particles. We also conducted investigations on the effect of alginate coating on CS-TPP particles to assess its potential influence on drug delivery. Additionally, the release properties of NRG-loaded particles subjected to ultrasonication treatment were monitored. Lastly, we investigated the impact of the composition and pH of the dissolution media as potential factors affecting the release properties of NRG.

4.4.2.1 CS-TPP

A dispersion was prepared by dispersing 39 mg of freeze-dried NRG-loaded CS-TPP particles, containing 4.4 mg of NRG, in 800 ml of water at 20°C under continuous magnetic stirring. The release profile of NRG from the CS-TPP particles is presented in Figure 4-60. During the initial 10 minutes, more than 70% of the loaded NRG was released, followed by a rapid release phase that extended until 120 minutes. Subsequently, a sustained release phase with a slower rate facilitated the liberation of the remaining portion of NRG (approximately 10%) from 120 minutes to 1680 minutes. The cumulative release of NRG from the CS-TPP particles gradually approached 100% after 4320 minutes.

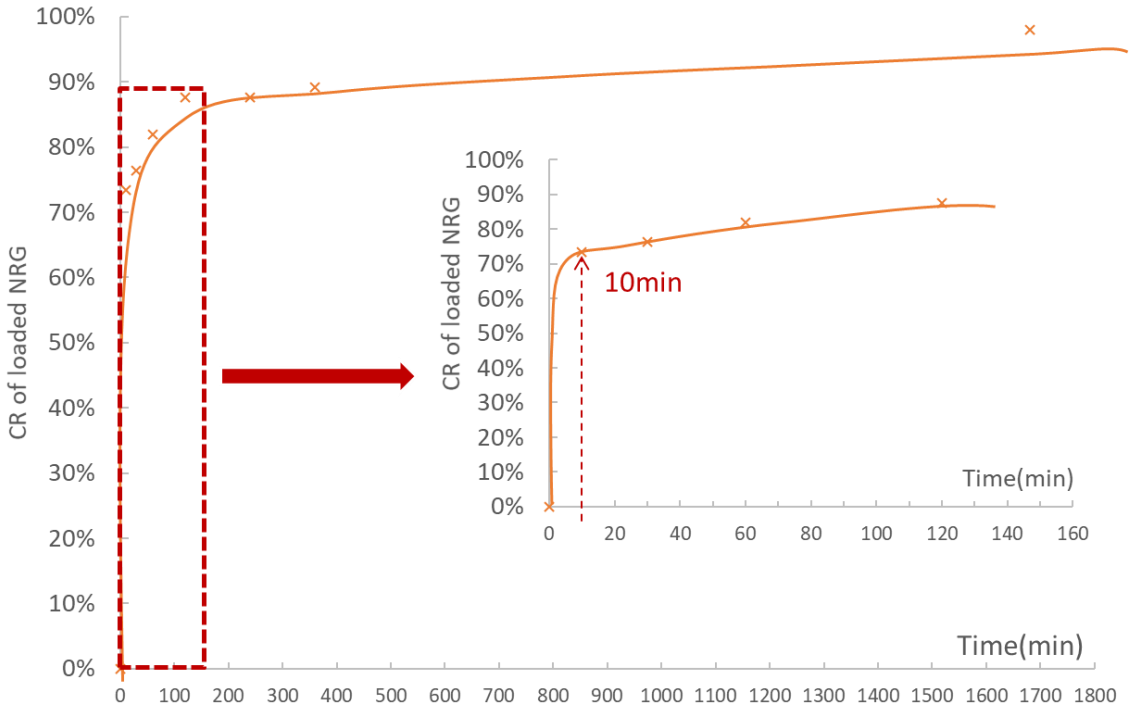


Figure 4-60 Dissolution of NRG loaded CS-TPP particles in water at 20 °C.

4.4.2.2 Ultrasonic treated CS-TPP particle

As mentioned previously, the introduction of ultrasonication treatment resulted in an increased proportion of small particles within the particle population. We were intrigued to investigate whether this change in particle size could impact the release properties of NRG from CS-TPP particles. To address this question, NRG-loaded CS-TPP particles were prepared, and three different durations of ultrasonication treatment (0.5 minutes, 1 minute, and 5 minutes) were employed. Additionally, a CS-TPP sample without ultrasonication treatment, was prepared as a control. All above mentioned particles contained 4.4 mg of NRG, and were lyophilized and subsequently redispersed in 800 ml of water at room temperature. The content of NRG in the dissolution media was monitored using UV spectrophotometry.

Figure 4-61 illustrates cumulative release of NRG from those particles. Release profile of NRG from ultrasonication treated particles were similar to non-treated particles. Both of them suffered rapid release in the first 10 min and then achieved to a plateau within the next 360min. Release from non-treated CS-TPP was approached to 100%, while release from ultrasonication treated particles stopped at 90%.

In comparison to the ultrasonication-treated particles, the untreated CS-TPP particles exhibited a higher degree of particle aggregation. However, the presence of particle aggregations did not appear to impede the release of NRG, suggesting that the structure of these aggregations remained sufficiently porous. Conversely, the ultrasonication treatment potentially resulted in the compression of partial aggregations, leading to a more compacted structure that influenced the release of NRG. Furthermore, the presence of small particles resulting from the dissociation of aggregations in the treated particles was expected to enhance the release process. However, the extent of this promotional effect was not

prominently observed in the results, suggesting that the loose structure of the aggregations in the untreated particles.

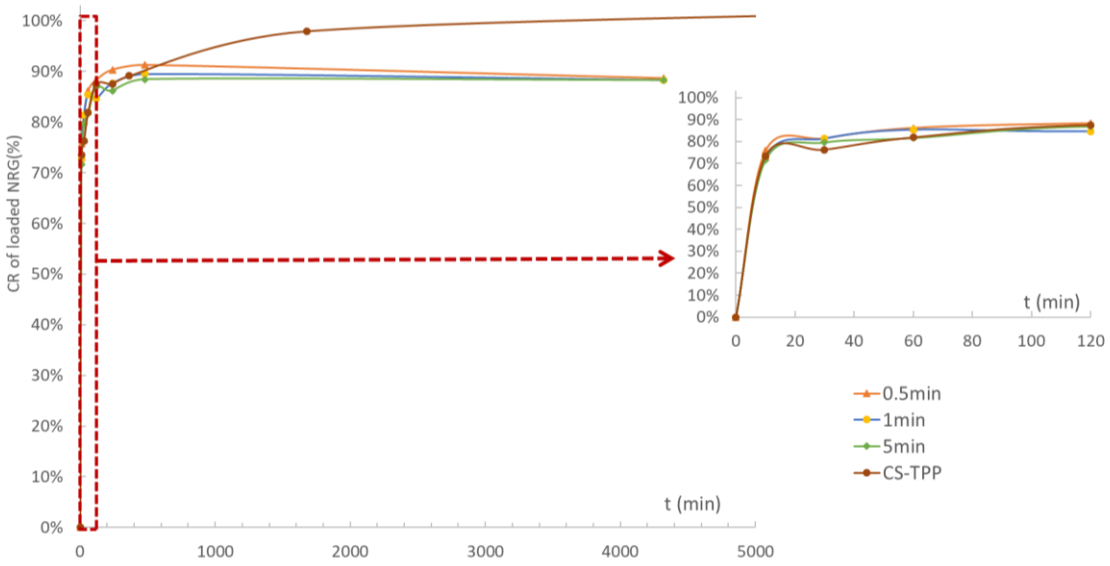


Figure 4-61 Cumulative release of NRG from CS-TPP and ultrasonic retreated CS-TPP samples in 800ml of water.

4.4.2.3 ALG coated CS-TPP

Successful preparation of ALG-coated CS-TPP particles was achieved by adding a suspension of CS-TPP into an ALG solution, followed by solidification of the resulting particles using a $CaCl_2$ solution. The introduction of ALG coating led to a change in the surface charge of the particles from positive to negative. With these questions in mind, we conducted an investigation to determine if the ALG coating would affect the release properties of NRG from CS-TPP particles. We compared the release properties of NRG from ALG coated CS-TPP particles with those of CS-TPP particles.

Figure 4-62 demonstrates that the release of NRG from ALG coated particles exhibited an initial burst release within the first 10 minutes, followed by a prolonged release phase until reaching a plateau. Initially, approximately 85% of NRG was detected in the dissolution media at the 10-minute mark. Subsequently, the release rate decreased, and a nearly linear relationship between cumulative release and time was observed until 360 minutes. After that, from 360 minutes to 2880 minutes, the release of NRG remained stable at approximately 95%.

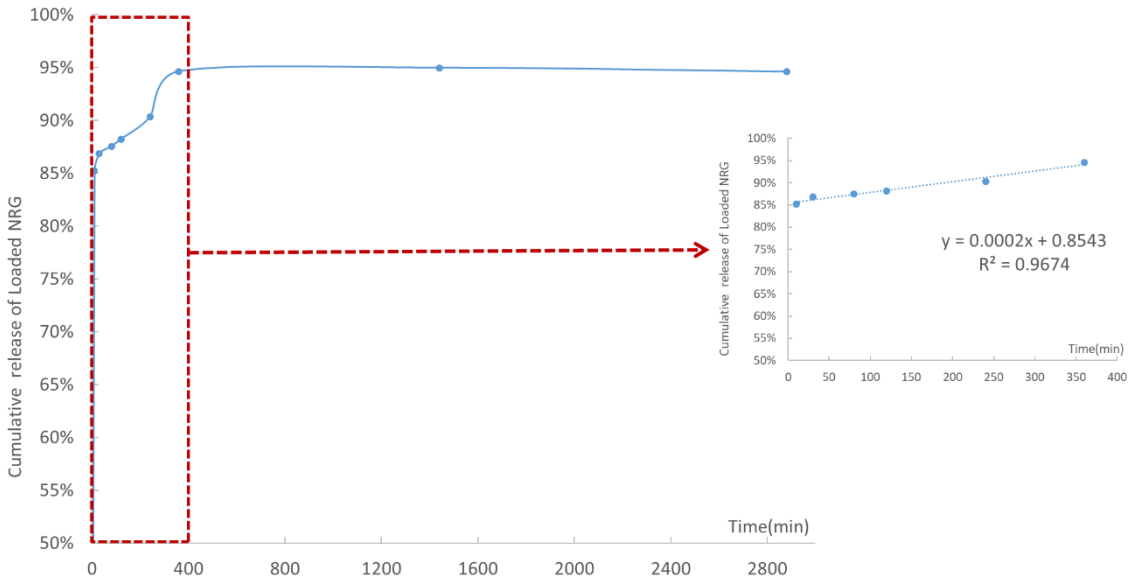


Figure 4-62 Cumulative release of NRG from ALG coated CS-TPP particles in 800 ml of water at 20°C

ALG coating did not hinder the release of NRG from the particles, as complete release was observed at the end of the dissolution test. However, after the initial burst release within the first 10 minutes, a zero-order drug release pattern was observed, indicating a more consistent release mechanism, which could be attributed to the complexity of the matrix structure induced by ALG.

The release profiles of NRG from CS-TPP particles and ALG-coated CS-TPP particles exhibited a high degree of similarity, as depicted in Figure 4-63. On the contrary, it is worth mentioning that the additional steps (washing, centrifugation) during the coating process led to a higher loss of the active molecule. ALG-coated CS-TPP particles exhibited lower encapsulation efficiency, implying that a greater amount of substances is required to deliver the same quantity of the target molecule in the ALG-coated vehicle.

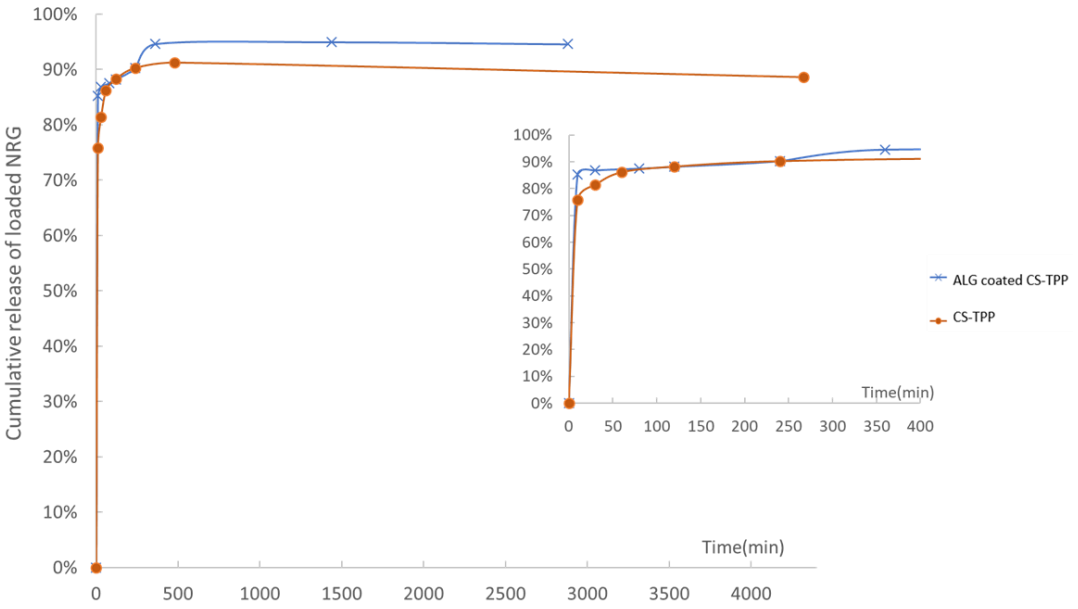


Figure 4-63 Cumulative release of NRG from ALG coated CS-TPP particles and CS-TPP particles

5 Conclusion and perspectives

In summary, Chitosan-Tripolyphosphate (CS-TPP) particles were successfully developed, optimized, characterized, and evaluated. The CS-TPP particles were optimized on the basis of various process variables such as CS concentration, volume of CS and TPP solutions, CS/TPP mass ratio, and temperature. Impact of those variables was investigated on the purpose to enable the prediction of formulation and preparation strategies for drug delivery systems. By gaining more insight into these aspects, it is possible to design DDSs in a more purpose-oriented and predictable way. Furthermore, the successful achievement of alginate coating on the surface of CS-TPP particles was accomplished under mild conditions. This coating may provide additional functionalities and can enhance the performance of the particles as drug carriers.

The CS-based particles were thoroughly characterized using various techniques including Zetasizer, Laser diffraction Size Analyzer, and SEM. The particle size of the CS-based particles exhibited a wide range, from 60 nm to over 200 µm. Notably, the addition of ALG coating to the particles resulted in an increase in both the average particle size and the broadness of the size distribution. This suggests that the ALG coating successfully modified the particle size and distribution.

In terms of surface charge (measured by zeta-potential), the CS-TPP particles exhibited relatively high negative surface charges, measuring above 30 mV. However, after the application of the ALG coating, the surface charges of the particles became positive. This change in surface charge further indicates the success of the surface coating process.

The characterization results obtained through these techniques provide valuable insights into the size and surface properties of the CS-based particles. The particle size range and the effect of ALG coating on particle size and surface charge are essential considerations for their potential applications as drug delivery vehicles or in other relevant fields.

Overall, the successful development, optimization, and characterization of CS-TPP particles, as well as the achievement of alginate coating, contribute to the advancement of drug delivery systems and offer potential for the design of more effective and targeted therapies.

In the second part of the study, the encapsulation of three polyphenol molecules, namely naringenin (NRG), naringin (NR), and catechin (CAT), into CS particles was conducted. These polyphenols have been extensively studied in the literature due to their reported benefits for human health. However, their practical applications are often hindered by challenges such as poor aqueous solubility and instability prior to reaching their intended target sites. To overcome these limitations, the encapsulation of these polyphenol molecules into CS particles was explored as a potential solution. CS particles have shown promise as drug carriers due to their biocompatibility, biodegradability, and ability to protect encapsulated molecules(Chuah et al., 2013; Hejazi and Amiji, 2003; Malathy and Priya, 2018). By encapsulating NRG, NR, and CAT within CS particles, it is anticipated that their solubility and stability issues can be addressed, thus enhancing their potential therapeutic applications.

The experimental conditions for the encapsulation of the polyphenol molecules, namely catechin (CAT), naringin (NR), and naringenin (NRG), into CS particles were established and optimized. Different separation methods were investigated to separate the free molecules from the CS particles. Filtration was found to be suitable for CAT, while centrifugation was more effective for NR and NRG due to the reduction in concentration observed after filtration through a cellulose membrane filter.

The encapsulation efficiency (EE%) of the active molecules was characterized using UV-Vis spectrometry to evaluate the affinity between the CS particles and the polyphenols. The results indicated that CS

particles were capable of effectively encapsulating NRG and CAT, as evidenced by high EE% values. However, the encapsulation of NR appeared to be less successful, possibly due to the specific properties of this molecule or its interaction with the CS particles.

Various variables, such as the initial amount of the polyphenol molecule and the solvent used for the dissolution of the molecule, were found to be influential factors affecting the encapsulation efficiency. Optimization of these variables is crucial to achieving high EE% and ensuring the efficient encapsulation of the polyphenols into the CS particles

These findings provide valuable insights into the encapsulation process and highlight the importance of understanding the specific properties and interactions between the active molecules and the CS particles. This knowledge can be utilized to further improve the encapsulation efficiency and enhance the potential applications of CS-based particles as effective carriers for polyphenol molecules as drug delivery systems.

In the final part of this study, the release kinetics of naringenin (NRG) from CS particles were extensively investigated. The aim was to understand the release behavior of NRG from different formulations and evaluate their potential as drug delivery systems.

During the release studies, a two-phased release profile was observed for NRG-loaded CS-TPP particles, sonicated-treated CS-TPP particles, and ALG-coated CS-TPP particles. The release profile consisted of an initial rapid burst release, followed by a prolonged release phase until a plateau approached to 100% was reached. This behavior suggests that the release of NRG from these formulations is influenced by multiple factors, such as the structure and composition of the particles.

Given the poor water solubility of NRG, special attention was given to ensuring a sink condition during the dissolution testing. A sink condition refers to maintaining a low concentration of the released drug in the release medium compared to its solubility, thereby avoiding potential saturation effects. To achieve this, a larger volume of release medium or methods to increase the solubility of NRG may be required. Results indicated that increasing the proportion of ethanol (EtOH) in the release medium up to 33% was favorable for solubilizing NRG without significantly altering the release properties of CS-TPP particles. However, to optimize the release experimental conditions, it would be beneficial to obtain NRG solubility data in a specific water-ethanol miscible system.

Due to limited availability of certain equipment, the investigation of release kinetics was focused on CS microparticles. However, it would be valuable to explore whether CS nanoparticles exhibit similar release characteristics. Comparing the release behavior between CS microparticles and nanoparticles could provide additional insights into the potential applications of CS-based nanoparticles as drug delivery systems.

By thoroughly investigating the release kinetics of naringenin (NRG) from CS particles and considering the sink condition, valuable insights can be gained into the release mechanism and behavior of NRG-loaded CS formulations. This knowledge is important for designing optimized drug delivery systems and ensuring effective release of NRG for its intended therapeutic applications. Further investigations on NRG solubility and the release behavior of CS nanoparticles would contribute to a comprehensive understanding of the release mechanism and aid in the optimization of CS-based drug delivery systems.

The findings of this study demonstrate that CS-TPP particles are a promising encapsulation system for the delivery of naringenin. This suggests that CS-TPP particles have the potential to be used as a delivery system for other bioactive molecules, including peptides, nucleic acids, and other similar compounds. The successful encapsulation and release of naringenin highlight the versatility and potential of CS-TPP

particles in various applications within the field of drug delivery and therapeutics. Further research and exploration are warranted to fully explore the capabilities of CS-TPP particles for the encapsulation and delivery of different bioactive molecules.

Starting from the results obtained from three different molecules, an important development would be to get further insights about the structural characteristics of molecules to be efficiently encapsulated in CS-TPP particles, i.e. defining the relevant molecular descriptors. In addition, by modifying the preparation process, it may possible to further adjust the size distribution and morphology of particles so as to reach a better control of release process.

List of figures

Figure 1-1 Chemical structure of chitin and chitosan and their sources including crustaceans, insects and fungi 21
Figure 1-2 Preparation of chitin and chitosan from crustacean marine waste(Sagheer et al., 2009; Huq et al., 2022) 22
Figure 1-3 Schematic overview of the versatility of chitosan applications in various fields. 25
Figure 1-4 Number of publications containing the keywords “chitin” or “chitosan” registered each year in SciFinder. Books, conferences, editorials, journal articles, preprints and reviews included. (Data from SciFinder, March 2023). 26
Figure 1-5 Number of patents relevant to the keywords “chitin” or “chitosan” in English published each year. (Data from WIPO, https://patentscope.wipo.int/search/en/result.jsf/(accessed on 1 March 2023)).....26
Figure 1-6 Schematic representation of the SEC-MALS system, (Adapted from Some, 2018). 27
Figure 1-7 Chitosan crosslinking gelation mechanisms. Graph adapted from Bellich et al. 2016 32
Figure 1-8 (a) Schematic representation of particulate formation through ionotropic gelation ionic gelation between positively charged chitosan and negatively charged counter-ions (e.g.TPP). (b) Schematic diagram of the preparation of ironically cross-linked chitosan nanoparticles via the traditional ionotropic gelation technique (Desai, 2016). 38
Figure 1-9 Transmission electron microscope, Institute Jean Lamour, campus ARTEM, Nancy 42
Figure 1-10 Atomic force microscopy (SMENA NT-MDT Microscope), Laboratoire Charles Coulomb (L2C), Montpellier 43
Figure 1-11 Schematic illustration of zeta potential and the Electrical double layer (from: Zetasizer Nano User Manual p229).....45
Figure 1-12 Zeta potential versus pH, Isoelectric point(Malvern Instruments, 2005).....46
Figure 1-13 Classification of polyphenols (Galanakis, 2018).....49
Figure 1-14 Structure of benzoic acid and cinnamon acid 50
Figure 1-15 Chemical Structures of Different Flavonoids. Chemical structure of naringenin, naringin and catechin(reprinted from Galanakis, 2018). 52
Figure 1-16 The solubility of naringenin in water gradually increases as the temperature increases. pH=4, temperature. (Reprinted form P. Zhang et al., 2013).....54
Figure 1-17 Chemical structure of catechin 56
Figure 1-18 Limitations of chitosan and polyphenol, and advantages of chitosan-polyphenol (Reprinted from (Pattnaik et al., 2022), Copyright 2022, Pattnaik et al). 59
Figure 3-1 chitosan structure and Chitosan 1H NMR spectrum at 343 K. 64
Figure 3-2 Process of purification of commercial chitosan. 66
Figure 3-3 Experimental photos of preparation CS-TPP particles via crosslinking under magnetic stirring at various temperatures. 69
Figure 3-4 Addition of CS-TPP into ALG solution under sonication within an ice bath. and the pulse on mode was used to help temperature control of samples during sonication treatment 73
Figure 3-5 Schematic introduction of encapsulation of active molecule by CS-TPP particles. 76
Figure 3-6 Schematic introduction of encapsulation of active molecule by ALG coated CS-TPP particles. 77
Figure 4-1 UV–Vis spectra of chitosan solutions (0.25, 0.5, 0.75, 1.5 mg/L, 1% acetic acid) at the range 200-500 nm. 84
Figure 4-2 UV absorbance at 292 nm vs concentration of chitosan solutions (1% acetic acid, v/v) and calibration curve with regression equation. 84
Figure 4-3 Infrared spectrum of commercial chitosan in the field 4000–500 cm–1 with assigned characteristic bonds (KBr tablet). 85
Figure 4-4 1H NMR spectrum of CD3COOD-D2O(2%, v/v) at 343 K (left) and 13C NMR spectrum of CD3COOD-D2O(2%, v/v) at 343 K (right). 86
Figure 4-5 1H NMR spectrum of DCl-D2O (2%, v/v) at 343 K. 86
Figure 4-6 1H NMR spectra of commercial (A,B)and purified chitosan (C,D) at 343K and at 300K. Obviously, 1H NMR spectra at 343K has stronger proton signal and the peaks of H-1(D) at 5.4 ppm were not visible at 300K for both commercial and purified chitosan. 87

Figure 4-7 1H NMR spectrum of purified chitosan (left) and our commercial chitosan (right) in DCl-D2O (2%, v/v) at 343 K. Protons were assigned in following orders: H-Ac, H-2(D), H2-6, H-1(D). 87
Figure 4-8 SEC-MALS spectrum of commercial chitosan (5 mg/L). 89
Figure 4-9 SEC-MALS spectrum of purified chitosan (5 mg/L). 90
Figure 4-10 Size distribution by intensity of samples prepared using raw chitosan (green) and purified chitosan (red). Upper side are samples prepared at room temperature, whereas below are samples prepared at 50°C. 92
Figure 4-11 UV-VIS spectra of naringenin diluted solutions from 190 nm to 500 nm. 93
Figure 4-12 UV-Vis absorbance of naringenin aqueous solutions with various concentrations at 289 nm. 93
Figure 4-13 UV-Vis absorbance spectra of naringenin dissolved in 33% EtOH 94
Figure 4-14 UV-Vis absorbance of naringenin dissolved in 33% EtOH at 289 nm. 94
Figure 4-15 1H NMR of naringenin in DMSO-d6 at 300 K with assignments. 95
Figure 4-16 UV-VIS spectra of naringin dilute solutions and absorbance data from 200 to 500 nm. 95
Figure 4-17 Calibration curve for UV-Vis spectrophotometric determination of naringin in aqueous solution (λmax = 282 nm) 96
Figure 4-18 1H NMR spectrum of naringin in the range δ 7.5– δ 2.5 (298K, 400 MHz). Sample was dissolved in DMSO-d6. The signals are assigned as follows: (1) H-3 cis (2) H-3 trans (3) H-2, (4) H-6 and H-8, (5) H-3' and H-5', (6) H-2' and H-6'. 96
Figure 4-19 UV-VIS spectra of catechin dilute solutions at range from 190 to 500 nm. 97
Figure 4-20 Calibration curve of catechin at 280 nm. 97
Figure 4-21 1H NMR spectrum of catechin in DMSO-d6 (10 mg/mL, 400 MHz, 298K) and assigned proton signals(A); (B) chemical shifts of catechin in DMSO-d6 (5.33 mg/mL, 600 MHz; 298K, reprinted from Pauli et al., 2014). .98
Figure 4-22 SEM micrographs of CS-TPP particles prepared by crosslinking of CS and TPP. experimental details including concentration volume. A: sample-021; B: sample-038; C,D: sample-012; E,F: sample-019 99
Figure 4-23 Combination of results of DLS (left) and SEM images (right) of sample-021, 012 and 038. 101
Figure 4-24 Appearance of samples. After addition of TPP and agitation for 1 hour. It was observed that the formed nanoparticle suspension became less turbid in following order: CS3TPP5> CS5TPP5> CS3TPP2.5. 102
Figure 4-25 CS-TPP particle suspensions, put them still on the bench and observe: newly prepared sample, after 30 min, after 3h30min, after one night and 2 days after preparation. 103
Figure 4-26 Particle size distribution on volume of CS-TPP microparticle (R= CS-TPP Mass Ratio). 104
Figure 4-27 Size distribution of sample-075 sample before(A) and after(B) sonication. 105
Figure 4-28 Size distribution by intensity of sample-026, sample-030 and sample-072. 106
Figure 4-29 Size evolution of ALG coated CS-TPP particles during coating process. 107
Figure 4-30 Zeta potential distribution of CS-TPP(sample-026, in red). CS-TPP-ALG (sample-030, green) and CS-TPP-ALG-Ca-W (sample-072, blue) samples. 107
Figure 4-31 Influence of concentration of chitosan on particle size and PDI. 108
Figure 4-32 (A)Size distribution by intensity of sample-009 (red), 007 (green) and 010 (blue). (B) Size distribution by intensity of sample-024 (red) and sample-029 (green). (C) Size distribution by intensity of sample-015 (red) and sample-012 (green). 110
Figure 4-33 Influence of Mass ratio of CS/TPP on particle size and PDI. Mass ratio of CS/TPP ranging from 2.5 to 9 had fluctuant effect on particle size, while PDI increased slightly when mass ratio of CS/TPP increased. 111
Figure 4-34 Influence of molar ratio of charges on particle formation(Average size(nm) in blue; PDI in orange). ... 111
Figure 4-35 Distribution of samples in terms of particle size and particle concentration 112
Figure 4-36 Process to start up preparation conditions of particles with expected size 113
Figure 4-37 UV-Vis spectra of CAT solution before (blue) and after (green) filtrated through 0.45 µm cellulose membrane filter. 114
Figure 4-38 UV-Vis spectra of NRG solution before (blue) and after (green) filtrated through 0.45 µm cellulose membrane filter. 115
Figure 4-39 UV-Vis spectra of NR solution before (blue) and after (green) filtrated through 0.45 µm cellulose membrane filter. 115
Figure 4-40 UV-Vis spectra of CAT loaded CS-TPP's supernatant obtained via centrifugation (green) and filtrate obtained via filtration (blue). 116

Figure 4-41 Appearance of samples (A) After addition of TPP (B) CS-TPP particle suspensions after 2 days of preparation: CS5TPP5, CS3TPP2.5, CS3TPP5 (from left to right) 117
Figure 4-42 Particle size evolution of ALG coated NRG loaded CS-TPP particles during coating process. The particle size greatly increased after addition of ALG and continuously increased after addition of Ca2+. 118
Figure 4-43 Volume weighted particle size distribution of blank CS-TPP particles and NRG/CAT loaded CS-TPP particles..... 120
Figure 4-44 EE% of NRG loaded in various CS-TPP systems (x: QNRG=5 mg; ●: QNRG=2 mg) 121
Figure 4-45 Influence of QNRG on EE% of CS-TPP-ALG particles 122
Figure 4-46 UV-Vis spectra of redispersed NR-loaded CS-TPP particles to monitor release of NR from these particles 123
Figure 4-47 CAT water solution with concentration of 5g/L at room temperature 124
Figure 4-48 Mixture of chitosan and catechin solution before(A) and after(B) addition of TPP solution 125
Figure 4-49 EE% of CAT loaded CS-TPP samples, QCAT =2mg (x: CAT was dissolved in 50%EtOH; ●: CAT was dissolved in EtOH) 126
Figure 4-50 EE% of CAT (in EtOH) loaded CS-TPP in different CS-TPP formulations (x: QCAT =5 mg; ●: QCAT =2 mg). 127
Figure 4-51 Two photos of newly prepared CS-TPP particles after centrifugation. Precipitate (pellet) of CS-TPP nanoparticles at the bottom of Eppendorf tube after centrifugation. 128
Figure 4-52 the appearance of pellet CS-TPP particles after centrifugation(A), and redispersed suspension of lyophilized CS-TPP particles (B) 128
Figure 4-53 Release of NRG from CS-TPP particles in various volume of water at room temperature. 130
Figure 4-54 Maximal amount of NRG released from CS-TPP particle within aqueous media with various volumes. When dissolution volume ranging from 10 ml to 100 ml, amount of released NRG was in good linear relation (R2> 0.99) with dissolution volume (Seen in the figure on upper side corner). 131
Figure 4-55 Dissolution of NRG from dialysis tube along time. Dissolution curve from 0 to 360 min was logarithmic shaped (Seen in upper right corner). 133
Figure 4-56 Dissolution of NRG from dialysis tube in the first 360 min was plotted against square root of time. 133
Figure 4-57 UV absorbance of liquid inside and outside the dialysis tube at 7200 minutes. 133
Figure 4-58 Release profile of NRG loaded CS-TPP dispersed in 10 ml of water, 10% EtOH and 33% EtOH. 135
Figure 4-59 Release profile of NRG loaded CS-TPP particles were dispersed in 800 ml of 33% EtOH and in water. 136
Figure 4-60 Dissolution of NRG loaded CS-TPP particles in water at 20 °C. 137
Figure 4-61 Cumulative release of NRG from CS-TPP and ultrasonic retreated CS-TPP samples in 800ml of water. 138
Figure 4-62 Cumulative release of NRG from ALG coated CS-TPP particles in 800 ml of water at 20°C 139
Figure 4-63 Cumulative release of NRG from ALG coated CS-TPP particles and CS-TPP particles 140
Figure Annex II-1 Calibration with PEO24k 169
Figure Annex II-2 Calibration check with PEO24k (3.03 g/L) 170
Figure Annex II-3 Commercial chitosan (10 g/L) 171
Figure Annex II-4 Commercial chitosan (5 g/L) 171
Figure Annex II-5 Purified chitosan (2.5 g/L) 172
Figure Annex II-6 Purified chitosan (5 g/L), inject volume: 50µl 173
Figure Annex II-7 Purified chitosan (5 g/L), inject volume: 100µl 174
Figure Annex II-8 Purified chitosan (5 g/L), inject volume: 150µl 175
Figure Annex III-1 UV-Vis spectra of washing liquids W1 (blue) and W2 (green), initial amount of NR added was 1 mg. 177
Figure Annex III-2 UV-Vis spectra of washing liquids of NR loaded CS-TPP particles W1 (blue) and W2 (green), initial amount of NR added was 5 mg. 178
Figure Annex III-3 UV-Vis spectra of washing liquids of NR loaded CS-TPP particles W1 (blue) and W2 (green), initial amount of NR added was 7.5 mg. 178
Figure Annex III-4 UV-Vis spectra of washing liquids of NRG loaded CS-TPP particles, W1 (blue) and W2 (green)... 179

List of tables

Table 1-1 Global annual production and price of chitin, chitosan and Dried shrimp shells. 22
Table 1-2 Preparation methods of chitosan relevant particles. The advantages and shortages of each methods and geometric dimension of obtained particles. The cartoon symbols present structural characteristiCS of these particles. 33
Table 1-3 Solubility data of naringenin from suppliers and in the literature 54
Table 1-4 λ_{max} of Naringenin in literature 55
Table 1-5 λ_{max} of Naringin 56
Table 1-6 λ_{max} data of catechin found in literature 58
Table 1-7 Examples of polyphenols loaded CS-TPP 60
Table 3-1 Experimental details of ^{1}H NMR spectroscopy 63
Table 3-2 Three samples prepared with different scale of batch to explore influence of batch volume on CS-TPP particle size and size distribution. 68
Table 3-3 Experimental conditions of samples prepared at room temperature and higher temperatures. Volume ratio of CS/TPP of those samples was fixed to 3. 69
Table 3-4 Three samples with various mass ratio CS/TPP and their size information. 71
Table 4-1 Product information of the three chitosan commercial samples used in this work 83
Table 4-2 Assigned protons of 1H NMR spectrum chitosan in D_2O/DCl at 343K. 88
Table 4-3 Deacetylation degree (DDA, %) determined of chitosan samples 88
Table 4-4 Average molar masses of commercial and purified chitosan samples determined by SEC-MALS. 91
Table 4-5 Linear regression equations of calibration curves of polyphenols 98
Table 4-6 Three CS-TPP samples prepared with various solutions of CS and TPP. Those samples were named based on the concentration of solutions used for preparation of these samples The mass ratio of CS/TPP and molar ratio of charges were also calculated. 102
Table 4-7 D [3, 2], SPAN and distribution mode of some CS-TPP microparticle samples. 103
Table 4-8 Size information of samples prepared by normal method and reverse method. 105
Table 4-9 Size and zeta-potential evolution of CS-TPP particles during ALG coating process. 106
Table 4-10 Particle size and polydispersity index of samples prepared at room temperature and higher temperatures. 109
Table 4-11 Preparation conditions of two samples with low mass ratio of CS/TPP. 110
After observation of 36 CS-TPP samples on focusing on their size and concentration of particles (Data seen in Table Annex I- 4-12). It is interesting to mention that, when particle concentration is below 3 g/L, particle size was often smaller than 240 nm (Expect for sample-037 and 073). Whereas, particles larger than 240 nm usually had particle concentration beyond 3 g/L. Figure 4-35 visualized this trend by tracking down particle size on concentration of particle of those samples, where samples dots were more likely to disperse in II and III zones but less likely in I and IV zones. 112
Table 4-13 Centrifugation conditions of samples 117
Table 4-14 Particle size, PDI and zeta potential of ALG coated NRG loaded CS-TPP particle. 118
Table 4-15 Particle size of blank CS-TPP particles and active molecule loaded CS-TPP particles 119
Table 4-16 EE% of NRG in CS-TPP particles. 121
Table 4-17 EE% of NRG loaded in ALG coated CS-TPP particles. 122
Table 4-18 EE% of NR in CS-TPP particles 123
Table 4-19 Encapsulation capacity of CS-TPP formulations of CAT(dissolved in water, in 50% EtOH and in EtOH). 125
Table 4-20 : Maximal concertation of naringenin during dissolution testing in media with various volume 130
Table Annex I-1 List of numerated sample with preparation conditions including concentrations and volumes of crosslinking agents and crosslinking temperature. 165
Table Annex I-2 List of CS-TPP nanoparticles with particle concentration and particle size. Detailed preparation conditions of samples can be found in Table 1. Sample were listed by the order that size increased. 167
Table Annex II-1 Raw data of SEC-MALS 176

Reference

Abbas, Z., Labbez, C., Nordholm, S., Ahlberg, E., 2008. Size-Dependent Surface Charging of Nanoparticles. J. Phys. Chem. C 112, 5715–5723. https://doi.org/10.1021/jp709667u

Abdel-Hafez, S.M., Hathout, R.M., Sammour, O.A., 2014. Towards better modeling of chitosan nanoparticles production: Screening different factors and comparing two experimental designs. International Journal of Biological Macromolecules 64, 334–340. https://doi.org/10.1016/j.ijbiomac.2013.11.041

Abdel-Rahman, R.M., Hrdina, R., Abdel-Mohsen, A.M., Fouda, M.M.G., Soliman, A.Y., Mohamed, F.K., Mohsin, K., Pinto, T.D., 2015. Chitin and chitosan from Brazilian Atlantic Coast: Isolation, characterization and antibacterial activity. International Journal of Biological Macromolecules 80, 107–120. https://doi.org/10.1016/j.ijbiomac.2015.06.027

Abdulah, R., Suradji, E.W., Subarnas, A., Supratman, U., Sugijanto, M., Diantini, A., Lestari, K., Barliana, M.I., Kawazu, S., Koyama, H., 2017. Catechin Isolated from Garcinia celebica Leaves Inhibit Plasmodium falciparum Growth through the Induction of Oxidative Stress. Pharmacogn Mag 13, S301–S305. https://doi.org/10.4103/pm.pm_571_16

Acosta, N., Sánchez, E., Calderón, L., Cordoba-Diaz, M., Cordoba-Diaz, D., Dom, S., Heras, Á., 2015. Physical Stability Studies of Semi-Solid Formulations from Natural Compounds Loaded with Chitosan Microspheres. Mar Drugs 13, 5901–5919. https://doi.org/10.3390/md13095901

Agnihotri, S.A., Aminabhavi, T.M., 2004. Controlled release of clozapine through chitosan microparticles prepared by a novel method. Journal of Controlled Release 96, 245–259. https://doi.org/10.1016/j.jconrel.2004.01.025

Akamo, A.J., Rotimi, S.O., Akinloye, D.I., Ugbaja, R.N., Adeleye, O.O., Dosumu, O.A., Eteng, O.E., Amah, G., Obijeku, A., Cole, O.E., 2021. Naringin prevents cyclophosphamide-induced hepatotoxicity in rats by attenuating oxidative stress, fibrosis, and inflammation. Food and Chemical Toxicology 153, 112266. https://doi.org/10.1016/j.fct.2021.112266

Alibaba, 2023. Chitosan Price, 2023 Chitosan Price Manufacturers & Suppliers | Made-in-China.com [WWW Document]. URL https://www.made-in-china.com/multi-search/Chitosan_Price/F2--CL_DM--PV_1356080000_19114_4374/1.html (accessed 3.6.23).

Álvarez-Álvarez, R., Botas, A., Albillos, S.M., Rumbero, A., Martín, J.F., Liras, P., 2015. Molecular genetics of naringeninbiosynthesis, a typical plant secondary metabolite produced by Streptomyces clavuligerus. Microbial Cell Factories 14, 178. https://doi.org/10.1186/s12934-015-0373-7

Amidi, M., Pellikaan, H.C., de Boer, A.H., Crommelin, D.J.A., Hennink, W.E., Jiskoot, W., 2008. Preparation and physicochemical characterization of supercritically dried insulin-loaded microparticles for pulmonary delivery. European Journal of Pharmaceutics and Biopharmaceutics 68, 191–200. https://doi.org/10.1016/j.ejpb.2007.05.007

Aranaz, I., Paños, I., Peniche, C., Heras, Á., Acosta, N., 2017. Chitosan Spray-Dried Microparticles for Controlled Delivery of Venlafaxine Hydrochloride. Molecules 22, 1980. https://doi.org/10.3390/molecules22111980

Arora, A., Byrem, T.M., Nair, M.G., Strasburg, G.M., 2000. Modulation of Liposomal Membrane Fluidity by Flavonoids and Isoflavonoids. Archives of Biochemistry and Biophysics 373, 102–109. https://doi.org/10.1006/abbi.1999.1525

Arozal, W., Louisa, M., Rahmat, D., Chendrana, P., Sandhiutami, N.M.D., 2021. Development, Characterization and Pharmacokinetic Profile of Chitosan-Sodium Tripolyphosphate Nanoparticles Based Drug Delivery Systems for Curcumin. Adv Pharm Bull 11, 77–85. https://doi.org/10.34172/apb.2021.008

ASTM, 2018. Test Method for Determining Degree of Deacetylation in Chitosan Salts by Proton Nuclear Magnetic Resonance (1H NMR) Spectroscopy. https://doi.org/10.1520/F2260-18

Atomic force microscopy [WWW Document], 2022. . Wikipedia. URL https://en.wikipedia.org/w/index.php?title=Atomic_force_microscopy&oldid=1089740675 (accessed 6.9.22).

Bark, K.-M., Yeom, J.-E., Yang, J.-I., Yang, I.-J., Park, C.-H., Park, H.-R., 2011. Spectroscopic Studies on the Oxidation of Catechin in Aqueous Solution. Bulletin of the Korean Chemical Society 32, 3443–3447. https://doi.org/10.5012/bkcs.2011.32.9.3443

Beri, R.G., Walker, J., Reese, E.T., Rollings, J.E., 1993. Characterization of chitosans via coupled size-exclusion chromatography and multiple-angle laser light-scattering technique. Carbohydrate Research 238, 11–26. https://doi.org/10.1016/0008-6215(93)87002-A

Bhathena, S.J., Velasquez, M.T., 2002. Beneficial role of dietary phytoestrogens in obesity and diabetes. The American Journal of Clinical Nutrition 76, 1191–1201. https://doi.org/10.1093/ajcn/76.6.1191

Bin-Jumah, M., Gilani, S.J., Jahangir, M.A., Zafar, A., Alshehri, S., Yasir, M., Kala, C., Taleuzzaman, M., Imam, S.S., 2020. Clarithromycin-Loaded Ocular Chitosan Nanoparticle: Formulation, Optimization, Characterization, Ocular Irritation, and Antimicrobial Activity [WWW Document]. International Journal of Nanomedicine. https://doi.org/10.2147/IJN.S269004

Biró, E., Németh, A.Sz., Feczkó, T., Tóth, J., Sisak, Cs., Gyenis, J., 2009. Three-step experimental design to determine the effect of process parameters on the size of chitosan microspheres. Chemical Engineering and Processing: Process Intensification 48, 771–779. https://doi.org/10.1016/j.cep.2008.10.001

Brimson, J.M., Prasanth, M.I., Kumaree, K.K., Thitilertdecha, P., Malar, D.S., Tencomnao, T., Prasansuklab, A., 2023. Tea Plant (Camellia sinensis): A Current Update on Use in Diabetes, Obesity, and Cardiovascular Disease. Nutrients 15, 37. https://doi.org/10.3390/nu15010037

Budincic, J.M., Petrovic, L., Dekic, L., Fraj, J., Bucko, S., Katona, J., Spasojevic, L., 2021. Study of vitamin E microencapsulation and controlled release from chitosan/sodium lauryl ether sulfate microcapsules. Carbohydr. Polym. 251, 116988. https://doi.org/10.1016/j.carbpol.2020.116988

Calvo, P., Remuñán-López, C., Vila-Jato, J.L., Alonso, M.J., 1997a. Novel hydrophilic chitosan-polyethylene oxide nanoparticles as protein carriers. Journal of Applied Polymer Science 63, 125–132. https://doi.org/10.1002/(SICI)1097-4628(19970103)63:1<125::AID-APP13>3.0.CO;2-4

Calvo, P., Remuñán-López, C., Vila-Jato, J.L., Alonso, M.J., 1997b. Development of positively charged colloidal drug carriers: Chitosan-coated polyester nanocapsules and submicron-emulsions. Colloid Polym Sci 275, 46–53. https://doi.org/10.1007/s003960050050

Caprifico, A.E., Foot, P.J.S., Polycarpou, E., Calabrese, G., 2020. Overcoming the Blood-Brain Barrier: Functionalised Chitosan Nanocarriers. Pharmaceutics 12, 1013. https://doi.org/10.3390/pharmaceutics12111013

CariÑo-Cortés, R., Álvarez-González, I., Martino-Roaro, L., Madrigal-Bujaidar, E., 2010. Effect of Naringin on the DNA Damage Induced by Daunorubicin in Mouse Hepatocytes and Cardiocytes. Biological and Pharmaceutical Bulletin 33, 697–701. https://doi.org/10.1248/bpb.33.697

Cavia-Saiz, M., Busto, M.D., Pilar-Izquierdo, M.C., Ortega, N., Perez-Mateos, M., Muñiz, P., 2010. Antioxidant properties, radical scavenging activity and biomolecule protection capacity of flavonoid naringenin and its glycoside naringin: a comparative study. Journal of the Science of Food and Agriculture 90, 1238–1244. https://doi.org/10.1002/jsfa.3959

Chatelet, C., 2001. Influence of the degree of acetylation on some biological properties of chitosan films. Biomaterials 22, 261–268. https://doi.org/10.1016/S0142-9612(00)00183-6

Cherniack, E.P., 2011. Polyphenols: planting the seeds of treatment for the metabolic syndrome. Nutrition 27, 617–623. https://doi.org/10.1016/j.nut.2010.10.013

Chinova, B., 2021. GRAS NOTICE FOR THE USE OF FIBER EXTRACTED FROM WHITE BUTTON MUSHROOMS AS AN ANTIMICROBIAL INGREDIENT IN FOOD AND BEVERAGE PRODUCTS.

Chuah, L.H., Billa, N., Roberts, C.J., Burley, J.C., Manickam, S., 2013. Curcumin-containing chitosan nanoparticles as a potential mucoadhesive delivery system to the colon. Pharmaceutical Development and Technology 18, 591–599. https://doi.org/10.3109/10837450.2011.640688

Cordenonsi, L.M., Sponchiado, R.M., Campanharo, S.C., Garcia, C.V., Raffin, R.P., Schapoval, E.E.S., 2017. Study of Flavonoids presente in Pomelo (Citrus máxima) by DSC, UV-VIS, IR, 1H AND 13C NMR AND MS 7.

CORDIS, 2019. KITOGREEN, HORIZON 2020 program [WWW Document]. The World's first vegetal chitosan biostimulant from non-GMO and renewable source on an industrial scale. URL https://cordis.europa.eu/project/id/875948

Cuevas-Valenzuela, J., Gonzalez-Rojas, A., Wisniak, J., Apelblat, A., Perez-Correa, J.R., 2014. Solubility of (+)-catechin in water and water-ethanol mixtures within the temperature range 277.6-331.2 K: Fundamental data to design polyphenol extraction processes. Fluid Phase Equilib. 382, 279–285. https://doi.org/10.1016/j.fluid.2014.09.013

Cui, C., Gan, L., Lan, X., Li, J., Zhang, C., Li, F., Wang, C., Yuan, C., 2019. Development of sustainable carrier in thermosensitive hydrogel based on chitosan/alginate nanoparticles for *in situ* delivery system. Polym. Compos. 40, 2187–2196. https://doi.org/10.1002/pc.25024

Dara, P.K., Mahadevan, R., Digita, P.A., Visnuvinayagam, S., Kumar, L.R.G., Mathew, S., Ravishankar, C.N., Anandan, R., 2020. Synthesis and biochemical characterization of silver nanoparticles grafted chitosan (Chi-Ag-NPs): in vitro studies on antioxidant and antibacterial applications. SN Appl. Sci. 2, 665. https://doi.org/10.1007/s42452-020-2261-y

Das, S., Singh, V.K., Dwivedy, A.K., Chaudhari, A.K., Upadhyay, N., Singh, P., Sharma, S., Dubey, N.K., 2019. Encapsulation in chitosan-based nanomatrix as an efficient green technology to boost the antimicrobial, antioxidant and in situ efficacy of Coriandrum sativum essential oil. International Journal of Biological Macromolecules 133, 294–305. https://doi.org/10.1016/j.ijbiomac.2019.04.070

Decuzzi, P., Pasqualini, R., Arap, W., Ferrari, M., 2008. Intravascular Delivery of Particulate Systems: Does Geometry Really Matter? Pharm Res 26, 235. https://doi.org/10.1007/s11095-008-9697-x

Desai, K.G., 2016. Chitosan Nanoparticles Prepared by Ionotropic Gelation: An Overview of Recent Advances. Crit Rev Ther Drug Carrier Syst 33, 107–158. https://doi.org/10.1615/CritRevTherDrugCarrierSyst.2016014850

Di Santo, M.C., D' Antoni, C.L., Domínguez Rubio, A.P., Alaimo, A., Pérez, O.E., 2021. Chitosan-tripolyphosphate nanoparticles designed to encapsulate polyphenolic compounds for biomedical and pharmaceutical applications − A review. Biomedicine & Pharmacotherapy 142, 111970. https://doi.org/10.1016/j.biopha.2021.111970

Dube, A., Nicolazzo, J.A., Larson, I., 2010. Chitosan nanoparticles enhance the intestinal absorption of the green tea catechins (+)-catechin and (−)-epigallocatechin gallate. European Journal of Pharmaceutical Sciences 41, 219–225. https://doi.org/10.1016/j.ejps.2010.06.010

Dudhani, A.R., Kosaraju, S.L., 2010. Bioadhesive chitosan nanoparticles: Preparation and characterization. Carbohydrate Polymers 81, 243–251. https://doi.org/10.1016/j.carbpol.2010.02.026

Eason, R., Campbell, A.M., 1978. Centrifugal Separations in Molecular and Cell Biology, in: Birnie, G.D., Rickwood, D. (Eds.), Centrifugal Separations in Molecular and Cell Biology. Butterworth-Heinemann, pp. 251–287. https://doi.org/10.1016/B978-0-408-70803-6.50012-1

Ebrahimi, M.H., Samadian, H., Davani, S.T., Kolarijani, N.R., Mogharabian, N., Salami, M.S., Salehi, M., 2020. Peripheral nerve regeneration in rats by chitosan/alginate hydrogel composited with Berberine and Naringin nanoparticles: in vitro and in vivo study. Journal of Molecular Liquids 318, 114226. https://doi.org/10.1016/j.molliq.2020.114226

El Knidri, H., Belaabed, R., Addaou, A., Laajeb, A., Lahsini, A., 2018. Extraction, chemical modification and characterization of chitin and chitosan. International Journal of Biological Macromolecules 120, 1181–1189. https://doi.org/10.1016/j.ijbiomac.2018.08.139

Elaissari, A. (Ed.), 2008. Colloidal nanoparticles in biotechnology. Wiley-Interscience, Hoboken, N.J.

El-Shabouri, M.H., 2002. Positively charged nanoparticles for improving the oral bioavailability of cyclosporin-A. International Journal of Pharmaceutics 249, 101–108. https://doi.org/10.1016/S0378-5173(02)00461-1

Esenaliev, R.O., 2000. Radiation and nanoparticles for enhancement of drug delivery in solid tumors. US6165440A.

EUCHIS, n.d. European Chitin Society - euchis.org [WWW Document]. URL https://euchis.org/ (accessed 2.22.23).

European Pharmacopoeia, 9. ed. ed, 2016. . Council of Europe, Strasbourg.

Facts & Factors, 2022. Chitosan Industry Trends, Share, Value, Analysis & Forecast Report [WWW Document]. URL https://www.globenewswire.com/en/news-release/2022/09/27/2523512/0/en/Demand-for-Global-Chitosan-Market-Size-to-Hit-26272-32-Mn-by-2028-Exhibit-a-CAGR-of-24-10-Chitosan-Industry-Trends-Share-Value-Analysis-Forecast-Report-by-Facts-Factors.html (accessed 2.28.23).

Fan, W., Yan, W., Xu, Z., Ni, H., 2012. Formation mechanism of monodisperse, low molecular weight chitosan nanoparticles by ionic gelation technique. Colloids and Surfaces B: Biointerfaces 90, 21–27. https://doi.org/10.1016/j.colsurfb.2011.09.042

FAO, 2019. FAO Yearbook. Fishery and Aquaculture Statistics 2019/FAO annuaire. Statistiques des pêches et de l'aquaculture 2019/FAO anuario. Estadísticas de pesca y acuicultura 2019. FAO. https://doi.org/10.4060/cb7874t

Ficarra, R., Tommasini, S., Raneri, D., Calabrò, M.L., Di Bella, M.R., Rustichelli, C., Gamberini, M.C., Ficarra, P., 2002. Study of flavonoids/beta-cyclodextrins inclusion complexes by NMR, FT-IR, DSC, X-ray investigation. J Pharm Biomed Anal 29, 1005–1014. https://doi.org/10.1016/s0731-7085(02)00141-3

Food and agriculture organization of united nations, 2014. The State of World Fisheries and Aquaculture 2014.

Fraga, C.G., Litterio, M.C., Prince, P.D., Calabró, V., Piotrkowski, B., Galleano, M., 2011. Cocoa flavanols: effects on vascular nitric oxide and blood pressure. J Clin Biochem Nutr 48, 63–67. https://doi.org/10.3164/jcbn.11-010FR

Frent, O.D., Vicas, L.G., Duteanu, N., Morgovan, C.M., Jurca, T., Pallag, A., Muresan, M.E., Filip, S.M., Lucaciu, R.-L., Marian, E., 2022. Sodium Alginate—Natural Microencapsulation Material of Polymeric Microparticles. International Journal of Molecular Sciences 23, 12108. https://doi.org/10.3390/ijms232012108

Fuior, E.V., Deleanu, M., Constantinescu, C.A., Rebleanu, D., Voicu, G., Simionescu, M., Calin, M., 2019. Functional Role of VCAM-1 Targeted Flavonoid-Loaded Lipid Nanoemulsions in Reducing Endothelium Inflammation. Pharmaceutics 11, 391. https://doi.org/10.3390/pharmaceutics11080391

Galanakis, C.M., 2018. Polyphenols: Properties, Recovery, and Applications. Elsevier.

Gan, Q., Wang, T., Cochrane, C., McCarron, P., 2005. Modulation of surface charge, particle size and morphological properties of chitosan–TPP nanoparticles intended for gene delivery. Colloids and Surfaces B: Biointerfaces 44, 65–73. https://doi.org/10.1016/j.colsurfb.2005.06.001

Gao, S., Hu, M., 2010. Bioavailability Challenges Associated with Development of Anti-Cancer Phenolics. Mini Rev Med Chem 10, 550–567.

Garbacki, N., Kinet, M., Nusgens, B., Desmecht, D., Damas, J., 2005. Proanthocyanidins, from Ribes nigrum leaves, reduce endothelial adhesion molecules ICAM-1 and VCAM-1. J Inflamm (Lond) 2, 9. https://doi.org/10.1186/1476-9255-2-9

Garg, U., Chauhan, S., Nagaich, U., Jain, N., 2019. Current Advances in Chitosan Nanoparticles Based Drug Delivery and Targeting. Adv Pharm Bull 9, 195–204. https://doi.org/10.15171/apb.2019.023

Ghormade, V., Pathan, E.K., Deshpande, M.V., 2017. Can fungi compete with marine sources for chitosan production? International Journal of Biological Macromolecules 104, 1415–1421. https://doi.org/10.1016/j.ijbiomac.2017.01.112

Ghosh, T.K., Jasti, B.R., 2004. Theory and Practice of Contemporary Pharmaceutics. CRC Press.

Giacalone, M., Di Sacco, F., Traupe, I., Topini, R., Forfori, F., Giunta, F., 2011. Antioxidant and neuroprotective properties of blueberry polyphenols: a critical review. Nutr Neurosci 14, 119–125. https://doi.org/10.1179/1476830511Y.0000000007

Gibaldi, M., Perrier, D., 2006. DRUGS AND THE PHARMACEUTICAL SCIENCES. Taylor & Francis Group.

Goldwasser, J., Cohen, P.Y., Lin, W., Kitsberg, D., Balaguer, P., Polyak, S.J., Chung, R.T., Yarmush, M.L., Nahmias, Y., 2011. Naringenin inhibits the assembly and long-term production of infectious hepatitis C virus particles through a PPAR-mediated mechanism. J Hepatol 55, 963–971. https://doi.org/10.1016/j.jhep.2011.02.011

Gooday, G.W., 1990. The Ecology of Chitin Degradation, in: Marshall, K.C. (Ed.), Advances in Microbial Ecology, Advances in Microbial Ecology. Springer US, Boston, MA, pp. 387–430. https://doi.org/10.1007/978-1-4684-7612-5_10

Gooneh-Farahani, S., Naghib, S.M., Naimi-Jamal, M.R., 2020. A Novel and Inexpensive Method Based on Modified Ionic Gelation for pH-responsive Controlled Drug Release of Homogeneously Distributed Chitosan Nanoparticles with a High Encapsulation Efficiency. Fibers Polym 21, 1917–1926. https://doi.org/10.1007/s12221-020-1095-y

Guo, D., Wang, J., Wang, X., Luo, H., Zhang, H., Cao, D., Chen, L., Huang, N., 2011. Double directional adjusting estrogenic effect of naringin from Rhizoma drynariae (Gusuibu). J. Ethnopharmacol. 138, 451–457. https://doi.org/10.1016/j.jep.2011.09.034

Guyot, S., Cheynier, V., Souquet, J.-M., Moutounet, M., 1995. Influence of pH on the Enzymic Oxidation of (+)-Catechin in Model Systems 5.

Hahn, T., Tafi, E., Paul, A., Salvia, R., Falabella, P., Zibek, S., 2020. Current state of chitin purification and chitosan production from insects. Journal of Chemical Technology & Biotechnology 95, 2775–2795. https://doi.org/10.1002/jctb.6533

Harmon, A.W., Patel, Y.M., 2004. Naringenin Inhibits Glucose Uptake in MCF-7 Breast Cancer Cells: A Mechanism for Impaired Cellular Proliferation. Breast Cancer Res Treat 85, 103–110. https://doi.org/10.1023/B:BREA.0000025397.56192.e2

Hasheminejad, N., Khodaiyan, F., Safari, M., 2019. Improving the antifungal activity of clove essential oil encapsulated by chitosan nanoparticles. Food Chemistry 275, 113–122. https://doi.org/10.1016/j.foodchem.2018.09.085

Hassan, R.A., Hozayen, W.G., Abo Sree, H.T., Al-Muzafar, H.M., Amin, K.A., Ahmed, O.M., 2021. Naringin and Hesperidin Counteract Diclofenac-Induced Hepatotoxicity in Male Wistar Rats via Their Antioxidant, Anti-Inflammatory, and Antiapoptotic Activities. Oxidative Medicine and Cellular Longevity 2021, e9990091. https://doi.org/10.1155/2021/9990091

He, X.-H., Wang, W., Deng, K., Xie, R., Ju, X.-J., Liu, Z., Chu, L.-Y., 2015. Microfluidic fabrication of chitosan microfibers with controllable internals from tubular to peapod-like structures. RSC Advances 5, 928–936. https://doi.org/10.1039/C4RA10696B

Hejazi, R., Amiji, M., 2003. Chitosan-based gastrointestinal delivery systems. Journal of Controlled Release 89, 151–165. https://doi.org/10.1016/S0168-3659(03)00126-3

Herdiana, Y., Wathoni, N., Shamsuddin, S., Muchtaridi, M., 2022. Drug release study of the chitosan-based nanoparticles. Heliyon 8, e08674. https://doi.org/10.1016/j.heliyon.2021.e08674

Hernández-Aquino, E., Muriel, P., 2018. Beneficial effects of naringenin in liver diseases: Molecular mechanisms. World Journal of Gastroenterology 24, 1679–1707. https://doi.org/10.3748/wjg.v24.i16.1679

Hirai, A., Odani, H., Nakajima, A., 1991. Determination of degree of deacetylation of chitosan by 1H NMR spectroscopy. Polymer Bulletin 26, 87–94. https://doi.org/10.1007/BF00299352

Hoffmann, S., Gorzelanny, C., Moerschbacher, B., Goycoolea, F., 2018. Physicochemical Characterization of FRET-Labelled Chitosan Nanocapsules and Model Degradation Studies. Nanomaterials 8, 846. https://doi.org/10.3390/nano8100846

Höfler, H.J., Averback, R.S., Hahn, H., Gleiter, H., 1993. Diffusion of bismuth and gold in nanocrystalline copper. Journal of Applied Physics 74, 3832–3839. https://doi.org/10.1063/1.354477

Hu, B., Pan, C., Sun, Y., Hou, Z., Ye, H., Hu, B., Zeng, X., 2008. Optimization of Fabrication Parameters To Produce Chitosan−Tripolyphosphate Nanoparticles for Delivery of Tea Catechins. Journal of Agricultural and Food Chemistry 56, 7451–7458. https://doi.org/10.1021/jf801111c

Hu, Y., Jiang, X., Ding, Y., Ge, H., Yuan, Y., Yang, C., 2002. Synthesis and characterization of chitosan–poly(acrylic acid) nanoparticles. Biomaterials 23, 3193–3201. https://doi.org/10.1016/S0142-9612(02)00071-6

Huang, K.-S., Yang, C.-H., Wang, Y.-C., Wang, W.-T., Lu, Y.-Y., 2019. Microfluidic Synthesis of Vinblastine-Loaded Multifunctional Particles for Magnetically Responsive Controlled Drug Release. Pharmaceutics 11, 212. https://doi.org/10.3390/pharmaceutics11050212

Huang, W.F., Tsui, C.P., Tang, C.Y., Yang, M., Gu, L., 2017. Surface charge switchable and pH-responsive chitosan/polymer core-shell composite nanoparticles for drug delivery application. Composites Part B: Engineering, Bio-inspired Nano-engineered Materials 121, 83–91. https://doi.org/10.1016/j.compositesb.2017.03.028

Huang, Y., Lapitsky, Y., 2011. Monovalent Salt Enhances Colloidal Stability during the Formation of Chitosan/Tripolyphosphate Microgels. Langmuir 27, 10392–10399. https://doi.org/10.1021/la201194a

Huether, S.E., McCance, K.L., 2019. Understanding Pathophysiology - E-Book. Elsevier Health Sciences.

Hunter, R.J., 2013. Zeta Potential in Colloid Science: Principles and Applications. Academic Press.

Huq, T., Khan, A., Brown, D., Dhayagude, N., He, Z., Ni, Y., 2022. Sources, production and commercial applications of fungal chitosan: A review. Journal of Bioresources and Bioproducts 7, 85–98. https://doi.org/10.1016/j.jobab.2022.01.002

Hwang, K.T., Jung, S.T., Lee, G.D., Chinnan, M.S., Park, Y.S., Park, H.J., 2002. Controlling Molecular Weight and Degree of Deacetylation of Chitosan by Response Surface Methodology. J. Agric. Food Chem. 50, 1876–1882. https://doi.org/10.1021/jf011167u

Jovanovic, S.V., Steenken, S., Tosic, M., Marjanovic, B., Simic, M.G., 1994. Flavonoids as Antioxidants 6.

Kailaku, S.I., 2014. Formulation of Nanoencapsulated Catechin with Chitosan as Encapsulation Material. Procedia Chemistry 7.

Kamat, V., Bodas, D., Paknikar, K., 2016. Chitosan nanoparticles synthesis caught in action using microdroplet reactions. Sci Rep 6, 22260. https://doi.org/10.1038/srep22260

Kanno, S.-I., Tomizawa, A., Hiura, T., Osanai, Y., Shouji, A., Ujibe, M., Ohtake, T., Kimura, K., Ishikawa, M., 2005. Inhibitory effects of naringenin on tumor growth in human cancer cell lines and sarcoma S-180-implanted mice. Biol Pharm Bull 28, 527–530. https://doi.org/10.1248/bpb.28.527

Kasaai, M.R., 2009. Determination of the degree of N-acetylation for chitin and chitosan by various NMR spectroscopy techniques: A review. J. Agric. Food Chem 57, 1667–1676. https://doi.org/10.1021/jf803001m

Kelly, K.L., Coronado, E., Zhao, L.L., Schatz, G.C., 2003. The Optical Properties of Metal Nanoparticles: The Influence of Size, Shape, and Dielectric Environment. J. Phys. Chem. B 107, 668–677. https://doi.org/10.1021/jp026731y

Khan, N., Mukhtar, H., 2013. Tea and Health: Studies in Humans. CPD 19, 6141–6147. https://doi.org/10.2174/1381612811319340008

Khan, N., Mukhtar, H., 2007. Tea polyphenols for health promotion. Life Sciences 81, 519–533. https://doi.org/10.1016/j.lfs.2007.06.011

Khayrova, A., Lopatin, S., Varlamov, V., 2021. Obtaining chitin, chitosan and their melanin complexes from insects. International Journal of Biological Macromolecules 167, 1319–1328. https://doi.org/10.1016/j.ijbiomac.2020.11.086

Khokhar, T.S., Memon, F.N., Memon, S.S., Memon, A.A., Bhatti, A.A., Memon, S., 2022. Naringenin solubilizing and pH dependent releasing properties of water soluble p-sulphonatocalix[4]arene. Supramolecular Chemistry 0, 1–11. https://doi.org/10.1080/10610278.2022.2061352

Kim, S.-K., 2010. Chitin, Chitosan, Oligosaccharides and Their Derivatives: Biological Activities and Applications, 1st ed. CRC Press.

Kumar, S.P., Birundha, K., Kaveri, K., Devi, K.T.R., 2015. Antioxidant studies of chitosan nanoparticles containing naringenin and their cytotoxicity effects in lung cancer cells. International Journal of Biological Macromolecules 78, 87–95. https://doi.org/10.1016/j.ijbiomac.2015.03.045

Kumirska, J., Czerwicka, M., Kaczyński, Z., Bychowska, A., Brzozowski, K., Thöming, J., Stepnowski, P., 2010. Application of Spectroscopic Methods for Structural Analysis of Chitin and Chitosan. Marine Drugs 8, 1567–1636. https://doi.org/10.3390/md8051567

Lakenbrink, C., Lapczynski, S., Maiwald, B., Engelhardt, U.H., 2000. Flavonoids and other polyphenols in consumer brews of tea and other caffeinated beverages. J Agric Food Chem 48, 2848–2852. https://doi.org/10.1021/jf9908042

Lam, P.-L., Lee, K.K.-H., Ho, Y.-W., Wong, R.S.-M., Tong, S.-W., Cheng, C.-H., Lam, K.-H., Tang, J.C.-O., Bian, Z.-X., Gambari, R., Kok, S.H.-L., Chui, C.-H., 2014. The development of chitosan based microcapsules as delivery vehicles for orally administered daunorubicin. RSC Adv. 4, 14109–14114. https://doi.org/10.1039/C4RA00195H

Lamarra, J., Rivero, S., Pinotti, A., 2016. Design of chitosan-based nanoparticles functionalized with gallic acid. Materials Science and Engineering: C 67, 717–726. https://doi.org/10.1016/j.msec.2016.05.072

Latańska, I., Rosiak, P., Paul, P., Sujka, W., Kolesińska, B., Latańska, I., Rosiak, P., Paul, P., Sujka, W., Kolesińska, B., 2021. Modulating the Physicochemical Properties of Chitin and Chitosan as a Method of Obtaining New Biological Properties of Biodegradable Materials, Chitin and Chitosan - Physicochemical Properties and Industrial Applications. IntechOpen. https://doi.org/10.5772/intechopen.95815

Lavertu, M., Xia, Z., Serreqi, A.N., Berrada, M., Rodrigues, A., Wang, D., Buschmann, M.D., Gupta, A., 2003. A validated 1H NMR method for the determination of the degree of deacetylation of chitosan.

Journal of Pharmaceutical and Biomedical Analysis 32, 1149–1158. https://doi.org/10.1016/S0731-7085(03)00155-9

Lee, M., Nah, J.-W., Kwon, Y., Koh, J.J., Ko, K.S., Kim, S.W., 2001. Water-Soluble and Low Molecular Weight Chitosan-Based Plasmid DNA Delivery. Pharm Res 18, 427–431. https://doi.org/10.1023/A:1011037807261

Lee, M.-H., Yoon, S., Moon, J.-O., 2004. The Flavonoid Naringenin Inhibits Dimethylnitrosamine-Induced Liver Damage in Rats. Biological and Pharmaceutical Bulletin 27, 72–76. https://doi.org/10.1248/bpb.27.72

Lee, Y., Ji, Y.R., Lee, S., Choi, M.-J., Cho, Y., 2019. Microencapsulation of Probiotic Lactobacillus acidophilus KBL409 by Extrusion Technology to Enhance Survival under Simulated Intestinal and Freeze-Drying Conditions. Journal of Microbiology and Biotechnology 29, 721–730. https://doi.org/10.4014/jmb.1903.03018

Lee, Y.H., Kim, S.C., Nam, K.D., Kim, T.H., Jung, B.O., Park, Y.-I., Synytsya, A., Park, J.K., 2022. Chitosan isolated from black soldier flies Hermetia illucens: Structure and enzymatic hydrolysis. Process Biochemistry 118, 171–181. https://doi.org/10.1016/j.procbio.2022.04.020

Li, D., Martini, N., Wu, Z., Wen, J., 2012. Development of an isocratic HPLC method for catechin quantification and its application to formulation studies. Fitoterapia 83, 1267–1274. https://doi.org/10.1016/j.fitote.2012.06.006

Li, J., Du, Y., Yang, J., Feng, T., Li, A., Chen, P., 2005. Preparation and characterisation of low molecular weight chitosan and chito-oligomers by a commercial enzyme. Polymer Degradation and Stability 87, 441–448. https://doi.org/10.1016/j.polymdegradstab.2004.09.008

Li, J., Wu, H., Jiang, K., Liu, Y., Yang, L., Park, H.J., 2021. Alginate Calcium Microbeads Containing Chitosan Nanoparticles for Controlled Insulin Release. Appl Biochem Biotechnol 193, 463–478. https://doi.org/10.1007/s12010-020-03420-9

Li, X., Kong, X., Shi, S., Zheng, X., Guo, G., Wei, Y., Qian, Z., 2008. Preparation of alginate coated chitosan microparticles for vaccine delivery. BMC Biotechnology 8, 89. https://doi.org/10.1186/1472-6750-8-89

Liang, J., Li, F., Fang, Y., Yang, W., An, X., Zhao, L., Xin, Z., Cao, L., Hu, Q., 2011. Synthesis, characterization and cytotoxicity studies of chitosan-coated tea polyphenols nanoparticles. Colloids and Surfaces B: Biointerfaces 82, 297–301. https://doi.org/10.1016/j.colsurfb.2010.08.045

Liang, J., Yan, H., Puligundla, P., Gao, X., Zhou, Y., Wan, X., 2017. Applications of chitosan nanoparticles to enhance absorption and bioavailability of tea polyphenols: A review. Food Hydrocolloids 69, 286–292. https://doi.org/10.1016/j.foodhyd.2017.01.041

Lim, L.Y., Wan, L.S.C., Thai, P.Y., 1997. Chitosan Microspheres Prepared by Emulsification and Ionotropic Gelation. Drug Development and Industrial Pharmacy 23, 981–985. https://doi.org/10.3109/03639049709149150

Ling, K., Wu, H., Neish, A.S., Champion, J.A., 2019. Alginate/chitosan microparticles for gastric passage and intestinal release of therapeutic protein nanoparticles. J. Control. Release 295, 174–186. https://doi.org/10.1016/j.jconrel.2018.12.017

Liu, F., Liu, L., Li, X., Zhang, Q., 2007. Preparation of chitosan–hyaluronate double-walled microspheres by emulsification-coacervation method. J Mater Sci: Mater Med 18, 2215–2224. https://doi.org/10.1007/s10856-007-3228-x

Liu, R., 2008. Water-Insoluble Drug Formulation, Second Edition. Taylor & Francis.

LKT Labs, n.d. Naringenin [WWW Document]. LKT Labs. URL https://lktlabs.com/product/naringenin/ (accessed 4.10.23).

Lu, C., Mu, B., Liu, P., 2011. Stimuli-responsive multilayer chitosan hollow microspheres via layer-by-layer assembly. Colloids and Surfaces B: Biointerfaces 83, 254–259. https://doi.org/10.1016/j.colsurfb.2010.11.029

Luo, Z., Murray, B.S., Yusoff, A., Morgan, M.R.A., Povey, M.J.W., Day, A.J., 2011. Particle-Stabilizing Effects of Flavonoids at the Oil−Water Interface. J. Agric. Food Chem. 59, 2636–2645. https://doi.org/10.1021/jf1041855

Lyklema, J., 2005. Fundamentals of Interface and Colloid Science: Particulate Colloids. Elsevier.

Maity, S., Mukhopadhyay, P., Kundu, P.P., Chakraborti, A.S., 2017. Alginate coated chitosan core-shell nanoparticles for efficient oral delivery of naringenin in diabetic animals—An in vitro and in vivo approach. Carbohydrate Polymers 170, 124–132. https://doi.org/10.1016/j.carbpol.2017.04.066

Malathy, S., Priya, R.I., 2018. Naringin Loaded Chitosan Nanoparticle for Bone Regeneration: A Preliminary in vitro Study. J Nanomed Nanotechnol 09. https://doi.org/10.4172/2157-7439.1000507

Maltese, F., Erkelens, C., Kooy, F. van der, Choi, Y.H., Verpoorte, R., 2009. Identification of natural epimeric flavanone glycosides by NMR spectroscopy. Food Chemistry 116, 575–579. https://doi.org/10.1016/j.foodchem.2009.03.023

Malvern Instruments, 2005. Tech Note: Zeta potential - An introduction in 30 minutes.

Mandal, R.S.K., Bhatt, S., Mv, J., 2019. Evaluation of encapsulated catechin in chitosan- sodium tripolyphosphate nanoparticle 7.

Mandel, S.A., Avramovich-Tirosh, Y., Reznichenko, L., Zheng, H., Weinreb, O., Amit, T., Youdim, M.B.H., 2005. Multifunctional Activities of Green Tea Catechins in Neuroprotection. NSG 14, 46–60. https://doi.org/10.1159/000085385

Martínez, J.P., Falomir, M.P., Gozalbo, D., 2014. Chitin: A Structural Biopolysaccharide with Multiple Applications, in: eLS. American Cancer Society. https://doi.org/10.1002/9780470015902.a0000694.pub3

Martins, E., Poncelet, D., Rodrigues, R.C., Renard, D., 2017. Oil encapsulation techniques using alginate as encapsulating agent: applications and drawbacks. Journal of Microencapsulation 34, 754–771. https://doi.org/10.1080/02652048.2017.1403495

Matsubara, T., Wataoka, I., Urakawa, H., Yasunaga, H., 2014. High-Efficient Chemical Preparation of Catechinone Hair Dyestuff by Oxidation of (+)-Catechin in Water / Ethanol Mixed Solution 4.

McCave, I.N., Bryant, R.J., Cook, H.F., Coughanowr, C.A., 1986. Evaluation of a laser-diffraction-size analyzer for use with natural sediments. Journal of Sedimentary Research 56, 561–564. https://doi.org/10.1306/212F89CC-2B24-11D7-8648000102C1865D

Md, S., Alhakamy, N.A., Akhter, S., Awan, Z.A.Y., Aldawsari, H.M., Alharbi, W.S., Haque, A., Choudhury, H., Sivakumar, P.M., 2020. Development of Polymer and Surfactant Based Naringenin Nanosuspension for Improvement of Stability, Antioxidant, and Antitumour Activity. Journal of Chemistry 2020, e3489393. https://doi.org/10.1155/2020/3489393

Mitra, S., Gaur, U., Ghosh, P.C., Maitra, A.N., 2001. Tumour targeted delivery of encapsulated dextran–doxorubicin conjugate using chitosan nanoparticles as carrier. Journal of Controlled Release, Proceeding of the International Symposium on Tumor Targeted Delivery Systems 74, 317–323. https://doi.org/10.1016/S0168-3659(01)00342-X

Mohan, K., Muralisankar, T., Jayakumar, R., Rajeevgandhi, C., 2021. A study on structural comparisons of α-chitin extracted from marine crustacean shell waste. Carbohydrate Polymer Technologies and Applications 2, 100037. https://doi.org/10.1016/j.carpta.2021.100037

Montasser, I., Fessi, H., Coleman, A.W., 2002. Atomic force microscopy imaging of novel type of polymeric colloidal nanostructures. European Journal of Pharmaceutics and Biopharmaceutics 54, 281–284. https://doi.org/10.1016/S0939-6411(02)00087-5

Moreno, J.A.S., Mendes, A.C., Stephansen, K., Engwer, C., Goycoolea, F.M., Boisen, A., Nielsen, L.H., Chronakis, I.S., 2018. Development of electrosprayed mucoadhesive chitosan microparticles. Carbohydrate Polymers 190, 240–247. https://doi.org/10.1016/j.carbpol.2018.02.062

Mori, T., Koyama, N., Tan, J., Segawa, T., Maeda, M., Town, T., 2019. Combined treatment with the phenolics (−)-epigallocatechin-3-gallate and ferulic acid improves cognition and reduces Alzheimer-like pathology in mice. J. Biol. Chem. 294, 2714–2731. https://doi.org/10.1074/jbc.RA118.004280

Mou, C.-L., Wang, W., Ju, X.-J., Xie, R., Liu, Z., Chu, L.-Y., 2019. Dual-responsive microcarriers with sphere-in-capsule structures for co-encapsulation and sequential release. Journal of the Taiwan Institute of Chemical Engineers 98, 63–69. https://doi.org/10.1016/j.jtice.2018.06.032

Mukhopadhyay, P., Chakraborty, S., Bhattacharya, S., Mishra, R., Kundu, P.P., 2015. pH-sensitive chitosan/alginate core-shell nanoparticles for efficient and safe oral insulin delivery. International Journal of Biological Macromolecules 72, 640–648. https://doi.org/10.1016/j.ijbiomac.2014.08.040

Munawar, A.M., Syeda, J., Wasan, K., Wasan, E., 2017. An Overview of Chitosan Nanoparticles and Its Application in Non-Parenteral Drug Delivery. Pharmaceutics 9, 53. https://doi.org/10.3390/pharmaceutics9040053

Musial, C., Kuban-Jankowska, A., Gorska-Ponikowska, M., 2020. Beneficial Properties of Green Tea Catechins. Int. J. Mol. Sci. 21, 1744. https://doi.org/10.3390/ijms21051744

Nair, R.S., Morris, A., Billa, N., Leong, C.-O., 2019. An Evaluation of Curcumin-Encapsulated Chitosan Nanoparticles for Transdermal Delivery. AAPS PharmSciTech 20. https://doi.org/10.1208/s12249-018-1279-6

Nanoparticle technology handbook, 3rd edition. ed, 2018. . Elsevier, Amsterdam.

Ngan, L.T.K., Wang, S.-L., Hiep, Đ.M., Luong, P.M., Vui, N.T., Đinh, T.M., Dzung, N.A., 2014. Preparation of chitosan nanoparticles by spray drying, and their antibacterial activity. Research on Chemical Intermediates 40, 2165–2175. https://doi.org/10.1007/s11164-014-1594-9

Nguyen, D.T., Phan, V.H.G., Lee, D.S., Thambi, T., Huynh, D.P., 2019. Bioresorbable pH- and temperature-responsive injectable hydrogels-incorporating electrosprayed particles for the sustained release of

insulin. Polymer Degradation and Stability 162, 36–46. https://doi.org/10.1016/j.polymdegradstab.2019.02.013

Niwa, T., Takeuchi, H., Hino, T., Kunou, N., Kawashima, Y., 1993. Preparations of biodegradable nanospheres of water-soluble and insoluble drugs with D,L-lactide/glycolide copolymer by a novel spontaneous emulsification solvent diffusion method, and the drug release behavior. Journal of Controlled Release 25, 89–98. https://doi.org/10.1016/0168-3659(93)90097-O

Oršolić, N., Gajski, G., Garaj-Vrhovac, V., Đikić, D., Prskalo, Z.Š., Sirovina, D., 2011. DNA-protective effects of quercetin or naringenin in alloxan-induced diabetic mice. European Journal of Pharmacology 656, 110–118. https://doi.org/10.1016/j.ejphar.2011.01.021

Özbaş-Turan, S., Akbuğa, J., Aral, C., 2002. Controlled Release of Interleukin-2 from Chitosan Microspheres. Journal of Pharmaceutical Sciences 91, 1245–1251. https://doi.org/10.1002/jps.10122

Panyam, J., Labhasetwar, V., 2003. Biodegradable nanoparticles for drug and gene delivery to cells and tissue. Adv Drug Deliv Rev 55, 329–347. https://doi.org/10.1016/s0169-409x(02)00228-4

Parmar, H.S., Jain, P., Chauhan, D.S., Bhinchar, M.K., Munjal, V., Yusuf, M., Choube, K., Tawani, A., Tiwari, V., Manivannan, E., Kumar, A., 2012. DPP-IV inhibitory potential of naringin: an in silico, in vitro and in vivo study. Diabetes Res Clin Pract 97, 105–111. https://doi.org/10.1016/j.diabres.2012.02.011

Patel, K., Singh, G.K., Patel, D.K., 2018. A Review on Pharmacological and Analytical Aspects of Naringenin. Chinese Journal of Integrative Medicine 24, 551–560. https://doi.org/10.1007/s11655-014-1960-x

Patil, S.B., Sawant, K.K., 2011. Chitosan microspheres as a delivery system for nasal insufflation. Colloids and Surfaces B: Biointerfaces 84, 384–389. https://doi.org/10.1016/j.colsurfb.2011.01.030

Pattnaik, A., Pati, S., Samal, S.K., 2022. Chitosan-Polyphenol Conjugates for Human Health. Life 12, 1768. https://doi.org/10.3390/life12111768

Pauli, G.F., Chen, S.-N., Simmler, C., Lankin, D.C., Gödecke, T., Jaki, B.U., Friesen, J.B., McAlpine, J.B., Napolitano, J.G., 2014. Importance of Purity Evaluation and the Potential of Quantitative 1H NMR as a Purity Assay. J. Med. Chem. 57, 9220–9231. https://doi.org/10.1021/jm500734a

Paulino, A.T., Simionato, J.I., Garcia, J.C., Nozaki, J., 2006. Characterization of chitosan and chitin produced from silkworm crysalides. Carbohydrate Polymers 64, 98–103. https://doi.org/10.1016/j.carbpol.2005.10.032

Pedroso-Santana, S., Fleitas-Salazar, N., 2020. Ionotropic gelation method in the synthesis of nanoparticles/microparticles for biomedical purposes. Polymer International 69, 443–447. https://doi.org/10.1002/pi.5970

Peng, C.-H., Chyau, C.-C., Chan, K.-C., Chan, T.-H., Wang, C.-J., Huang, C.-N., 2011. Hibiscus sabdariffa Polyphenolic Extract Inhibits Hyperglycemia, Hyperlipidemia, and Glycation-Oxidative Stress while Improving Insulin Resistance. J. Agric. Food Chem. 59, 9901–9909. https://doi.org/10.1021/jf2022379

Phan, A.N.Q., Bach, L.G., Nguyen, T.D., Le, N.T.H., 2019. Efficient Method for Preparation of Rutin Nanosuspension Using Chitosan and Sodium Tripolyphosphate Crosslinker. Journal of Nanoscience and Nanotechnology 19, 974–978. https://doi.org/10.1166/jnn.2019.15925

Prabha, S., Zhou, W.-Z., Panyam, J., Labhasetwar, V., 2002. Size-dependency of nanoparticle-mediated gene transfection: studies with fractionated nanoparticles. International Journal of Pharmaceutics 244, 105–115. https://doi.org/10.1016/S0378-5173(02)00315-0

Prasanth, M.I., Sivamaruthi, B.S., Chaiyasut, C., Tencomnao, T., 2019. A Review of the Role of Green Tea (Camellia sinensis) in Antiphotoaging, Stress Resistance, Neuroprotection, and Autophagy. Nutrients 11, 474. https://doi.org/10.3390/nu11020474

Prego, C., Fabre, M., Torres, D., Alonso, M.J., 2006. Efficacy and Mechanism of Action of Chitosan Nanocapsules for Oral Peptide Delivery. Pharm Res 23, 549–556. https://doi.org/10.1007/s11095-006-9570-8

Raja Kumar, S., Mohd Ramli, E.S., Abdul Nasir, N.A., Ismail, N.H.M., Mohd Fahami, N.A., 2019. Preventive Effect of Naringin on Metabolic Syndrome and Its Mechanism of Action: A Systematic Review. Evidence-Based Complementary and Alternative Medicine 2019, e9752826. https://doi.org/10.1155/2019/9752826

Rathore, P., 2020. Formulation development, in vitro and in vivo evaluation of chitosan engineered nanoparticles for ocular delivery of insulin. RSC Advances 11.

Renugadevi, J., Prabu, S.M., 2010. Cadmium-induced hepatotoxicity in rats and the protective effect of naringenin. Experimental and Toxicologic Pathology 62, 171–181. https://doi.org/10.1016/j.etp.2009.03.010

Reportlinker, 2023. Global Chitin and Chitosan Derivatives Market to Reach $24.9 Billion by 2030 [WWW Document]. URL https://www.globenewswire.com/news-release/2023/02/17/2610744/0/en/Global-Chitin-and-Chitosan-Derivatives-Market-to-Reach-24-9-Billion-by-2030.html (accessed 3.6.23).

Ruh, M.F., Zacharewski, T., Connor, K., Howell, J., Chen, I., Safe, S., 1995. Naringenin: A weakly estrogenic bioflavonoid that exhibits antiestrogenic activity. Biochemical Pharmacology 50, 1485–1493. https://doi.org/10.1016/0006-2952(95)02061-6

Sachdeva, A.K., Kuhad, A., Chopra, K., 2014. Naringin ameliorates memory deficits in experimental paradigm of Alzheimer's disease by attenuating mitochondrial dysfunction. Pharmacology Biochemistry and Behavior 127, 101–110. https://doi.org/10.1016/j.pbb.2014.11.002

Saraf, S., Jain, S., Sahoo, R.N., Mallick, S., 2020. Lipopolysaccharide derived alginate coated Hepatitis B antigen loaded chitosan nanoparticles for oral mucosal immunization. International Journal of Biological Macromolecules 154, 466–476. https://doi.org/10.1016/j.ijbiomac.2020.03.124

Satoskar, R.S., Rege, N., Bhandarkar, S.D., 2017. Pharmacology and Pharmacotherapeutics. Elsevier Health Sciences.

Scalbert, A., Johnson, I.T., Saltmarsh, M., 2005a. Polyphenols: antioxidants and beyond. The American Journal of Clinical Nutrition 81, 215S-217S. https://doi.org/10.1093/ajcn/81.1.215S

Scalbert, A., Manach, C., Morand, C., Rémésy, C., Jiménez, L., 2005b. Dietary Polyphenols and the Prevention of Diseases. Critical Reviews in Food Science and Nutrition 45, 287–306. https://doi.org/10.1080/1040869059096

Sehrawat, N., Upadhyay, S.K., Sharma, A.K., Kumar, S., Yadav, M., 2021. Emerging Renoprotective Role of Citrus Flavonoid Naringin: Current Pharmaceutical Status and Future Perspectives. Curr Pharmacol Rep 7, 96–101. https://doi.org/10.1007/s40495-021-00256-7

Seidi, F., Khodadadi Yazdi, M., Jouyandeh, M., Dominic, M., Naeim, H., Nezhad, M.N., Bagheri, B., Habibzadeh, S., Zarrintaj, P., Saeb, M.R., Mozafari, M., 2021. Chitosan-based blends for biomedical applications. International Journal of Biological Macromolecules 183, 1818–1850. https://doi.org/10.1016/j.ijbiomac.2021.05.003

Semalty, A., Semalty, M., Singh, D., Rawat, M.S.M., 2010. Preparation and characterization of phospholipid complexes of naringenin for effective drug delivery. J Incl Phenom Macrocycl Chem 67, 253–260. https://doi.org/10.1007/s10847-009-9705-8

SFly, 2019. SFly - PRODUCTEUR DE CHITINE, CHITOSAN - HERMETIA ILLUCENS [WWW Document]. SFLY producteur de chitine chitosan. URL http://sflyproteins.fr/ (accessed 3.29.19).

Shadab, M., Alhakamy, N.A., Aldawsari, H.M., Asfour, H.Z., 2019. Neuroprotective and Antioxidant Effect of Naringenin-Loaded Nanoparticles for Nose-to-Brain Delivery. Brain Sci. 9, 275. https://doi.org/10.3390/brainsci9100275

Sheikholeslami, Z.S., Salimi-Kenari, H., Imani, M., Atai, M., Nodehi, A., 2017. Exploring the effect of formulation parameters on the particle size of carboxymethyl chitosan nanoparticles prepared via reverse micellar crosslinking. Journal of Microencapsulation 34, 270–279. https://doi.org/10.1080/02652048.2017.1321047

Shit, S.C., Shah, P.M., 2014. Edible Polymers: Challenges and Opportunities. Journal of Polymers 2014, 1–13. https://doi.org/10.1155/2014/427259

Shulman, M., Cohen, M., Soto-Gutierrez, A., Yagi, H., Wang, H., Goldwasser, J., Lee-Parsons, C.W., Benny-Ratsaby, O., Yarmush, M.L., Nahmias, Y., 2011. Enhancement of naringenin bioavailability by complexation with hydroxypropyl-β-cyclodextrin. [corrected]. PLoS One 6, e18033. https://doi.org/10.1371/journal.pone.0018033

Soe, Z.C., Poudel, B.K., Nguyen, H.T., Thapa, R.K., Ou, W., Gautam, M., Poudel, K., Jin, S.G., Jeong, J.-H., Ku, S.K., Choi, H.-G., Yong, C.S., Kim, J.O., 2019. Folate-targeted nanostructured chitosan/chondroitin sulfate complex carriers for enhanced delivery of bortezomib to colorectal cancer cells. Asian Journal of Pharmaceutical Sciences 14, 40–51. https://doi.org/10.1016/j.ajps.2018.09.004

Sreekumar, S., Goycoolea, F.M., Moerschbacher, B.M., Rivera-Rodriguez, G.R., 2018. Parameters influencing the size of chitosan-TPP nano- and microparticles. Scientific Reports 8. https://doi.org/10.1038/s41598-018-23064-4

Sreekumar, S., Lemke, P., Moerschbacher, B.M., Torres-Giner, S., Lagaron, J.M., 2017. Preparation and optimization of submicron chitosan capsules by water-based electrospraying for food and bioactive packaging applications. Food Additives & Contaminants: Part A 34, 1795–1806. https://doi.org/10.1080/19440049.2017.1347284

Stuhr, U., Striffler, T., Wipf, H., Natter, H., Wettmann, B., Janssen, S., Hempelmann, R., Hahn, H., 1997. An investigation of hydrogen diffusion in nanocrystalline Pd by neutron spectroscopy. Journal of Alloys and Compounds 253–254, 393–396. https://doi.org/10.1016/S0925-8388(96)03062-9

Sun, B., Zhang, M., Shen, J., He, Z., Fatehi, P., Ni, Y., 2019. Applications of Cellulose-based Materials in Sustained Drug Delivery Systems. Current Medicinal Chemistry 26, 2485–2501.

Szafraniec-Szczęsny, J., Janik-Hazuka, M., Odrobińska, J., Zapotoczny, S., 2020. Polymer Capsules with Hydrophobic Liquid Cores as Functional Nanocarriers. Polymers 12, 1999. https://doi.org/10.3390/polym12091999

Tang, D.-W., Yu, S.-H., Ho, Y.-C., Huang, B.-Q., Tsai, G.-J., Hsieh, H.-Y., Sung, H.-W., Mi, F.-L., 2013. Characterization of tea catechins-loaded nanoparticles prepared from chitosan and an edible polypeptide. Food Hydrocolloids 30, 33–41. https://doi.org/10.1016/j.foodhyd.2012.04.014

Thakur, A., Taranjit, 2011. Preparation of Chitosan Nanoparticles: A Study of Influencing Factors. Presented at the THE 10TH ASIAN INTERNATIONAL CONFERENCE ON FLUID MACHINERY, Kuala Lumpur (Malaysia), pp. 299–300. https://doi.org/10.1063/1.3653728

Tharanathan, R.N., Kittur, F.S., 2003. Chitin — The Undisputed Biomolecule of Great Potential. Critical Reviews in Food Science and Nutrition 43, 61–87. https://doi.org/10.1080/10408690390826455

Thielecke, F., Boschmann, M., 2009. The potential role of green tea catechins in the prevention of the metabolic syndrome – A review. Phytochemistry 70, 11–24. https://doi.org/10.1016/j.phytochem.2008.11.011

Tommasini, S., Calabrò, M.L., Raneri, D., Ficarra, P., Ficarra, R., 2004. Combined effect of pH and polysorbates with cyclodextrins on solubilization of naringenin. Journal of Pharmaceutical and Biomedical Analysis 36, 327–333. https://doi.org/10.1016/j.jpba.2004.06.013

Vinogradov, S.V., Bronich, T.K., Kabanov, A.V., 2002. Nanosized cationic hydrogels for drug delivery: preparation, properties and interactions with cells. Advanced Drug Delivery Reviews 54, 135–147. https://doi.org/10.1016/S0169-409X(01)00245-9

Wan, A., Sun, Y., Li, W., Li, H., 2008. Transmission electron microscopy and electron diffraction study of BSA-loaded quaternized chitosan nanoparticles. Journal of Biomedical Materials Research Part B: Applied Biomaterials 86B, 197–207. https://doi.org/10.1002/jbm.b.31006

Watson, R.R., Preedy, V.R., Zibadi, S. (Eds.), 2014. Polyphenols in human health and disease. Elsevier/Academic Press, Amsterdam ; Boston.

Xun, X.-M., Zhang, Z.-A., Yuan, Z.-X., Tuhong, K., Yan, C.-H., Zhan, Y.-F., Kang, G.-P., Wu, Q.-Y., Wang, J., 2023. Novel caffeic acid grafted chitosan-sodium alginate microcapsules generated by microfluidic technique for the encapsulation of bioactive peptides from silkworm pupae. Sustainable Chemistry and Pharmacy 32, 100974. https://doi.org/10.1016/j.scp.2023.100974

Yan, N., Chen, X., 2015. Sustainability: Don’t waste seafood waste. Nature News 524, 155. https://doi.org/10.1038/524155a

Yang, X.-L., Ju, X.-J., Mu, X.-T., Wang, W., Xie, R., Liu, Z., Chu, L.-Y., 2016. Core–Shell Chitosan Microcapsules for Programmed Sequential Drug Release. ACS Appl. Mater. Interfaces 8, 10524–10534. https://doi.org/10.1021/acsami.6b01277

Yilma, A.N., Singh, S.R., Morici, L., Dennis, V.A., 2013. Flavonoid Naringenin: A Potential Immunomodulator for Chlamydia trachomatis Inflammation. Mediators of Inflammation 2013, e102457. https://doi.org/10.1155/2013/102457

Zeng, J.-B., He, Y.-S., Li, S.-L., Wang, Y.-Z., 2012. Chitin Whiskers: An Overview. Biomacromolecules 13, 1–11. https://doi.org/10.1021/bm201564a

Zeng, W., Liu, Z., Li, Y., Zhu, S., Ma, J., Li, W., Gao, G., 2017. Development and characterization of cores–shell poly(lactide-co-glycolide)-chitosan microparticles for sustained release of GDNF. Colloids and Surfaces B: Biointerfaces 159, 791–799. https://doi.org/10.1016/j.colsurfb.2017.08.052

Zhang, H., Zhai, Z., Wang, Yueying, Zhang, J., Wu, H., Wang, Yingying, Li, C., Li, D., Lu, L., Wang, X., Chang, J., Hou, Q., Ju, Z., Zhou, D., Meng, A., 2013. Resveratrol ameliorates ionizing irradiation-induced long-term hematopoietic stem cell injury in mice. Free Radical Biology and Medicine 54, 40–50. https://doi.org/10.1016/j.freeradbiomed.2012.10.530

Zhang, H., Zhao, Y., 2015. Preparation, characterization and evaluation of tea polyphenol–Zn complex loaded β-chitosan nanoparticles. Food Hydrocolloids 48, 260–273. https://doi.org/10.1016/j.foodhyd.2015.02.015

Zhang, J., Zhang, P., Liu, T., Zhou, L., Zhang, L., Lin, R., Yang, G., Wang, W., Li, Y., 2015. Solubility of naringin in ethanol and water mixtures from 283.15 to 318.15K. Journal of Molecular Liquids 203, 98–103. https://doi.org/10.1016/j.molliq.2014.12.039

Zhang, P., Lin, R., Yang, G., Zhang, J., Zhou, L., Liu, T., 2013. Solubility of Naringenin in Ethanol and Water Mixtures. J. Chem. Eng. Data 58, 2402–2404. https://doi.org/10.1021/je4000718

Zhang, W., Jin, X., Li, H., Wei, C., Wu, C., 2019. Onion-structure bionic hydrogel capsules based on chitosan for regulating doxorubicin release. Carbohydrate Polymers 209, 152–160. https://doi.org/10.1016/j.carbpol.2019.01.028

Zhang, X., Zhang, Y., Gao, W., Guo, Z., Wang, K., Liu, S., Duan, Z., Chen, Y., 2021. Naringin improves lipid metabolism in a tissue-engineered liver model of NAFLD and the underlying mechanisms. Life Sciences 277, 119487. https://doi.org/10.1016/j.lfs.2021.119487

Zhang, Y., Zhang, X., Ding, R., Zhang, J., Liu, J., 2011. Determination of the degree of deacetylation of chitosan by potentiometric titration preceded by enzymatic pretreatment. Carbohydrate Polymers 83, 813–817. https://doi.org/10.1016/j.carbpol.2010.08.058

Zhou, D.-Y., Wu, Z.-X., Yin, F.-W., Song, S., Li, A., Zhu, B.-W., Yu, L.-L. (Lucy), 2021. Chitosan and Derivatives: Bioactivities and Application in Foods. Annu. Rev. Food Sci. Technol. 12, 407–432. https://doi.org/10.1146/annurev-food-070720-112725

Zhu, H., Poojary, M.M., Andersen, M.L., Lund, M.N., 2019. Effect of pH on the reaction between naringenin and methylglyoxal: A kinetic study. Food Chemistry 298, 125086. https://doi.org/10.1016/j.foodchem.2019.125086

Zielinska, K., Shostenko, A.G., Truszkowski, S., 2014. Analysis of chitosan by gel permeation chromatography. High Energy Chem 48, 72–75. https://doi.org/10.1134/S0018143914020143

Zu, Y., Li, C., Fu, Y., Zhao, C., 2006. Simultaneous determination of catechin, rutin, quercetin kaempferol and isorhamnetin in the extract of sea buckthorn (Hippophae rhamnoides L.) leaves by RP-HPLC with DAD. Journal of Pharmaceutical and Biomedical Analysis 41, 714–719. https://doi.org/10.1016/j.jpba.2005.04.052

Annex I. Preparation conditions of CS-TPP particles

Table Annex I-0-1 List of numerated sample with preparation conditions including concentrations and volumes of crosslinking agents and crosslinking temperature.

Sample	C_{Cs} (g/L)	C_{TPP} (g/L)	V_{Cs} (ml)	V_{TPP} (ml)	Temperature[2] (°C)
001	0.6	1	50	20	RT
002	3	1	50	20	RT
003	3	1	50	20	RT
004	1	1	10	8	RT
005	2	1	8	6.4	RT
006	2	1	50	15	RT
007	2	1	100	30	50
008	2	1	15	5	45
009	2	1	100	30	RT
010	2	1	100	30	RT
011	2	1	100	30	RT
012	2	1	100	30	50
013	2	1	50	15	RT
014	2	1	10	3	RT
015	2	1	50	15	RT
016	2	1	100	30	RT
017	2	1	100	30	RT
018	2	1	15	5	45
019*	2	1	100	30	RT
020	2	5	10	3.2	RT
021	3	1	8	9.6	RT
022	3	1	15	5	45
023	3	1	10	12	RT
024	3	1	10	3.3	45
025	3	1	50	20	RT
026	3	1	10	3.3	45
027	3	1	50	20	RT
028	3	1	50	20	45
029	3	1	10	3.3	RT
030	3	1	10	3.3	45

[2] RT: room temperature, 20 ±2 °C

031	3	1	10	3.3	45
032	3	1	10	3.3	45
033	2	1	15	5	45
034	3	1	10	3.3	45
035	3	1	10	3.3	45
036	3	1	10	3.3	45
037	4	5	10	3.3	RT
038	4	1	50	15	45
039	5	5	10	4	RT
040	5	1	10	3	RT
041	5	2.67	30	10	RT
042*	5	1	30	10	RT
043*	5	1	30	10	RT
044	5	1	160	40	RT
045	5	5	200	80	RT
046	5	1	20	40	RT
047	5	5	160	40	RT
048	5	5	160	40	RT
049	5	5	80	32	RT
050	5	5	80	32	RT
051	5	5	80	16	RT
052	5	1	80	160	RT
053	5	1	80	160	RT
054	5	1	80	100	RT
055	5	1	72	90	RT
056	5	5	160	80	RT
057	5	5	30	10	RT
058	10	5	50	20	RT
059	5	5	50	20	RT
060	30	5	9	6	RT
061	5	5	80	32	RT
062	5	5	80	32	RT
063	5	5	80	32	RT
064	3	1	39	13	45
065	3	1	10	3.3	45
066	3	1	10	3.3	45
067	3	1	39	13	45
068	3	1	10	3.3	45
069	3	0.5	50	20	RT
070	5	1	10	3.3	RT
071	3	1	15	5	45

072	3	1	15	5	45
073	3	1	15	5	45
074	3	1	15	5	45
075	3	1	15	5	45
076	3	1	15	5	45
077	10	5	50	20	RT
078	5	5	50	20	RT
079	3	1	39	13	RT
080	3	1	39	13	RT
081	3	5	10	3.3	RT
082	3	2.5	10	3.3	RT
083	5	5	10	4	RT
084*	5	1	10	3.3	RT
085	1	1	10	3.3	RT

* Sample prepared by reverse method

Table Annex I-0-2 List of CS-TPP nanoparticles with particle concentration and particle size. Detailed preparation conditions of samples can be found in Table 1. Sample were listed by the order that size increased.

Sample	Particle concentration (g/L)	Z-average(nm)	Sample	Particle concentration (g/L)	Z-average(nm)
002	0.6	64	079	2.5	172
021	1.9	81	015	1.8	176
005	1.6	99	025	2.4	189
069	2.3	109	037	4.2	199
001	0.7	111	073	8.6	204
068	2.5	111	026	2.5	220
006	1.8	115	003	2.4	227
007	1.8	122	027	2.5	228
008	1.8	124	028	2.5	236
009	1.8	125	039	5.0	237
010	1.8	126	040	4.1	243
011	1.8	136	078	5.0	267
022	2.5	136	077	8.6	277
012	1.8	138	041	4.4	285
013	1.8	139	029	2.5	314
023	1.9	140	038	3.3	390
014	1.8	158	050	5.0	417
024	2.5	160	074	5.0	501

Annex II. SEC MALS

Size exclusion chromatography (SEC-MALS, Size exclusion chromatography with multi-angle laser light scattering detectors) allows the determination of the molecular mass and the investigation of the molar mass distribution of polysaccharides.

Chitosan (C2395, 5-20 mPa·s, 0.5% in 0.5% Acetic Acid at 20°C) was purchased from TCI chemicals (Tokyo). Purified chitosan sample was prepared in lab by above mentioned method. This method was used to evaluate the average molar masses (MW) of commercial and purified chitosan. The average molar mass was determined using the use of PEO standard (PEO 24K, Malvern). For each sample, a solution was made by dissolving the polysaccharides to be tested at 2% w/v in a buffer acetate (0.3 M acetic acid; 0.3 M sodium acetate; pH=4.5). This buffer has been filtered on a membrane with a porosity of 0.45 µm (Durapore® 47 mm diameters, Millipore) at 20°C. Buffer acetate also served as the mobile phase for chromatography. The analyzes were carried out at 30°C at a flow rate of 0.35 mL/min with an injection volume of 50, 100 and 150 µL and using a viscometer of the Viscotek A4000M type (column 7.8 mm in internal diameter and 30 cm in long). A SEC-MALLS VISCOTEK 305 TDA (Malvern instruments) and a Shimadzu HPLC pump (Shimadzu) were used to conduct the molecular weight determination. 100 uL of sample was injected unless stated otherwise.

Table Annex II-1: Experimental conditions of SEC-MALS

Viscometer	SEC-MALLS VISCOTEK 305 TDA
Pump	Shimadzu HPLC pump
Detector	RALS only
Buffer	Acetic acid 170 mM, acetate 200 mM (pH 4.5)
Column	Malvern A4000 (Polymethyl-methacrylate)
Flow rate	0.35 mL/min
Temperature	30°C
Solvent RI	1.331

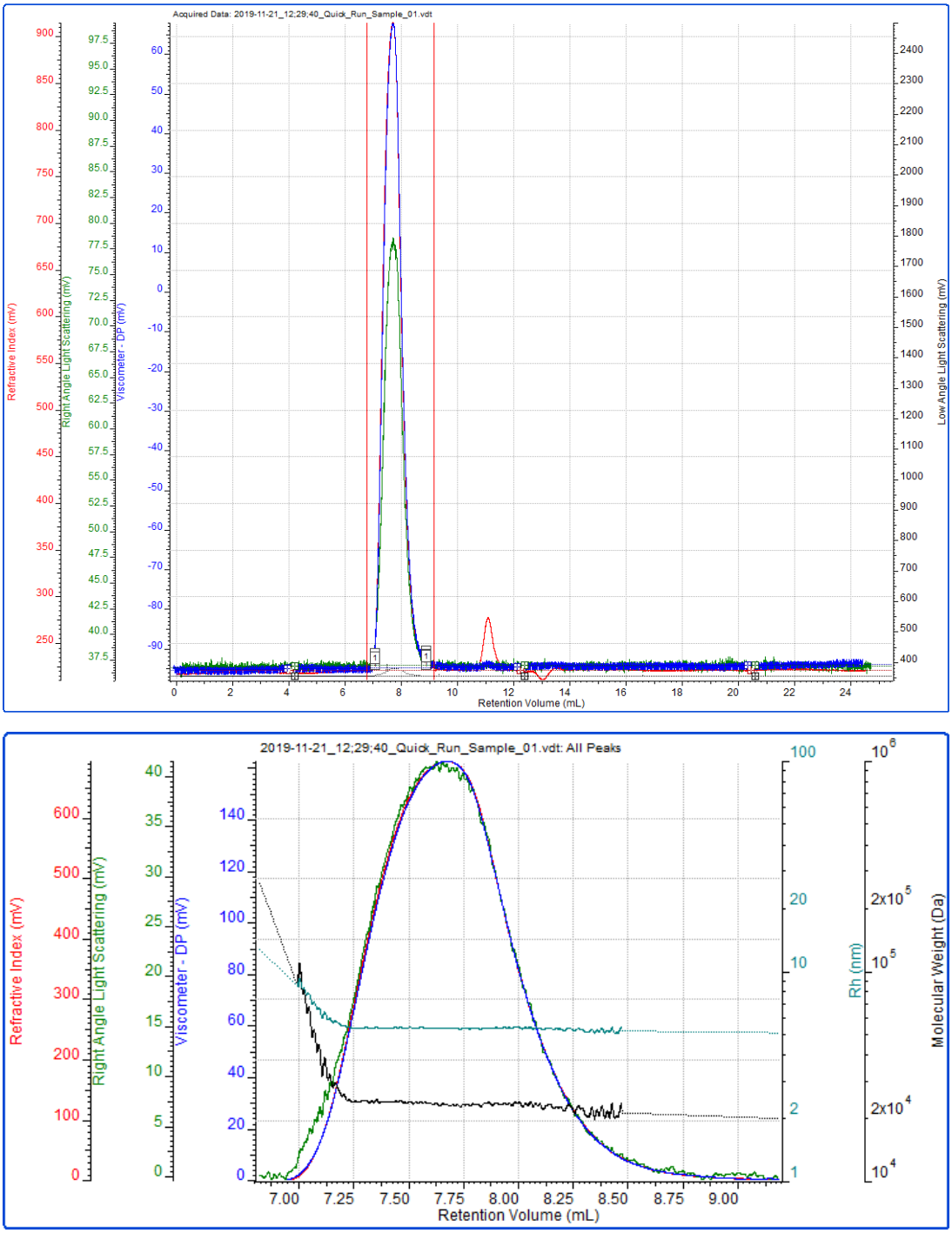
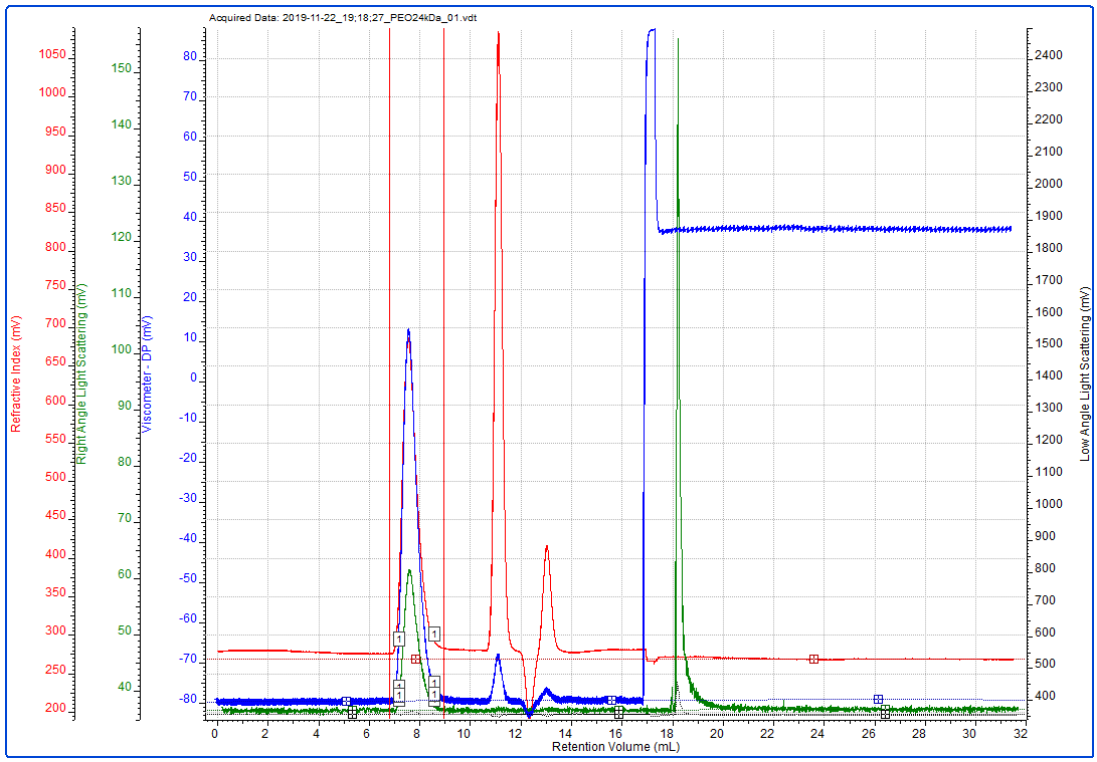


Figure Annex II -1 Calibration with PEO24k

PEO24k @ 3.03 g/L to check calibration



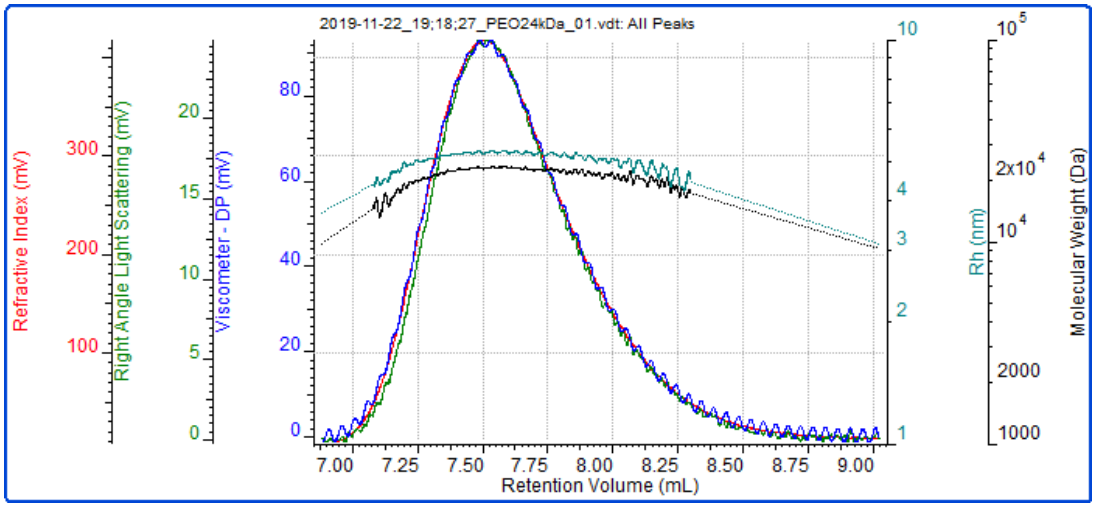


Figure Annex II-2 Calibration check with PEO24k (3.03 g/L)

Optimization concentration of chitosan

Commercial chitosan 10 g/L was too much concentrated for SEC-MALS. While 5 g/L was more suitable as concentration.

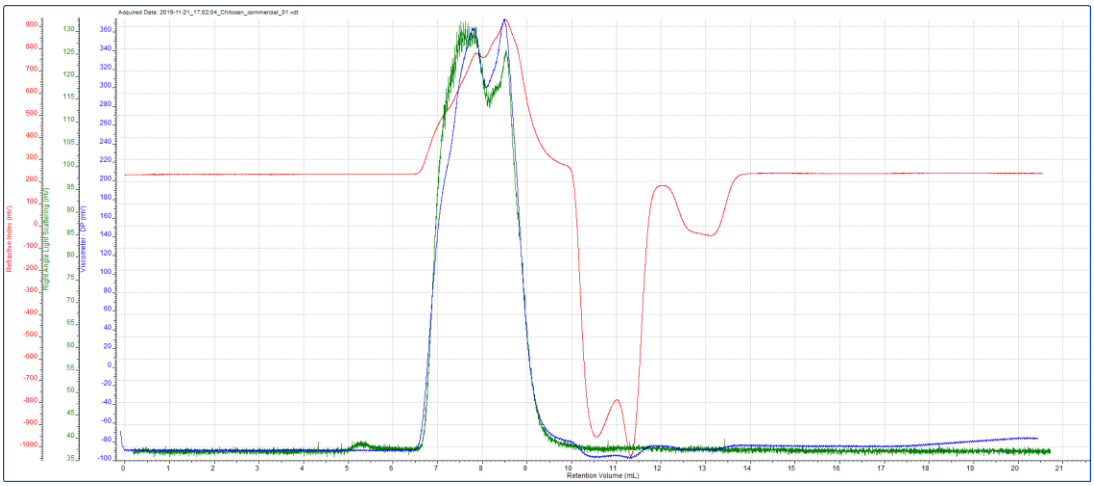


Figure Annex II-3 Commercial chitosan (10 g/L)

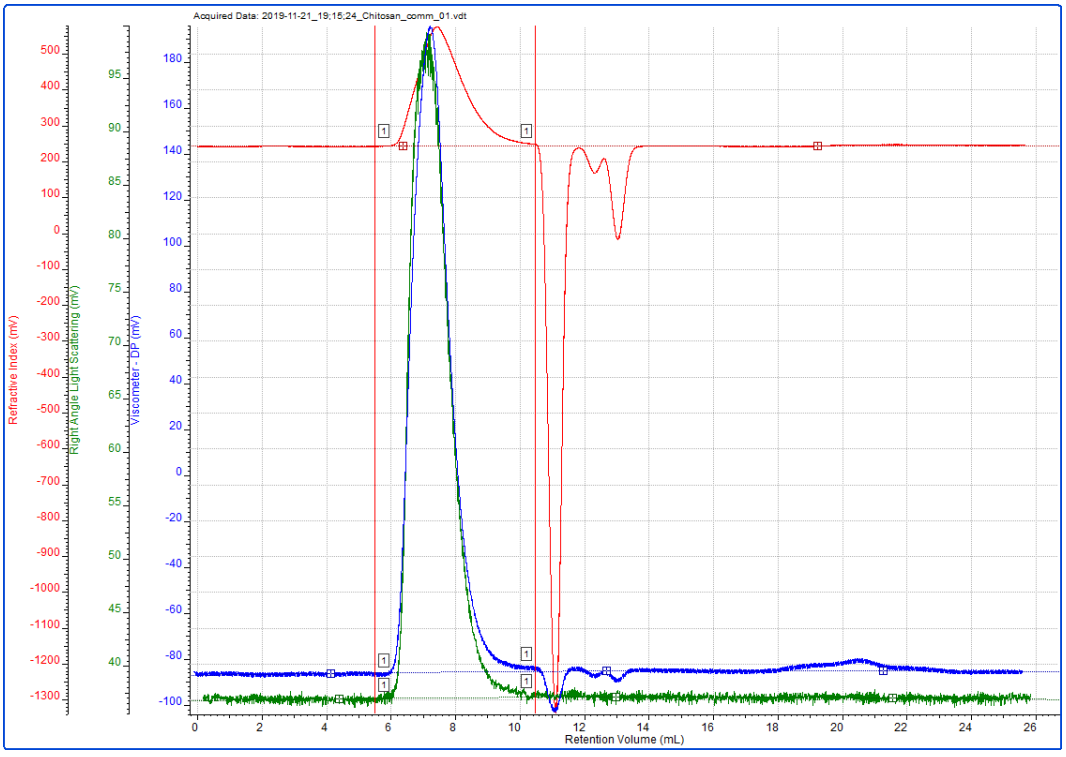


Figure Annex II-4 Commercial chitosan (5 g/L)

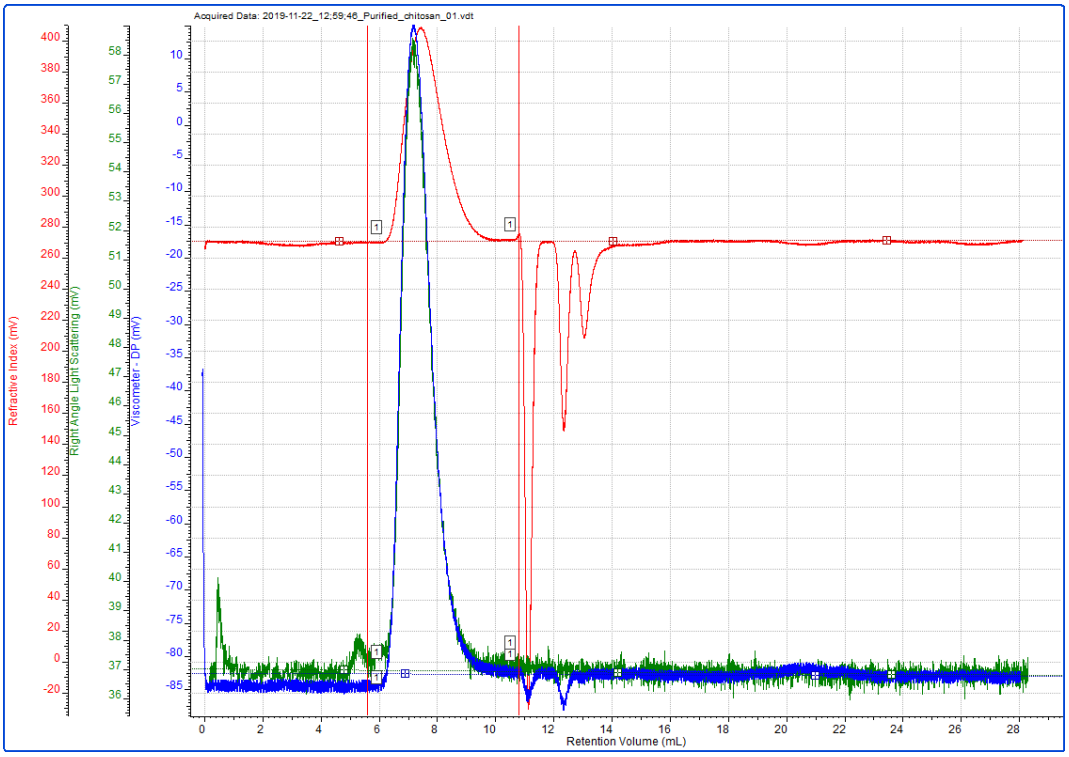


Figure Annex II-5 Purified chitosan (2.5 g/L)

Optimization of injected volume

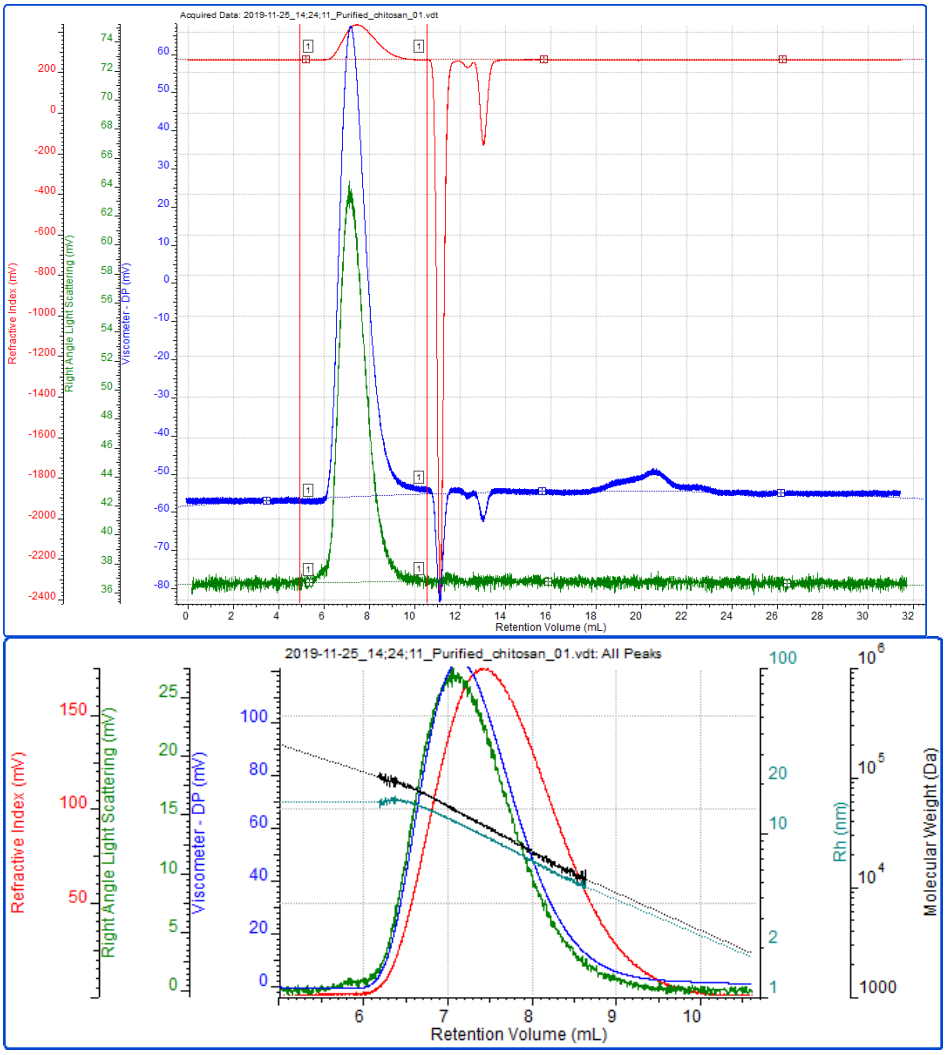


Figure Annex II-6 Purified chitosan (5 g/L), inject volume: 50µl

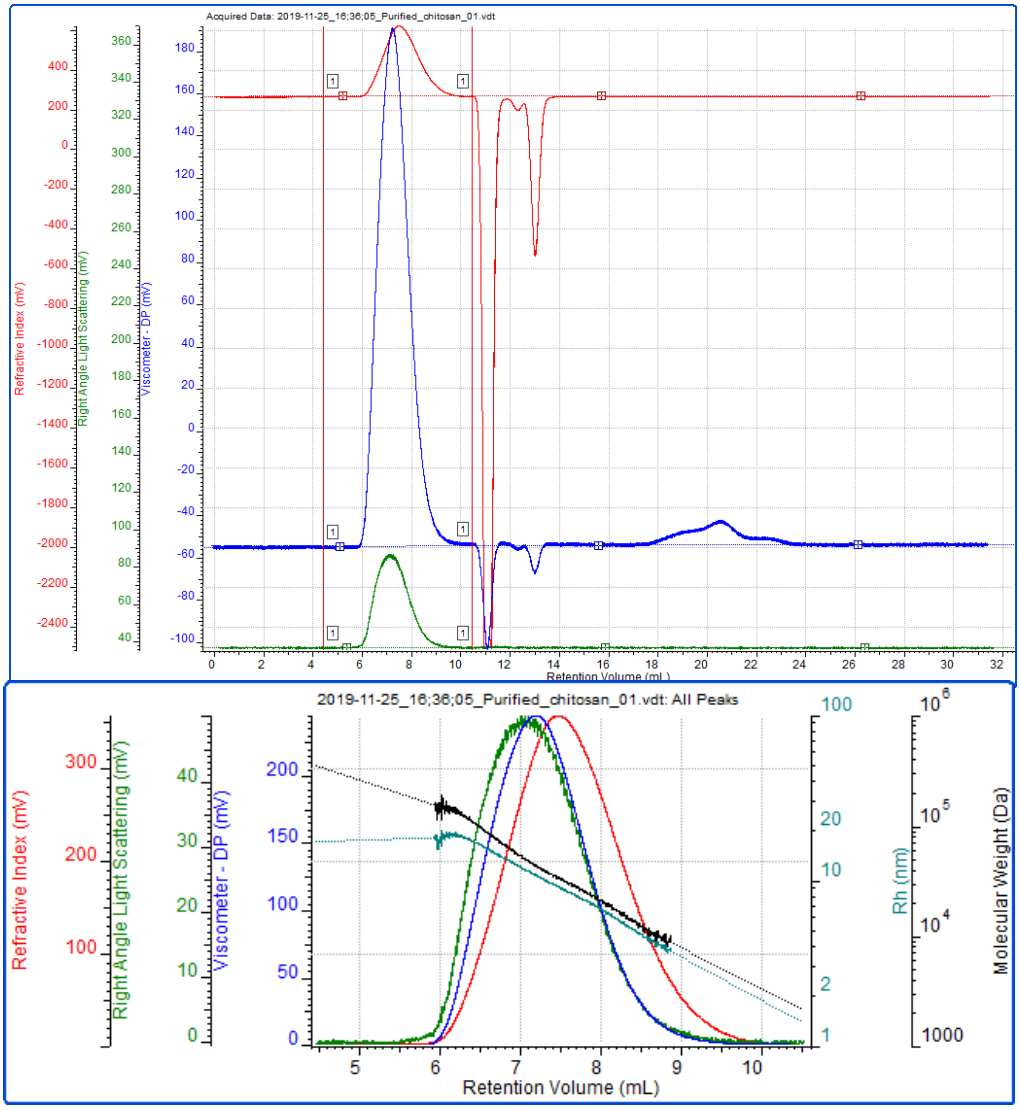


Figure Annex II-7 Purified chitosan (5 g/L), inject volume: 100µl

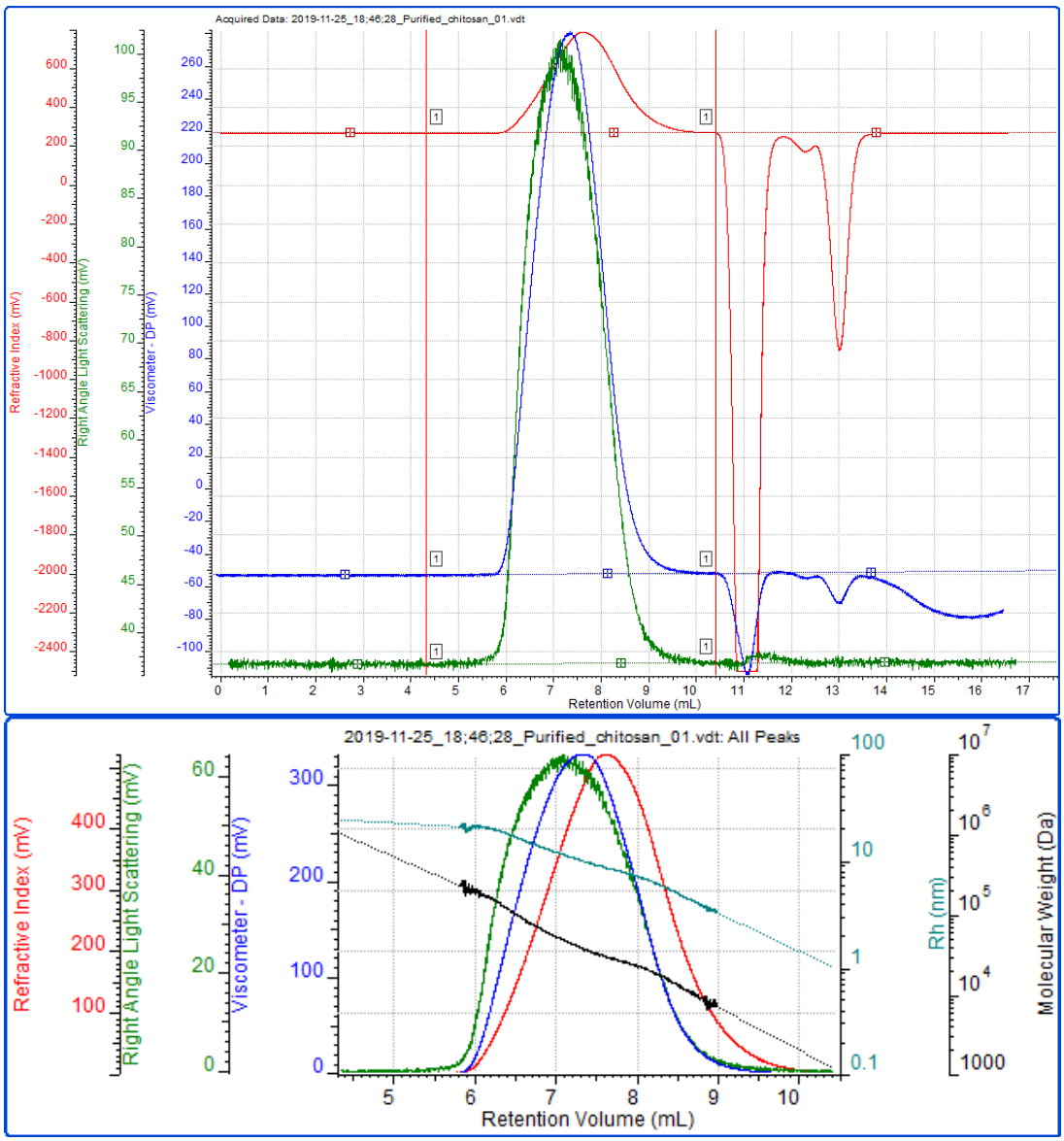


Figure Annex II-8 Purified chitosan (5 g/L), inject volume: 150µl

Sample	Commercial chitosan @ 5 g/L	Purified chitosan @ 2.5 g/L	Purified chitosan @ 5 g/L	Purified chitosan @ 5 g/L	Purified chitosan @ 5 g/L
Sample concentration(g/L)	5	2.5	5	5	5
Input (µL)	50	50	50	100	150
Ret Vol (mL)	7.388	7.393	7.407	7.452	7.597
Mw (Da)	44406	34965	35306	36882	36266
Mw/Mn	1.682	1.403	1.483	1.593	1.704
IV (dL/g)	1.6536	1.3915	1.3900	1.4327	1.4308
Rh(w) (nm)	10.09	8.88	8.88	9.04	8.96
Rg(w) (nm)	0.00	0.00	0.00	0.00	0.00
Wt Fr (Peak)	1.0000	1.0000	1.0000	1.0000	1.0000
RI Area (mVmL)	551.38	207.22	296.35	608.06	909.99
RALS Area (mVmL)	85.94	26.12	37.00	78.28	115.61
IVDP Area (mVmL)	377.96	117.97	168.73	358.96	540.53
Input Concentration (mg/mL)	5.0000	2.5000	5.0000	5.0000	5.0000
Calculated Concentration (mg/mL)	4.5757	1.7196	4.9186	5.0461	5.0345
Recovery %	91.5140	68.7855	98.3721	100.9214	100.6893

Table Annex II-II-1 Raw data of SEC-MALS

Annex III. Encapsulation washing step

NR solution (containing 1, 5 and 7.5 mg, respectively) was added into 10 mL of CS solution (5 g/L) under mild magnetic stirring.

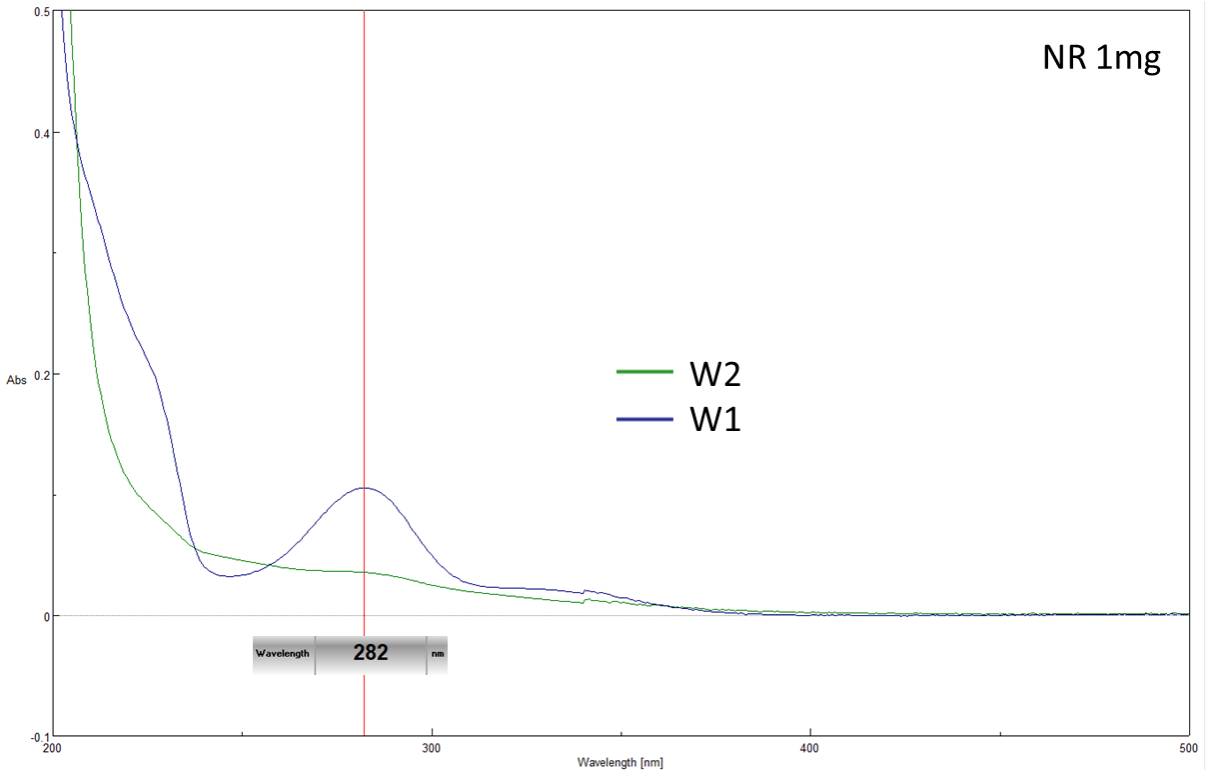


Figure Annex III-1 UV-Vis spectra of washing liquids W1 (blue) and W2 (green), initial amount of NR added was 1 mg.

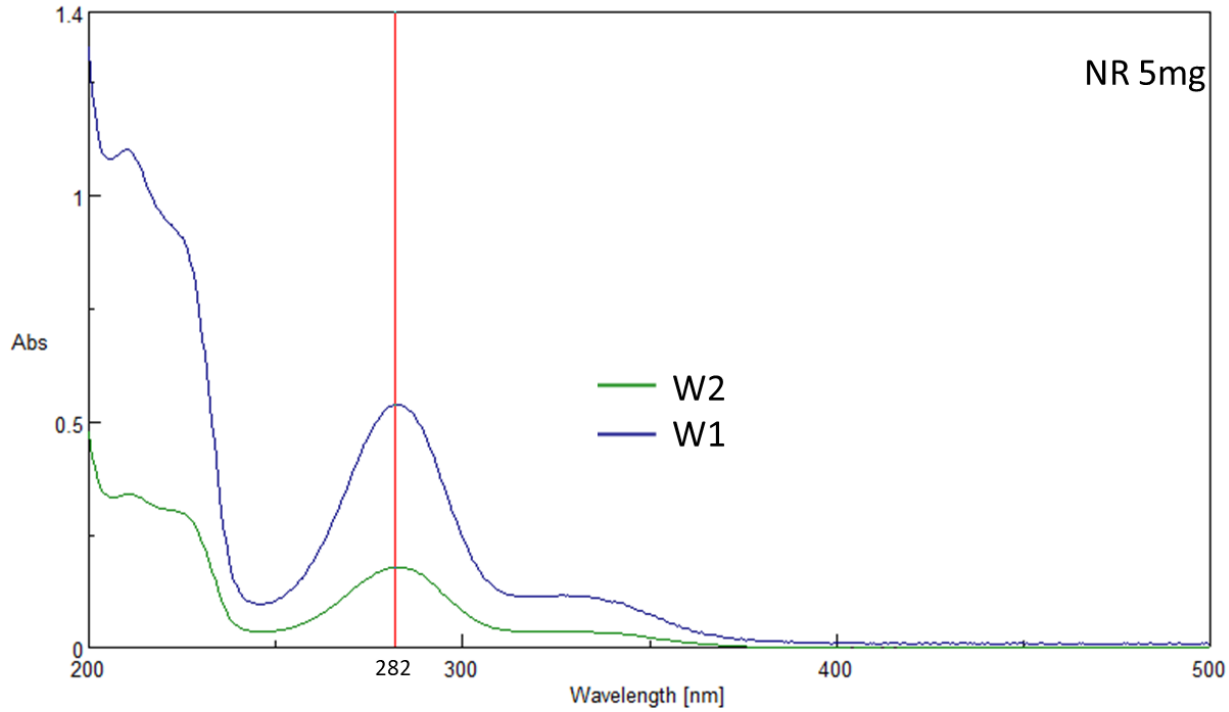


Figure Annex III-2 UV-Vis spectra of washing liquids of NR loaded CS-TPP particles W1 (blue) and W2 (green), initial amount of NR added was 5 mg.

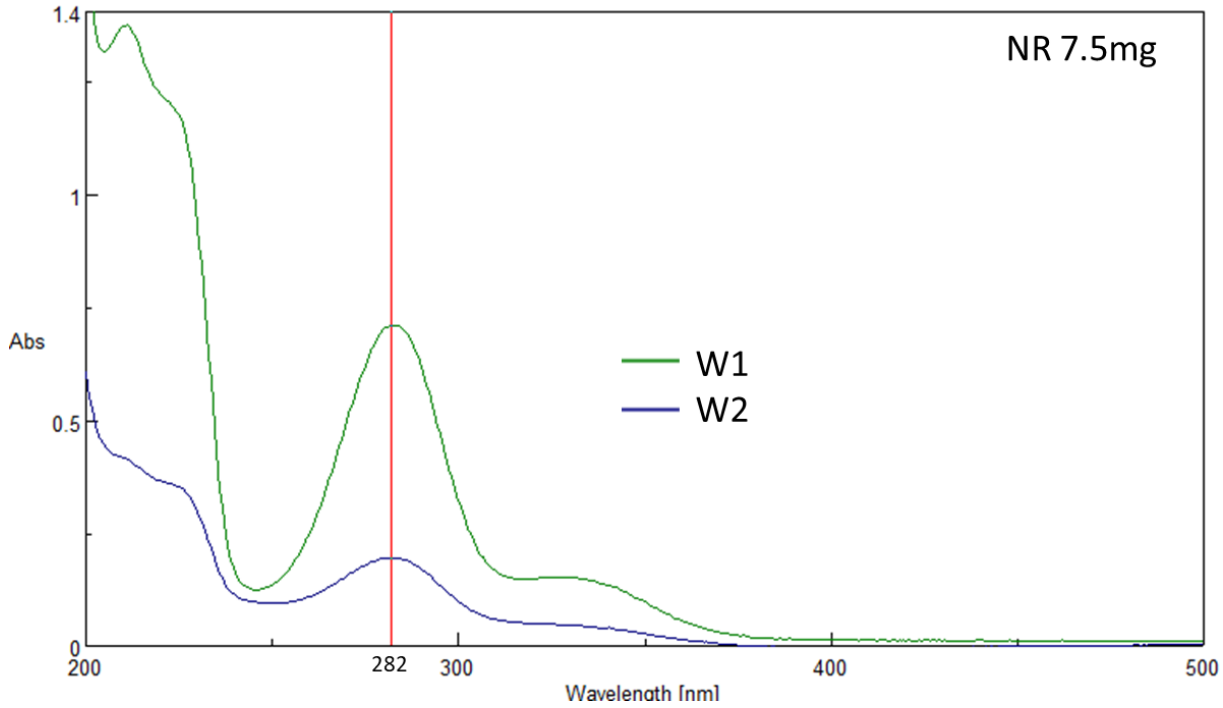


Figure Annex III-3 UV-Vis spectra of washing liquids of NR-loaded CS-TPP particles W1 (blue) and W2 (green), initial amount of NR added was 7.5 mg.

Sequentially, 4 mL of TPP (5 g/L) solution was dropped and wisely added into a mixture of CS-NR solution. Then, mixed solution was stirred for at least 1 hour to make sure full gelation of CS-TPP particles and encapsulation of NR. After, the mixed suspension was transferred into an Eppendorf tube and centrifuged (5000rpm, 10min, 20°C). The pellet obtained was washed twice with 10 mL of water and washing liquids were labeled as W1 and W2, respectively. W1, and W2 were measured UV-Vis spectrophotometrically to determine the content of NR.

Low UV absorbance (even no detectable) of NR at 282 nm was observed in W2 (Figure A1, A2 and A3). The amount of NR in W2 were calculated and were equal to 3%, 1% and 1% of the total amount of NR added, respectively. Similarly, the UV absorbance of NRG in W1 was low and undetectable in W2 at 289 nm. 1% of total NRG was found in W1 and quantity in W2 was negligible.

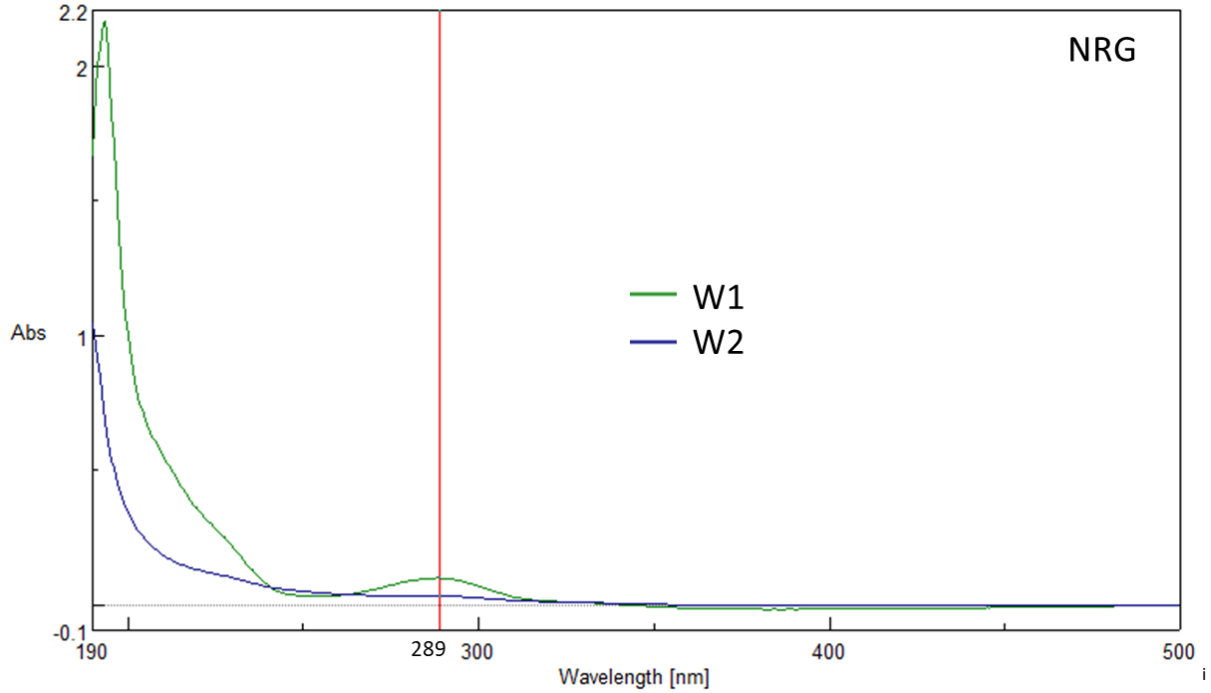


Figure Annex III-4 UV-Vis spectra of washing liquids of NRG-loaded CS-TPP particles, W1 (blue) and W2 (green)

The quantity of free NR and NRG molecules in W2 was negligible, therefore, two rounds of washing are sufficient for removing them from the CS-TPP particles.